# Application of sputtering to micro gas chromatography : a novel collective stationary phase disposition technique for micro gas chromatography columns fabrication : feasibility, evaluations and oilfield applications.

Raphael Haudebourg

# THÈSE

PRÉSENTÉE A

## L'UNIVERSITÉ PIERRE ET MARIE CURIE

ÉCOLE DOCTORALE DE CHIMIE PHYSIQUE
ET DE CHIMIE ANALYTIQUE DE PARIS CENTRE

Par **Raphaël HAUDEBOURG**

Laboratoire des Sciences Analytiques,
Bioanalytiques et Miniaturisation

POUR OBTENIR LE GRADE DE

**DOCTEUR**

# Application of sputtering to micro gas chromatography

**a novel collective stationary phase deposition technique for micro gas chromatography columns fabrication: feasibility, evaluations and oilfield applications**

***Application de la pulvérisation cathodique à la chromatographie en phase gazeuse miniature***

***une nouvelle technique de dépôt collectif de la phase stationnaire pour la fabrication de micro colonnes sur puce: faisabilité, caractérisations, et applications pétrolières***

Directeur de thèse : **Jérôme VIAL**

Soutenue le : 05/02/2014, devant la commission d'examen formée de :

| | | |
|---|---|---|
| **M. Carlo BICCHI** | Professeur à l'Université de Turin | Rapporteur |
| **M. Jérôme RANDON** | Professeur à l'Université Claude Bernard de Lyon | Rapporteur |
| **M. Jacques FATTACCIOLI** | Maître de Conférences à l'Université Pierre et Marie Curie de Paris | Examinateur |
| **M. Franck LAUNAY** | Professeur à l'Université Pierre et Marie Curie de Paris | Examinateur |
| **M. Michel SABLIER** | Directeur de Recherches au CRCC de Paris | Examinateur |
| **M. Jérôme BREVIERE** | Directeur de Département à GeoServices, Schlumberger | Examinateur |
| **M. Jérôme VIAL** | Maître de Conférences à l'ESPCI ParisTech | Directeur de thèse |
| **M. Didier THIEBAUT** | Chargé de Recherche CNRS à l'ESPCI ParisTech | Co-directeur de thèse |

# Application of sputtering to gas chromatography

**A novel collective stationary phase deposition technique for micro gas chromatography columns fabrication: feasibility, evaluations and oilfield applications.**

A thesis submitted in fulfillment of the requirements for the degree of
**Doctor of Philosophy in Analytical Chemistry**

At the
**Doctoral School of Physical Chemistry and Analytical Chemistry of Paris (ED388, Pierre & Marie Curie University), FRANCE**

In partnership with the
**Laboratory of Analytical and Bioanalytical Sciences and Miniaturization ESPCI ParisTech, FRANCE**

And
**Schlumberger MEMS Technology Center Elancourt, FRANCE**

By
**Raphael HAUDEBOURG**

To

| | | |
|---|---|---|
| **Mr. Carlo BICCHI** | Professor at the University of Turin | Reporter |
| **Mr. Jerome RANDON** | Professor at the University Claude Bernard of Lyon | Reporter |
| **Mr. Jacques FATTACCIOLI** | Associate professor at the University Pierre et Marie Curie of Paris | Examiner |
| **Mr. Franck LAUNAY** | Professor at the University Pierre et Marie Curie of Paris | Examiner |
| **Mr. Michel SABLIER** | Research manager at the CRCC of Paris | Examiner |
| **Mr. Jerome BREVIERE** | Department manager at GeoServices, Schlumberger | Examiner |
| **Mr. Jerome VIAL** | Associate professor at the ESPCI ParisTech | Thesis supervisor |
| **Mr. Didier THIEBAUT** | CNRS Research fellow at the ESPCI ParisTech | Thesis co-supervisor |

Defended
**February 5th 2014**

# Statement of original authorship

The work contained in this thesis has not been previously submitted to meet requirements for an award at this or any other higher education institution. To the best of the author's knowledge and belief, this thesis does not contain previously published or written by another person material except where due reference is made.

Date:

Signature:

# Table of contents

# List of tables and figures

# Foreword

The research work presented in this report is the fruit of a “CIFRE” collaboration (French industrial convention of education through research). From March 2010 to January 2014, it implied Schlumberger, the leading oilfield services company, as the industrial collaborator, the ESPCI ParisTech, the top-ten transdisciplinary graduate engineering school, as the academic collaborator, and the Doctoral School of Pierre & Marie Curie University in Physical Chemistry and Analytical Chemistry, as the educational and administrative host. It was conducted at Schlumberger MEMS TC (Micro Electro-Mechanical Systems Technical Center), at GeoServices (a Schlumberger subsidiary), at the ESPCI LSABM (Laboratory of Analytical and Bioanalytical Sciences and Miniaturization), and at the ESIEE Paris (Graduate Engineering School in Electrotechnics and Electronics). It is transdisciplinary, standing at the crossroads of analytical chemistry (fundamental and applied), micro engineering (including micro fabrication, packaging, thermal management), automation (including hard- and software developments), and petro chemistry.

The purpose of this foreword is to justify the author’s will to intend this report to the industrial community as well as to the academic one, to the international scientific community as well as to the French one, and to micro fabrication or petroleum engineers as well as to analytical chemistry researchers. Therefore, the author made the two following choices (in agreement with the Doctoral School): first, this report is written in English (instead of French, which is usually recommended for thesis manuscripts; a 7-pages summary of the thesis in French is proposed page 172); then, the introduction of the thesis will begin with a short and basic description of elementary gas chromatography notions (I.A.), for non-specialists; finally, this report, meant to be read, purports to be as synthetic as possible. The hurried expert reader is of course allowed to directly jump to sections I.B. and I.C., which are respectively dedicated to a basic description of the use of gas chromatography in oilfield services and to MEMS technology, or even to next chapters. A few additional notions, too marginal to be defined in the body of the report for readability reasons but occasionally useful, are followed by an asterisk and defined in a short glossary at the end of the report.

This version of the report is non-confidential, and, therefore, all sections related to the specific application developed in partnership with GeoServices do not appear. However, it is obviously possible for any interested reader to ask for confidential information and/or the full version of the report, at the author address: raphael.haudebourg@gmail.com.

Anyway, the author wishes to all kinds of readers a pleasant time through this manuscript.

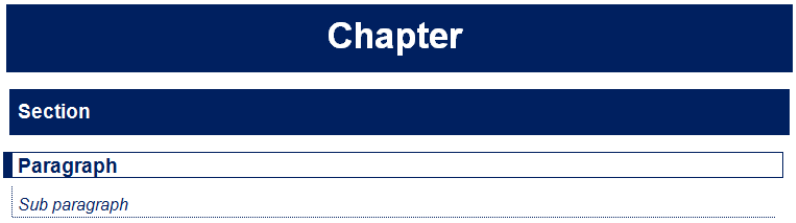

# I. Introduction

As mentioned in the foreword, the first section of this introduction will firstly be intended to gas chromatography (GC) non-specialists, and has two main purposes, which are crucial for the understanding of the method: the description of the different types of GC columns and detectors, and the definitions of the thermodynamic and kinetic evaluations of a GC column. Then, emphasis will be put on the use of GC in oilfield services and on miniaturized systems and their contribution to this technique. In the five last sections of this introduction chapter, problem will be stated, research justified, approach and methodology described, scope delimited, and finally report structure outlined.

## I.A. Fundamental notions of gas chromatography

### I.A.1. Gas chromatography general principle

Chromatography is a chemical analysis technique aiming at the separation, identification, and quantification of the different species in a mixture. Gas chromatography refers to the use of this technique for the analysis of gaseous mixtures (gaseous under standard conditions or after easy vaporization). On figure 1 is displayed the general functioning principle of a Gas Chromatograph (GC), the apparatus enabling the process.

The apparatus consists of three main components:

- an injector, which allows the injection of the sample to analyze into the column,
- a column, similar to a tube, which allows the separation of the different species in the sample,
- a detector, which allows the measurement of a physical value at the end of the column.

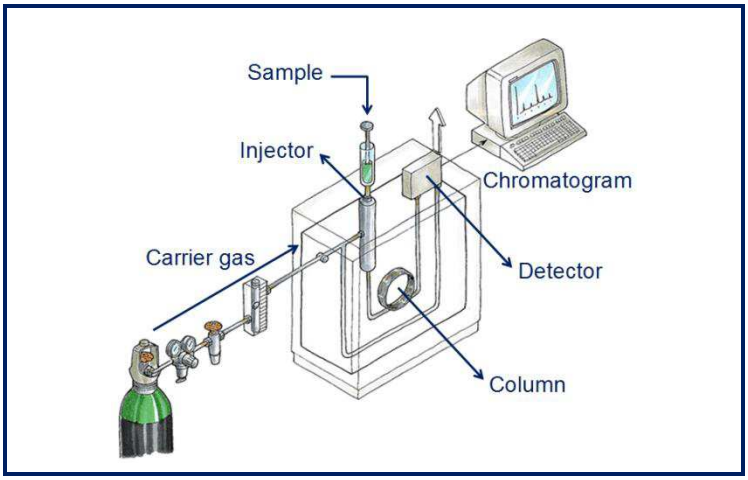


*Fig. 1: GC general principle*

A continuous stream of a carrier gas (usually helium, but also nitrogen or hydrogen) passes through the column towards the detector. The sample to analyze is injected upstream of the column and percolates through the column. The recording over time of the electronic signal returned by the detector placed downstream of the column is called the chromatogram, which consists in a succession of peaks corresponding to the different species eluting out of the column at different times (retention times, $t_R$).

## I.A.2. Separation mechanism in a gas chromatography column

The column consists of a tubing, whose length is generally comprised between 5 cm and 50 m, depending on the type of column (see I.A.3.), and whose inner diameter is generally comprised between 100 µm and 1 mm. The column is packed (or its inner walls are coated) by an adsorbing material, named the stationary phase (by opposition to the carrier gas also named mobile phase). The separation mechanism is displayed on figure 2.

In this cross-sectional view of the tubing, the inner walls of the column (in black) are coated with a thin film of stationary phase (green). A two components (red and blue) mixture (purple) is injected upstream of the column (left) and carried through it towards the detector (right) thanks to the carrier gas stream (big black arrows). During the percolation, the molecules of the sample diffuse laterally (small black arrows) and adsorb and desorb several times on the stationary phase. The strength of the adsorption is a thermodynamic value and is specific to a couple adsorbent-adsorbed molecule. Thus, molecules that weakly adsorb on the stationary phase (red) elute before molecules that strongly adsorb (blue). If all the parameters are relevantly chosen, the chromatogram results in two separated peaks, the first one corresponding to the less retained compound (red).

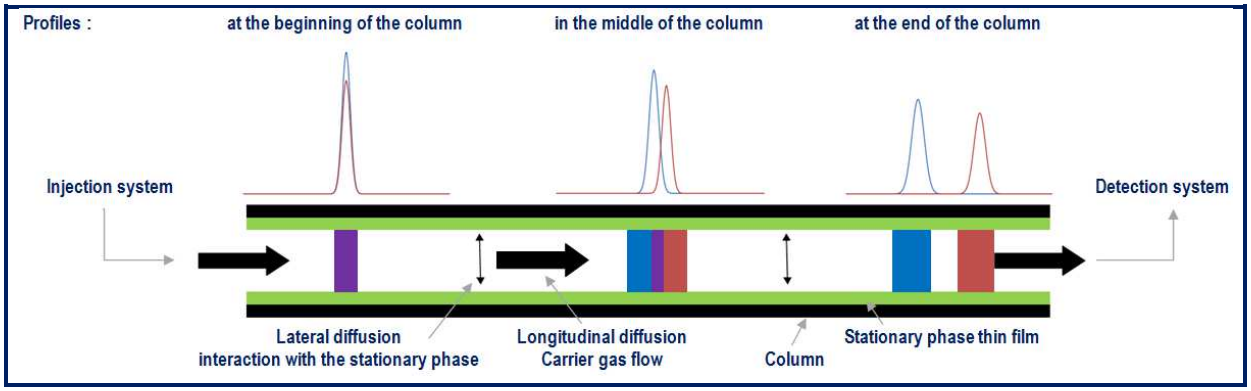


*Fig. 2: separation mechanism in a column*

## I.A.3. Different types of gas chromatography columns

In a basic approach, there are 3 main types of conventional GC columns, according to the layout of the stationary phase inside the column (see figure 3).

- Packed columns are filled with porous solid grains. They are often short and wide, to compensate the high pressure drop induced by the low permeability of the inner structure. Retention is ensured by small diffusion lengths. First GC columns were of this type.

- Porous Layer Open Tubular (PLOT) columns are coated with a thin film of a porous solid monolithic structure. Retention is ensured by a longer length, made possible by the high permeability of the column.

- Wall Coated Open Tubular (WCOT) columns are coated with a thin film of a gel material. Although their layout seems to be quite similar to PLOT columns at first sight, retention mechanisms are different (dissolution of the analyte in the liquid stationary phase, contrary to surface physi-sorption of the analyte on the surface of the porous solid stationary phase), and their length is often longer to enable separation. They represent the most used type of columns.

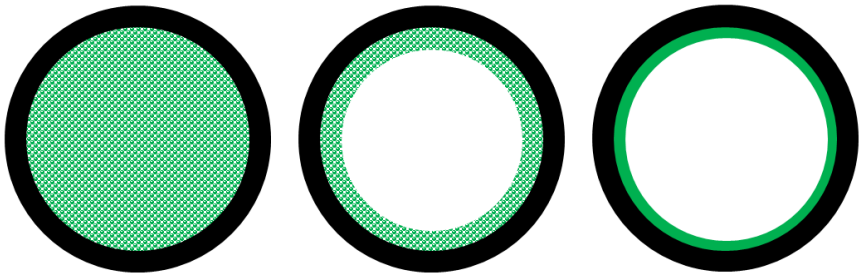


*Fig. 3: the three main types of GC columns: packed column, Porous Layer Open Tubular column (PLOT) and Wall Coated Open Tubular column (WCOT)*

## I.A.4. Injectors and detectors

The injection of the sample into the flow line of the apparatus can be executed manually by the user with a syringe, or automatically by a robot. It is also possible to use a switch injection system, the first step being the loading of the sample into a sampling loop, the second step being the unloading of the sample from the loop to the main flow line. Loop injectors are widely used for automated tasks. Moreover, they enable multidimensional chromatography (several columns in parallel in the same system).

The continuous measurement of a physical value at the end of the column is performed by a detector. The main types of detectors are:

- Flame Ionization Detector (FID), whose response is proportional to the instantaneous quantity of C-H bonds in the detector chamber; it is a robust detector with relatively low detection and quantification limits; however, it is not universal (only C-H bonds-containing molecules can be detected) and it requires hydrogen supply;

- Thermal Conductivity Detector (TCD), which signal is proportional to the difference of thermal conductivity in the main flow line and in a carrier gas reference flow line; it generally shows poorer performances than FID, but it is universal and requires no other gases than the carrier gas;

- many other types of detector exist (e.g. optical, specific to one atom, mass detection), but are of lower interest here.

Generally, the area of the chromatographic peak displayed by the detection system is linked to the injected quantity of the corresponding analyte (proportional in the linear domain of the detector). A typical chromatogram and the relevant values for evaluation are displayed on figure 4.

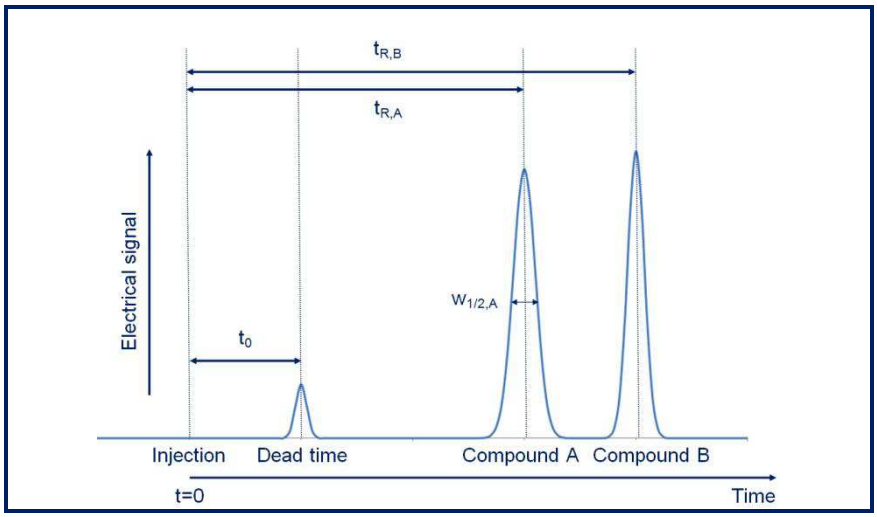


*Fig. 4: typical chromatogram and relevant values*

## I.A.5. Thermodynamic evaluation of a gas chromatography column

The thermodynamic behavior of a column (towards one compound) is characterized by the retention factor k:

$$k = \frac{K}{\beta}$$

- where K is the distribution coefficient of the compound between the stationary phase and the mobile phase; if $\Delta_r H°$, $\Delta_r G°$ and $\Delta_r S°$ are respectively the standard enthalpy, Gibbs free energy, and entropy associated to the adsorption equilibrium, T the temperature in Kelvin, R the ideal gas constant (8.314 $J.K^{-1}.mol^{-1}$), K is ruled by the following equation:

$$\Delta_r G° = \Delta_r H° - T\Delta_r S° = -RT \ln K \quad \text{or} \quad K = K° \exp(-\Delta_r H°/RT) \quad \text{with} \quad K° = \exp(\Delta_r S°/R)$$

- and where β is the phase ratio of the column, which is the ratio between the geometric volume of mobile phase, or void, inside the column, and the volume of stationary phase inside the column; e.g., for a round-section open tubular column with an inner diameter $d_c$, and coated with a $e_f$-thick thin film of stationary phase, $\beta = d_c/4e_f$.

k is experimentally measured thanks to the following relation:

$$k = \frac{t_R - t_0}{t_0}$$

where $t_R$ is the retention time of the compound and $t_0$ the zero retention time, dead time or flight time, corresponding to percolation time of a non-retained compound (see figure 4).

The main use of k is to give a universal and dimensionless value of the retention of one compound in one column, for comparison purposes. Moreover, adsorption heat $|\Delta_r H°|$ is easily exhibited by the plot of the logarithm of k against 1/RT at different temperatures (Van't Hoff plot). Finally, the plot of ln k against column's and stationary phase's dimensions, and the possible deviation to ideality, gives precious information about the influence of such parameters on the thermodynamic behavior of the column.

As a consequence of the thermodynamic behavior of a GC column, a higher column temperature will result in a weaker retention. To decrease the retention times of the most retained compounds in the mixture, without decreasing the retention of the less retained (which would generally result in a poorer resolution), chromatographists apply linear temperature ramps to the column. By choosing the appropriate temperature programming parameters (start temperature, slope in °C/min, and stop time), it is possible to shorten analysis time without losing separation quality, compared to isothermal conditions. An obvious demonstration of this will be shown in IV.B.3, but the key point here is to keep in mind that column thermal management is a crucial issue in gas chromatography.

The last thermodynamic quantity to be introduced here is the selectivity $k_A/k_B$ of a stationary phase between two compounds A and B. This value is generally useful for the comparison between the thermodynamic behaviors of two different stationary phases from different columns which could not have the same phase ratio β for practical reasons. By using two retained compounds, the value of β can be passed-by, which is of the most helpful utility when this value cannot be accurately known (for instance in the case of solid stationary phases with unknown porosities). Investigated differences can obviously concern stationary phase type or material, but also structure, porosity, or hydration, in the case of solid stationary phases.

## I.A.6. Kinetic evaluation of a gas chromatography column

The plate theory predicts Gaussian shapes for chromatographic peaks in ideal conditions. The broadening of the peaks (considered as a Dirac delta function at the injection) is ruled by three phenomena:

- a multiple path effect, occurring almost only in packed columns, and independent of the carrier gas velocity,
- a longitudinal diffusion effect (along the column axis), proportional to the diffusion coefficient of the analyte in the mobile phase, and inversely proportional to the carrier gas velocity,
- a resistance to mass transfer effect, both due to the high density of the stationary phase and of the inhomogeneous radial velocity profile of the mobile phase, and is proportional to it.

These three phenomena are respectively represented in the three terms of the Van Deemter equation:

$$H = A + \frac{B}{u} + Cu$$

where u is the carrier gas velocity, where A, B and C three constants related to the analyte, the stationary phase structure, and the mobile phase nature, and where H is the plate height.

The name of plate height, or Height Equivalent to a Theoretical Plate (HETP), comes from an historical analogy of chromatographic separation with fractionation distillation (as well as the name of “column” for the separating element). This plate height is linked to the efficiency of the retention of one compound on one column under one set of experimental parameters by the simple following relation:

$$N = \frac{L}{H}$$

where L is the length of the column; N, also named efficiency, is thus the number of plates in the column (again, for one compound and one column under one set of experimental parameters).

N is calculated from the data processing of the chromatogram by the following equation:

$$N = 5.54 \left(\frac{t_R}{w_{1/2}}\right)^2$$

where $w_{1/2}$ is the half-height width of the peak (see figure 4). In other words, the retention of one compound on one column is said to be efficient when the column is able to retain the most the compound with a low peak broadening, i.e. when the number of plates is high, i.e. when the plate height is small. Nowadays, numbers of plates often exceed 10000 plates per meter in open columns (a few 10 to a few 100 meters long). Efficiency is sometimes expressed in number of plates per second to take into account pressure drop effects and consequences on analyses time in the comparison of different columns (open or packed…): acknowledged limit value for open columns is around 1000 plates per second.

The plot of HETP against u (regulated through the pressure difference applied to the column, and calculated with $u=L/t_0$) is called a Van Deemter plot, and has a typical shape as shown on figure 5.

The relevance of the value of efficiency to assess the performance of a separation is demonstrated on figure 5a. At low velocities, peak summits are better separated than at high velocities, but peak broadening is more important, which results in a poor separation; on the contrary, at high velocities, peak broadening is low, but peak summits are closer to each other on the time axis, also resulting in a poor separation. Therefore, efficiency reaches a maximum (and plate height reaches a minimum, see figure 5b) at an optimal velocity. The values of the minimal plate height $H_{min}$ and of the optimal velocity $u_{opt}$ can be extracted from Van Deemter equation as following:

$$H_{min} = A + 2\sqrt{BC} \qquad \text{and} \qquad u_{opt} = \sqrt{\frac{B}{C}}$$

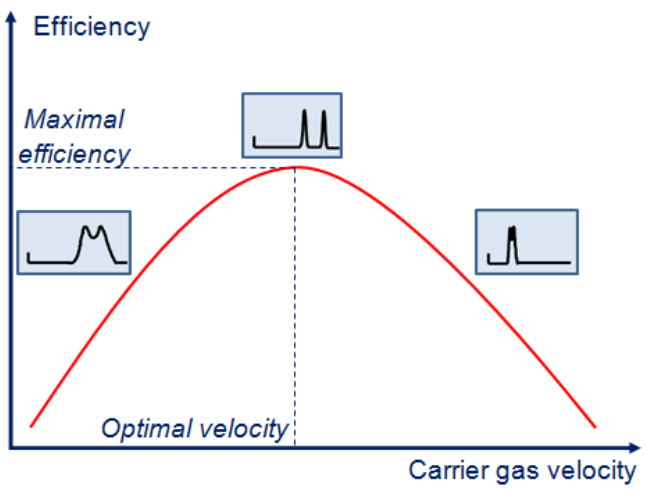


*Fig. 5a: schematic plot of efficiency (number of plates N) as a function of carrier gas velocity in the example of the separation of two compounds*

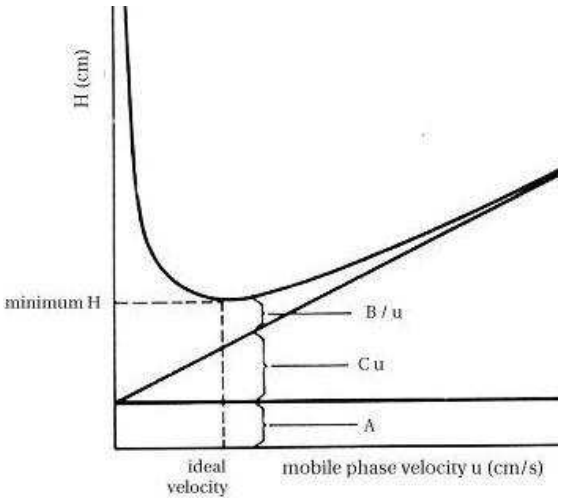


*Fig. 5b: typical Van Deemter plot of plate height H against carrier gas velocity u, showing the three terms of the Van Deemter equation*

*Fig. 5: illustration of the notion of efficiency*

## I.A.7. Other significant values

Four last simple and intuitive values of the highest relevance for this report are introduced here:

- separation time $t_{tot}$, which is the overall time required to complete the separation, from the injection to the return of the signal to the baseline after the peak of the most retained compound in the mixture to analyze;

- resolution $R_{AB}$ of the separation between two compounds A and B, calculated as following:

$$R_{AB} = 1.18\frac{t_{R,B} - t_{R,A}}{(w_{1/2,A} + w_{1/2,B})}$$

  a resolution higher than 1.25 is generally mandatory for quantitative purposes, however, in particular cases (compounds in similar quantities, high signal to noise ratio) a value of 0.75 can be sufficient (see also separation number, in the glossary);

- peak asymmetry As, quantifying the deviation to ideal Gaussian peaks (especially in the case of tailing peaks), calculated as following:

$$As = \frac{w_{1/10,R}}{w_{1/10,L}}$$

where $w_{1/10,R}$ is the right half-width of the peak at 10% of maximal height (distance from the point at peak midpoint to the right tailing edge measured at 10%), and $w_{1/10,L}$ the left half-width of the peak at 10% of maximal height (distance from the point at peak midpoint to the left edge measured at 10%); the further As from 1, the more asymmetric the peak.

### I.A.8. Gas chromatography common applications

GC has been applied to applications in which the targeted compounds are easily vaporizable (gaseous and stable below 300°C). These applications include biology, chemistry, pharmacology, water pollution, biological and chemical warfare agent or drug detection, food- and beverage-processing, oil and petroleum etc.

Moreover, GC has been commonly used for the monitoring (autonomous and cycled detection and quantification) of pollutants in air, such as Volatile Organic Compounds*.

And last, but not least, GC is also first choice technique for the monitoring of gases such as light hydrocarbons (C1-C9, and more commonly C1-C5, cyclic and aromatic compounds), or permanent gases ($O_2$, $N_2$, $CO_2$, and the dangerous $H_2S$), in oil- and gas field environments.

As a study led in partnership with Schlumberger, this report focuses on this last domain of application.

## I.B. Use of gas chromatography in oilfield services

### I.B.1. Targeted compounds

Oil analysis, from crude to refined, is crucial in petroleum industry. Table 1 gathers the main categories of chemical compounds commonly found in oilfield environment and refining industry. Excepted metal and salt traces, and hydrocarbons heavier than C16, the compounds are vaporizable below 300°C and are directly compatible with most GC available on the market. Hydrocarbons (paraffins, cycloalkanes, alkenes, aromatics and naphtalenes), but also functionalized compounds (sulfides, amines, alcohols, ketones, ethers and esters) can be detected and quantified with a FID. Analyses beyond C100 (with simulated distillation) are routinely performed.

Therefore, GC has been commonly used in petroleum industry. Contrary to liquid chromatography, where the sampling, the transportation of the sample from the sampling point to the lab, and the conservation of the sample before analysis, are generally uncomplicated steps, gas chromatography can also be used in direct on-field real-time monitoring. In the following paragraph, one of the best examples of the use of GC-based light hydrocarbons monitoring in oilfield industry is introduced.

### I.B.2. Schlumberger confidential paragraph

This example of GC monitoring in oilfield industry was purposely chosen, as the first application of the discovery presented in this report (see III.D., and IV.C.).

| | Compound | Category | Occurrence | Boiling point (°C) | FID detection |
|---|---|---|---|---|---|
| $O_2$ | Oxygen | Permanent gas | Abundant | -183 | N |
| $N_2$ | Nitrogen | Permanent gas | Abundant | -196 | N |
| $CO_2$ | Carbon Dioxide | Permanent gas | Abundant | -57 | N |
| $H_2O$ | Water | Permanent gas | Abundant | 100 | N |
| C1 | Methane | Paraffins | Abundant | -160 | Y |
| C5 | Pentane | Paraffins | Abundant | 36 | Y |
| C10 | Decane | Paraffins | Abundant | 174 | Y |
| C20 | Isosane | Paraffins | Abundant | 343 | Y |
| cC6 | Cyclohexane | Cycloalkanes | Occasional | 81 | Y |
| Eth | Ethene | Alkenes | Abundant | -104 | Y |
| Bnz | Benzene | Aromatics | Abundant | 80 | Y |
| Nph | Naphtalene | Naphtalenes | Abundant | 218 | Y |
| $H_2S$ | Hydrogen Sulfide | Sulfides | Occasional | -60 | N |
| DMS | Dimethyl Sulfide | Sulfides | Traces | 41 | Y |
| MA | Methyl Amine | Amines | Traces | -6 | Y |
| PH | Phenol | Alcohols | Traces | 182 | Y |
| Ni | Nickel | Metal | Traces | 2913 | N |
| NaCl | Sodium Chloride | Salt | Traces | 1413 | N |

*Table 1: examples of chemical constituents in oilfield environment (Y=yes, N=no)*

### I.B.3. Schlumberger confidential paragraph



## I.C. MEMS technology developments and miniaturization

### I.C.1. General background

Micro electro-mechanical systems (MEMS) are made up of components between 1 to 100 micrometers in size; MEMS generally range in size from 20 micrometers to 20 millimeters. They usually consist of one or several components that interact with the surroundings such as a micro sensor, and sometimes of a central unit that processes data (microprocessor). Because of the large surface area to volume ratio of MEMS, surface effects such as electrostatics, adsorption and wetting dominate over volume effects such as inertia or thermal mass.

The potential of very small machines was appreciated before the technology existed that could make them. MEMS became practical once they could be fabricated using modified semiconductor device fabrication technologies, normally used to make electronics. The economies of scale, ready availability of cheap high-quality materials, ability to incorporate electronic functionality and advantaging crystallographic and mechanical properties have made silicon the most attractive material in MEMS fabrication. Table 2 sums up some of the earliest and most significant milestones in MEMS technology history.

The starting substrate of a process is generally a blank silicon wafer (see figure 9a). Processes are divided in four categories: deposition, patterning, etching and dicing. A substrate can undergo up to 100 processes during fabrication. The processes, very diversified in each category and quite complex, are briefly introduced in the following paragraph, in order to then understand the contribution of MEMS technology to microfluidics.

| Date | Event |
|---|---|
| 1948 | Invention of the Germanium transistor |
| 1954 | Discovery of piezo resistive effect in Germanium and Silicon |
| 1958 | First integrated circuit |
| 1959 | Famous Feynman's speech on the potentialities of miniaturization |
| 1959 | First silicon pressure sensor demonstrated |
| 1966 | Radio frequency sputtering of dielectric films* |
| 1967 | Anisotropic deep silicon etching patented |
| 1968 | Resonant Gate Transistor Patented (Surface Micromachining Process) |
| 1970s | Bulk etched silicon wafers used as pressure sensors (Bulk Micromachining Process) |
| 1971 | Invention of the microprocessor |
| 1979 | HP micro machined ink-jet nozzle |
| 1979 | Publication of the paper "An air analyzer fabricated on a silicon wafer"* |
| 1982 | LIGA (lithography, electroplating, and molding) process patented* |
| 1982 | Disposable blood pressure transducer |
| 1985 | Crash sensor by Airbag |
| 1986 | Invention of the atomic force microscope |
| 1986 | Silicon wafer bonding patented* |
| 1988 | Batch fabricated pressure sensors via wafer bonding |
| 1994 | Bosch process for Deep Reactive Ion Etching patented* |

*Table 2: earliest and major MEMS milestones;*
** Inventions with direct implications in the present study*

## I.C.2. Usual processes

### *I.C.2.01 Deposition*

One of the basic building blocks in MEMS processing is the ability to deposit thin films of material with an accurate thickness, generally between a few nanometers to about 100 micrometers. There are two types of deposition processes, as follows.

- Physical vapor deposition ("PVD"), in which a material is removed from a target, and deposited on the surface of substrate, in a vacuum system. This includes sputtering, in which an ion beam liberates atoms from a target, and evaporation, in which a material is evaporated from a target using either heat (thermal evaporation) or an electron beam (e-beam evaporation).

- Chemical vapor deposition ("CVD"), in which a stream of source gas reacts on the substrate in order to grow the desired material. This can be further divided into categories depending on the details of the technique, for example, LPCVD (Low Pressure chemical vapor deposition) and PECVD (Plasma Enhanced chemical vapor deposition).

Oxide films can also be grown by the technique of thermal oxidation, in which the silicon wafer is exposed to oxygen and/or steam, to form a thin surface layer of silicon dioxide.

### *I.C.2.02 Patterning*

Photolithography (figure 9b) uses light to transfer a geometric pattern from a mask to a light-sensitive chemical photoresist deposited on the substrate. A series of chemical treatments then either engraves the exposure pattern into (negative resist), or enables deposition of a

new material in the desired pattern upon (positive resist), the material underneath the photo resist.

Other more specific lithography techniques exist, such as electron, ion or X-ray beam lithography, and follow the same principle. Ion track technology and diamond patterning are other patterning techniques.

### *I.C.2.03 Etching*

Etching consists in removing specific volumes from layers. Combined with lithography, it is used to create geometrical shapes in the substrate (e.g. by removing to a fixed depth the regions of the substrate that are not protected by resist).

Etching is wet when the material to remove is dissolved when immersed in a chemical solution, or dry when it is sputtered or dissolved using reactive ions in a plasma or a vapor phase etchant. Etching can be isotropic or anisotropic, highly selective or poorly selective.

Deep Reactive Ion Etching (DRIE, figure 9c) is a common highly anisotropic etching process used to create deep penetration, steep-sided holes and trenches in substrates, typically with high aspect ratios.

### *I.C.2.04 Dicing*

After having prepared a large number of MEMS devices on a silicon wafer, individual dies have to be separated. Wafer dicing may then be performed either by sawing using a cooling liquid or a dry laser process called stealth dicing.

*Fig. 9a: blank silicon wafers before processing (diameters 2 to 12 inches, 5 to 30 cm)*

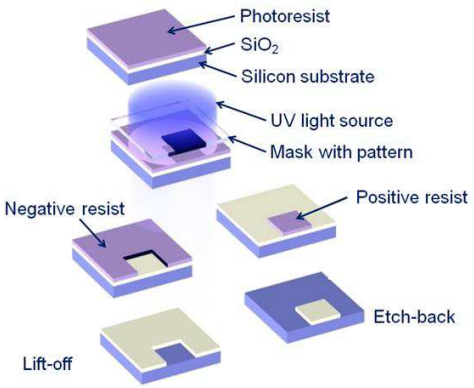


*Fig. 9b: photolithography schematic process: the pattern of the mask is negatively or positively transferred to the substrate*

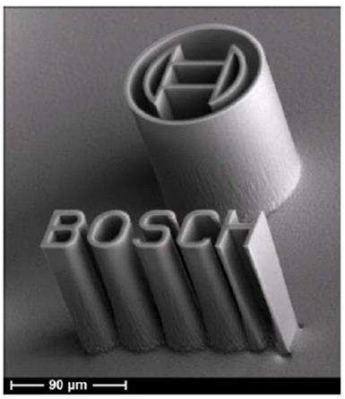


*Fig. 9c: SEM picture of a geometrical structure on a silicon wafer obtained by DRIE with a standard Bosch process*

*Fig. 9: substrate micro machining processes*

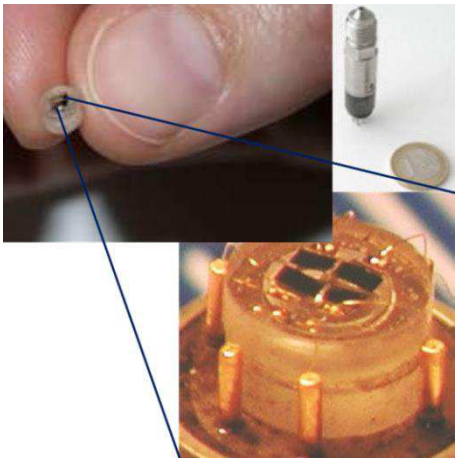

*Figure 10a: micro sapphire-based pressure sensor (chip and packaging).*

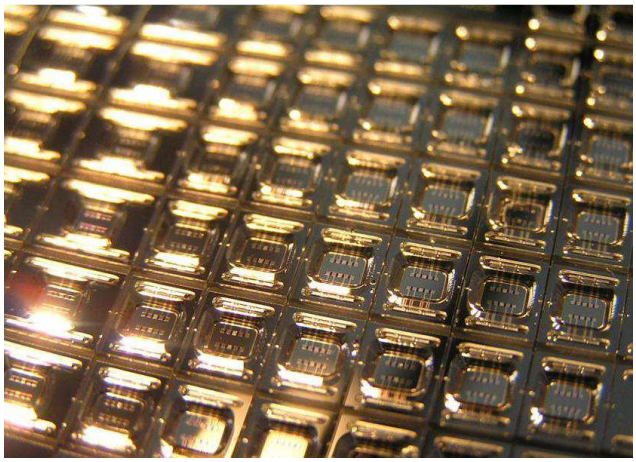

*Figure 10b: batch fabrication of micro thermal conductivity detectors; unit size is 7x5mm²; 100 units are fabricated on one wafer.*

*Fig. 10: two examples of sensors designed and fabricated at MEMS TC*

## I.C.2. Applications of MEMS technology

Common and historical applications of MEMS technology are electronics and physical micro sensors fabrication. For instance, Schlumberger MEMS TC has been designing and developing MEMS-based pressure (figure 10a), temperature, thermal conductivity (figure 10b, also see I.C.3, figure 13, and appendix A), density, viscosity, seismic, acceleration and rotation embedded sensors, for surface or down hole tools.

Both due to the great variety of materials available for deposition, and to surface effects predominance, MEMS deposition techniques have been utilized in the fabrication of adsorption-based or oxidation-reduction chemical sensors, mainly for gas detection.

MEMS technology has finally been used for the design and fabrication of a new generation of micro fluidic circuits. By combining etching and bonding technologies, it became possible to create various shapes of circuits and functions for very specific purposes (e.g. flow channels and mixers, droplet producers and breakers). Thanks to the increase of the resolution of micro machining processes, fluidic circuits can integrate longer serpentine-shaped channels and more functions in smaller volumes. This, in addition to the increase of wafer sizes (figure 9a), increases the number of units that can be fabricated on one wafer. MEMS thus contributed to improve gas chromatography technology as suggested in next paragraph.

## I.C.3. Perspectives of silicon-based gas chromatography

First and foremost, it has to be reminded here to the non-specialist reader that a gas chromatograph is a bulky laboratory equipment. Typical dimension is 50 cm (see figure 11a). GC conventional columns are coiled to form a cylinder (figure 11b) which is placed in the GC oven (typical dimension 30 cm) for temperature programming. Due to the big volume of the GC oven, temperature ramps are generally limited to 100°C/min, and cooling times (between two analyses) are several minutes-long. Moreover, gas supply implies additional heavy

equipment, such as carrier gas bottle, hydrogen generator or bottle, air compressor and filters. Finally, an analogical to numerical converting unit and a computer are necessary to control the system and to process the data.

Consequently, a conventional gas chromatograph is not a portable equipment, and, in oilfield, even less a surface or down hole tool-embedded sensor, contrary to most MEMS devices. It is also an expensive equipment (purchase, maintenance, replacement, human operating, power consumption, helium supply), mainly dedicated to laboratory analyses, which are usually longer than 1 minute, whereas MEMS are designed to be batch-fabricated in great quantity, mainly out of relatively low-cost raw materials, easily replaceable, autonomous, low-powered, and dedicated to in-situ fast monitoring.

However, GC technology was recently enough miniaturized so that a few models of portable gas chromatographs were commercialized (figure 12). Miniaturization was here achieved by basically reducing the size of each component in the gas chromatograph (injection system, valves and actuators, column, detector, electronic boards…), avoiding the resort to external supplies (computer, power), and using air as carrier gas. This approach, enabling to perform analyses almost anywhere on the surface, is a major advance in the domain, but yet struggles to overcome limitations in terms of analysis time and whole cycle time (preparation plus analysis). Indeed, even size-reduced, column blocks still show high thermal capacities, and stationary phase choice can be constraining.

The improvements allowed by silicon micro machining technologies in micro fluidics leads one to believe that all these limitations could be overcome by the developments of MEMS-based gas chromatographs (extremely small size and adequate thermal properties). As it will be further developed in the literature review, the first attempt to fabricate a GC-based gas analyzer on a silicon wafer dates back to 1979. Ever since, efforts have been made to fully enable this technology. As an example, MEMS TC has developed since the middle 2000s a MEMS injector, a MEMS column and a MEMS detector for a hypothetical MEMS-based gas chromatograph (figure 13).


*Fig. 11a: GC by Varian (model 3800)*

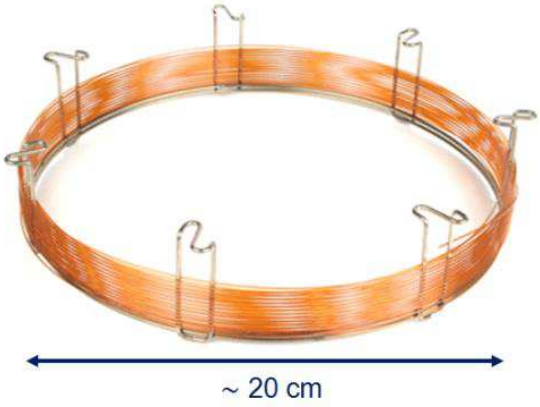


*Fig. 11b: coiled GC column*

*Fig. 11: dimensions of conventional GC equipment*

*Fig. 12: examples of recently commercialized portable gas chromatographs: C2V (top left), Torion (top right), SLS (bottom left) and Defiant Tech (bottom right)*

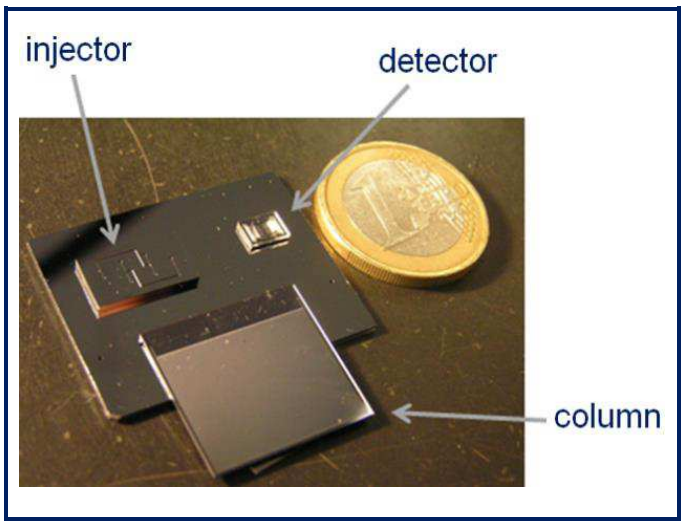


*Fig. 13: the three silicon micro machined components of a gas chromatograph as developed at MEMS TC:*

- *A pneumatic injector (with micro valves and micro actuators)*
- *A 2.2 m-long, (100 µm)²-square section serpentine column*
- *A micro thermal conductivity detector (see also appendix A)*

## I.D. Problem statement

Usually, silicon micro machined gas chromatography columns are fabricated following the same schematic process, as displayed on figure 14:

- etching of a spiral or serpentine channel into the substrate (silicon wafer); the shape and dimensions of the etching are ruled by the type of etching and the parameters chosen;
- bonding of a Pyrex cover on the substrate to close the channel and form a tubing;
- insertion of the stationary phase (coating gel, packing solid, or in-situ growth of a coating or filling solid structure).

Numerous studies on the fabrication and the performances of such columns have been published, as it will be shown in the literature review (II.). Poly dimethyl siloxane (PDMS) is a common gel stationary phase providing highly efficient conventional gas chromatography columns, and is likewise the most reported stationary phase in micro machined columns. Conventional solid packings insertion into extremely miniaturized columns is laborious, gives poor results, and is poorly reported in the literature. Solid coatings are rarely reported and mainly consist of carbon nanotubes (CNTs) in-situ growth. Solid monoliths in-situ growth, common in conventional and micro liquid chromatography, is as recent as recent can be (2013) in micro gas chromatography.

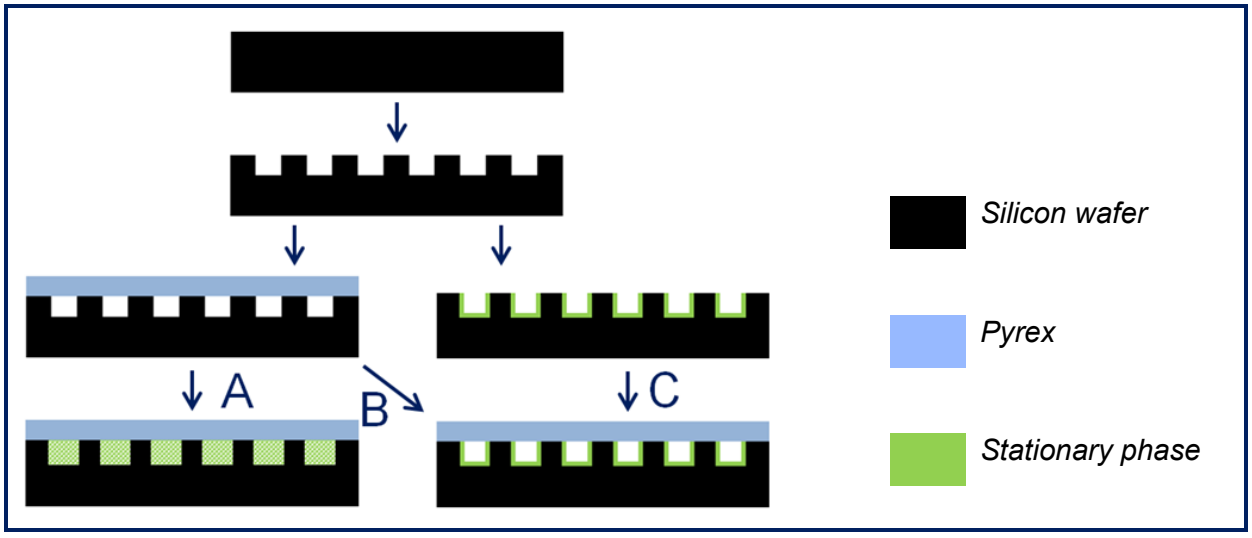


*Fig. 14: schematic process of micro columns fabrication (cross-section view of substrate): starting from a blank silicon wafer, channels are etched with chosen shape and dimensions; then the wafer is either bonded to a Pyrex lid and diced (left), either covered with a thin layer of stationary phase (e.g. carbon nanotubes) (right); in the first case, a solid material (e.g. silica gel, graphitized carbon, alumina or molecular sieve) is packed or a monolith structure is grown inside the column (process A), or the inner walls of the column are coated with a gel material (e.g. PDMS) (process B); in the second case, the wafer is bonded to a Pyrex lid and diced (process C).*

Each one of these four main types of stationary phases was tested at MEMS TC on micro columns, with the aim of fast analysis of light hydrocarbons (C1-C5), which is the first targeted application, and showed significant limitations. These preliminary results are not the author's direct production (though implicated) and will thus not be thoroughly developed in the body of this report, but, as essential to the full understanding of the problem, will be detailed and illustrated in appendix B, and summed up in this introduction:

- retention of lighter compounds (C1 and C2) on PDMS is clearly not strong enough for short to average (< 2m) micro columns; in this case, retention can only be achieved by drastically increasing the length of the column (or decreasing the temperature), and, therefore, overall analysis time and column's chip size; moreover, process is not collective, and judgment on the precision of the coating is strongly reserved;

- conventional solid packings (silica gel, graphitized carbon, alumina and molecular sieve) insertion is hardly compatible with extreme miniaturization and clean room batch fabrication (big and polluting particles); process is not collective and very tedious, and packing is clearly barely reproducible;

- CNTs growth process is collective, but requires high facility and safety level; besides, retention mechanisms on carbon successfully enable lighter alkanes separation but often provide excessive peak asymmetry and tailing;

- silica-based monoliths in-situ growth appears to be a promising process, but does not perfectly match the criteria of collective fabrication and remains a very recent technique in gas chromatography.

In the light of what precedes, the problem statement is clear:

**The problem is to find a material, rather solid, which could be used as an adequate stationary phase for the fast but full separation of light hydrocarbons (typically C1-C5, in less than 10 s), and an insertion process in micro machined gas chromatography columns, which could be collective, reproducible, industry-ready and compatible with clean room facilities and the rest of column's fabrication process.**

## I.E. Sputtering as a potential solution; justification of the research

As previously mentioned (I.C.2.01), sputtering (figures 15 and 16) is a common deposition technique in silicon micro machining technology. Owing to its nature, this process is fully compatible with clean room batch fabrication and with the rest of the fabrication process of the columns. Likewise, it is collective and enables the deposition of an accurately controlled layer of the chosen material in the different columns etched in the wafer.

Moreover, most materials used commonly as solid stationary phases in conventional gas chromatography, and especially for the separation of light hydrocarbons (such as silica, alumina, and graphite), are available as targets for sputtering (figure 16).

Reservations can be expressed arguing that sputtering usually produces very dense and lowly porous layers, which is in contradiction with the functioning principle of PLOT columns (I.A.3.). Without a certain porosity, it may be impossible to perform the separation of very light compounds on such short columns. Nevertheless, it is shown that only layers deposited parallel to the target or substrate plan (as are the floors of the channels) are dense and non-porous, and that layers deposited perpendicularly to these plans (as are the walls of the channels) are porous. This will be discussed in the literature review.

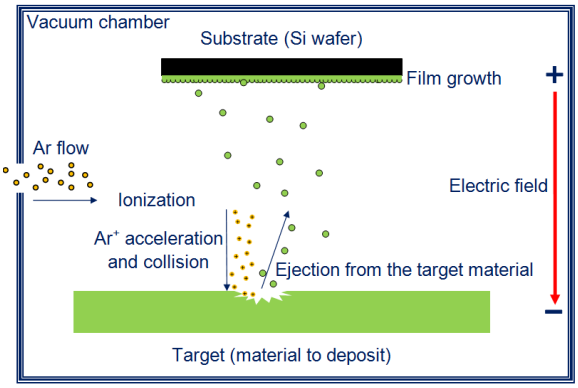


*Fig. 15: scheme of the sputtering process: an argon flow penetrating inside a vacuum chamber is ionized and Argon cations are accelerated towards a target (made of the material to deposit) connected to the cathode. Target sputtering induces ejection of target material atoms which are then deposited as a thin layer on the substrate (silicon wafer) placed directly opposite of the target. Film thickness is proportional to sputtering time.*


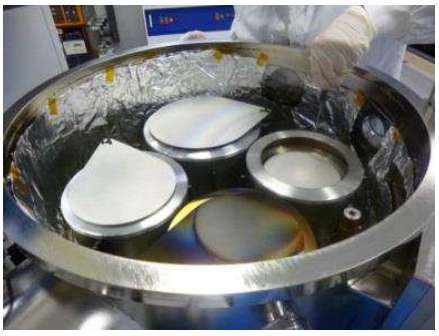

*Fig. 16: pictures of MEMS TC clean room sputtering machine:*

*top: the sputtering machine itself*

*middle: the silica target used in the present study (diameter 15 cm, thickness 3 mm), bonded to a copper backing plate*

*bottom: inside the vacuum chamber, with four different targets, for multi material processes; movable covers are used for remote controlling of the accurate start of the deposition (the substrate is placed over the targets, over the covers).*

Therefore, it is very surprising that absolutely no studies on sputtered mineral materials used as stationary phases in micro machined gas chromatography columns have been published. This said, the author is very pleased to have worked on this previously unreported field of investigation, especially as a first preliminary C1-C2-C3 separation on a silica sputtered micro column was obtained at MEMS TC at the end of 2009 (see also appendix B).

Starting from there, the launching of more thorough research project was an obvious necessity.

## I.F. Approach and methodology

As suggested by the background of this discovery, the research work mainly consisted of the scientific validation (or reject) of the method. This report is therefore firstly about basic evaluation of the micro columns: functioning and failure rates, optic observations, possible separations demonstrations, and preliminary process robustness and results precision tests.

In an academic approach, advanced kinetic and thermodynamic evaluations were performed, to enable publication and comparison with reported state of the art. Emphasis was put on the tests of different stationary phases and columns. The influence of different parameters, such as stationary phase material, deposition pressure and thickness, or column type and dimensions, on the chromatographic properties of the column was studied. To this purpose, different stationary phase materials were purchased, and different column models were designed during the thesis.

In an industrial approach, temperature-programming enabling and fast C1-C5 separations obtaining was the top priority. It implied the design and fabrication of a self-made hard- and software, and the research and development of the appropriate heating and cooling methods. Emphasis was first put on real conditions use and then on targeted XXXXXXXXXXX application (GeoServices became implied in the project at the beginning of 2012). Matching requirements and overcoming unexpected troubles was then a major activity. Other potential applications were of course not forgotten.

To precise and close this section, the author wishes to introduce here (table 3) the different parts and people (title and function) directly implied in the production of the results presented in this report.

**Schlumberger MEMS TC, Elancourt**

Bertrand Bourlon
Research Engineer
*Project functional and administrative supervisor (until 04/2012)*

Kamran Danaie
Process Engineer
*Columns fabrication (except stationary phase sputtering) at the ESIEE; technical advisor*

Emna Zoghlami
Intern (02-08/2013)
*Cooling systems and columns evaluation*

Pierre Guibal
Intern (07-12/2009)
*Preliminary tests of conventional stationary phases; first separations on silica sputtered columns*

Nicolas Renoux
Engineering Manager
*Administrative supervisor (from 01/2013)*

**LSABM, ESPCI ParisTech**

Jerome Vial
Research Manager
*Thesis director*

Didier Thiebaut
Research Manager
*Thesis co-director*

Zineb Matouk
Intern (02-07/2013)
*Columns evaluation*

Patrick Sassiat
Technical advisor

Imadeddine Azzouz
PhD student (2010-2013)
*Research on in-situ-grown silica-based monolithic GC stationary phases*

**Analytical Measurements Department, Roissy**

Jerome Breviere
Department Manager
*Project functional manager (from 04/2012)*

Pawel Kasprzykowski
Research Engineer
*Industrial development (from 06/2013)*

*Table 3: people and institutions directly implied in the project*

Raphael Haudebourg
Intern (03/2010), temp (08/2010),
PhD Student (02/2011-01/2014)
(CIFRE LSABM – MEMS TC)

## I.G. Delimitations of scope

Due to the maturity of the project (totally new), to columns fabrication and evaluation time (~1 month), to available equipment, and to the number of people immediately dedicated to the production of results and reports (between 1 and 3 depending on the phase), the present report does not deal with the following items:

- clean room fabrication process advanced optimization: the targeted application of sputtering (stationary phase deposition) drove the initial choice of the deposition parameters, but they remained constant for each target (except, of course, deposition time and, occasionally, deposition pressure); the influence of these parameters, though mentioned in the literature review, was not studied; moreover, some troubles encountered in the fabrication process (described in III.A.5.) still require solutions to pass the step of industrialization, but they will only be suggested in this report;

- exhaustive robustness and precision tests: basic tests (on 4 columns and 3 wafers, and on 50 temperature cycles) were led for a first quantitative evaluation of this crucial aspect of the method; however, exhaustive statistic tests are absolutely necessary for method total validation and, until now, no studies in real conditions on a far higher amounts of columns, wafers and temperature cycles have been led;

- extra-column effects evaluation: columns studies were led with a conventional laboratory GC equipment (Varian 3800), which was the most robust, stable and easy to handle and the less trouble causing apparatus available; however, this apparatus may not be totally adequate for micro columns kinetic evaluation: indeed, dead volumes* have probably a greater influence on analyses performed with very low volume micro machined columns, compared to conventional columns, by causing non-negligible peak broadening; the study of these extra-column effects could not be led here, and columns efficiencies exhibited in this report might be slightly underestimated;

- separation tests of other compounds than hydrocarbons and permanent gases: studies mainly focused on C1-C4 (or C5) separations; the separation of other compounds (permanent gases, heavier or cyclic alkanes, unsaturated and aromatic hydrocarbons) was occasionally tested; but no other compounds were injected, neither oilfield-related (sulfides, amines, alcohols, ethers, ketones, esters), nor non-oilfield-related;

- quantity analyses: no study on the influence of the injected quantity on columns behavior or detector was led (except for µ-TCD evaluation, see appendix A); injected quantities were arbitrary chosen, ensuring sufficient signal to noise ratio, and avoiding column overloading or resolution loss; obviously, injected quantities were kept constant in compared studies;

- definition of a standard and optimized utilization method: the temperature-programming system was developed to demonstrate fast separations of light hydrocarbons; parameters

were judiciously chosen to exhibit high quality separations (in terms of speed and resolution), but, obviously, they are not to be automatically transferred to specific application; accurate utilization methods for specific applications were not developed here, be it XXXXXXXXXXX or any other potential applications;

⌦ integration with both the micro injector and the micro detector developed at MEMS TC: another potential and most promising application of micro machined columns is of course their integration in a fully micro machined system, including micro injector and micro detector as shown on figure 13, and micro flow lines, micro electric boards etc; this was not the main objective of this research work.

## I.H. Outline of the report

The body of this report will begin with a thorough literature review on micro gas chromatography, accompanied by major and relevant references on gas chromatography, XXXXXXXXXXX, and sputtering. This will give scientific credit and complete the pedagogical introduction above. It will also enable comparison of the quantitative results obtained in this study with the state of the art.

After a summary of evaluated columns, materials and methods used in this research work will then be exhaustively and accurately described, along with the possible troubles encountered. They will deal with gas chromatographic equipment, micro columns fabrication, temperature-programming enabling, columns evaluation methods, and prototype development for XXXXXXXXXXX.

The heart of this report will naturally be dedicated to the display of the results obtained experimentally, along with their interpretation and immediate implications. The discussion will follow the same thread than in the previous chapter, namely temperature programming, columns evaluation and prototype for XXXXXXXXXXX. Columns evaluations will include functioning, optic (visual and microscopic), precision, thermodynamic, kinetic, hydration and temperature-programmed evaluations, and will involve different parameters such as stationary phase material and deposition protocol, or columns type and dimensions.

A conclusion will finally close the report, by gathering the academic and industrial implications of the study, by clearly defining the limitations of the impact of the research work presented in this report, and by opening perspectives and suggesting practical further work, for both academic and industrial research.

At the end of the document, the reader will find three appendices, on micro thermal conductivity detector evaluation, on experienced limitations of other stationary phases in micro machined columns, and on temperature programming system, followed by a list of abbreviations and symbols used in this report, a semi-indexed, glossary, the list of publications and communications related to the present work, acknowledgements, and abstracts in French and in English.

# II. Literature review

As explained in the outline of the report, the aim of this literature review is to give scientific credit and complete the pedagogical introduction above. Although it will mainly deal with micro gas chromatography (first report, columns designs and fabrication processes, up- and downstream components developments, computer modeling, stationary phases, applications), it will also mention major and relevant references on gas chromatography (with constant focus on hydrocarbons separation), XXXXXXXXXXX, and sputtering.

## II.A. Gas chromatography

### II.A.1. Reference books

Most of the general notions and quantitative theories on gas chromatography utilized in this report come from the Gas Chromatography Practical Manual by Tranchant[1], the ESPCI 2nd year Analytical Sciences lesson manuscript by Hennion, and the book of Chromatography Theory by Cazes and Scott[2]. General notions include gas chromatography principle, description of the components, types of columns, injectors and detectors, applications, stationary phases, thermodynamic and kinetic theory, and practical advises for the chromatographist.

### II.A.2. Common stationary phases

#### *II.A.2.01 Gels and liquids for WCOT columns*

Long and branched hydrocarbon chains such as squalane (figure 17a), apiezon and apolane have been historically used as stationary phases for the separation of light hydrocarbons [1,3,4]. Siloxane-based polymers such as poly dimethyl siloxane (PDMS, figure 17b) have then been the most used stationary phases in WCOT columns [1,5-7]. As mentioned in the introduction, indicated by the literature, and observed in appendix B, the retention of these stationary phases towards the lighter alkanes (C1-C2-C3) is not strong enough to enable separation, unless by compensating with a very long column[7], with corresponding drawbacks (cf. I.D.). Another limitation of hydrocarbon chains-based stationary phases is their low temperature range of utilization (below 120°C for squalane, below 200°C for apiezon and apolane), in possible contradiction with the use in fast temperature-programmed applications. Finally, the usual insertion process in the column (dissolution of the stationary phase in a solvent, insertion of the liquid solution in the blank column, and evaporation of the solvent) does not match the criteria of collective and reproducible insertion process in silicon micro machined columns, and of full compatibility with clean room batch fabrication (see also appendix B).

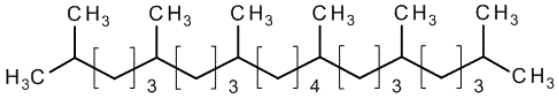

*Fig. 17a: squalane molecule*

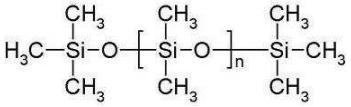

*Fig. 17b: poly dimethyl siloxane*

Other organic polymer-based stationary phases, such as polyethylene glycol, polypropylene glycol, polyesters, have also commonly been used in gas chromatography, with relatively similar properties and limitations as polysiloxane stationary phases. Obviously, other major stationary phases of this type exist, but are not dedicated to the separation of lighter hydrocarbons, but rather to more polar compounds or specific functionalized groups[1].

### *II.A.2.02 Solid adsorbents for packed columns*

Silica-, alumina-, and carbon-based packing adsorbents, as well as porous organic polymers, and, more specifically, ammonium salts, are more appropriate for the targeted separation of light hydrocarbons and permanent gases, and have commonly been used for this purpose. Figure 18 displays typical chromatograms obtained on such stationary phases.

- The use of silica gel has been widely reported, as by Patton in 1955[8], Greene in 1957[9] (see figure 18a), Kiselev[10] in 1964 and Snyder in 1966[11];

- Similarly, numerous studies on the utilization of alumina have been published, as by Patton (1955[8]), Greene (1956[9,12], see figure 18a), and Hoffmann (1966[13,14]);

- Patton (1955[8]), Greene (1956[12]), and Corcia (1978[15,16], see figure 18b) reported the use of graphite-packed columns;

- Molecular sieves (or zeolites) were also reported, for instance in 1973 by Smith[17] and Garilli[18] or in 1986 by Andronikashvili[19], although they seem to be mainly intended to permanent gases separations of heavier alkanes separations.

- Porous organic polymers (such as styrene divinyl benzene copolymers), as reported for instance by Papic[20] in 1968 (see figure 18c), are now widely commercialized as well;

- More specifically, ammonium salts (molybdenum phosphate, tungsten phosphate and silicate) were successfully used for the separation of C1-C4 hydrocarbons by Nayak[21] (see figure 18d);

Other specific adsorbents exist (other organic porous polymers, such as cellulose, metallic complexes, such as zirconium phosphates, or organic clays such as kaolinite or bentonite), but are not dedicated to the separation of lighter hydrocarbons[1,22].

Although the stationary phases described above in this paragraph are perfectly appropriate for the separation of permanent gases and C1-C5 hydrocarbons, they seem to hardly match the criteria of collective and reproducible insertion process in silicon micro machined columns, of full compatibility with clean room batch fabrication, as well as gel-coated columns, and of fast analysis. This last aspect was studied by Jonker, who enabled a C1-C4 separation in 0.15 second on a packed column (see figure 19), by resorting to an input pressure of 64 bar[23], which is a strong limitation for both conventional and numerous specific applications (see also appendix B).

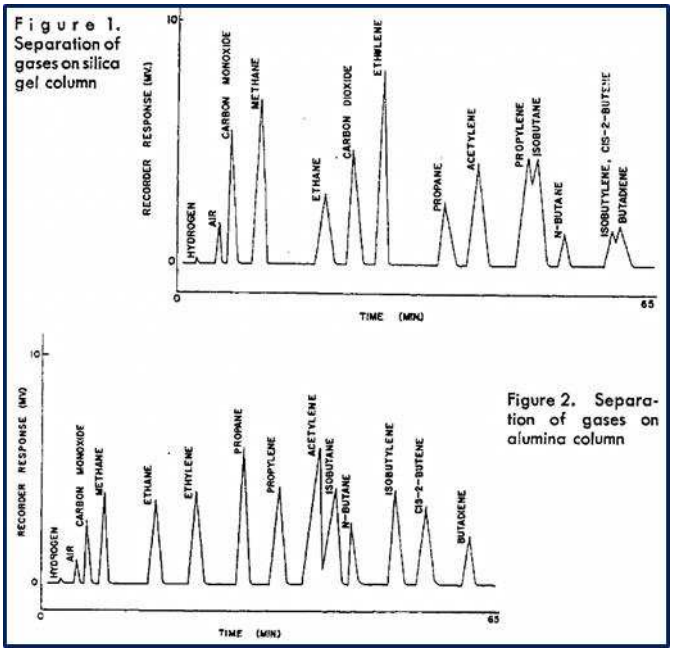


*Fig. 18a: on silica gel and alumina[9]*
*Column 20 ft, Mesh 20-40,*
*helium 70cc, 5°C=>155°C in 65 min*

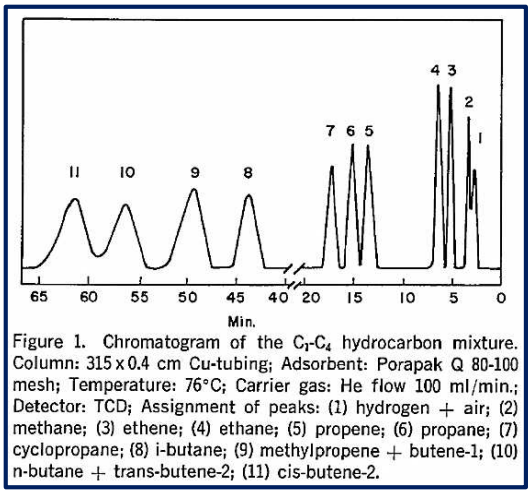


Figure 1. Chromatogram of the $C_1$-$C_4$ hydrocarbon mixture. Column: 315 x 0.4 cm Cu-tubing; Adsorbent: Porapak Q 80-100 mesh; Temperature: 76°C; Carrier gas: He flow 100 ml/min.; Detector: TCD; Assignment of peaks: (1) hydrogen + air; (2) methane; (3) ethene; (4) ethane; (5) propene; (6) propane; (7) cyclopropane; (8) i-butane; (9) methylpropene + butene-1; (10) n-butane + trans-butene-2; (11) cis-butene-2.

*Fig. 18c: on organic polymer[20]*

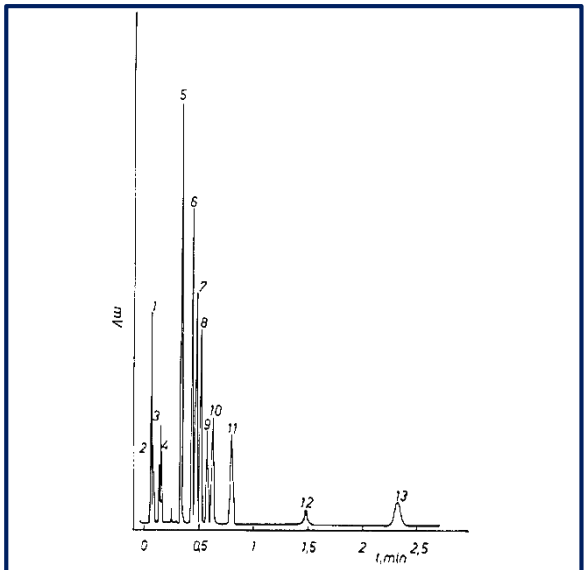


**Figure 5.** Chromatogram showing the separation of $C_4$ hydrocarbons including isopentane and pentane. Column, 0.9-mm i.d., length, 108 cm; packing, Carbopack C (60–33 μm) + 0.19% picric acid; carrier gas, hydrogen; pressure drop, 12 atm; dead time, 4.4 s; temperature, 50 °C. Eluates, (1) methane, (2) ethane, (3) propane, (4) propene, (5) isobutane, (6) 1-butene, (7) butane, (8) isobutene, (9) *cis*-2-butene, (10) *trans*-2-butene, (11) butadiene, (12) isopentane, (13) pentane

*Fig. 18b: on graphite[15]*

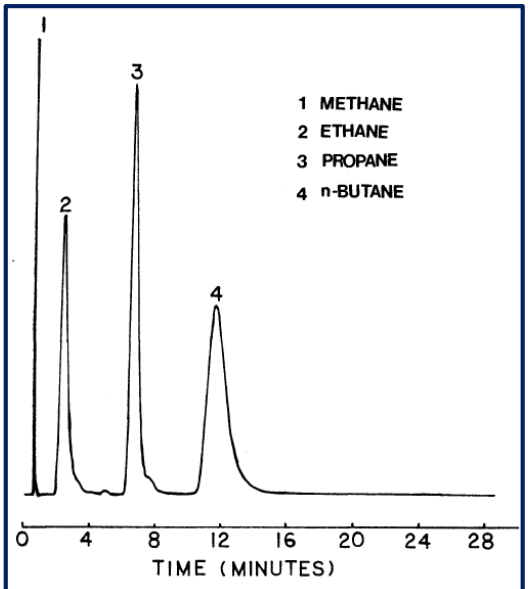


**Figure 3.** Separation of $C_1$–$C_4$ saturates over a 6-ft × ⅛-in. ammonium tungstosilicate (20% on glass beads) column: initial temperature, 323°K; initial time, 2 min; heating rate, 20°K/min; final temperature, 443°K; final time, 30 min; carrier gas, $N_2$; flow rate, 10 mL/min; detector, FID.

*Fig. 18d: on ammonium tungsto silicate[21]*

*Fig. 18: use of gas-solid chromatography in packed columns*
*for the separation of permanent gases and/or light hydrocarbons*

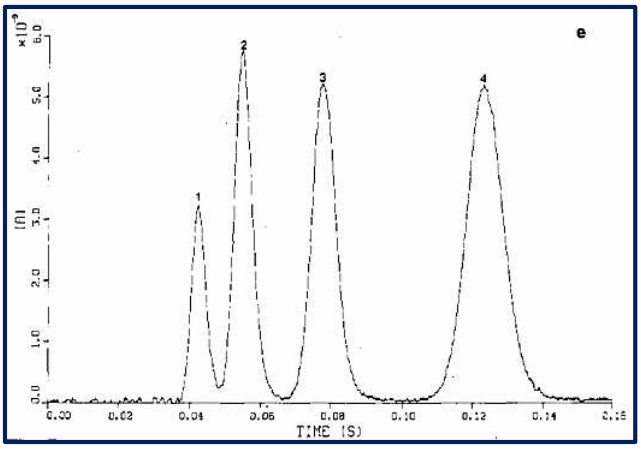


*Fig. 19: ultra-high speed C1-C4 separation by GC with a micro particulate packed column (length 3.2 cm, diameter 1.19 mm, silica particles LiChrosorb Si-60, diameter 10 µm), carrier gas helium, detection FID, T=100°C, P=64 bars, N=650 for butane[23].*

### *II.A.2.03 Solid adsorbents for PLOT columns*

Using the same materials historically used for columns packing, various types of PLOT columns were reported. In 1988, Henrich demonstrated the potentialities of the use of PLOT columns and their ability to separate permanent gases and light hydrocarbons (figure 20), as well as packed columns[24]. Ji[25], in 1999, and Berezkin[26], in 2008, published thorough reviews on the topic, respectively on the preparations, applications and future directions of various types of PLOT columns, and on capillary gas adsorption chromatography. In a first approximation, PLOT columns are expected to provide higher efficiencies and faster analyses, but lower sample capacity*, compared to packed columns. Figure 21 displays typical chromatograms obtained on such stationary phases.

Concerning silicon dioxide and aluminum dioxide, a first approach consisted in forming a thin layer of adsorbent by oxidizing and activating column's material inside the column: Mohnke used ammonia to activate the glass of a fused-silica capillary and separated hydrogen isotopes[27], and Petitjean oxidized the surface of an aluminum tube to directly obtain a thin layer of alumina in a column (5 µm in a 15 meters long, 0.51-diameter column), and a total C1-C5 separation in 15 minutes[28].

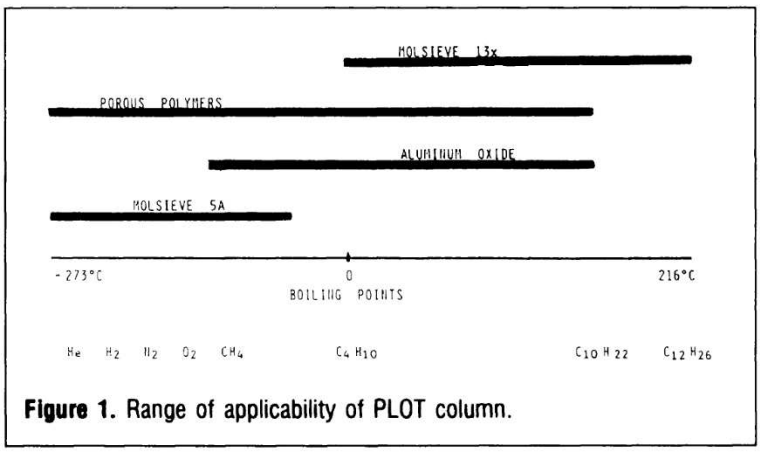


*Figure 20: range of applicability of molecular sieve, porous polymer and alumina PLOT columns, according to Henrich[24]*

A second approach, drawing inspiration from gel stationary phases insertion processes (dissolution, insertion of the liquid solution, evaporation of the solvent), was used by Schwartz to coat 60 meters long, 0.51 mm-diameter capillaries with a thin layer (20 µm) of silica gel and obtain a 11 minutes long C1-C5 analysis[29] (see also figure 21a); De Nijs[30], after Kirkland[31], and following a similar process, performed a total analysis of C1-C4 hydrocarbons in 5 minutes on a 30 meters long, 0.32 mm-diameter column coated with a 8 µm thick porous alumina layer (figure 21b).

This second approach has also been used for the fabrication of molecular sieve and organic porous polymer (figure 21c) PLOT columns[24]. More recently, sol-gel processes were used by Tanaka (2000[32,33]) or Korolev (2006[34]) to grow monolithic silica-based structures in fused-silica capillaries, obtaining fast separations of light hydrocarbons (for instance C1-C4 in less than 15 seconds at 86 bars[35], figure 21d).

Last, but not least, carbon-based materials have also been widely used as porous layers in PLOT columns. Havenga resorted to graphite PLOT columns to perform rapid analyses of coke oven gas[36] (permanent gases, combustion gases and C1-C3 in 10 minutes on a commercial CarboPLOT 007 column), followed by Bruner for environmental analyses[37,38] (C1-C5 in 6 minutes on a 30 meters long, 0.25 mm-diameter column, figure 21f). Finally, carbon nanotubes layers were in-situ synthetized by Saridara to separate methane, ethane and alkenes in less than 5 minutes with a 3 meters long, 0.5 mm-diameter column, coated with a 2-15 µm-thick layer of CVD synthetized CNTs[39] (figure 21e).

### *II.A.2.04 Conclusion*

In the light of what precedes, the starting hypothesis according to which sputtering (cf. I.E.) could be used as a solid stationary phase deposition technique for the separation of light hydrocarbons seems to hold. Indeed, by depositing thin layers of adsorbents in micro channels by sputtering (between the etching and the bonding steps), PLOT-like micro columns could be fabricated, thus respecting the criteria of collective fabrication. Several of the common adsorbents used in PLOT columns for the separation of light hydrocarbons, such as silica, alumina, and graphite, are available as target materials for sputtering.

Before discussing the details and the expected implications of the use of this technique (II.C.), an exhaustive review on micro gas chromatography (columns and other components fabrication processes and designs, heating methods and computer science contributions, utilized stationary phases, and targeted applications) is compulsory. The recent and significant interest of the scientific community towards gas chromatography miniaturization and its applications is clearly demonstrated by the fast increasing number of publications on the topic since 2005, and even more since the beginning of the present work (2010). As an example, two very specific reviews on micro gas chromatography columns heating methods and stationary phases, cited above in this report, were published in 2012 and 2013.

At the end of the following section, a summary of efficiencies reached by the different designs of micro columns and types of stationary phases will be exhibited, to enable comparison with kinetic results displayed in Chapter IV.

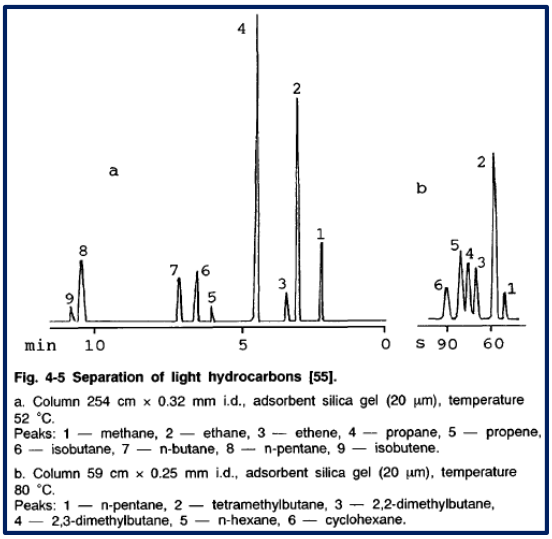


**Fig. 4-5 Separation of light hydrocarbons [55].**

a. Column 254 cm × 0.32 mm i.d., adsorbent silica gel (20 μm), temperature 52 °C.
Peaks: 1 — methane, 2 — ethane, 3 — ethene, 4 — propane, 5 — propene, 6 — isobutane, 7 — n-butane, 8 — n-pentane, 9 — isobutene.

b. Column 59 cm × 0.25 mm i.d., adsorbent silica gel (20 μm), temperature 80 °C.
Peaks: 1 — n-pentane, 2 — tetramethylbutane, 3 — 2,2-dimethylbutane, 4 — 2,3-dimethylbutane, 5 — n-hexane, 6 — cyclohexane.

*Fig. 21a: on a silica gel PLOT column[26]*

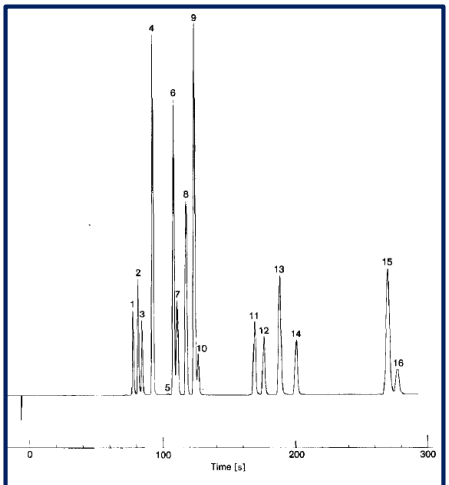


**Figure 3**

**Fast analysis of $C_1$–$C_4$ hydrocarbons.**

**Column: 30 m × 0.32 mm fused silica aluminum oxide PLOT column.**

**Conditions: oven temperature, 60°C; carrier gas, 1.80 bar He; detection, FID 4 × $10^{-11}$ Afs; injection, split 1 : 25 of 20 μl gas mixture $C_1$–$C_4$; pressure aqualizer, 5.0 bar He.**

**1 = methane; 2 = ethane; 3 = ethene; 4 = propane; 5 = cyclopropane; 6 = propene; 7 = ethyne; 8 = isobutane; 9 = *n*-butane; 10 = propadiene; 11 = 1-butene; 12 = *trans*-2-butene; 13 = isobutene; 14 = *cis*-2-butene; 15 = 1,3-butadiene; 16 = propyne.**

*Fig. 21b: on an alumina PLOT column[30]*

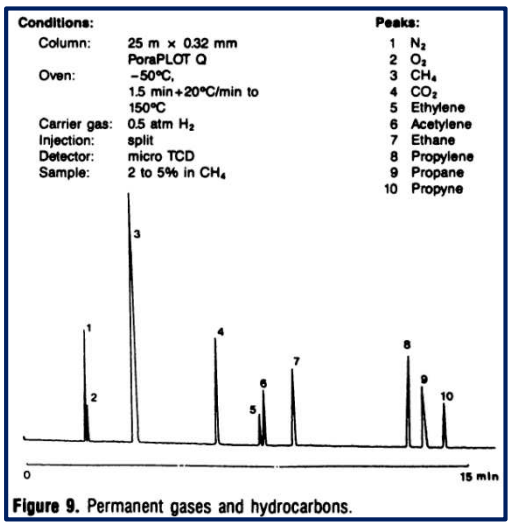


**Figure 9.** Permanent gases and hydrocarbons.

*Fig. 21c: on a PoraPLOT column[24]*

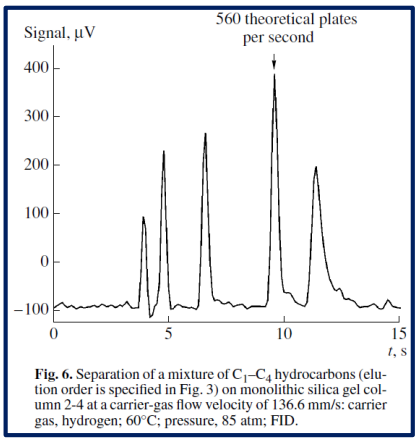


**Fig. 6.** Separation of a mixture of $C_1$–$C_4$ hydrocarbons (elution order is specified in Fig. 3) on monolithic silica gel column 2-4 at a carrier-gas flow velocity of 136.6 mm/s: carrier gas, hydrogen; 60°C; pressure, 85 atm; FID.

*Fig. 21d: on a monolithic silica gel column[35]*

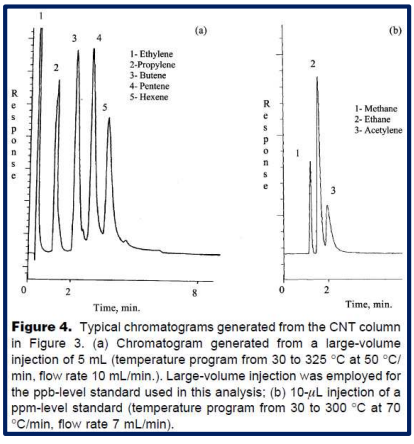


**Figure 4.** Typical chromatograms generated from the CNT column in Figure 3. (a) Chromatogram generated from a large-volume injection of 5 mL (temperature program from 30 to 325 °C at 50 °C/min, flow rate 10 mL/min.). Large-volume injection was employed for the ppb-level standard used in this analysis; (b) 10-μL injection of a ppm-level standard (temperature program from 30 to 300 °C at 70 °C/min, flow rate 7 mL/min).

*Fig. 21e: on a CNTs PLOT column[39]*

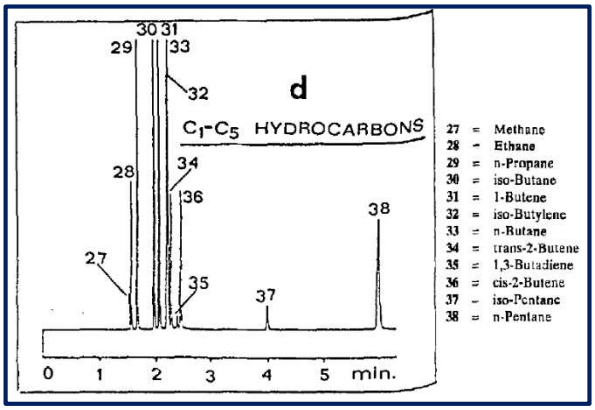


*Fig. 21f: on a graphite PLOT column[37]*

*Fig. 21: use of gas-solid chromatography in PLOT columns for the separation of light hydrocarbons*

## II.B. Micro gas chromatography

The perspectives of miniaturized gas chromatography are numerous, as described by Yashin (on portable GC[40]), De Mello (on chip-embedded GC[41]), Wise (on MEMS in general, and MEMS-based GC in particular[42]), Azzouz (on stationary phases for micro columns[43]), or Wang (on column and micro column heating[44], as well as Smith[45]) in their respective reviews: increase of the range of potential applications, measure automation, production and maintenance cost decrease, lower power consumption, high speed temperature programming enabling (and, thus, faster analyses) are the more often cited.

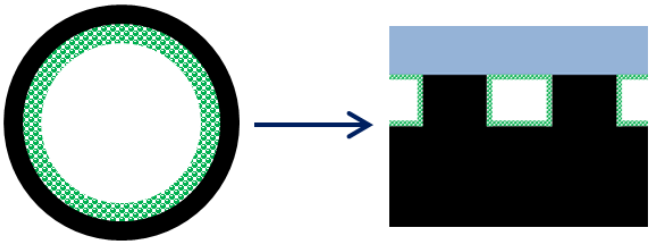

*Fig. 22: how to adapt conventional PLOT columns fabrication techniques to silicon micro machining processes?*

### II.B.1. How it all began

After a PhD defended on the subject in 1975, Terry published in 1979 the first paper dealing with the fabrication of a whole gas chromatographic air analyzer on a silicon wafer (figure 23).

A 200 µm wide, 30 µm deep, and 1.5 m long column was fabricated on a 200 µm thick, 5 cm-diameter silicon wafer[46]. A layer of silicon dioxide (approximately 1 µm thick) was thermally grown on the wafer to serve as an etch mask in the silicon etching step. Using a standard photoresist and photolithography process, a spiral pattern was defined in the silicon dioxide on the front side of the silicon wafer; the oxide was removed where the groove was to be formed, exposing the silicon surface. The wafer was then placed in an isotropic silicon etching solution where the spiral pattern, defined by the silicon dioxide, was etched into the silicon. Next, the wafer was re-oxidized and feed-through holes were defined and etched by photolithography through the wafer. An anisotropic etchant was utilized to minimize the volume of these holes. The silicon wafer was then cleaned and stripped of all oxide, and anodically bonded to a Pyrex cover plate, forming the spiral groove into an enclosed capillary tube. A commercial PDMS stationary phase (OV-101) was used to coat the inner walls of the column, following standard coating process (dissolution in a solvent, coating of the liquid, removal of the solvent).

Mainly intending his discovery to air analysis, he also designed and fabricated a micro valve injector and a micro thermal conductivity detector (see II.B.4.), and obtained a separation of C5-C7 and chlorine alkanes. Plate number reached 2300 (1530 plates per meter) for heptane.

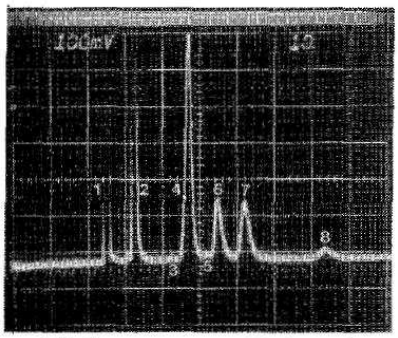

Fig. 8. Miniature GC chromatogram of hydrocarbons on OV-101 stationary phase. Peak 1 nitrogen; 2 n-pentane; 3 3-methylpentane; 4 n-hexane plus chloroform; 5 2,4-dimethyl pentane; 6 1,1,1-trichloroethane; 7 cyclohexane; 8 n-heptane.

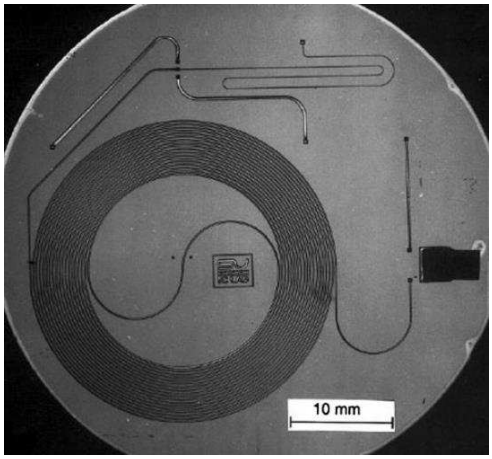


*Fig. 23: separation obtained by Terry (left) with the first silicon-based gas chromatographic system (right), including column, injector and detector[46].*

## II.B.2. Columns etching processes and designs

### *II.B.2.01 Isotropic etching (semi-circular or circular channels)*

The same method was used in many other research works.

In 1997, Hannoe[47] developed an ultrasonic-based method for the corn-shaped etching of in- and outlet holes. Simple fused-silica capillaries were then easily glued to the connection holes with polyimide glue (figure 24).

To improve chromatographic properties of such systems, the fabrication of circular channels instead of strongly asymmetric semi-circular channels was then reported.

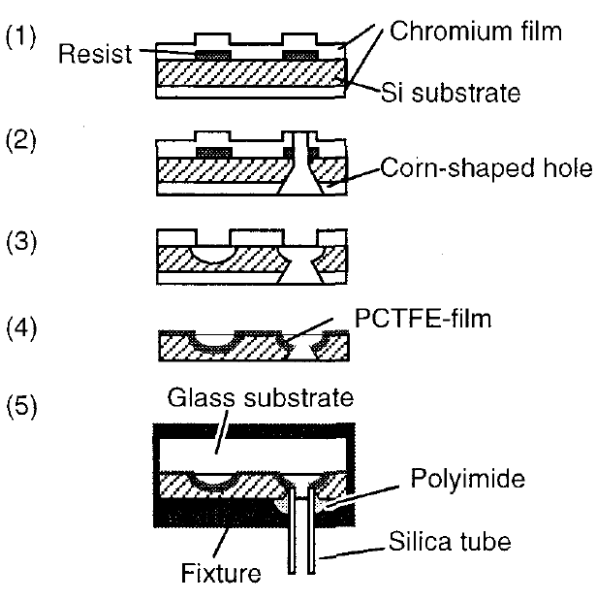


Fig. 3 Fabrication process for micro-column

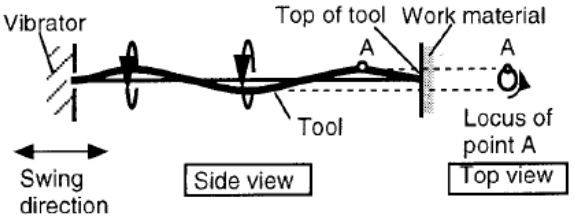


Fig. 12 Resonance state of needle tool

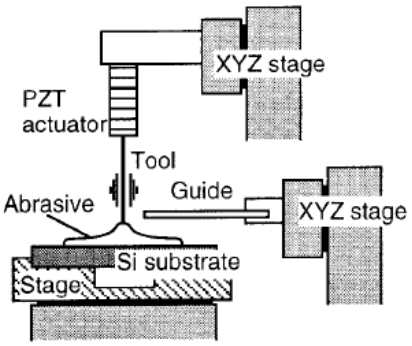


Fig. 13 Apparatus for ultrasonic machining

*Fig. 24: column (left) and holes (right) fabrication processes, as reported by Hannoe[47]*

Tjerkstra in 1997[48], followed by De Boer in 2000[49], provided accurate description of BCT (Burried Column Technology) and of wafer-wafer aligned bonding, two processes enabling the fabrication of quasi circular channels. In BCT (figure 25), isotropic etching for the formation of the circular channel is performed after a preliminary step of anisotropic (vertical) etching, and the last step consists in the closing of the hole up the channel (usually with silicon nitride). In wafer-wafer bonding (figure 26), two wafers are isotropically etched with chiral patterns to form semi-circular channels, and bonded together to form circular channels; alignment control and accuracy are, of course, crucial.

Recently, Potkay (2007) used BCT for the development of a low-power micro gas chromatography column[50] (see also II.B.3), as well as Radadia (2009, cf. figure 25)[51]. Pai (2008) used wafer-wafer bonding technology after coating the semi-circular channels of both wafers with stationary phase[52]. Lewis (2010) transferred isotropic etching and wafer-wafer bonding technologies to glass to fabricate a glass-based circular-section column[53]. In 1998, Yu reported the development of a full silicon-based system, including injector and detector, and the separation of a C1-C6 mixture, with a wafer-wafer bonded circular column[54]. Nevertheless, the display of the chromatogram in the published paper is of poor quality and allows to doubt as for the claimed result (figure 26b).

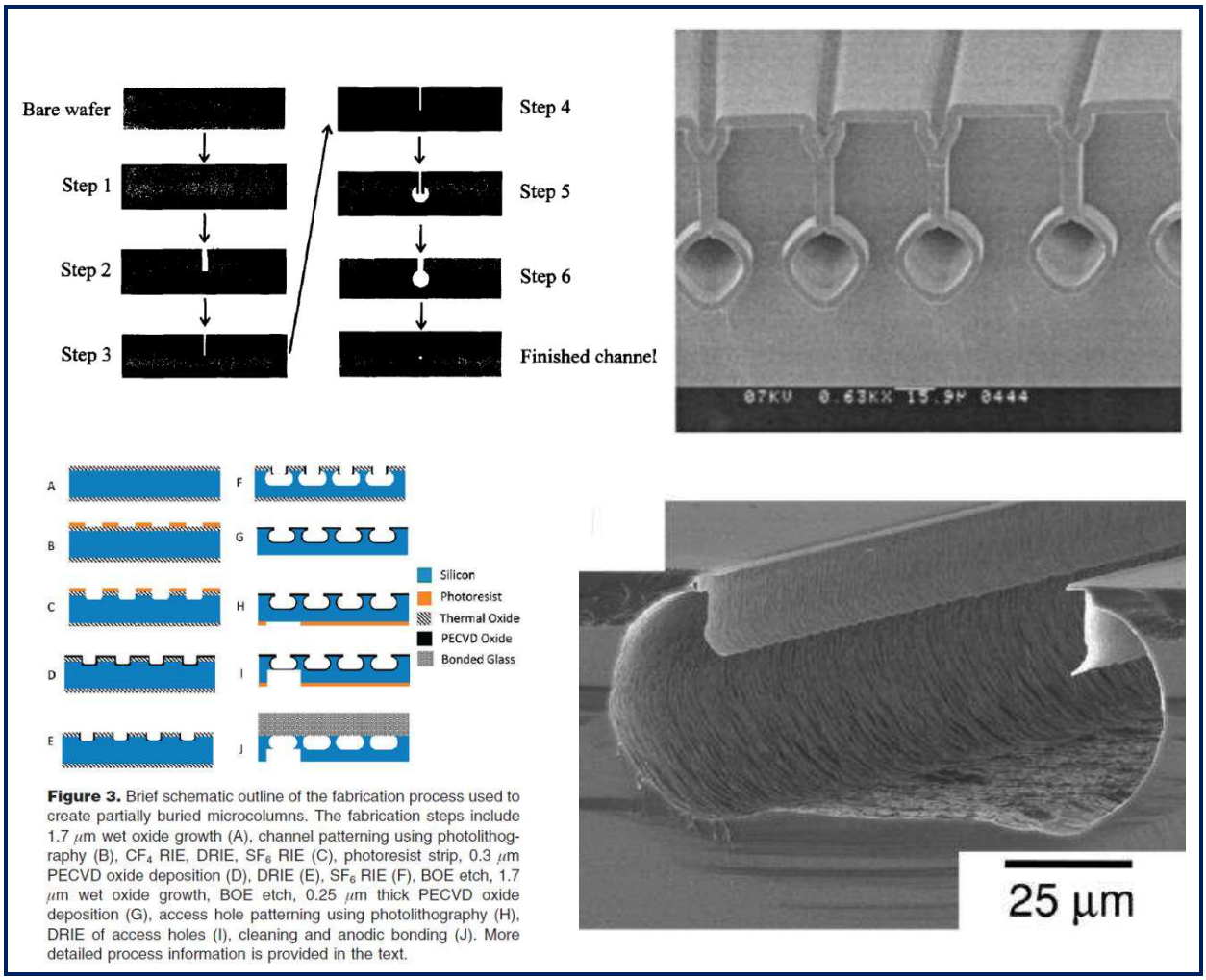


**Figure 3.** Brief schematic outline of the fabrication process used to create partially buried microcolumns. The fabrication steps include 1.7 $\mu$m wet oxide growth (A), channel patterning using photolithography (B), $CF_4$ RIE, DRIE, $SF_6$ RIE (C), photoresist strip, 0.3 $\mu$m PECVD oxide deposition (D), DRIE (E), $SF_6$ RIE (F), BOE etch, 1.7 $\mu$m wet oxide growth, BOE etch, 0.25 $\mu$m thick PECVD oxide deposition (G), access hole patterning using photolithography (H), DRIE of access holes (I), cleaning and anodic bonding (J). More detailed process information is provided in the text.

*Fig. 25: process flow (left) and SEM pictures (right) of buried channels obtained by BCT, as reported by De Boer and Tjerkstra[48,49] (top) and Radadia[51] (bottom)*

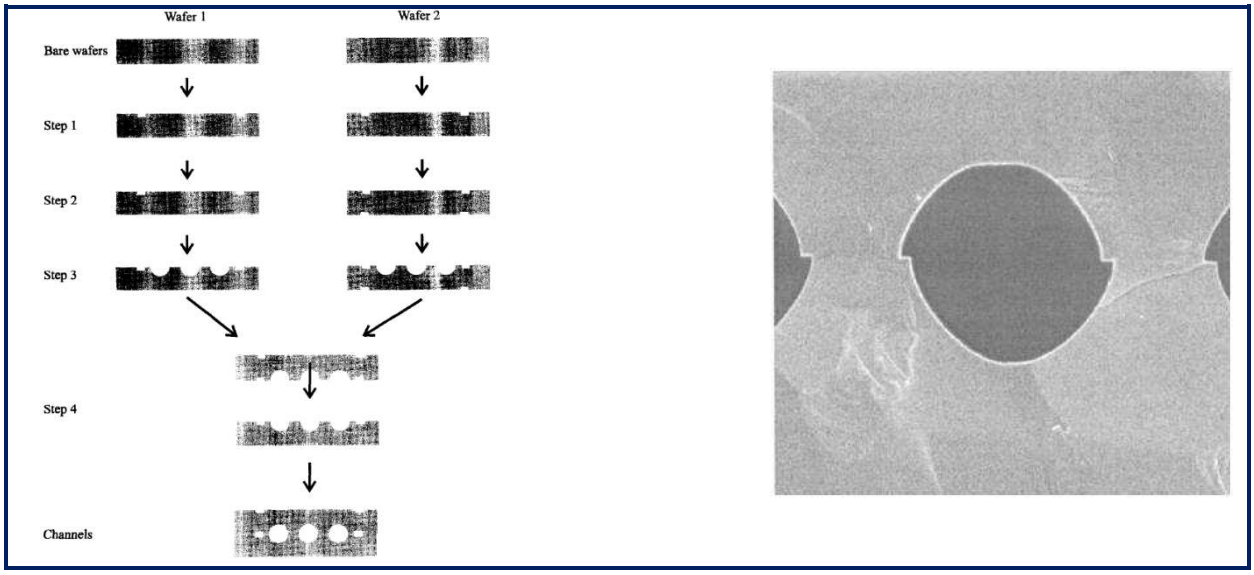


*Fig. 26a: process flow (left) and SEM picture (right) of circular channels obtained by isotropic etching and wafer-wafer bonding, as reported by De Boer and Tjerkstra[48,49]*

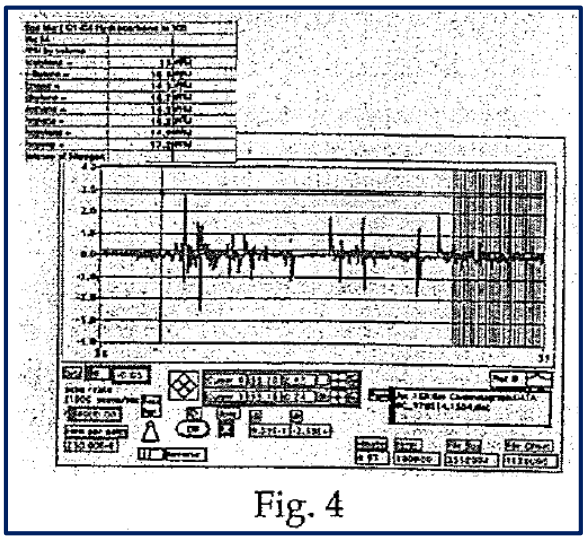


*Fig. 26b: C1-C6 (?) separation obtained by Yu with a full silicon-based system, including injector and detector*

### *II.B.2.02 Anisotropic etching (square channels)*

The same method was then followed in many other research works, among which the specific investigation and optimization of the HARSE process (High Aspect Ratio Silicon Etching) for this purpose by Matzke[55], the considerable contribution of Agah and the University of Michigan[56,57], and more recent developments by Sun[58,59] (cf. figure 27).

Compared to semi-circular channels, square channels present a better symmetry (which generally improve kinetic performances), and occupy less space; indeed, for an identical channel section and length (i.e. an identical column volume), the diameter of a semi-circular channel is $\sqrt{8/\pi}$=1.6 times bigger than the side of a square channel; moreover, with HARSE processes and rectangular section (vertical dimension bigger than horizontal dimension), space saving can be even higher.

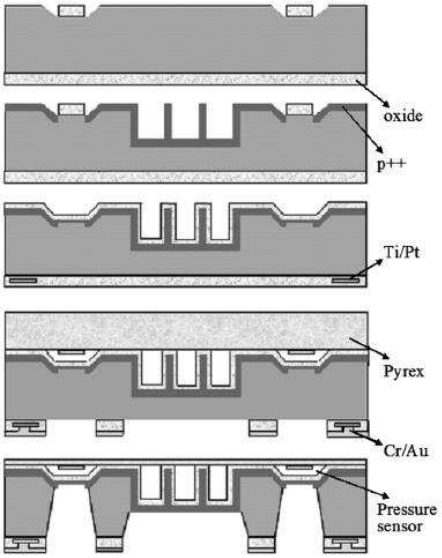


*process flow*

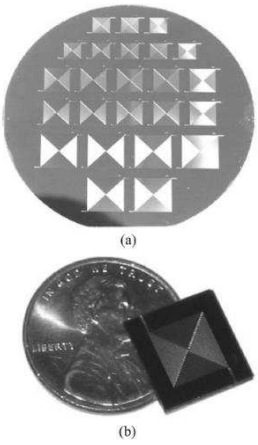


*(a) wafer containing 25-cm, 50-cm, and 1-m-long silicon-glass columns (width 250 µm, depth 150 µm) (b) closer view of a 25-cm-long column*

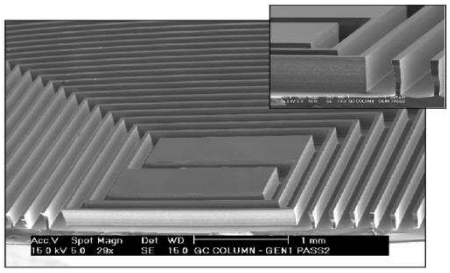


*SEM micrograph*

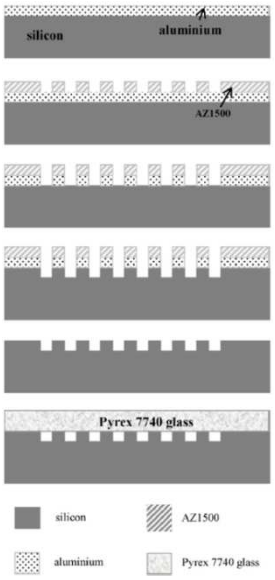


*process flow*

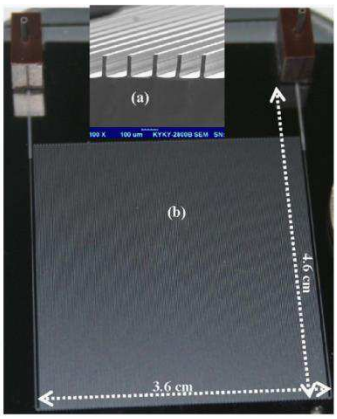


*(a) SEM micrograph, (b) picture of a micro machined column (100 µm x 100 µm x 6 m)*

*Fig. 27: process flow and pictures of square-channel micro machined columns by Agah[56,57] (left) and Sun[58,59] (right)*

Buried channels have the same advantages (and even more concerning symmetry), but imply more complex processes than square channels. Besides, stationary phase insertion can only be achieved after columns sealing, which compromises the compatibility with clean room conventional collective deposition processes (such as sputtering).

A last advantage of square channels compared to other types of channels is the possibility to create various high aspect ratio structures such as micro pillars inside the channel bed, as described in the following subparagraph.

### *II.B.2.03 Micro structure etching in channels*

In 2009, Ali (figure 28a) reported the first design and fabrication of square section micro columns with micro pillars (or micro posts)[60]. The aim was to transfer the advantages of conventional packed columns (high separating power in small lengths and high sample capacity through greater stationary phase surface) to micro machined columns. Such designs were baptized “semi-packed”.

The same year, Nishiyama (figure 28b) studied the effect of micro pillar density on kinetic performances of semi-packed GC columns[61]. Highest efficiency was provided by highest density.

In 2013, Sun (figure 28c) replaced square-section posts by circular-section posts[62].

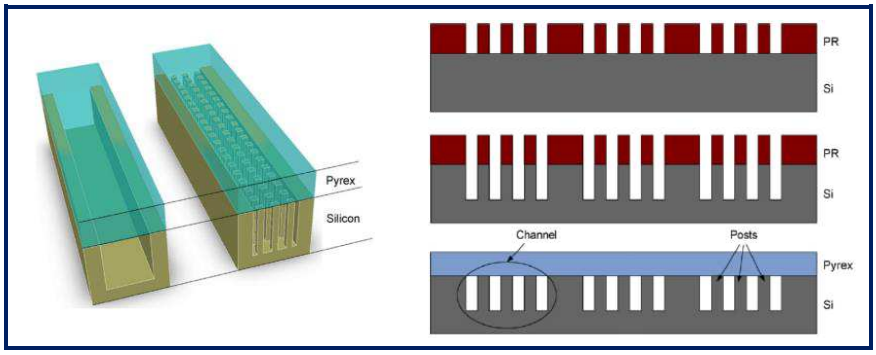


*Fig. 28a: design of semi-packed channel compared to open channel (left) and simplified flow of semi-packed micro machined columns (right) as reported by Ali[60].*

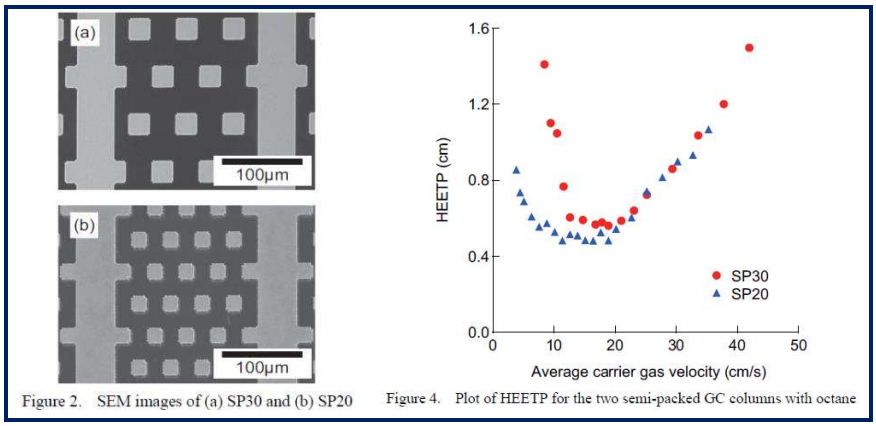


*Fig. 28b: comparison of the kinetic performances of semi-packed micro columns with different packing densities as reported by Nishiyama[61].*

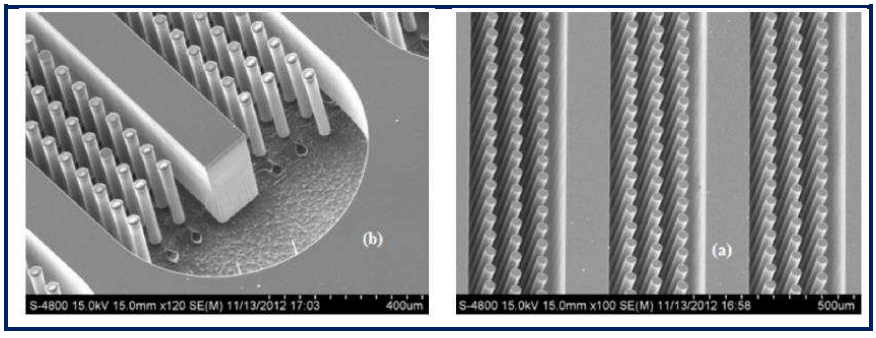


*Fig. 28c: SEM images of circular-section posts in a semi-packed micro column by Sun[62].*

### *II.B.2.04 Influence of tubing shape*

In 2010, a study on the influence of tubing shape on the kinetic performances of micro GC columns was published by Radadia[63]. Three different shapes were experimentally evaluated (serpentine, spiral and square spiral, figure 29), in terms of efficiency, resolution, and separation of real mixtures. For all of these three criteria, the serpentine shape was found to be the best one. This quantitative study confirmed the intuition according to which flow asymmetries were more compensated in serpentine than in spiral tubings.

### *II.B.2.05 Conclusion*

Taking account of the volume occupied by the channels, channel symmetry, process simplicity, possible compatibility with batch deposition techniques such as sputtering, possible compatibility with semi-packed designs, and influence of tubing shape, anisotropically-etched square section serpentine design seems to be the most appropriate in the present context.

In most developments, column's chips were equipped with a heating system, to enable temperature-programming, as briefly summarized in next paragraph.

## II.B.3. Heating methods

Chip thermal management has been widely reported and used in MEMS technology, including gas sensor applications[64-66]. It has generally consisted of electro- or plasma- on-chip-deposited metallic micro filaments for direct resistive heating. Most chosen metals were gold, platinum, tungsten and chromium-nickels alloy[67], for their high conductivity, resistance to oxidation, and compatibility with MEMS deposition techniques.

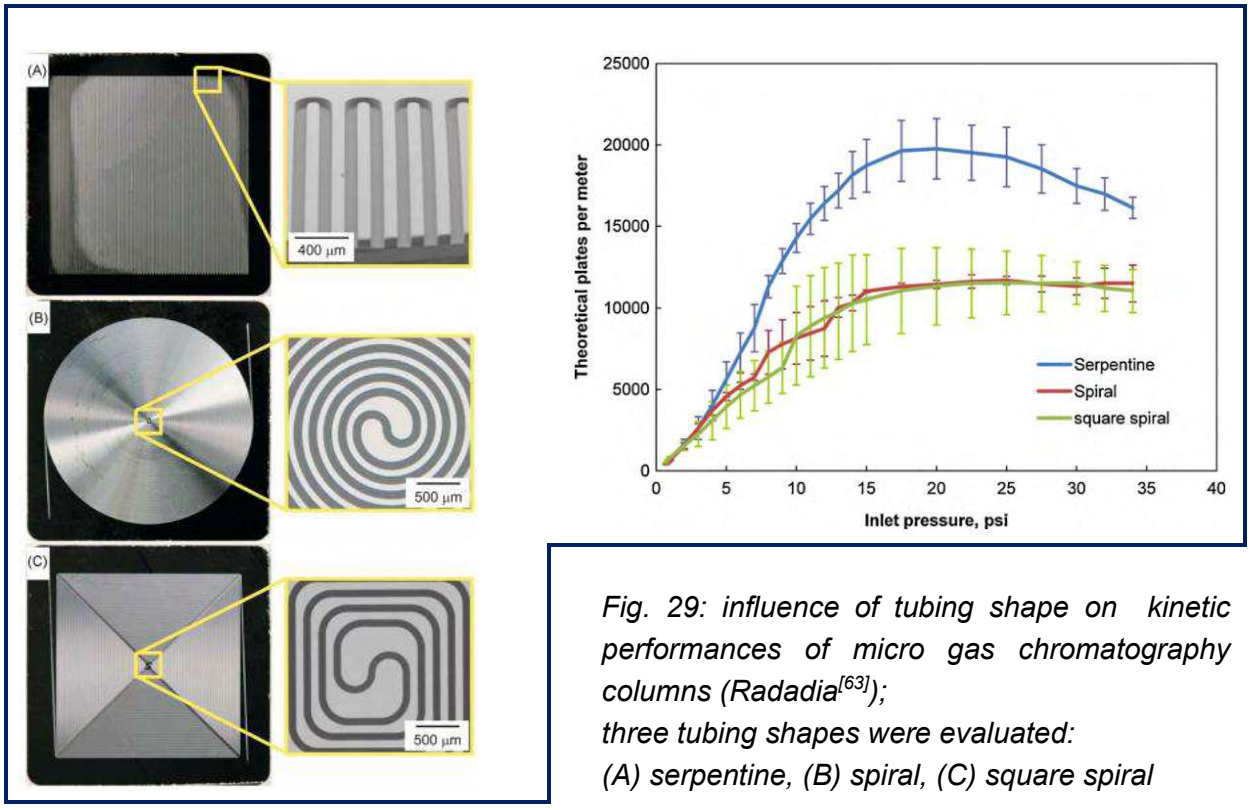


*Fig. 29: influence of tubing shape on kinetic performances of micro gas chromatography columns (Radadia[63]);*
*three tubing shapes were evaluated:*
*(A) serpentine, (B) spiral, (C) square spiral*

This kind of micro heating technology was used by Agah[57] to equip his gas chromatography chip with a temperature-programming system (figure 30a). However, micro heaters have rather been dedicated to maintain chips to a specified temperature, or to provide relatively slow temperature ramps (for instance, between 5°C/s and 40°C/min).

Fast and homogeneous chip heating has rather been provided by filament serpentine deposition covering the whole surface of the chip, as optimized by, for instance, Pasupuleti[67] or Roy[68], and summarized in a very recent review (2012) by Wang[44] (cf. figure 30b).

With adapted heating filaments, ramps up to 10°C/s were reached by Agah[57], and up to 26°C/s[70], and even 60°C/s[71], by Reid and Stadermann, for ultra-fast separations of C6-C10 or oxygenated hydrocarbons in 2 seconds with carbon nanotubes as stationary phase (see also II.B.6).

In 2012, Luong experienced and discussed the limitations of ultra-fast heating[69], notably concerning strong baseline drifts encountered during minute-long separations (cf. figure 30c). System stabilization by habituation and subtracting algorithms were proposed.

Potkay answered the issue of low-power temperature-programming by designing and BCT-fabricated in-vacuum-suspended micro channels (figure 30d). Heat losses usually occurring to the surrounding air were lowered with a vacuum environment (supporting structure excepted)[50].

Whereas heating methods and optimization have been subjects of numerous studies, the problem of cooling has been poorly reported. Wang mentioned the use of Peltier device (with heat sink and fans) in his review[44]. This basic system was for instance used by Lewis[53]. Yet, in the context of cycled measurements (automate successive fast analyses), cooling time is crucial. Indeed, the whole interest of performing ultra-fast temperature ramps and beating records in terms of separation time can be made worthless if cooling down the column from the high end temperature to the low start temperature for the next analysis is too long.

Once completed with the appropriate temperature-programming system, the column's block is purposed to be placed in a whole flow line. The next paragraph is dedicated to a (very short and qualitative) summary of the use of MEMS technology in the fabrication of miniaturized up- and downstream components of the GC column, such as injector, detector, and pre concentrator. It will provide both references that will be used in appendix A, and credit to the concept of pocket gas chromatography, in which this work perfectly fits.

### II.B.4. Up- and downstream components and integration

An integrated system, in addition to the column's block and to fluidic and electrical connections (carrier gas and sample supply, electric board and micro processing unit), must be equipped with injection and detection systems; it can also be equipped with an intern calibration system, a pre concentrator/focuser (PCF) and a micro pump. Figure 31 displays an example of the first generation of MEMS integrated gas chromatographs, by Lu[72].

### *II.B.4.01 Injectors*

As well as conventional injectors, micro injectors are of two types: pneumatic or mechanical (cf. figure 32a). Both types consist of a network of channels (sample-, injection-, and waste line, sampling loop). In pneumatic micro injectors (such as reported by Terry[46,73], Bruns[74], or developed at MEMS TC[75,76]), the pressure necessary for valve actuation is provided by the carrier gas; in mechanical injectors (such as developed at MEMS TC as well), valve opening and closing is provided by the displacement a moving part on an immovable one.

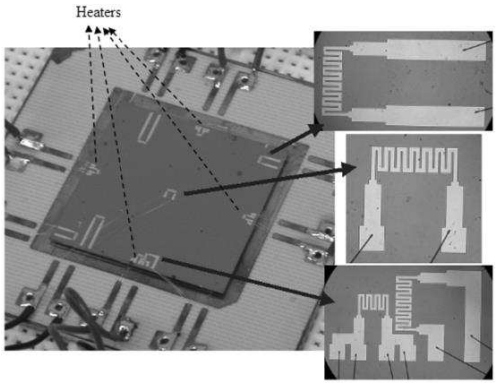


*Fig. 30a: 3 m-long GC column on a (3.3 cm)² chip equipped with micro heaters, as firstly reported by Agah[56]*

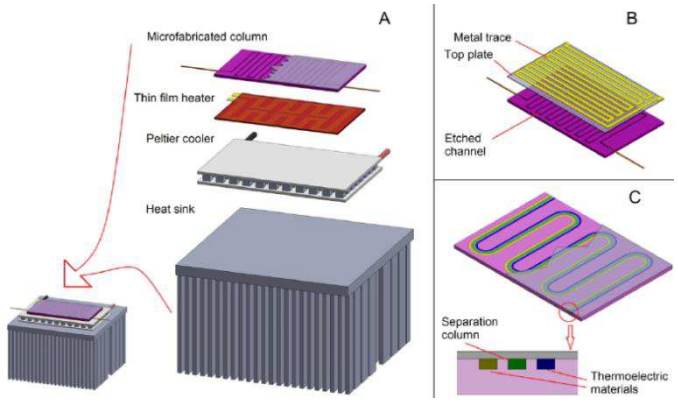


*Fig. 30b: micro column temperature-programming systems, as summarized by Wang[44] (A: external heater, B: on-chip heater, C: internal heating and cooling with Peltier strips)*

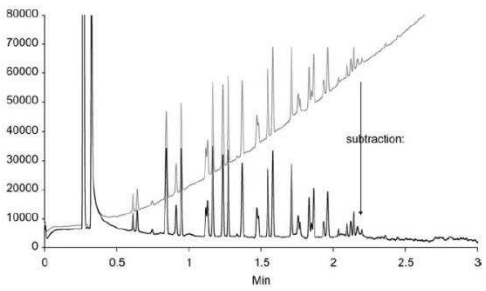


*Fig. 30c: typical baseline drift issues encountered during fast heating and solved by Luong[69]*

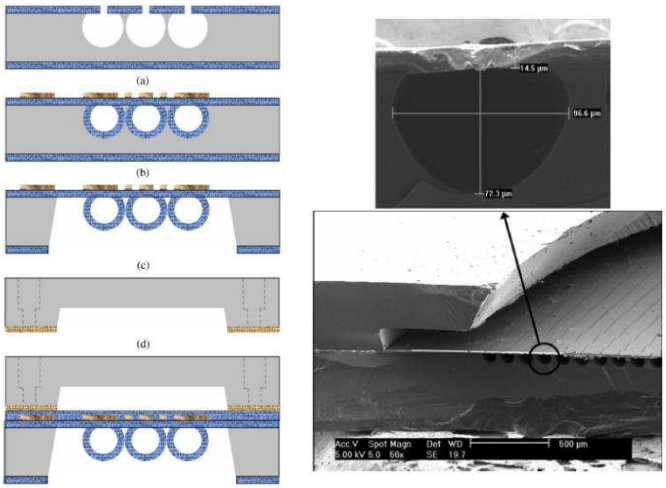


*Fig. 30d: in-vacuum-suspended micro columns for low-power thermal management, as designed, fabricated and reported by Potkay (left: process; right: SEM image)*

*Fig. 30: heating and temperature-programming problematics in micro gas chromatography*

### *II.B.4.02 Detectors*

The relative simplicity, along with robustness and universality, has made the thermal conductivities detector (TCD) the first and most reported detector to be miniaturized. A TCD usually consists of four resistors forming a Wheatstone bridge, two of them being immerged in the main flow line downstream of the column, and two of them being immerged in a reference flow line continuously swept by the carrier gas; the resistors are slightly heated with a constant voltage, and the temperature of the resistors (and, thus, their resistance) depends on the thermal transfer from the resistors to the surrounding gas in the channels, which in turns depends on the nature of the surrounding gas; thus, when both lines are only swept by carrier gas (no analyte in the detector), the four resistances are equal, the bridge is balanced and the signal is null; when an analyte (in a given concentration in the carrier gas) flows out of the column, the value of two resistances changes, the bridge is unbalanced and a signal appears. The main drawback of TCDs is their relatively high detection limit and poor sensibility; bridge perfect balancing is crucial to ensure widest quantification range possible. Micro TCD were designed and fabricated by Terry[46,73], Yu[54], Sorge[81], Cruz[82], or at MEMS TC[77] (see figure 32b, left). To avoid bridge unbalancing due to flow difference between column line and reference line, Narayanan proposed to place two resistors at the beginning of the column, and two at the end, thus removing the reference line (figure 32b, right), and obtained satisfying results[78].

Zimmermann designed and fabricated a micro machined flame ionization detector[83] (FID), and Reddy reported the use of an optical micro detector based on Fabbry Perrot interferometry[79] (figure 32c). Metal-oxide micro sensors (based on the electrical measurement of oxidation-reduction processes) were also reported[72,84].

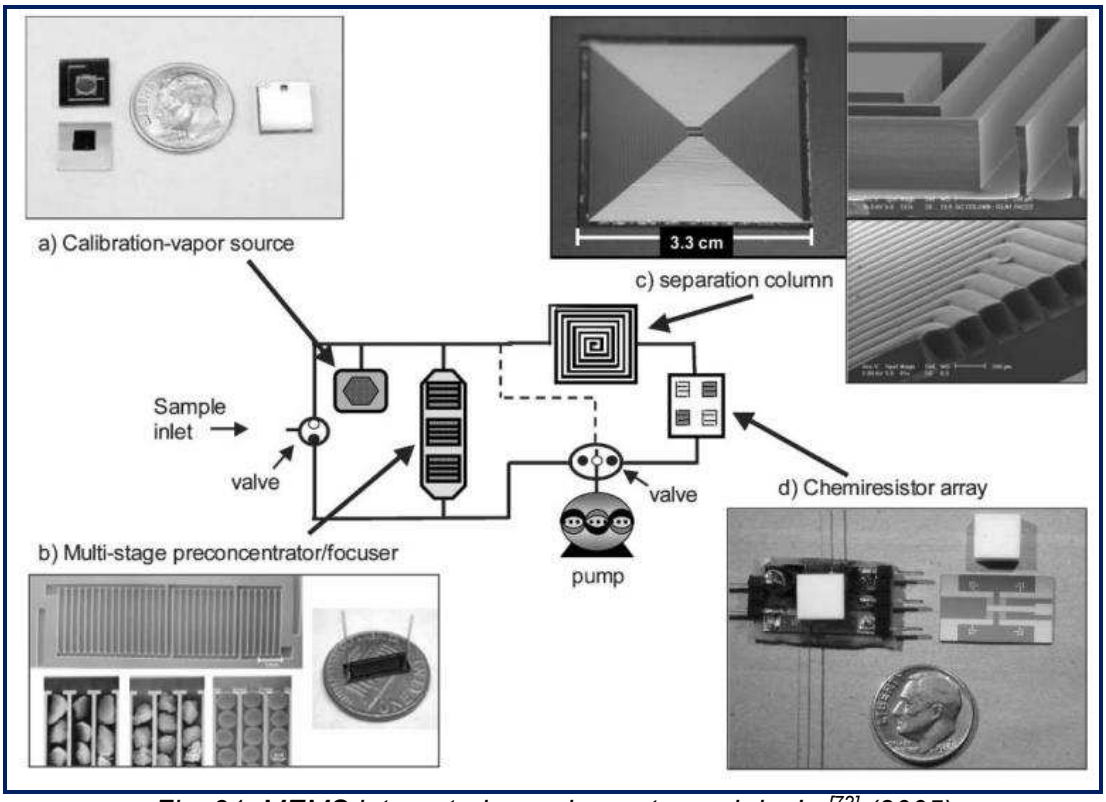


*Fig. 31: MEMS integrated gas chromatograph by Lu[72] (2005)*

### *II.B.4.03 Pre concentrators and calibration vapor source*

Pre concentrators/focusers are useful for the detection of trace-level compounds, and were for instance micro machined and integrated by Agah[56,57] and Wise[42] (figure 33), Lu[72] (figure 31), Zampolli[85], or Serrano[80] (figure 32c). Saridara reported the use of a carbon nanotubes MEMS PCF for methane pre concentration[86].

A calibration vapor source was integrated by Lu[72] (figure 31) or Wise[42] (figure 33) for intern calibration of the embedded detector (internal standard).

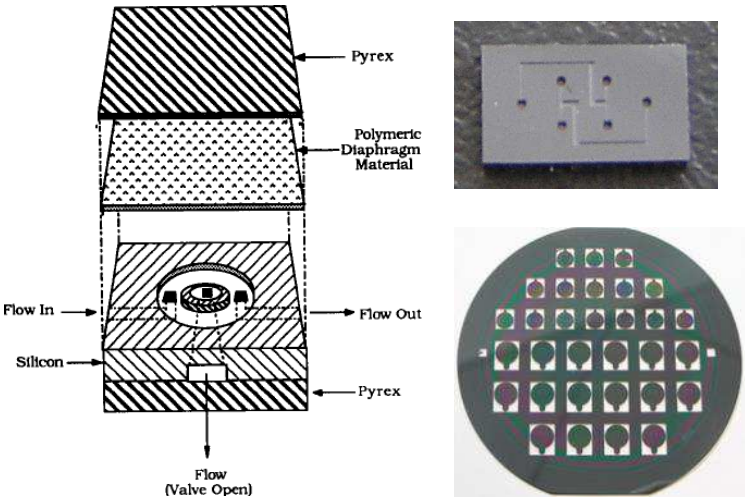


*Fig. 32a:*
*examples of micro injectors:*
*<u>left:</u>*
*pneumatic injector by Bruns[74]*
*<u>top right:</u>*
*pneumatic injector developed at MEMS TC by Nachef[75,76];*
*chip size 4x7x1 mm³*
*<u>bottom right:</u>*
*wafer with two-parts mechanical injectors developed at MEMS TC*

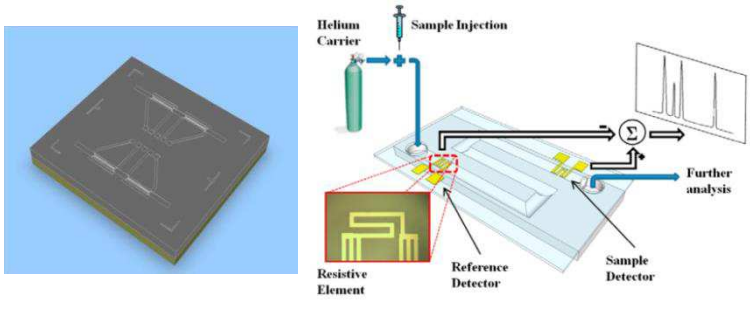


*Fig. 32b:*
*examples of micro TCDs*
*<u>left:</u>*
*as developed at MEMS TC[77];*
*chip size 4x6x1 mm³*
*<u>right:</u>*
*without reference line, as reported by Narayanan[78]*

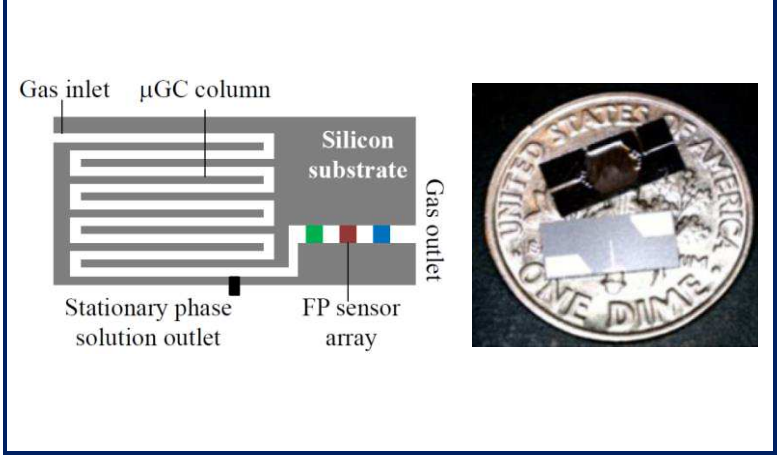


*Fig. 32c:*
*other examples of micro machined elements*
*<u>left:</u>*
*Fabbry-Perrot optical detector for micro GC, as invented by Reddy[79]*
*<u>right:</u>*
*micro machined PCF chip (front side and back side) as developed by Serrano[80]*

*Fig. 32: examples of up- and downstream MEMS components*

## II.B.5. Computer science contribution

Over the last 15 years, computer science improvements have contributed to model and optimize micro gas chromatographic components.

A most interesting study by Spangler determined the theoretical loss of efficiency caused by square sections compared to circular sections[87]. The plot of the resistance to mass transfer in gas phase coefficient (part of the C term in the Van Deemter equation, cf. I.A.6) against retention factor (as displayed in figure 34a) for both sections exhibited expected lower kinetic performances for square sections compared to circular sections. For relatively weak retentions, as in the present context of light alkanes separations, the difference was less significant than for strong retentions.

Agah resorted to computer modeling to choose the length and width of his column (figure 34b), and to calculate heat losses while heating[56].

Vangelooven used advanced micro fluidic simulation to indicate how to optimize semi-packing shapes, dimensions and position of gas chromatography columns[88] (figure 34c).

Earlier, Wong modeled transport in gas chromatography columns for the Micro-Chem Lab™[89], and Chen led thermal analyses simulations on the micro channel flow in miniature thermal conductivity detectors[90].

## II.B.6. Stationary phases

The last, but not least, material aspect of micro gas chromatography discussed in this literature review deals with stationary phases. Stationary phase choice is driven by the two following criteria: the targeted application (i.e. the targeted compounds to separate), and the compatibility of the insertion process in the column with requirements (e.g. coating or packing uniformity or collective insertion).

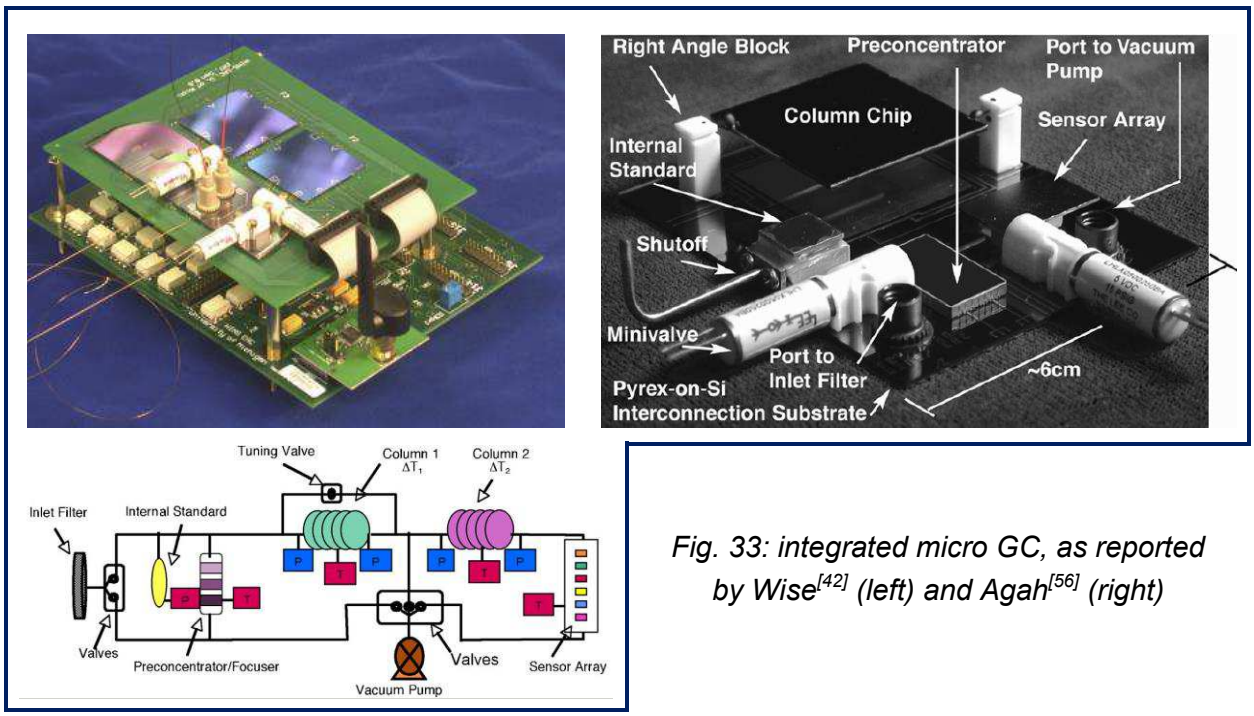


*Fig. 33: integrated micro GC, as reported by Wise[42] (left) and Agah[56] (right)*

A review on stationary phases utilized in micro gas chromatography columns fabrication was published by Azzouz in 2013 and co-authored by the author of the present manuscript[43]. This paragraph is an exhaustive yet short summary on this specific topic, while details and quantitative precisions can be found in the review.

### *II.B.6.01 Coating gel stationary phases*

Following a conventional process of static coating, for instance described and optimized by Reidy[91] (figure 35a) for micro gas chromatography, poly dimethyl siloxane commercial stationary phases were utilized in a huge majority of studies[43]. Terry[46,73], Matzke[55], Yu[54], Agah[56,57], Lu[72], Potkay[50], Wise[42], Ali[60], Nishino[92], Radadia[51], Sun[58], Lorenzelli[93], Narayanan[78], Yu[54], as most works on the topic, resorted to PDMS to coat their micro columns. Naturally, targeted compounds were of higher boiling points or polarity than C1-C5 hydrocarbons, and coating process (dissolution of the stationary phase in a solvent, coating of one column, and evaporation of the solvent) was not first purported to be collective and reproducible. A PDMS micro column, fabricated at Schlumberger and evaluated by Azzouz at the ESPCI was proven able to separate a C1-C3-C4-C5 mixture but C1-C2 separation could not be performed[94].

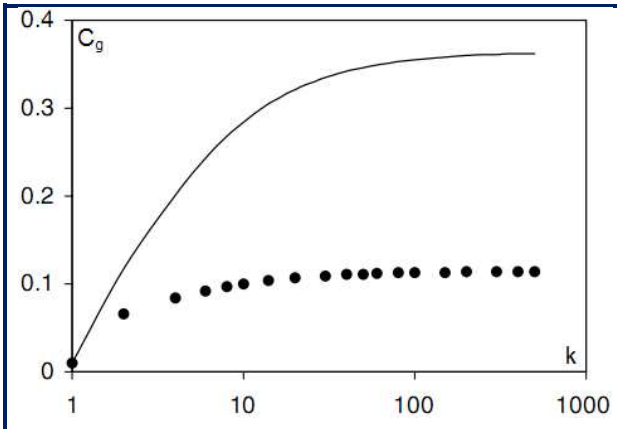


*Fig. 34a: resistance to mass transfer coefficient as a function of retention factor for circular- (dots) and square- (line) sections of GC columns, as reported by Spangler[87]*

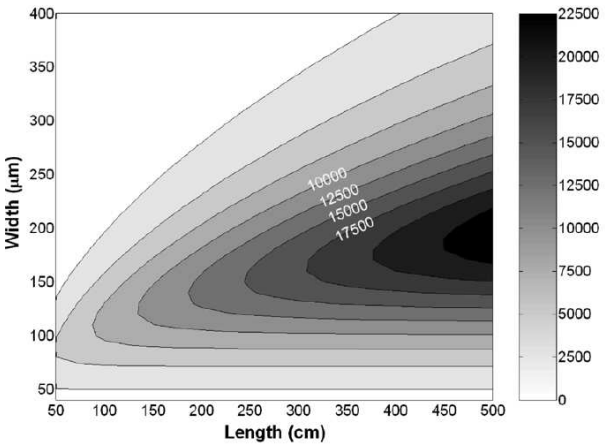


*Fig. 34b: predicted number of plates as a function of column width and length for a 250 µm deep, square-section, PDMS-coated micro column, as used by Agah[56]*

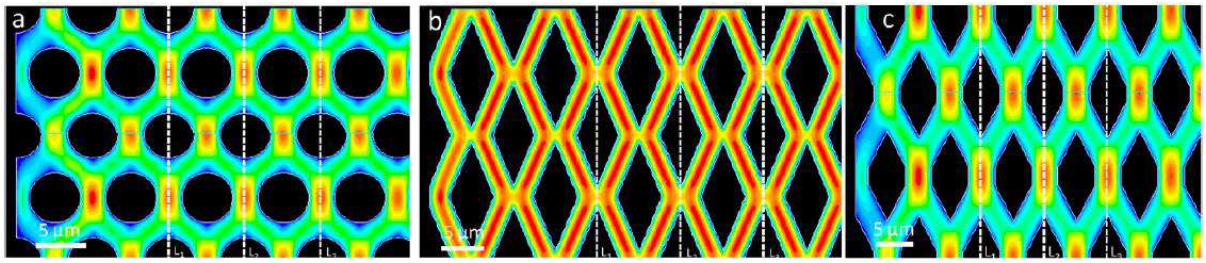


*Fig. 34c: optimized shapes, dimensions and positions of semi-packing structures for micro gas chromatographic applications, by Vangelooven[88]; diamond shape (b) was recommended*

*Fig. 34: examples of computer science contribution to micro gas chromatography*

Pai utilized (poly(methyldi(1,1,1-trifluoro-2-trifluoromethyl-2-hydroxypent-4-enyl)silane, also named HCSFA2, to coat two wafers with semi-circular channels[52], as already mentioned in II.B.2.01.

### *II.B.6.02 Packing solid stationary phases*

Very few studies reported the use of solid packings as stationary phases. The significant work of Zampolli[84,85,95], who utilized Carbograph (carbon molecular sieve) for the separation of aromatic volatiles, can yet be mentioned here. In this case, after encapsulation, the spiral column was filled with the powder by applying vacuum to the outlet and slowly dripping small amounts of mesh into the inlet (figure 35b). The flow realized by the vacuum pump moved the mesh through the column until reaching a small metal filter located at the column outlet. Packing materials were also tested at MEMS TC as preliminary studies, and the corresponding results are presented in appendix B.

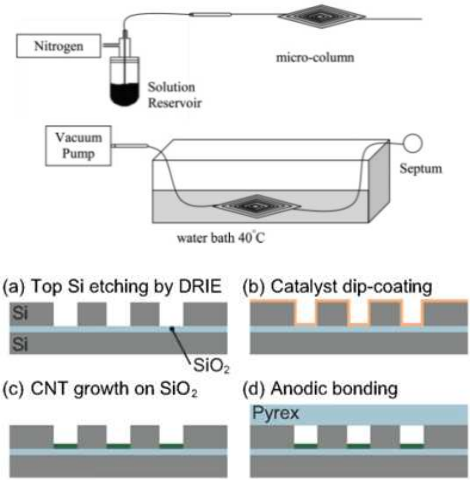


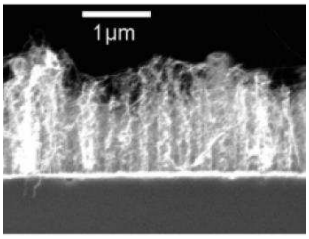


*Fig. 35a (top left): usual static process for PDMS coating, by Reidy[91]; up: coating; down: solvent evaporation*
*Fig. 35b (top right): carbon molecular sieve-packed micro column by Zampolli[84] (75 cm, depth 0.8 mm, width 1 mm)*
*Fig. 35c (bottom): CNTs micro column fabrication (left) and channel floor SEM image (right) as reported by Nakai[96]*

*Fig. 35: micro columns gel-coating, packing and porous layer-coating*

### *II.B.6.03 Porous layer stationary phases*

A different approach, aiming at coating collectively all the columns on one wafer before bonding and dicing, was attempted, mainly with carbon nanotubes (CNTs) as the stationary phase. CNTs were grown by chemical vapor deposition (CVD) by flushing the wafer with inert and carbon-wealth gas mixture (such as argon and ethylene) and utilizing an appropriate and accurate temperature program. Stadermann[71], Nakai[96], and Reid[70] fabricated such columns, respectively for C6-C10 or oxygenated hydrocarbons, C6-C14 and C6-C11 analyses. However, a CNT micro column, fabricated at Schlumberger and evaluated by Azzouz at the ESPCI[94], was proven able to separate a C1-C3-C4 mixture (in 0.4 minute, without temperature programming). Tests led on this column at MEMS TC are detailed in appendix B.

Electro-deposited bare- or functionalized gold layers were also occasionally reported, for the separation of heavier hydrocarbons (>C10)[43].

A recent PhD thesis by Azzouz[97] demonstrated the possibility to transfer silica porous monoliths synthesis into micro columns, and to obtain a 2 minutes-long C1-C4 complete

separation (figure 36). 1750 plates were obtained for ethane separation (with a corresponding plate height of 0.6 mm) on a 1 m-long, 75 µm x 75 µm wide micro column. The author of the present manuscript took part in the production of these results by sputtering a thin silica bond coat inside the micro channels before synthesis, and by providing gas samples. This promising work remained to be confirmed, in terms of batch fabrication and precision.

Eventually, poly chloro tetra fluoro ethylene (PCTFE, a type of Teflon) was sputtered into the uncovered channels before bonding by Hannoe in 1997[47]. Although no viable chromatographic result was reported from this study, Hannoe mentioned other alternatives (especially among plasma-deposited amino-acid films), and had after all a most interesting approach, very similar to the one chosen in the present work.

### *II.B.6.04 Conclusion*

Most reported stationary phase insertion processes consisted in transferring usual coating or packing techniques from conventional columns to silicon micro machined columns. To mimic conventional PLOT columns, only a few very specific approaches were attempted.

To conclude this section on micro gas chromatography, the two next paragraphs consist of summaries of the various applications of micro gas chromatography and compared kinetic performances of micro columns reported in the literature.

## II.B.7. Applications

The first developments of silicon-based micro chromatographs were intended to spacecraft applications[40] (including Terry[46], which PhD work was led in partnership with the NASA). Over the past 15 years, two applications have represented the majority of reported applications, namely chemical warfare agent detection (Frye-Mason[98], Pai[52], Potkay[50]), and environment contamination (by volatile organic compounds) monitoring (Zampolli[84,85,95], Lu[72], Nishino[92], Lewis[53], Sun[58,59]). Biological applications were occasionally published, as for instance by Lorenzelli, for the monitoring of the homovanillic acid and vanillylmandelic acid (VMA) ratios in mass population screening for neuroblastoma diagnosis and prognosis[93], or by Hintikka, for the detection of anabolic steroids[99].

While polar and/or complex compounds or hydrocarbons heavier than C4 have easily been separated, no micro gas chromatographic system dedicated to the fast monitoring of permanent gases and natural gas was found.

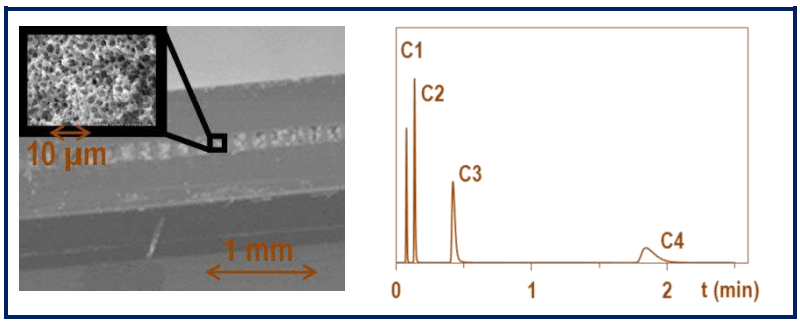


*Fig. 36: micro column with monolithic porous silica, SEM image (left) and C1-C4 separation (right), by Azzouz[97]*

## II.B.8. Summary of reported kinetic performances of micro columns

Table 4 displays a comparative summary of reported micro columns kinetic performances. As mentioned in II.B.6, most micro columns were coated with PDMS as the stationary phase. These columns were less (or as) efficient than commercial PDMS columns (which provide ~5- to 10000 plates per meter); efficiency losses were mainly due to the not perfectly circular shapes of column sections; Radadia reported an astonishing number of plates per meter of 18700. Apart from this reference, semi-packed designs allowed increased efficiencies compared to open ones. Solid layers, such as CNTs or thiol-functionalized gold, also gave satisfying results, respectively with 2500 and 7200 plates per meter.

| **Ref** | **[46]** | **[54]** | **[56]** | **[72]** | **[57]** | **[91]** |
|---|---|---|---|---|---|---|
| **Date** | 1979 | 1998 | 2005 | 2005 | 2006 | 2006 |
| **By** | Terry | Yu | Agah | Lu | Agah | Reidy |
| **Channel** | ~rectangular | $Si^2$-bond circular | rectangular | rectangular | rectangular | rectangular |
| **Section** | 200 µm x 30 µm | 100 µm | 150 µm x 250 µm | 150 µm x 240 µm | 150 µm x 250 µm | 150 µm x 250 µm |
| **Column** | Circular spiral | Circular spiral | Square spiral | Square spiral | Square spiral | Square spiral |
| **Length** | 150 cm | 560 cm | 300 cm | 300 cm | 25 cm | 300 cm |
| **S. Ph.** | **PDMS** | **PDMS** | **PDMS** | **PDMS** | **PDMS** | **PDMS** |
| **Comp.** | C7 | ? | Cumene | ? | C8 | C8 |
| **N** | **2300** | **40000** | **8000** | **6500** | **625** | **12500** |
| **N (/m)** | **1533** | **7143** | **2667** | **2167** | **2500** | **4167** |
| **HETP** | **0.65 mm** | **0.14 mm** | **0.38 mm** | **0.46 mm** | **0.40 mm** | **0.25 mm** |

| **Ref** | **[50]** | **[60]** | **[96]** | **[92]** | **[61]** | **[51]** |
|---|---|---|---|---|---|---|
| **Date** | 2007 | 2009 | 2009 | 2009 | 2009 | 2009 |
| **By** | Potkay | Ali | Nakai | Nishino | Nishiyama | Radadia |
| **Channel** | BCT | semi-packed | rectangular | rectangular | semi-packed | BCT |
| **Section** | 90 µm | 150 µm x 180 µm | 160 µm x 250 µm | 200 µm x 100 µm | 180 µm x 230 µm | ~165 µm x 65 µm |
| **Column** | Square spiral | Square spiral | Serpentine | Circular spiral | Serpentine | Serpentine |
| **Length** | 100 cm | 100 cm | 100 cm | 856 cm | 100 cm | 34 cm |
| **S. Ph.** | **PDMS** | **PDMS** | **CNT** | **PDMS** | **Parylene** | **PDMS** |
| **Comp.** | C10 | C9 | C10 | C16 | C8 | C10 |
| **N** | **2000** | **10000** | **2500** | **35000** | **2500** | **872** |
| **N (/m)** | **2000** | **10000** | **2500** | **4089** | **2500** | **2564** |
| **HETP** | **0.50 mm** | **0.10 mm** | **0.40 mm** | **0.24 mm** | **0.40 mm** | **0.39 mm** |

| **Ref** | **[58]** | **[53]** | **[63]** | **[100]** | **[62]** | **[97]** |
|---|---|---|---|---|---|---|
| **Date** | 2009 | 2009 | 2010 | 2012 | 2013 | 2013 |
| **By** | Sun | Lewis | Radadia | Shakeel | Sun | Azzouz |
| **Channel** | rectangular | $SiO_2^2$-bond circular | rectangular | rectangular | semi-packed | rectangular |
| **Section** | 100 µm x 100 µm | 320 µm | 100 µm x 100 µm | 30 µm x 250 µm | 300 µm x 350 µm | 75 µm x 75 µm |
| **Column** | Serpentine | Square spiral | Serpentine | Serpentine | Serpentine | Serpentine |
| **Length** | 600 cm | 140 cm | 300 cm | 25 cm | 200 cm | 100 cm |
| **S. Ph.** | **PDMS** | **PDMS** | **PDMS** | **Au-Thiol** | **PDMS** | **Monoliths** |
| **Comp.** | Toluene | Toluene | C8 | ? | Phenol (?) | C2 |
| **N** | **4850** | **2000** | **56100** | **1800** | **19000** | **1750** |
| **N (/m)** | **808** | **1429** | **18700** | **7200** | **9500** | **1750** |
| **HETP** | **1.24 mm** | **0.70 mm** | **0.05 mm** | **0.14 mm** | **0.11 mm** | **0.57 mm** |

*Table 4: comparative summary of micro columns kinetic performances (S. Ph.=stationary phase, Comp.=probe analyte for kinetic evaluation)*

# II.C. Sputtering

Sputtering has been a conventional deposition technique for more than 50 years (cf. I.C.1). A very wide and various range of materials (metals, alloys, ceramics, oxides, nitrides) are compatible with sputtering and are commercially available as targets. The general principle of sputtering deposition was described in I.E.; in this section, a few central or detail points of this technique will be discussed, due to their crucial influence on the targeted application. As the best candidates for light hydrocarbons separation, silica, alumina and graphite sputter-deposited layers will deserve special emphasis.

## II.C.1. Sputtering parameters

### *II.C.1.01 Sputtering mode and power*

Historically, the first plasma-enhanced depositions were made with conductive target materials (metals, alloys, graphite) and a constant anode-cathode polarization. The deposition of isolating materials, such as ceramics, oxides, nitrides, could not be performed as well, due to charge accumulations on the target. To overcome this issue, a new type of deposition mode was developed, consisting in switching the anode-cathode polarization at a high frequency. The first mode is called DC (direct continue) and the second one RF (radio frequency).

In both cases, sputtering power is set by the user, and generally ranges between 100 and 1000 W.

### *II.C.1.02 Gases and pressure*

Sputtering is usually performed by a neutral in-situ-ionized gas, commonly argon. Oxides, nitrides or hydrogenated compounds can be directly sputtered and deposited; another approach consists in depositing the pure metal (for instance silicon in the case of silica) with an additional gas (for instance oxygen in the case of silica, nitrogen, hydrogen). Gas supply in the chamber is flow-controlled and set by the user.

Sputtering gas (and possibly additional gases) pressure in the vacuum chamber is a crucial parameter. With a too low pressure, plasma cannot be initiated or self-sustained, and with a too high pressure, layer quality can be lowered. Common pressure order of magnitude for sputter deposition is ~1 mT – 20 mT (0.13 Pa – 2.6 Pa).

### *II.C.1.03 Deposition time*

Layer thickness is directly proportional to deposition time. Deposition rate is measured on a gauge wafer during process definition, and strongly depends on the deposited material (from a few nm/hour to a few µm/hour).

Next paragraph's purpose is to (briefly) summarize the influence on the parameters above on layer micro structure reported in the literature.

## II.C.2. Sputter-deposited layers micro structure

### *II.C.2.01 Influence of atomic deposition process*

Layer growth initiation is driven by a nucleation phenomenon: due to weak attractive forces, deposited atoms trend to first form aggregates, as shown on figure 37a. As the layer grows, an effect of shadowing keeps the homogenous arriving of new atoms to perfectly fill the voids, and induces a columnar growth.

In 1986, Thornton reported a structure zone model for the description of sputtered-deposited thin film morphologies[101]. On a 3D diagram with argon pressure and substrate temperature as the parameter axes, four structures zone were identified (figure 37 b&c):

- at low temperatures (for substrates kept at room temperatures during sputtering), and higher pressures, the structure consists of tapered crystallites separated by voids and therefore porous;
- at high temperatures, and regardless of the pressure, the structure consists of columnar grains;
- at even higher temperatures (close to the melting point of the target material), and regardless of the pressure, columnar structure disappears and recrystallized grains appear;
- at intermediate temperatures, and especially as pressure decreases, a transition structure consists of densely packed fibrous grains.

*Fig. 37: sputter-deposited films structure:*

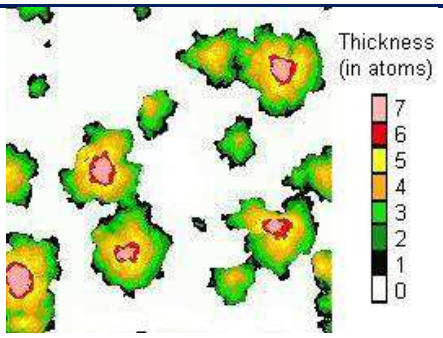


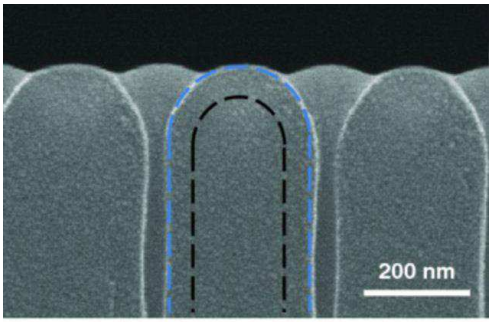


*Fig. 37a (top left): simulation of nuclear growth during the first instants of a sputter deposition*

*Fig. 37b (bottom left): SEM image of the columnar structure of sputter-deposited silica, as reported by Soo Lee[102]*

*Fig. 37c (bottom right): Thornton structure zone model[101]; $T_m$ is the target material melting point (e.g. $T/T_m$=0.15 for room-temperature-deposited silica)*

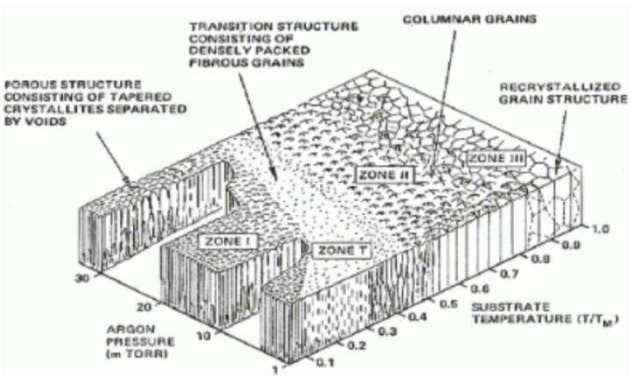

In the general context of device fabrication, where dense, homogeneous, non-porous, and smooth layers are targeted, along with low temperature depositions (for other practical reasons), this represents an obstacle to circumvent. However, in the present context, porous layers with high surface to volume ratios for adsorption are targeted, and the starting hypothesis remains valid.

### *II.C.2.02 Influence of deposition parameters*

A specific study by Bhatt in 2007 on sputtered silica is summarized on figure 38a[103]. Deposition rate was increased with increasing RF-power and increasing argon pressure, while surface roughness was increased with decreasing RF-power and decreasing film thickness (see also figure 40a). Deposition rates ranged between 4 and 18 nm/min (0.93 to 4.2 hours/µm).

Ito used spectroscopic ellipsometry and positron annihilation to determine overall volume nano porosity of sputter-deposited silica films, at various argon pressures and for various thicknesses[104]. Overall porosity was confirmed to increase along with pressure, but also with thickness (figure 38b).

Miyazaki exhibited similar results with sputter-deposited Ti-Ni films (figure 38c)[105].

Whereas it appears to be advantaging to use high deposition pressures (increased deposition rate and porosity, and decrease of argon content in the layer[106]), RF-power choice results from a compromise between greater specific surface area and faster deposition.

### *II.C.2.03 Influence of substrate structure*

In most applications, layers are deposited on flat and smooth surfaces, in a plan parallel to the target's one. In this potential specific application, not only the channel's floors, but also the side walls, are coated with a film of sputtered material. This detail appears to be in fact crucial, at least for the two following reasons:

- a study by Pulugurtha demonstrated the influence of substrate orientation (angle between target plan and substrate plan) on deposited layer structure[107]; for a 90° orientation, the columnar structure was even more pronounced, and porosity was increased in densely packed zones (figure 39a). In the present context, this implies that side-wall layers, which are deposited perpendicularly to target and substrate plan, are expected to show a higher adsorption surface than floor layers;

- due to the nature of the DRIE process (in a first approximation, very short successions of isotropic etching, which results in a vertical etching), side walls show a regular surface roughness, as shown for instance by Defforge[108] (figure 39b). This phenomenon, named scalloping, is expected to accentuate the effect of nucleation and shadowing during sputtering introduced above.

Therefore, side walls, which represent 2/3 of the coated surface, can be expected to provide enough adsorption surface, even in unfavorable deposition conditions (low pressure, high power).

*Fig. 38: influence of deposition parameters on sputter-deposited layers structure*

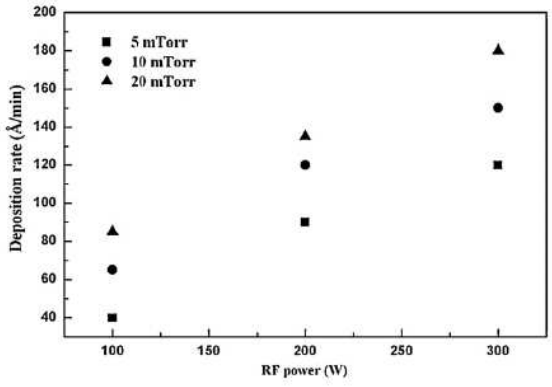


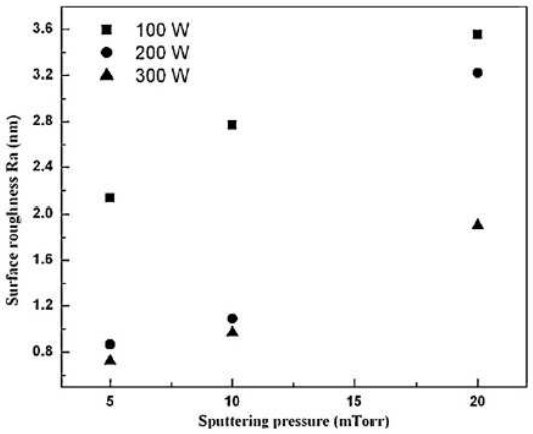


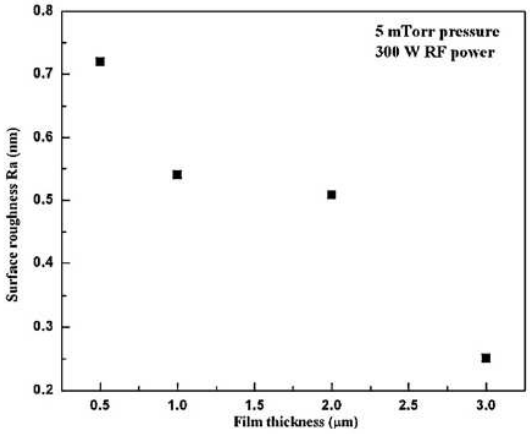


*Fig. 38a: influence of Ar pressure, RF power, and film thickness on deposition rate (left) and surface roughness (below) of sputter-deposited silica films, as reported by Bhatt[103]*

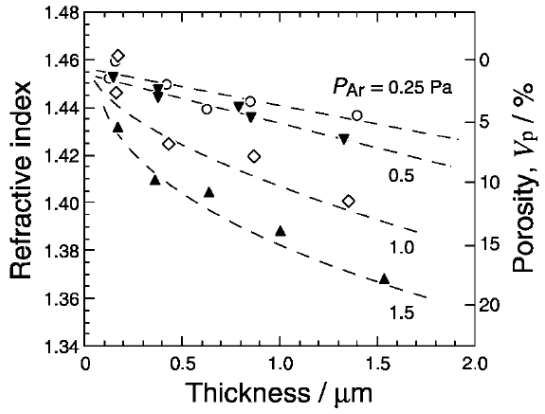


*Fig. 38b: variations of refractive index at 630 nm of RF-sputtered silica at various Ar pressure (1.9 to 11 mT) as reported by Ito[104]; overall porosity was estimated by an optical relation (Lorentz-Lorenz equation).*

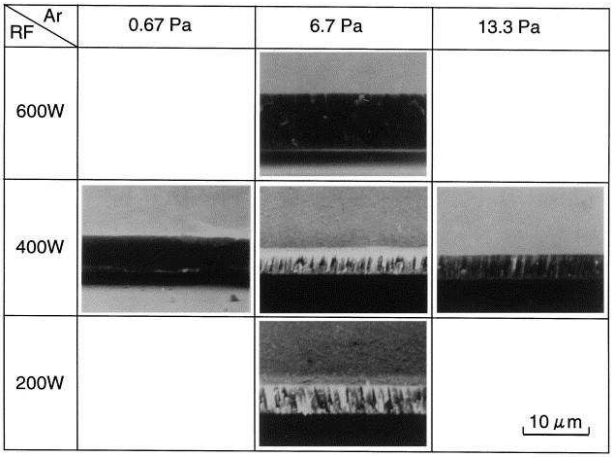


*Fig. 38c: SEM images showing the structure of Ti-Ni thin films formed under various sputtering conditions, as reported by Miyazaki[105]*

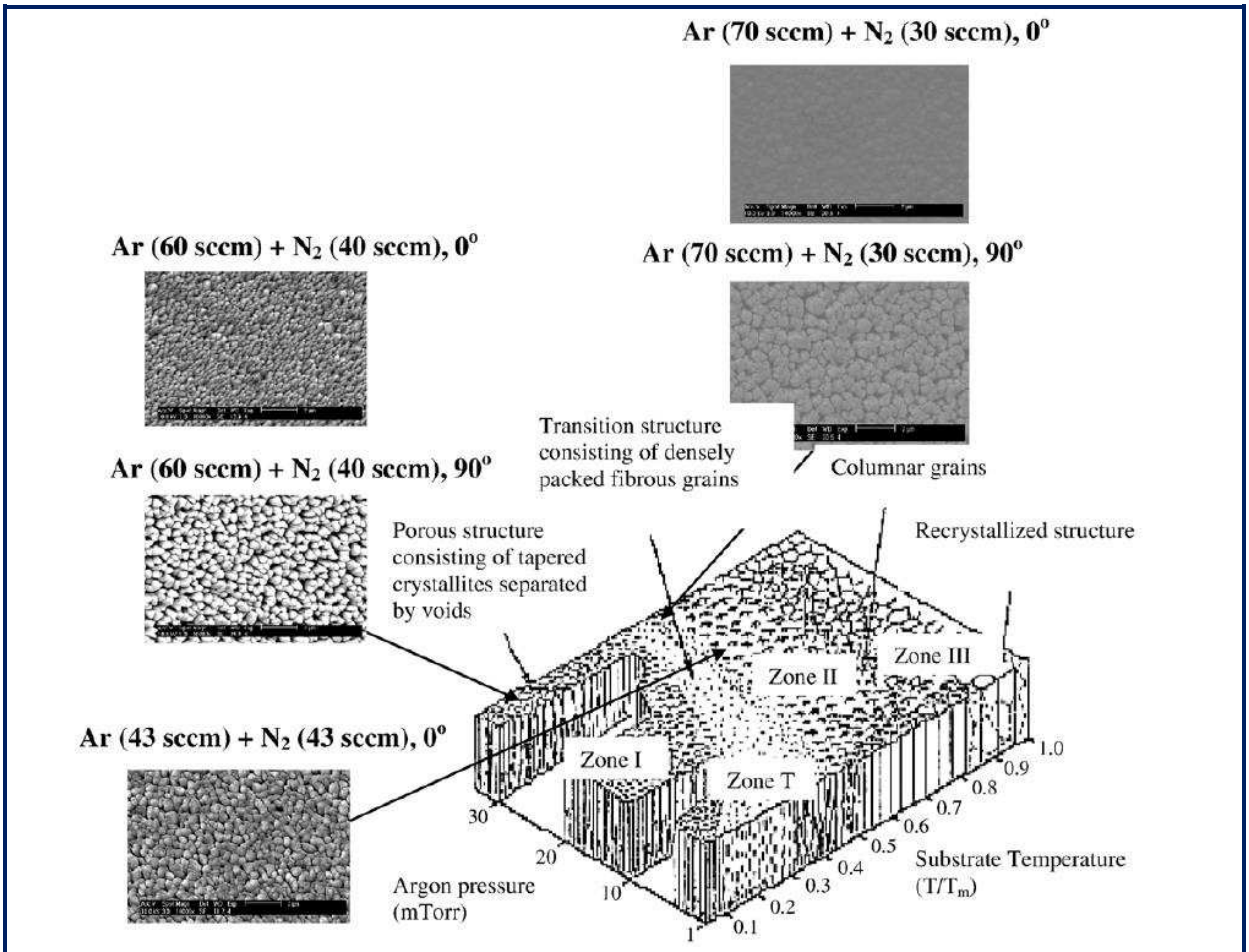


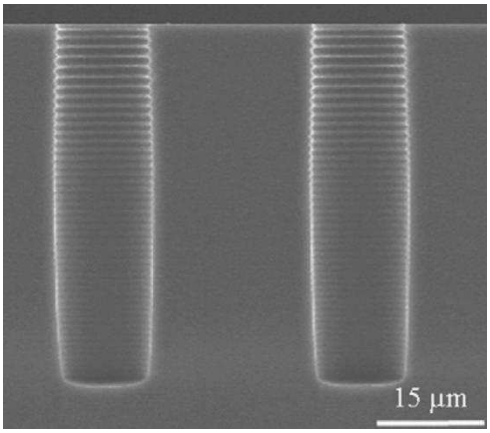


*Fig. 39: illustrations of the influence of substrate on sputter-deposited layers:*

*Fig. 39a (top): Thornton structure zone model, completed with the effect of substrate orientation on the structure of CrN sputter-deposited films (angle with target plan in °), as reported by Pulugurtha[107].*

*Fig. 39b (bottom left): SEM image of DRI-etched holes, clearly illustrating the scalloping effect (vertical surface regular roughness due to DRIE process), as reported by Defforge[108].*

## II.C.3 Chosen target materials

Three target materials appear to be the best candidates so far: silica, alumina and graphite. Two other ones were also selected: magnesia and titania. This paragraph deals with sputtering processes and/or structures obtained with these materials. However, parameters choices as described in Chapter III will be driven by sputtering machine and targets suppliers advices, and by micro processing engineers at Schlumberger and the ESIEE recommendations, as well as conventional literature reports.

### *II.C.3.01 Silica*

Silica ($SiO_2$) deposition, commonly used for the insertion of isolating layers in micro electronics, was partially described above. To complete this description, studies by Wu[109], Flamm[110] and Fujiyama[111] have to be mentioned. Silica direct deposition appears to be a better approach compared to silicon deposition under oxygen partial pressure, in the aim of porous, low-density, structures. Finally, AFM images of surface roughness by Bhatt are displayed on figure 40a.

### *II.C.3.02 Alumina*

Alumina ($Al_2O_3$) has been widely used as a wear-resistant coating for tribological applications because of its good abrasion resistance, dimensional stability, resistance to thermal shock, and mechanical strength at high temperatures. Numerous studies, such as reported by Chou[112], or Schütze[113] (see also figure 40b), described alumina deposition (with or without oxygen), with processes very similar to the ones used for silica deposition.

### *II.C.3.03 Graphite*

In the 70s-80s, there had been a growing interest for amorphous or graphite carbon thin films due to their unique combination of useful properties[114] (see figure 40d). These properties include high hardness and wear resistivity, chemical inertness to both acids and alkaline, lack of magnetic response, and an optical band gap adjustable with deposition conditions. Carbon thin films were then used as protective coatings on magnetic or optical devices. Due to major advances in carbon technologies over the past 20 years, modern carbon materials (e.g. fullerenes, carbon nanotubes, see also II.B.6.03, diamonds) and their most interesting properties, have been preferred to amorphous or graphite carbon coatings.

### *II.C.3.04 Magnesia*

Magnesium oxide (MgO), or magnesia, has well-known strong adsorption properties (for instance towards water) and has been widely used as a drying agent. Just left to aluminum and silicon in the periodic table, and commonly present as a cation in zeolites, magnesium was used as oxide in liquid chromatography for the separation of unsaturated hydrocarbons, amines and alcohols (e.g. by Nobuhara[115]). Regarding sputter-deposited magnesia examples, Vuoristo investigated layer adhesion and structure on various metal substrates[116]; Villegier reported the deposition of sputtered magnesia for the fabrication of high-quality adjustable tunnel barriers[117]; Yan, with a similar purpose, used a magnesium target under oxygen partial pressure[118]; finally, Ghekiere studied growth mechanisms[119], as shown on figure 40e.

### *II.C.3.05 Titania*

Titanium dioxide ($TiO_2$), or titania, was occasionally used in liquid[120,121], supercritical[122], and gas-solid chromatography[123]. In MEMS technology, sputter-deposited titania was for instance studied by Martin[124] (figure 40e) or Heo[125], respectively with and without additional oxygen. It needs to be highlighted here that sputter-deposited titania was recently (2011) used by Boulousis as stationary phase in micro machined silicon chips for the separation of phosphopeptides through affinity liquid chromatography[126].

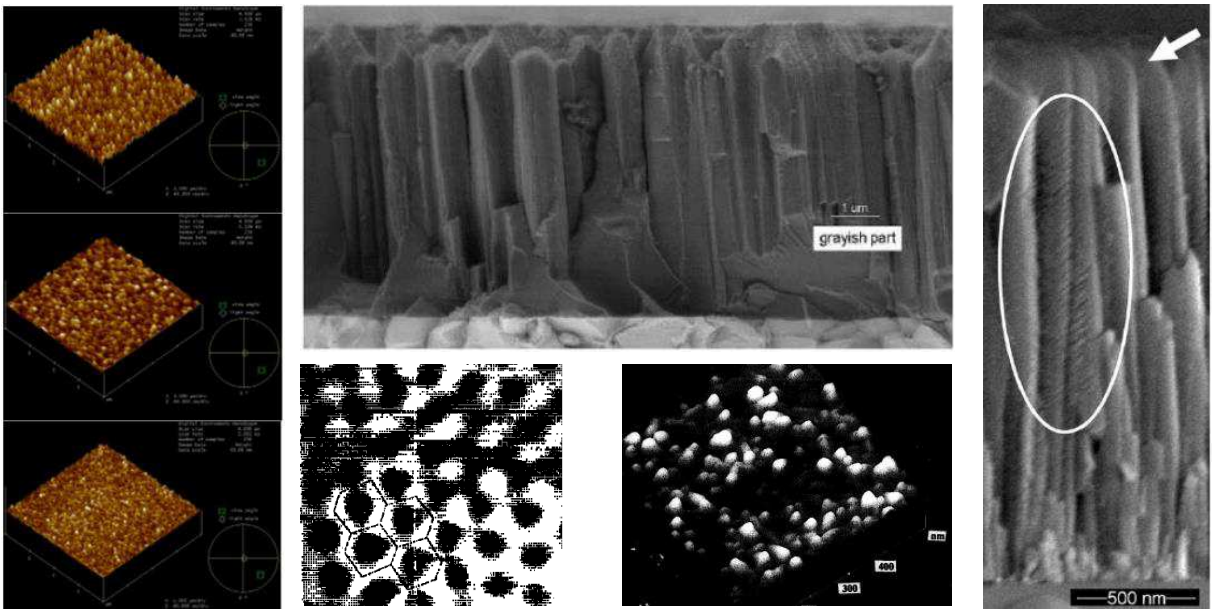


*Fig. 40a (left): AFM images of silica surface, showing the evolution of the roughness of a 5 µm-thick film along with sputtering power (100 W, 200 W, 300 W from top to bottom)[103]*
*Fig. 40b (middle top): SEM image of alumina[113]*
*Fig. 40c (right): SEM image of magnesia[119]*
*Fig. 40d (middle bottom left): STM image of graphite, with drawn hexagonal structure[114]*
*Fig. 40e (middle bottom right): AFM image of titania[124]*

*Fig. 40: various examples of sputter-deposited materials of first interest in chromatography*

### II.C.4. Conclusion

Sputter-deposited materials appear to be appropriate stationary phases in PLOT-like micro columns for the separation of light hydrocarbons. Firstly because silica, alumina and graphite are compatible with sputtering and have been widely reported in the literature, as well as magnesia and titania, to a lower extent; secondly because sputter-deposited layers are not perfectly packed and smooth (which would compromise retention), but show a columnar structure with a specific porosity, especially on the side walls of the channel. The present research work will thus endeavor to evaluate the influence of the sputtered material and of the sputtering parameters (mainly thickness and pressure) on the chromatographic properties of the columns.

Whereas a summary of micro machined columns kinetic evaluations has already been displayed in II.B.8, a summary of thermodynamic properties, and, with more accuracy, of alkanes adsorption heats, on silica, alumina and graphite is compulsory, to enable comparison with the results displayed further in this study.

## II.D. Adsorption properties of silica, alumina and graphite

Hydrocarbons adsorption mechanisms and thermodynamics on silica[127-136], alumina[136-139] and graphite[38,138,140-144] have been widely reported. In a basic approach, evaluation methods can be sorted in 3 categories: chromatographic (Van't Hoff plot of a column containing the

adsorbent as stationary phase), optical (changes in the spectroscopic properties of the adsorbent due to adsorption), and mechanical (changes in the weight of the adsorbent due to adsorption, measured by micro gravimetry).

Interactions are due to common intermolecular Van Der Waals forces between the adsorbent and the adsorbate (physisorption). Light hydrocarbons are not intrinsically polarized, but show high polarizability: in the case of polar adsorbents (here, silica, alumina, magnesia and titania), Debye forces (permanent dipole – induced dipole) between adsorbent and adsorbate prevail; in the case of non-polar adsorbents (here, graphite, which has a high polarizability[145], as well as hydrocarbons), London forces (induced dipole - induced dipole) prevail. Therefore, alkanes retention increases with polarizability, which increases with molecule size (i.e. along with number of carbon atoms and boiling point). Numerous studies reported the variation of adsorption heats of n-alkanes according to carbon number on various adsorbents, such as Kiselev[127], Dernovaya[131], or a review by Rouquerol[146] (see figure 41).

In this short section, a summary of light alkanes adsorption heats, on silica, alumina and graphite is presented, to enable comparison with the results displayed further in this study; then, the prediction of peak shape from adsorption type will be discussed; finally, the influence of hydration and column overloading will be mentioned. Discussions will focus on C1-C4 hydrocarbons each time the possibility is given.

## II.D.1. Short summary of reported adsorption heats

As shown on table 5, adsorption strength appears to increase from silica to graphite through alumina, and with specific area, in addition to increase with carbon number. Data from figure 41 and table 5 will be compared with results obtained in thermodynamic evaluation (IV.B.3.).

## II.D.2. Adsorption isotherms and prediction of peak shapes

In ideal adsorption chromatography, the distribution coefficient K is independent of the concentrations of the analyte in the mobile and in the stationary phase, and the relation between both concentrations (adsorption isotherm) is linear. In this case, the resulting chromatographic peak is symmetrical. Actually, distribution coefficient value depends on the concentrations, and the relation between them is non-linear; therefore, real adsorption isotherms generally show a slight or strong concavity or convexity near the origin, depending on the couple adsorbent-adsorbate. In the case of a concave isotherm, resulting chromatographic peak is tailing; in the case of a convex isotherm, it shows a leading front (see figure 42a)[1].

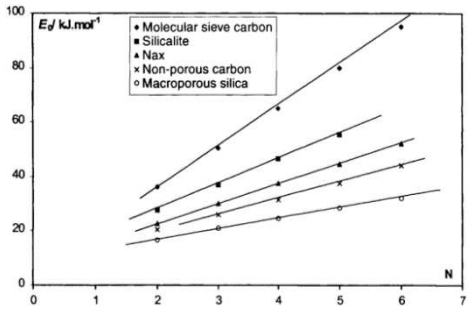


*Fig. 41: summary of linear alkanes adsorption heats for different adsorbents as a function of carbon number, by Rouquerol[146]; silicalite is a polymorph of silica having a structure analogous to the zeolites; Nax is a molecular sieve of formula Na $2Al_2O_3$ $2.45SiO_2$ $6H_2O$.*

| Ref. | Method | Adsorbent | Type (specific surface area if mentioned) | Adsorbate | Ads. heat |
|---|---|---|---|---|---|
| [127] | IGC | Silica | Mesoporous gel (720 m²/g) | C2 | 24.9 kJ/mol |
| | | | | C3 | 33.1 kJ/mol |
| | | | Macroporous gel (20 m²/g) | C2 | 16.7 kJ/mol |
| | | | | C3 | 21.8 kJ/mol |
| [128] | IGC | | Mesoporous gel (800m²/g) | C3 | 33.1 kJ/mol |
| [129] | Spe | | Macroporous gel (150 m²/g) | C5 | 23.9 kJ/mol |
| [130] | Grv | | Mesoporous gel (670 m²/g) | C4 | 39.4 kJ/mol |
| [131] | IGC | | Macroporous gel (100 m²/g) | C6 | 37.2 kJ/mol |
| [134] | Grv | | Mesoporous gel (980 m²/g) | C2 | 26.4 kJ/mol |
| | | | | C3 | 37.7 kJ/mol |
| [136] | IGC | Alumina | Mesoporous gel (20 m²/g) | C6 | 25.1 kJ/mol |
| [139] | Cpu | | - | C4 | 25.6 kJ/mol |
| [38] | IGC | Carbon | Graphite, Carbopack (8 m²/g) | C5 | 39.4 kJ/mol |
| [144] | | | Graphite, Carbobond | C2 | 34.0 kJ/mol |
| [70] | | | CNT (micro column) | C10 | 46.2 kJ/mol |

*Table 5: short summary of reported adsorption heats of light alkanes on silica, alumina and graphite; IGC=Inverse Gas Chromatography, Spe=Spectroscopy, Grv=Gravimetry, Cpu=computer modeling*

Reported studies on the adsorption of light alkanes on silica[130,132-135,147] or graphite[142] all converge to the same conclusion: adsorption isotherms are pronouncedly concave, and slight or strong peak tailing is common in adsorption chromatography of hydrocarbons on silica, alumina, or graphite. This phenomenon will be mentioned during the evaluation of chromatographic properties of the columns fabricated in this research work. Indeed, peak non-ideality can be both due to kinetic phenomena (peak broadening because of extra-column effects, of channel and tubing shape, and of stationary phase layout), and to thermodynamic phenomena (peak tailing due to non-linear adsorption isotherm, hysteresis effects between adsorption and desorption).

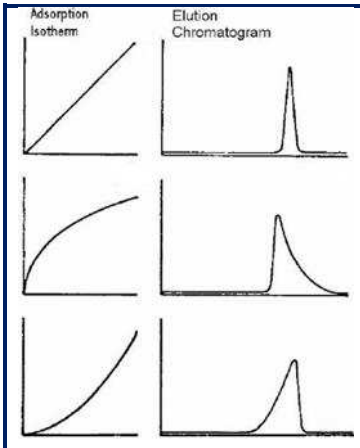


*Fig. 42a: schematic relation between adsorption isotherm type (from top to bottom: linear, concave, convex) and peak shape (symmetric, tailing, leading).*

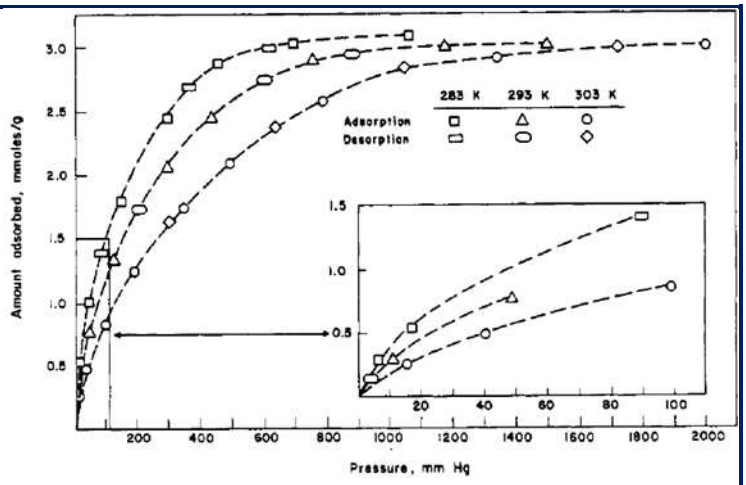


*Fig. 42b: adsorption and desorption isotherms of C4 on silica gel, as reported by Al-Sahhaf[130]; concavity is strongly marked.*

*Fig. 42: adsorption isotherms and peak shapes*

### II.D.3. Effects of hydration and overloading

Water undesired adsorption affects retention properties of the gas chromatography column; the drop of adsorption heat of polyethylene particles on silica surfaces for different degrees of hydration was for instance quantitatively studied by Nalaskowski through AFM[148]. In the present context of oilfield environment, the presence of water and the effects of hydration have to be taken into account. And more generally, the activation or reactivation of polar adsorbents such as silica or alumina prior to use is highly recommended by the literature, for instance by flushing the column with carrier gas (dry and inert) in the oven above 100°C, to remove the adsorbed water[1].

Column overloading also modifies thermodynamic properties of the column; non-linear changes in partition coefficient along with concentrations close of saturation points were as well reported, especially for silica[130]. Although minimal concentrations possible were used in the present work, definitive conclusions on peak asymmetries cannot be proposed in the absence of thorough quantitative analysis (as mentioned in I.G.).

### II.D.4. Conclusions

Standard and relatively similar values of adsorption heats of light hydrocarbons on silica, alumina, and graphite were exhibited to enable comparison of thermodynamic performances of sputtered silica, alumina and graphite as stationary phases for micro columns. A tailing shape is expected for chromatographic peaks of light hydrocarbons on those stationary phases. Adsorbent hydration by water has to be taken into account.

Before the general conclusion of this literature review, a few references on XXXXXXXXXX technology will be given in the following section.

## II.E. Schlumberger confidential section

## Conclusion

In this literature review, it has first been shown that porous-layer open tubular columns with silica, alumina, or graphite as stationary phases, have been commonly used in gas chromatography for the separation of very volatile hydrocarbons.

In the main section dedicated to micro gas chromatography, it clearly appeared that numerous and successful efforts have been made to relevantly miniaturize the technology, including column fabrication process, fast heating enabling, up- and downstream components design and integration, and computer modeling. However, stationary phase

insertion processes were mainly transferred from conventional gas chromatography and seemed to be barely compatible with collective fabrication and C1-C5 fast separations. In a few cases, interesting PLOT-mimicking approaches were reported (polymer plasma sputtering, chemically-grown carbon nanotubes, functionalized electro-deposited gold), but showed similar drawbacks. Kinetic performances of reported micro columns were basically summarized.

Sputtering as a potential solution was then introduced: indeed, this deposition technique is fully compatible with batch fabrication, and silica, alumina, graphite, but also magnesia and titania, have commonly been used as target materials in micro systems fabrication; moreover, it has been demonstrated that sputter-deposited layers can show a porous columnar structure, which is even enhanced on the side walls of the channels and with appropriate sputtering parameters.

To enable thermodynamic evaluation and comparison of sputter-deposited layers, general adsorption properties of silica, alumina and graphite towards light alkanes were summarized. This section also gave indications on expected chromatographic peak shapes and layer hydration effect.

Finally, a significant application in which this research work could perfectly fit (in case of success) was presented. Thus, the demonstrated interest of the academic community for the topic was completed with a challenging industrial objective.

To make an end of this review, it has to be mentioned that mass-produced, low bulk and low thermal mass micro columns perfectly fit in multidimensional chromatography challenges, as early suggested by Agah[57] in 2006, or most recently developed by Liu[154] (2012) or Chen[155] (2013), as shown on figure 44. With this approach, analyses accuracy and throughput could be even more improved.

*Fig. 44: multidimensional micro gas chromatography as an analysis quality and speed enhancer*

*Fig. 44a (top right): as suggested by Agah[57]*
*Fig. 44b (bottom left): as developed by Liu[154]*
*Fig. 44c (bottom right): as developed by Chen[155]*

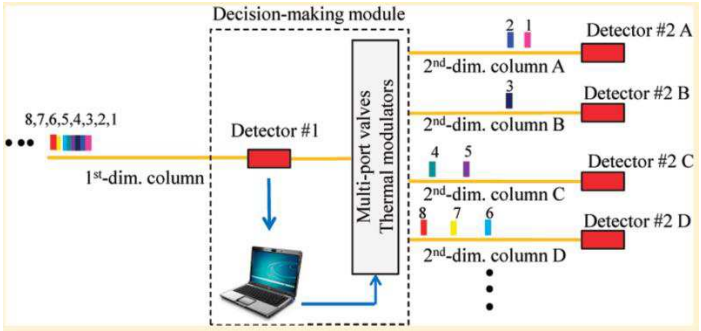


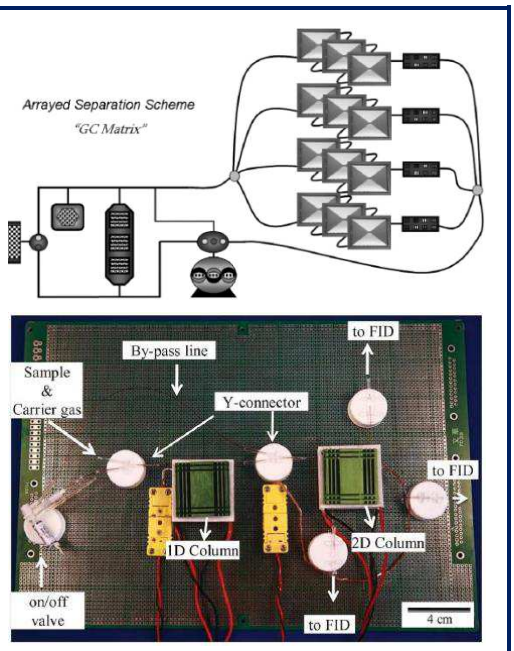

# Bibliography

[1] J. Tranchant, *Manuel pratique de chromatographie en phase gazeuse*, Masson, 4th edition, **1995**.

[2] J. Cazes and R. P. W. Scott, *Chromatography theory*, Marcel Dekker Inc., 1st edition, **2002**.

[3] J. A. Rijks and C. A. Cramers, *Chromatographia*, **1974**, *7 (3)*, 99-106.

[4] C. D. Wick, J. I. Siepmann, W. L. Klotz and M. R. Schure, *Journal of Chromatography A*, **2002**, *954 (1–2)*, 181-190.

[5] J. K. Haken, *Journal of Chromatography A*, **1977**, *141 (3)*, 247-288.

[6] J. K. Haken, *Journal of Chromatography A*, **1984**, *300 (C)*, 1-77.

[7] W. Averill and L. S. Ettre, *Nature*, **1962**, *196 (4860)*, 1198-1199.

[8] H. W. Patton, J. S. Lewis and W. I. Kaye, *Analytical Chemistry*, **1955**, *27 (2)*, 170-174.

[9] S. A. Greene, *Analytical Chemistry*, **1957**, *29 (7)*, 1055.

[10] A. V. Kiselev, Y. U. S. Nikitin, R. S. Petrova, K. D. Shcherbakova and Y. A. I. Yashin, *Analytical Chemistry*, **1964**, *36 (8)*, 1526-1533.

[11] L. R. Snyder, *Separation Science*, **1966**, *1 (2-3)*, 191-218.

[12] S. A. Greene, M. L. Moberg and E. M. Wilson, *Analytical Chemistry*, **1956**, *28 (9)*, 1369-1370.

[13] R. L. Hoffmann, G. R. List and C. D. Evans, *Journal of the American Oil Chemists' Society*, **1966**, *43 (12)*, 675-677.

[14] R. L. Hoffmann and C. D. Evans, *Analytical Chemistry*, **1966**, *38 (10)*, 1309-1312.

[15] A. Di Corcia, A. Liberti and R. Samperi, *Journal of Chromatography A*, **1978**, *167 (C)*, 243-252.

[16] A. D. Corcia, *Analytical Chemistry*, **1978**, *50 (7)*, 1000-1003.

[17] K. A. Smith and R. J. Dowdell, *Journal of Chromatographic Science*, **1973**, *11 (12)*, 655-658.

[18] F. Garilli, L. Fabiani, U. Filia and V. Cusi, *Journal of Chromatography A*, **1973**, *77 (1)*, 3-10.

[19] T. G. Andronikashvili, V. G. Berezkin, N. A. Nadiradze and L. Y. Laperashvili, *Journal of Chromatography A*, **1986**, *365 (C)*, 269-277.

[20] M. Papic, *Journal of Chromatographic Science*, **1968**, *6 (9)*, 493-494.

[21] V. S. Nayak and R. N. Pandey, *Journal of Chromatographic Science*, **1990**, *28 (12)*, 617-620.

[22] A. G. Datar, P. S. Ramanathan and M. Sankar Das, *Indian J Technol*, **1974**, *12 (3)*, 127-129.

[23] R. J. Jonker, H. Poppe and J. F. K. Huber, *Analytical Chemistry*, **1982**, *54 (14)*, 2447-2456.

[24] L. H. Henrich, *Journal of Chromatographic Science*, **1988**, *26 (5)*, 198-205.

[25] Z. Ji, R. E. Majors and E. J. Guthrie, *Journal of Chromatography A*, **1999**, *842 (1–2)*, 115-142.

[26] V. G. e. Berezkin and J. De Zeeuw, *Capillary gas adsorption chromatography*, **2008**.

[27] M. Mohnke and W. Saffert, in *Fourth International Gas Chromatography Symposium*, **1962**.

[28] D. L. Petitjean and C. J. Leftault, *Journal of Chromatographic Science*, **1963**, *1 (3)*, 18-21.

[29] R. D. Schwartz, D. J. Brasseaux and G. R. Shoemake, *Analytical Chemistry*, **1963**, *35 (4)*, 496-499.

[30] R. C. M. de Nijs, *HRC & CC. Journal of high resolution chromatography & chromatography communications*, **1981**, *4 (12)*, 612-615.

[31] J. J. Kirkland, *Analytical Chemistry*, **1963**, *35 (9)*, 1295-1297.

[32] N. Ishizuka, H. Minakuchi, K. Nakanishi, N. Soga, H. Nagayama, K. Hosoya and N. Tanaka, *Analytical Chemistry*, **2000**, *72 (6)*, 1275-1280.

[33] N. Ishizuka, H. Minakuchi, K. Nakanishi, K. Hirao and N. Tanaka, *Colloids and Surfaces A: Physicochemical and Engineering Aspects*, **2001**, *187–188 (0)*, 273-279.

[34] A. A. Korolev, V. E. Shiryaeva, T. P. Popova and A. A. Kurganov, *Russ. J. Phys. Chem.*, **2006**, *80 (4)*, 609-614.

[35] A. A. Korolev, V. E. Shiryaeva, T. P. Popova and A. A. Kurganov, *Journal of Analytical Chemistry*, **2007**, *62 (4)*, 313-318.

[36] W. J. Havenga and E. R. Rohwer, *Journal of High Resolution Chromatography*, **1992**, *15 (6)*, 381-386.

[37] F. Bruner, L. Lattanzi, F. Mangani and M. Attaran Rezaii, *Chromatographia*, **1994**, *38 (1-2)*, 98-108.

[38] F. Bruner, G. Bertoni and P. Ciccioli, *Journal of Chromatography A*, **1976**, *120 (2)*, 307-319.

[39] C. Saridara and S. Mitra, *Analytical Chemistry*, **2005**, *77 (21)*, 7094-7097.

[40] Y. I. Yashin and A. Y. Yashin, *Journal of Analytical Chemistry*, **2001**, *56 (9)*, 794-805.

[41] A. de Mello, *Lab on a Chip*, **2002**, *2 (3)*, 48N-54N.

[42] K. D. Wise, *Sensors and Actuators A: Physical*, **2007**, *136 (1)*, 39-50.

[43] I. Azzouz, J. Vial, D. Thiébaut, R. Haudebourg, K. Danaie, P. Sassiat and J. Breviere, *Anal Bioanal Chem*, **2013**, 1-14.

[44] A. Wang, H. D. Tolley and M. L. Lee, *Journal of Chromatography A*, **2012**, *1261*, 46-57.

[45] P. A. Smith, *Journal of Chromatography A*, **2012**, *1261*, 37-45.

[46] S. C. Terry, J. H. Jerman and J. B. Angell, *IEEE Transactions on Electron Devices*, **1979**, *26 (12)*, 1880-1886.

[47] S. Hannoe, I. Sugimoto, K. Yanagisawa and H. Kuwano, in *International Conference on Solid-state Sensors and Actuators*, **1997**, 515-518.

[48] R. W. Tjerkstra, M. de Boer, E. Berenschot, J. G. E. Gardeniers, A. van den Berg and M. C. Elwenspoek, *Electrochimica Acta*, **1997**, *42 (20–22)*, 3399-3406.

[49] M. J. De Boer, R. W. Tjerkstra, J. W. Berenschot, H. V. Jansen, G. J. Burger, J. G. E. Gardeniers, M. Elwenspoek and A. Van den Berg, *Microelectromechanical Systems, Journal of*, **2000**, *9 (1)*, 94-103.

[50] J. A. Potkay, G. R. Lambertus, R. D. Sacks and K. D. Wise, *Journal of Microelectromechanical Systems*, **2007**, *16 (5)*, 1071-1079.

[51] A. D. Radadia, R. D. Morgan, R. I. Masel and M. A. Shannon, *Analytical Chemistry*, **2009**, *81 (9)*, 3471-3477.

[52] R. S. Pai, D. R. Mott, J. L. Stepnowski, R. A. McGill, B. A. Higgins and D. L. Simonson, in *Technologies for Homeland Security, 2008 IEEE Conference on*, **2008**, 150-154.

[53] A. C. Lewis, J. F. Hamilton, C. N. Rhodes, J. Halliday, K. D. Bartle, P. Homewood, R. J. P. Grenfell, B. Goody, A. M. Harling, P. Brewer, G. Vargha and M. J. T. Milton, *Journal of Chromatography A*, **2010**, *1217 (5)*, 768-774.

[54] C. M. Yu, M. Lucas, J. C. Koo, P. Stratton, T. DeLima and E. Behymer, in *Micro-Electro-Mechanical Systems*, **1998**, 481-486.

[55] C. M. Matzke, R. J. Kottenstette, S. A. Casalnuovo, G. C. Frye-Mason, M. L. Hudson, D. Y. Sasaki, R. P. Manginell and C. C. Wong, in *SPIE Conference on Micromachining and Microfabrication Process Technology*, **1998**, 262-268.

[56] M. Agah, J. A. Potkay, G. Lambertus, R. Sacks and K. D. Wise, *Journal of Microelectromechanical Systems*, **2005**, *14 (5)*, 1039-1050.

[57] M. Agah, G. R. Lambertus, R. Sacks and K. Wise, *Journal of Microelectromechanical Systems*, **2006**, *15 (5)*, 1371-1378.

[58] J. Sun, D. Cui, Y. Li, L. Zhang, J. Chen, H. Li and X. Chen, *Sensors and Actuators B: Chemical*, **2009**, *141 (2)*, 431-435.

[59] J. Sun, D. Cui, H. Cai, H. Li, X. Chen, L. Du and L. Zhang, *Sensor Letters*, **2011**, *9 (2)*, 655-658.

[60] S. Ali, M. Ashraf-Khorassani, L. T. Taylor and M. Agah, *Sensors and Actuators B: Chemical*, **2009**, *141 (1)*, 309-315.

[61] S. Nishiyama, T. Nakai, M. Shuzo, J. J. Delaunay and I. Yamada, in *IEEE*, **2009**, 1935-1938.

[62] J. Sun, D. Cui, X. Chen, L. Zhang, H. Cai and H. Li, *Journal of Chromatography A*, **2013**, *1291 (0)*, 122-128.

[63] A. D. Radadia, A. Salehi-Khojin, R. I. Masel and M. A. Shannon, *Sensors and Actuators, B: Chemical*, **2010**, *150 (1)*, 456-464.

[64] M. Baroncini, P. Placidi, A. Scorzoni, G. Cardinali, L. Dori and S. Nicoletti, in *VLSI Technology, Systems, and Applications, 2001. Proceedings of Technical Papers. 2001 International Symposium on*, **2001**, 164-167.

[65] K. Zhang, S. Chou and S. Ang, *International Journal of Thermal Sciences*, **2007**, *46 (6)*, 580-588.

[66] J. Lee, H.-Y. Lee, S.-E. Moon, J.-H. Kwak, S.-J. Park, J.-H. Park, K.-H. Park and J. Kim, in *Nanotechnology, 2008. NANO'08. 8th IEEE Conference on*, **2008**, 476-479.

[67] P. K. Pasupuleti, thesis submitted for the Degree of Master of Science at the Graduate Faculty of the Louisiana State University, USA, D$^{pmt}$ of Mechanical Engineering, **2005**.

[68] S. Roy, T. Majhi, A. Kundu, C. Sarkar and H. Saha, *Sensor Letters*, **2011**, *9 (4)*, 1382-1389.

[69] J. Luong, H. Cai, R. Gras and J. Curvers, *Journal of Chromatographic Science*, **2012**, *50 (3)*, 245-252.

[70] V. R. Reid, M. Stadermann, O. Bakajin and R. E. Synovec, *Talanta*, **2009**, *77 (4)*, 1420-1425.

[71] M. Stadermann, A. D. McBrady, B. Dick, V. R. Reid, A. Noy, R. E. Synovec and O. Bakajin, *Analytical Chemistry*, **2006**, *78 (16)*, 5639-5644.

[72] C. J. Lu, W. H. Steinecker, W. C. Tian, M. C. Oborny, J. M. Nichols, M. Agah, J. A. Potkay, H. K. L. Chan, J. Driscoll, R. D. Sacks, K. D. Wise, S. W. Pang and E. T. Zellers, *Lab on a Chip - Miniaturisation for Chemistry and Biology*, **2005**, *5 (10)*, 1123-1131.

[73] J. H. Jerman and S. C. Terry, *Environment International*, **1981**, *5 (2)*, 77-83.

[74] M. W. Bruns, in *Proceedings of the 1992 International Conference on Industrial Electronics, Control, Instrumentation, and Automation*, **1992**, 1640-1644 vol.3.

[75] K. Nachef, T. Bourouina, F. Marty, K. Danaie, B. Bourlon and E. Donzier, *Microelectromechanical Systems, Journal of*, **2010**, *19 (4)*, 973-981.

[76] K. Nachef, P. Guieze, E. Donzier and B. Bourlon, 20120021529, **2012**.

[77] B. C. Kaanta, W. H. Steinecker, O. Zhdaneev, G. R. Lambertus, H. Chen, X. Zhang, B. Bourlon and E. Donzier, WO/2011/044547, **2011**.

[78] S. Narayanan, B. Alfeeli and M. Agah, in *Proc. Eurosensors XXIV*, **2010**, 29-32.

[79] K. Reddy, J. Liu, M. K. K. Oo and X. Fan, **2012**.

[80] G. Serrano, T. Sukaew and E. T. Zellers, *Journal of Chromatography A*, **2013**, *1279 (0)*, 76-85.

[81] S. Sorge and T. Pechstein, *Sensors and Actuators, A: Physical*, **1997**, *63 (3)*, 191-195.

[82] D. Cruz, J. P. Chang, S. K. Showalter, F. Gelbard, R. P. Manginell and M. G. Blain, *Sensors and Actuators, B: Chemical*, **2007**, *121 (2)*, 414-422.

[83] S. Zimmermann, S. Wischhusen and J. Mueller, in *SPIE Conference on Micromachined Devices and Components*, **1999**, 238-245.

[84] S. Zampolli, I. Elmi, J. Stürmann, S. Nicoletti, L. Dori and G. C. Cardinali, *Sensors and Actuators, B: Chemical*, **2005**, *105 (2)*, 400-406.

[85] S. Zampolli, I. Elmi, F. Mancarella, P. Betti, E. Dalcanale, G. C. Cardinali and M. Severi, *Sensors and Actuators, B: Chemical*, **2009**, *141 (1)*, 322-328.

[86] C. Saridara, S. Ragunath, Y. Pu and S. Mitra, *Analytica Chimica Acta*, **2010**, *677 (1)*, 50-54.

[87] G. E. Spangler, *Journal of Microcolumn Separations*, **2001**, *13 (7)*, 285-292.

[88] J. Vangelooven and G. Desmet, *Journal of Chromatography A*, **2010**, *1217 (52)*, 8121-8126.

[89] C. C. Wong, D. R. Adkins, G. C. Frye-Mason, M. L. Hudson, R. Kottenstette, C. M. Matzke, J. N. Shadid and A. G. Salinger, in *SPIE Conference on Microfluidic Devices and Systems II*, **1999**, 120-129.

[90] K. Chen and Y. E. Wu, *Sensors and Actuators, A: Physical*, **2000**, *79 (3)*, 211-218.

[91] S. Reidy, G. Lambertus, J. Reece and R. Sacks, *Analytical Chemistry*, **2006**, *78 (8)*, 2623-2630.

[92] M. Nishino, Y. Takemori, S. Matsuoka, M. Kanai, T. Nishimoto, M. Ueda and K. Komori, *IEEJ Transactions on Electrical and Electronic Engineering*, **2009**, *4 (3)*, 358-364.

[93] L. Lorenzelli, A. Benvenuto, A. Adami, V. Guarnieri, B. Margesin, V. Mulloni and D. Vincenzi, *Biosensors and Bioelectronics*, **2005**, *20 (10 SPEC. ISS.)*, 1968-1976.

[94] I. Azzouz, J. Vial, D. Thiebaut, P. Sassiat, F. Marty, K. Danaie, M. Bockrath, J. Wong, R. Haudebourg and B. Bourlon, *Spectra Analyse*, **2011**, *282*, 46-51.

[95] J. Sturmann, W. Benecke, S. Zampolli, I. Elmi, G. C. Cardinali and W. Lang, in *Solid-State Sensors, Actuators and Microsystems, 2005. Digest of Technical Papers. TRANSDUCERS '05. The 13th International Conference on*, **2005**, 2083-2086 Vol. 2.

[96] T. Nakai, J. Okawa, S. Takada, M. Shuzo, J. Shiomi, J. J. Delaunay, S. Maruyama and I. Yamada, in *Olfaction and Electronic Nose: Proceedings of the 13 International Symposium*, **2009**, 249-252.

[97] I. Azzouz, thesis submitted for the Degree of Doctor in Philosophia at the University Pierre et Marie Curie of Paris, France, D$^{pmt}$ of Analytical Chemistry, **2013**.

[98] C. Frye-Mason, R. P. Manginell, E. J. Heller, C. M. Matzke, S. A. Casalnuovo, V. M. Hietala, R. J. Kottenstette, P. R. Lewis and C. C. Wong, in *Microprocesses and Nanotechnology Conference, 1999. Digest of Papers. Microprocesses and Nanotechnology '99. 1999 International*, **1999**, 60-61.

[99] L. Hintikka, M. Haapala, S. Franssila, T. Kuuranne, A. Leinonen and R. Kostiainen, *Journal of Chromatography A*, **2010**, *1217 (52)*, 8290-8297.

[100] H. Shakeel, G. Rice and M. Agah, in *Micro Electro Mechanical Systems (MEMS), 2012 IEEE 25th International Conference on*, **2012**, 823-826.

[101] J. A. Thornton, *Journal of Vacuum Science & Technology A: Vacuum, Surfaces, and Films*, **1986**, *4 (6)*, 3059-3065.

[102] U. Soo Lee, J. Sik Choi, B. Seob Yang, S. Oh, Y. Jang Kim, M. Sook Oh, J. Heo and H. Joon Kim, *ECS Solid State Letters*, **2013**, *2 (6)*, R13-R15.

[103] V. Bhatt and S. Chandra, *Journal of Micromechanics and Microengineering*, **2007**, *17 (5)*, 1066-1077.

[104] K. Ito, R. Yu, Y. Kobayashi, K. Sato, K. Hirata, H. Togashi, Y. Michida, R. Suzuki and T. Ohdaira, *Nippon Seramikkusu Kyokai Gakujutsu Ronbunshi/Journal of the Ceramic Society of Japan*, **2004**, *112 (1306)*, 338-341.

[105] S. Miyazaki and A. Ishida, *Materials Science and Engineering: A*, **1999**, *273–275 (0)*, 106-133.

[106] G. C. Schwartz and R. E. Jones, *IBM Journal of Research and Development*, **1970**, *14 (1)*, 52-60.

[107] S. R. Pulugurtha, D. G. Bhat, M. H. Gordon and J. Shultz, *Surface and Coatings Technology*, **2007**, *202 (4–7)*, 755-761.

[108] T. Defforge, X. Song, G. Gautier, T. Tillocher, R. Dussart, S. Kouassi and F. Tran-Van, *Sensors and Actuators A: Physical*, **2011**, *170 (1–2)*, 114-120.

[109] W. F. Wu and B. S. Chiou, *Applied Surface Science*, **1996**, *99 (3)*, 237-243.

[110] D. Flamm, F. Frost and D. Hirsch, *Applied Surface Science*, **2001**, *179 (1–4)*, 95-101.

[111] H. Fujiyama, T. Sumomogi and T. Endo, *Journal of Vacuum Science and Technology, Part A: Vacuum, Surfaces and Films*, **2002**, *20 (2)*, 356-361.

[112] T. C. Chou, T. G. Nieh, S. D. McAdams and G. M. Pharr, *Scripta Metallurgica et Materiala*, **1991**, *25 (10)*, 2203-2208.

[113] A. Schütze and D. T. Quinto, *Surface and Coatings Technology*, **2003**, *162 (2–3)*, 174-182.

[114] N. H. Cho, D. K. Veirs, J. W. Ager, M. D. Rubin, C. B. Hopper and D. B. Bogy, *Journal of Applied Physics*, **1992**, *71 (5)*, 2243-2248.

[115] K. Nobuhara, M. Kato, M. Nakamura, M. Takami and S. Kaneko, *Journal of Chromatography A*, **1995**, *704 (1)*, 45-53.

[116] P. Vuoristo, T. Mantyla and P. Kettunen, *Journal of Vacuum Science & Technology A: Vacuum, Surfaces, and Films*, **1986**, *4 (6)*, 2932-2937.

[117] J. C. Villegier, M. Radparvar, L. Yu and S. M. Faris, *Magnetics, IEEE Transactions on*, **1989**, *25 (2)*, 1227-1230.

[118] L. Yan, C. M. Lopez, R. P. Shrestha, E. A. Irene, A. A. Suvorova and M. Saunders, *Applied Physics Letters*, **2006**, *88 (14)*, 142901-142901-3.

[119] P. Ghekiere, S. Mahieu, G. De Winter, R. De Gryse and D. Depla, *Thin Solid Films*, **2005**, *493 (1–2)*, 129-134.

[120] M. Zaharescu, T. Cserháti and E. Forgács, *Journal of Liquid Chromatography and Related Technologies*, **1997**, *20 (18)*, 2997-3007.

[121] J. Ge, L. Zhao, L. R. Chen and Y. P. Shi, *Journal of Chromatographic Science*, **2010**, *48 (1)*, 29-34.

[122] R. E. Paproski, J. Cooley and C. A. Lucy, *Journal of Chromatography A*, **2005**, *1095 (1-2)*, 156-163.

[123] G. J. S. Vint and C. S. G. Phillips, *Journal of Chromatography A*, **1984**, *292 (1)*, 263-271.

[124] N. Martin, C. Rousselot, C. Savall and F. Palmino, *Thin Solid Films*, **1996**, *287 (1–2)*, 154-163.

[125] C. H. Heo, S.-B. Lee and J.-H. Boo, *Thin Solid Films*, **2005**, *475 (1–2)*, 183-188.

[126] G. Boulousis, K. Tsougeni, K. Ellinas, A. Speliotis, A. Tserepi and E. Gogolides, in *Proc. Eurosensors XXV*, **2011**, 717-720.

[127] A. V. Kiselev and Y. I. Yashin, *Petroleum Chemistry U.S.S.R.*, **1965**, *4 (3)*, 221-228.

[128] J. J. Haydel and R. Kobayashi, *Industrial & Engineering Chemistry Fundamentals*, **1967**, *6 (4)*, 546-554.

[129] W. Hertl and M. L. Hair, *The Journal of Physical Chemistry*, **1968**, *72 (13)*, 4676-4682.

[130] T. A. Al-Sahhaf, E. D. Sloan and A. L. Hines, *Industrial & Engineering Chemistry Process Design and Development*, **1981**, *20 (4)*, 658-662.

[131] L. I. Dernovaya and Y. A. Eltekov, *Journal of Chromatography A*, **1990**, *520 (0)*, 47-54.

[132] C. A. Grande and A. E. Rodrigues, *Industrial & Engineering Chemistry Research*, **2001**, *40 (7)*, 1686-1693.

[133] M. A. Hernández, J. A. Velasco, M. Asomoza, S. Solís, F. Rojas, V. H. Lara, R. Portillo and M. A. Salgado, *Energy & Fuels*, **2003**, *17 (2)*, 262-270.

[134] B. L. Newalkar, N. V. Choudary, U. T. Turaga, R. P. Vijayalakshmi, P. Kumar, S. Komarneni and T. S. G. Bhat, *Microporous and Mesoporous Materials*, **2003**, *65 (2–3)*, 267-276.

[135] H. Vinh-Thang, Q. Huang, M. Eić, D. Trong-On and S. Kaliaguine, *Langmuir*, **2005**, *21 (11)*, 5094-5101.

[136] S. Faramawy, A. Y. El-Naggar, A. M. El-Fadly, S. M. El-Sabagh and A. A. Ibrahim, *Arabian Journal of Chemistry*, **2011**.

[137] L. H. Klemm and S. K. Airee, *Journal of Chromatography A*, **1964**, *13 (C)*, 40-47.

[138] G. L. Hargrove and D. T. Sawyer, *Analytical Chemistry*, **1968**, *40 (2)*, 409-413.

[139] P. de Sainte Claire, K. C. Hass, W. F. Schneider and W. L. Hase, *The Journal of Chemical Physics*, **1997**, *106 (17)*, 7331-7342.

[140] L. A. Kartsova and A. A. Makarov, *Russian Journal of Applied Chemistry*, **2002**, *75 (11)*, 1725-1731.

[141] I. Halasz and C. Horvath, *Analytical Chemistry*, **1964**, *36 (7)*, 1178-1186.

[142] J. H. Clint, *Journal of the Chemical Society, Faraday Transactions 1: Physical Chemistry in Condensed Phases*, **1972**, *68 (0)*, 2239-2246.

[143] M. A. Castro, S. M. Clarke, A. Inaba, T. Arnold and R. K. Thomas, *The Journal of Physical Chemistry B*, **1998**, *102 (51)*, 10528-10534.

[144] C. Szopa, R. Sternberg, D. Coscia, F. Raulin and C. Vidal-Madjar, *Journal of Chromatography A*, **2000**, *904 (1)*, 73-85.

[145] C. Vidal-Madjar and E. Bekassy-Molnar, *The Journal of Physical Chemistry*, **1984**, *88 (2)*, 232-238.

[146] J. Rouquerol, F. Rouquerol and K. S. W. Sing, *Adsorption by powders and porous solids*, Academic Press, 1st edition, **1998**.

[147] M.-G. Olivier and R. Jadot, *Journal of Chemical & Engineering Data*, **1997**, *42 (2)*, 230-233.

[148] J. Nalaskowski, J. Drelich, J. Hupka and J. D. Miller, *Langmuir*, **2003**, *19 (13)*, 5311-5317.



[154] J. Liu, M. K. Khaing Oo, K. Reddy, Y. B. Gianchandani, J. C. Schultz, H. M. Appel and X. Fan, *Analytical Chemistry*, **2012**, *84 (9)*, 4214-4220.

[155] B. X. Chen, T. Y. Hung, R. S. Jian and C. J. Lu, *Lab on a Chip*, **2013**, *13 (7)*, 1333-1341.

# III. Materials and methods

This chapter is dedicated to the detailed description of the materials and methods used in this study for the different types of evaluations of the micro columns. To this purpose, micro columns fabrication will first be described, from computer designing to bench completion through micro processing, followed by hard- and software developments for temperature-programming; then, chromatographic setups, including samples, and columns evaluation methods will be specified; finally, the attempt of XXXXXXXXXXX will be reported.

⌦ Possible troubles encountered during the implementations of these methods will naturally also be described, and indicated with the preceding symbol.

At the end of this chapter, the reader will find a useful summary of evaluated columns.

## III.A. Micro columns fabrication

Whole column fabrication process is presented in this section, including computer drawing of the masks, clean room micro machining at the ESIEE and at MEMS TC, and provisional column completion (electric and fluidic connections). This section will be completed by SEM images of fabricated columns, and with observed limitations in the fabrication process.

### III.A.1. Computer designing

#### *III.A.1.01 Columns*

Columns were drawn at MEMS TC using L-EDIT software by Tanner Tools. Inspiring from the literature, four columns masks were designed in this study, to evaluate the influence of the different geometrical parameters of the columns; column chip size was 2 cm x 2 cm, and nine serpentine columns were drawn per 4 inch (=10 cm) diameter wafer:

- A regular design, with nine 100 µm wide and 220 cm long columns (figure 45a); these columns were intended to be etched at a depth of 100 µm;

- A variable width design, with two 100 µm wide, two 75 µm wide, two 50 µm wide, two 30 µm and one 20 µm wide columns; columns length was also 220 cm; these columns were intended to be etched at a depth of 100 µm or 50 µm (figure 46a);

- A semi-packed design, with nine 200 µm wide and 110 cm long columns (figure 45b and 46b); 10 µm x 10 µm square pillars were drawn, with 20 µm distance between the centers of two pillars, and with the corners oriented along the axis of the flow (rather than the edges); these columns were intended to be etched at a depth of 100 µm;

- A short-length design, with three 100 cm long and six 50 cm columns; to compensate column length decrease, column width was as well decreased, to 75 µm (figure 45c); these columns were intended to be etched at a depth of 75 µm;

A last type of design, intended to solid packing, was designed for preliminary tests prior to this study, as explained in appendix B; column chip size was 3 cm x 2 cm, and columns were 450 µm wide, 200 µm deep, and 44 cm long (figure 45d).

A first semi-packed design was early created, and was replaced by the semi-packed design described above (see also figure 46b). Both designs were identical in terms of column and pillar dimension and density, but differed in terms of pillar position: in the oldest design, pillars centers were shifted from one row to another (not in the newest design). Replacement was due to inappropriateness of the oldest design (only two columns per wafer, no compliance with later standard filament mask). Difference, initially due to inattention, eventually enabled interesting comparison of thermodynamic and kinetic performances between both designs (silica was tested on both designs).

### *III.A.1.02 Inlet and outlet holes*

Inlet and outlet holes mask (figure 47 & 48) was designed during the preliminary study detailed in appendix B, and remained unchanged for the whole study. Indeed, holes mask consisted of a constellation of numerous holes regularly arranged (far more than the 18 theoretically necessary for a 9 column wafer): thus, columns masks could be created and modified without having to recreate a specific holes mask each time.

Holes were designed with a diameter of 400 µm, and intended to be etched at a depth of 300 µm, so that usual 360 µm-diameter fused-silica capillaries could fit in, and stay in position while gluing (see paragraph III.A.4.01).

### *III.A.1.03 Platinum filaments*

Two filaments drawings per chip were designed to enable temperature programming through platinum sputtering deposition: a narrow and long high resistance filament for temperature sensing, and a wide and short low resistance filament for resistive heating. Platinum was chosen for basic reasons of appropriateness and availability at the ESIEE.

The filaments were designed taking account of the two following constraints:

- To keep number of fabrication steps and of masks as low as possible, both sensing and heating filaments had to be formed during the same deposition process, and, thus, to have the same thickness; moreover, heating filament length was sought to be as long as possible, to enable maximal covering of the surface of the chip, in order to provide the most homogeneous heating, whereas sensing filament length was sought to be as short as possible to occupy the less surface possible on the chip. Therefore, filament width was the main adjustable parameter.

- Targeting 20°C/s for temperature ramps performances, and calculating chip thermal capacity (0.43 J/K, see table 6), a minimal input power of 8.6 W was estimated; but anticipating thermal capacity decrease with temperature, resistance increase with temperature, and strong power losses (convection in air, conduction in solid support, radiation), this value was, in a first attempt, multiplied by 10. Knowing usual voltages

available in bench or industrial power supplies (0 – 24 V or 30 V), the first chosen resistance value for heaters was 10 Ω ($P_{30V}$=90 W).

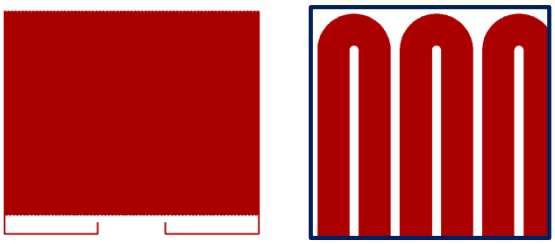

Fig. 45a: regular design
width 100 µm, length 220 cm
(variable width design: 20, 30, 50, 75 µm)

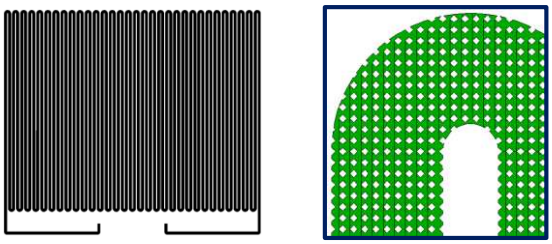

Fig. 45b: semi-packed design
width 200 µm, length 110 cm, pillars
10 µm x 10 µm, centers distance 20 µm

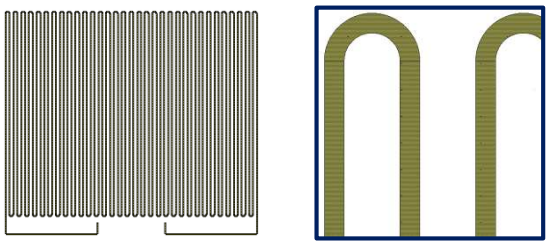

Fig. 45c: short-length design
width 75 µm, lengths 100 cm and 50 cm

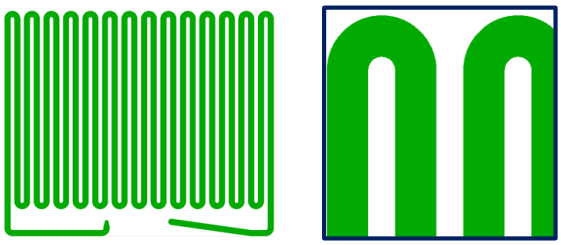

Fig. 45d: to-pack design
width 450 µm, length 44 cm

*Figure 45: the different column designs used in this study (packed design: see appendix B)*

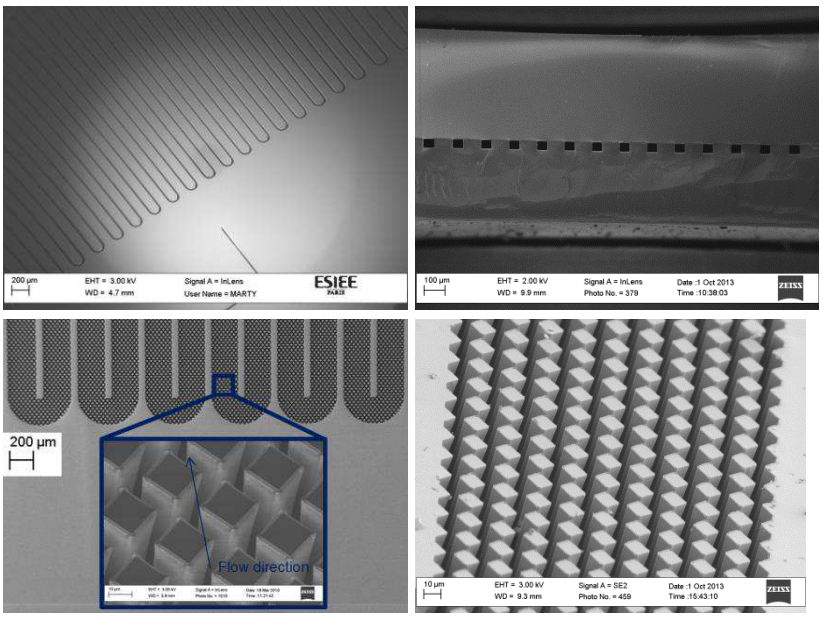


*Fig. 46a (top): open*
*<u>left:</u> top view of a 20 µm wide, 100 µm deep column, before Pyrex bonding*
*<u>right:</u> cross-section view of a 50 µm wide, 50 µm deep column, after Pyrex bonding*

*Fig.46b (bottom): semi-packed*
*<u>left:</u> top view of oldest design with sputtered silica*
*<u>right:</u> top view of newest design with sputtered alumina*

*Fig. 46: examples of SEM images from the different designs*

Three designs of heating filaments were first designed (figure 47 left, table 7), and one was finally chosen after short comparison (see also IV.A.1.) for standard production purposes for GeoServices (figure 47 right).

Large bonding pads were drawn at the extremities of the filaments to enable conventional stain soldering in a first approach, and to remain compatible with more appropriate but less available electrical connections (e.g. wire bonding, vertical screws).

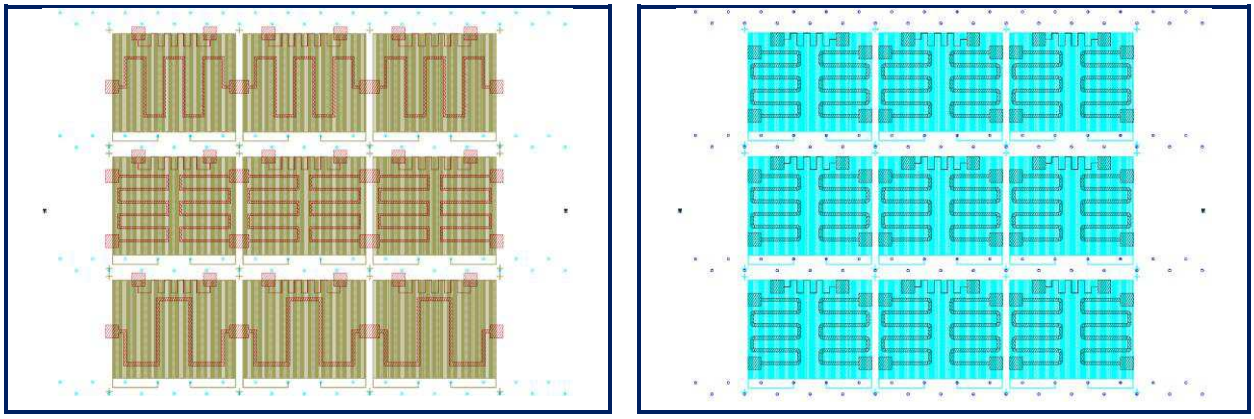

*Fig. 47: superimposed view of the three drawn masks:*
*holes + columns (regular design here) + platinum filaments (left: 1st design, right: 2nd design)*

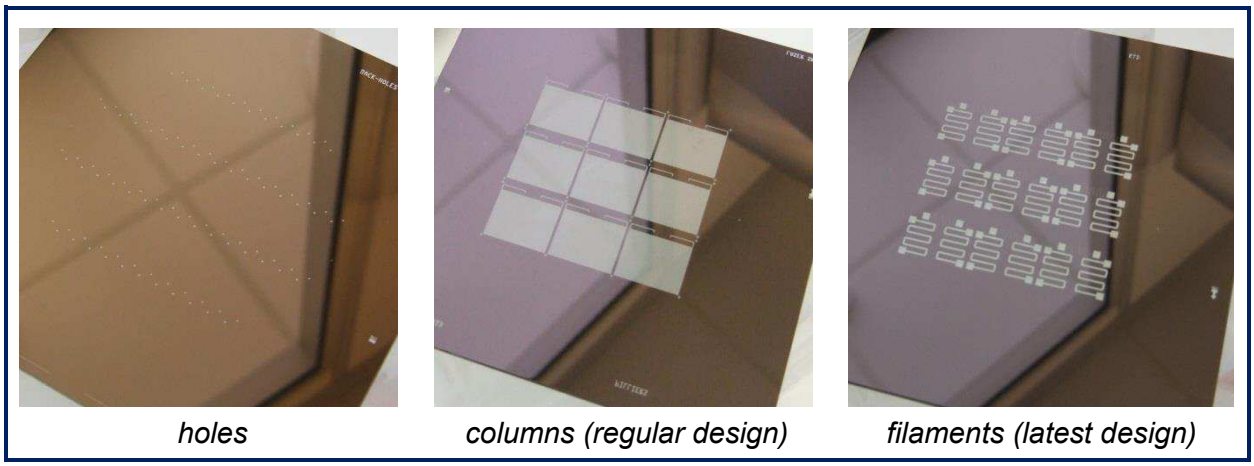

*holes* *columns (regular design)* *filaments (latest design)*

*Fig. 48: pictures of the 3 masks used in a process*

| Material | Density | Volume (1 chip) | Mass (1 chip) | Thermal capacity | Thermal capacity (1 chip) |
|---|---|---|---|---|---|
| Silicon | 2.33 g/cm$^3$ | (2 cm)² x 400 µm | 0.37 g | 700 J/K/kg | 0.26 J/K |
| Pyrex | 2.23 g/cm$^3$ | (2 cm)² x 250 µm | 0.22 g | 750 J/K/kg | 0.17 J/K |

*Table 6: silicon and Pyrex physical properties and dimensions*
*for the calculation of chip thermal capacity (0.43 J/K)*

| Filament | Length | Width | Resistance for a 500 nm thick film |
|---|---|---|---|
| Heater 1 | 4.90 cm | 1000 µm | 10.14 Ω |
| Heater 2 | 2 x 5.00 cm | 500 µm | 10.35 Ω |
| Heater 3 | 5.80 cm | 1200 µm | 10.01 Ω |
| Sensor | 1.95 cm | 30 µm | 134.6 Ω |

*Table 7: targeted platinum ($\rho_{Pt}$=105 nΩ.m) filaments characteristics*

## III.A.2. Clean room fabrication process

The whole column clean room fabrication process was performed at the ESIEE by Kamran Danaie, except stationary phase sputtering, which was performed at MEMS TC by the author.

### *III.A.2.01 Clean room process flow at the ESIEE*

Following usual columns fabrication steps reported in the literature, a process was implemented at the ESIEE, as displayed on table 8, and illustrated on figure 49. DRIE depth inaccuracy was measured to be between negligible and 4%.

| | Step | Details |
|---|---|---|
| 01 | Standard Cleaning | Si substrate, 4 inches, 400 µm thick |
| 02 | Oxidation | Thermal oxidation in oven, target 400 nm (40 min) |
| 03 | Back Side Protection | Oven annealing 15 min at 110°C, photoresist 1.7 µm |
| 04 | Front Side Oxide Etch | Etchant: BHF; 7 min |
| 05 | Photoresist Strip | Equipment: Matrix; 4 min |
| **06** | **Photolithography: filaments (back side)** | Shinetsu 3 manual coating, 2900 rpm, annealing: oven, 110°C, 15 min, insolation (MA150, 6.5 mW/cm$^2$, 9.8 s, PEB), development (PRD238, 2min30) |
| **07** | **Platinum Sputtering (target: 10 Ω)** | RF Etch-back (90W, 0.3 $10^{-2}$ mbar, 90 s), Pt DC deposition (9200 Å, 200 W, $10^{-2}$ mbar, 14min25s) |
| 08 | Photoresist Strip | Acetone + Ultrasounds : 20 min |
| 09 | Aluminum Sputtering (back side) | 8000 Å, DC, 500 W, 8 min |
| **10** | **Photolithography: holes (back side)** | Falcon (PFR 1.2 µm), annealing: oven, 110°C, 15 min, insolation (MA150, 3.4 mW/cm$^2$), development (PRD238, 1 min, hard bake) |
| 11 | Plasma $O_2$ | Nextral, 50 W, 50 cc, 6.67.$10^{-5}$ bar, 90 s |
| 12 | Aluminum Etching (back side) | AlEtch, 30°C, 9 min |
| 13 | $SiO_2$ Etching | DRIE Auto, $CHF_3$, 1500 W, -10°C, 0.3 Pa, 1min45 |
| 14 | Photoresist Strip | Equipment: Matrix; 4 min |
| **15** | **Photolithography: columns (front side)** | Shinetsu 3 manual coating, 2900 rpm, annealing: oven, 110°C, 15 min, insolation (MA150, 6.5 mW/cm$^2$, 9.8 s, PEB), development (PRD238, 2min30) |
| **16** | **DRIE (holes)**, Target : (400 µm – column depth) | 1800 W source, 80 W substrate, 300 cc $SF_6$ (6 s), 150 cc $C_4F_8$ (2 s), flow 29% (4.02 Pa), 10 min + 34 min + 3 min 30 |
| **17** | **DRIE (Columns)**, Target : 50 µm, 75 µm or 100µm | 1500 W source, 50 W substrate, 300 cc $SF_6$ (6 s), 200 cc $C_4F_8$ (2 s), flow 34% (4.12 Pa), 10 min + 14 min |
| 18 | Aluminum Etching (back side) | AlEtch, 60°C, 10 min |
| 19 | *Stationary phase sputtering* | *(at MEMS TC, cf. III.A.2.02)* |
| 20 | Photoresist strip | Acetone + Ultrasounds : 30 min |
| 21 | Pyrex Cleaning | substrate 4 in, 250 µm thick, $H_2SO_4$ + $H_2O_2$ (1:1) : 15 min |
| **22** | **Si/Pyrex Bonding** | |
| **23** | **Dicing** | |

*Table 8: columns fabrication technical process flow*


Oxidation and annealing ovens

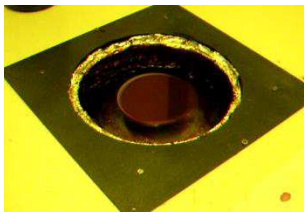

Photoresist spin coating

Photolithography machine

Sputtering machine (for Al & Pt)


Chemical treatments bench

DRIE machine

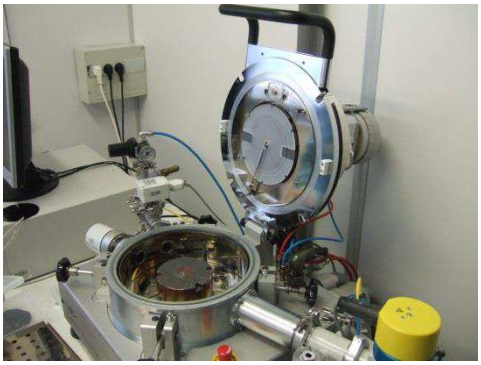

Bonder

Dicing saw

*Fig. 49: virtual visit of ESIEE clean room equipment involved in micro columns fabrication*

### *III.A.2.02 Sputtering at MEMS TC*

Sputtering was performed at MEMS TC; sputtering machine pictures were displayed in I.E.. Deposited layer thickness and homogeneity were measured with a mechanical profilometer (DekTak 200-Si) after deposition on a blank wafer with an adhesive tape strip on it. After removal of the adhesive strip, thickness was found to vary of 10% for silica between the center of the wafer and farthest potentially etched point. Due to angle and shadowing effects, a layer deposited in a column was always thinner than a layer deposited on a blank wafer, which was even more pronounced for semi-packed columns. Real thicknesses were measured through SEM (see next paragraph), and do not correspond to deposition rates displayed in table 9, along with main sputtering parameters.

Sputtering process general description can be split into the following steps:

- setting of the airlock at ambient pressure (sputtering chamber always remains in vacuum, except while shutdowns, for target change for instance);
- loading of the wafer in the airlock and depressurizing of the airlock (~$1.3 \times 10^{-5}$ mbar);
- airlock-chamber gate opening, remote loading of the wafer from the airlock to the chamber, gate closing, remote positioning of the substrate in front of the chosen target (a movable cover hided the substrate from the target);
- waiting for the pressure in the chamber to reach below $4.10^{-7}$ mbar, opening gas flow, waiting for the pressure to stabilize at $P_{initiation}$, and initiation of the plasma;
- waiting for the stabilization of the plasma, setting pressure to $P_{deposition}$, and waiting for the plasma to stabilize again;
- setting deposition time, starting deposition on the substrate by remote removing of the cover between the target and the substrate;
- at the end of deposition time, deposition of a new layer on the substrate with the same process, or unloading of the wafer from the chamber and from the airlock, and re-setting the air lock in vacuum (after loading another substrate or not).

| Process | Target | Mode | $P_{initiation}$ | $P_{deposition}$ | Power | Deposition rate (µm/hour) | Ar | $O_2$ | $N_2$ |
|---|---|---|---|---|---|---|---|---|---|
| Silica 1 | $SiO_2$ | RF | 30 mT | 3 mT | 600 W | 3 | 80 cc | 0 cc | 0 cc |
| Silica 2 | $SiO_2$ | RF | 50 mT | 50 mT | 600 W | 1.2 | 80 cc | 0 cc | 0 cc |
| Graphite | C | DC | 30 mT | 3 mT | 800 W | 0.78 | 80 cc | 0 cc | 0 cc |
| Alumina | $Al_2O_3$ | RF | 30 mT | 3 mT | 800 W | 1.67 | 80 cc | 0 cc | 0 cc |
| Titania | $TiO_2$ | RF | 22,5 mT | 22,5 mT | 200 W | $0.28.10^{-3}$ | 80 cc | 8,9 cc | 0 cc |
| Magnesia | MgO | RF | 20 mT | 20 mT | 400 W | 0.32 | 80 cc | 0 cc | 0 cc |

*Table 9: summary of chosen parameters (and observed deposition rates on gauge wafers) for the different targets used as stationary phases in this study; unless contrary mention, process silica 1 was used for silica deposition*

Stationary phase films had to be deposited as successive layers with breaks between depositions to avoid excessive heating of the substrate during deposition. Indeed, deposited layers were far thicker (several µm) than typical layers usually deposited by sputtering in MEMS technology (several nm to a few hundreds nm), and, therefore, cooling system performances were not adequate for hours long depositions. As substrate was to be kept from excessive heating during deposition (to avoid photoresist cohesive baking with the silicon or the stationary phase, and to keep deposited structure as columnar as possible), deposition process was split into ½ hour depositions spaced with ¼ hour break. Thus, cooling fluid (water) temperature was kept at 19°C in the circuit during the whole process, as indicated by the chilling units.

## III.A.3. SEM observations of deposited layers

SEM images of on-column deposited layers were taken at the ESIEE at different times of the thesis, first to measure actually deposited thicknesses, then for qualitatively observe the structure of the films, for the different stationary phases, designs of columns, or sputtering pressure. Several examples were chosen for their relevance and are displayed in this paragraph.

⌦ It should be mentioned here that direct porosity measurements were attempted on gauge wafers with sputter-deposited silica, via spectroscopic ellipsometry, both with Dr. B. Gallas at the NanoSciences Institute of Paris, and with Dr. V. Rouessac at the European Institute on Membranes of Montpellier. The inability to measure any porosity sufficient to induce retention, and the following discussions, led to the understanding of the presence of two different kinds of layer structures, one on channel floors (and gauge wafers), densely packed and non-porous, and one channel side walls, columnar and porous.

### *III.A.3.01 Silica*

First depositions and SEM observations were carried out with silica (figure 50).

The expected columnar structure of the layer was clearly observed on the side-walls of regular channels (figures 50 a&d). Void typical size could not be accurately measured, but was estimated in the range 1-10 nm. Channel floor deposited layers appeared denser, as expected (figure 50c).

Deposition rate in channels was naturally lower than in gauge wafers, and deposited thickness was found not to be homogeneous on the channel: for a (100 µm)² regular channel and a 120 min long deposition process at 3 mT (figure 50a), measured thickness was 3.2 µm at the middle of channel floor, 3 µm at the top of the side walls, and 2.2 µm at the bottom corners of the channels. This inhomogeneity, also due to shadowing effects, was naturally more pronounced in narrow-width channels, for instance respectively 2.6 µm, 1 µm and 0.75 µm in a 100 µm x 30 µm channel (figure 50b), with the same process (time and pressure). Again with the same process, layer thickness in semi-packed columns (figures 50 e&f) was measured to be around 0.5 µm in channel floor and around 1 µm at pillar top.

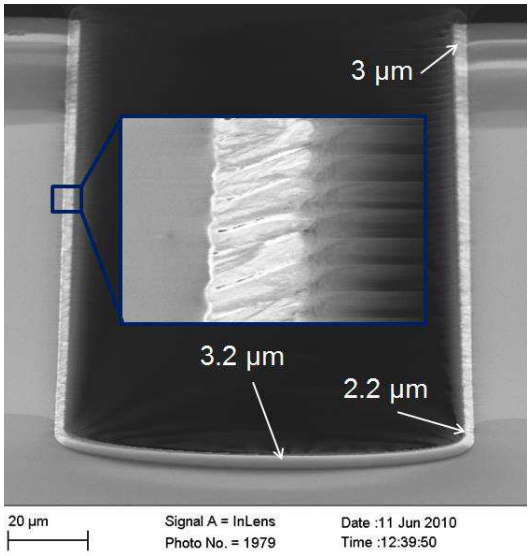


*Fig. 50a: cross-section view of a (100 µm)² regular channel, with 120 min long silica deposition, before Pyrex bonding*

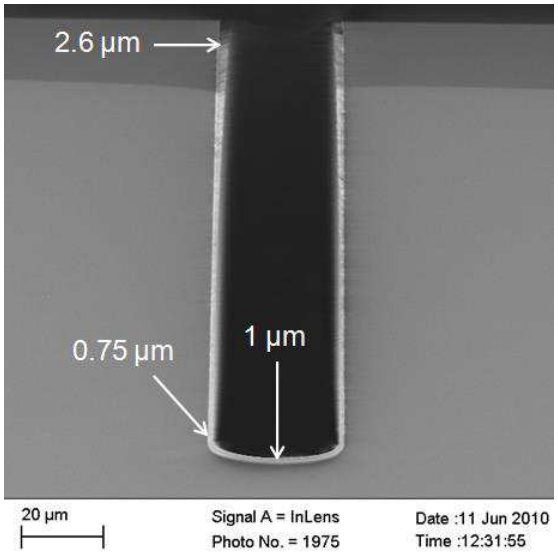


*Fig. 50b: cross-section view of a 100 µm x 30 µm channel, with 120 min long silica deposition, before Pyrex bonding*

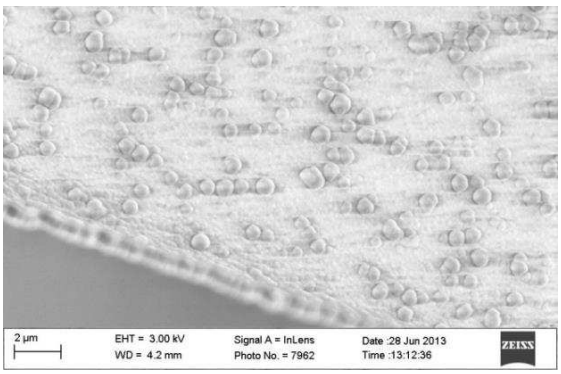


*Fig. 50c: surface view of channel floor covered by sputter-deposited silica (120 min, process 50 mT), regular column*

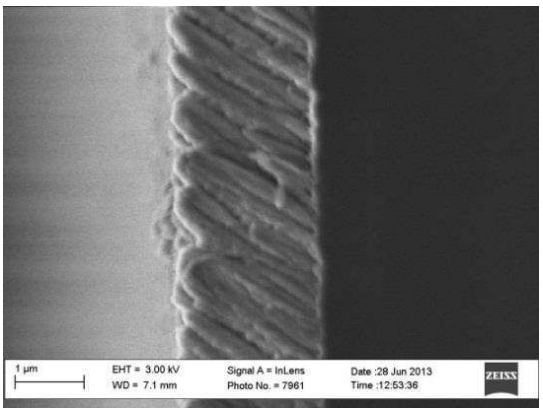


*Fig. 50d: cross-section view of channel side wall with sputter-deposited silica (300 min, process 50 mT), regular column*

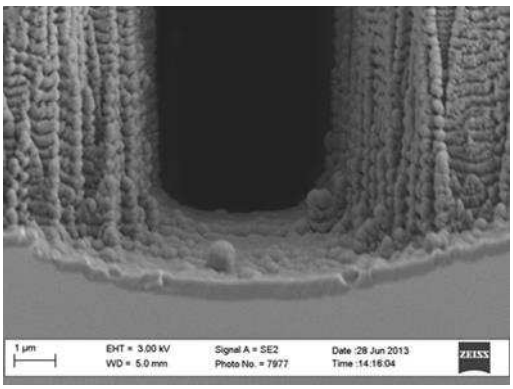


*Fig. 50e: cross-section view at the bottom of two pillars in a semi-packed channel, process silica 120 min*

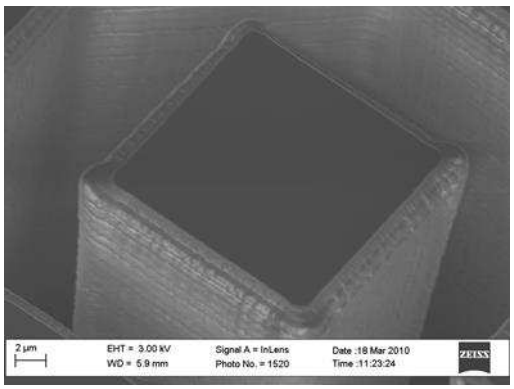


*Fig. 50f: top view of a pillar in a semi-packed channel, process silica 120 min*

*Fig. 50: SEM images of sputter-deposited silica layers*

Unexpectedly, process pressure increase strongly decreased deposition rate (by a factor 2.5, see table 9 and figures 50 a&d), and targeted porosity increase could not be clearly observed.

On the contrary, scalloping effect consequences (cf. II.C.2.03) were clearly observed on semi-packed columns pillars (figure 50f).

### *III.A.3.02 Alumina*

The same considerations were observed with alumina, which aspect was very similar to silica (columnar structure was slightly less pronounced). Figure 51 displays the top view of pillars with sputter-deposited alumina. The scalloping effect could again be clearly observed.

### *III.A.3.03 Graphite*

Scalloping effect was also clearly observed on regular channels with sputter-deposited graphite (figures 52 a&c), but very poorly on semi-packed columns (figure 52c). Figure 52a perfectly illustrates the difference of structure between side-wall layers and floor layers.

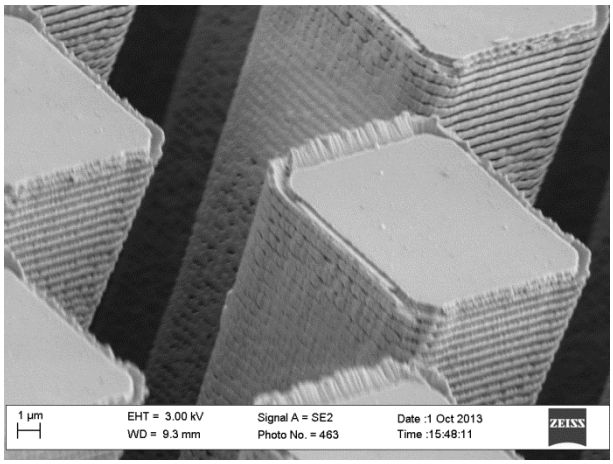


*Fig. 51: top view of semi-packed column pillars, before Pyrex bonding, with 1 µm thick sputter-deposited alumina (120 min)*

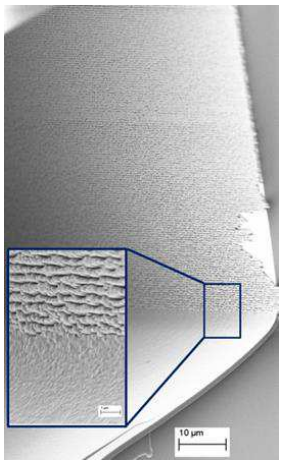


*Fig. 52a: ¾ view of a (100 µm)² channel (200 min)*

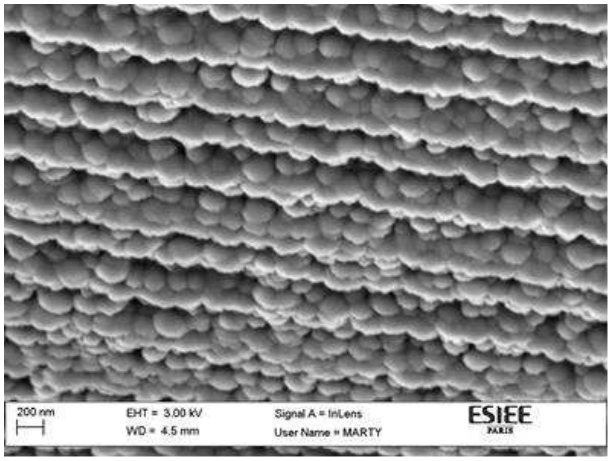


*Fig. 52b: side wall surface view of a regular channel (80 min)*

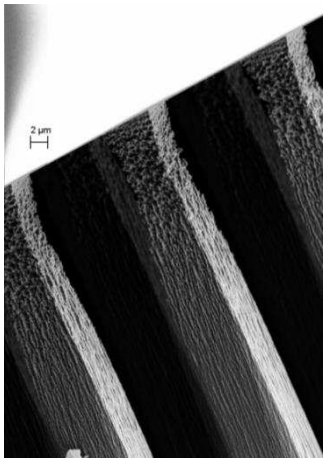


*Fig. 52c: pillars (60 min)*

*Fig. 52: SEM images of sputter-deposited graphite layers*

### *III.A.3.04 Magnesia*

Similar observations were made on magnesia (figure 53).

### *III.A.3.05 Titania*

Due to the very low deposition rates encountered with titania (as forecast by gauge depositions), no tangible structure could be observed with this material, in spite of the very long deposition time chosen (480 min), as shown on figure 54.

### *III.A.3.06 Conclusions*

A porous columnar structure on channel side walls, a densely packed structure on channel floors, and scalloping effect were observed with silica, alumina, graphite and magnesia.

Thickness inhomogeneities were observed, more pronounced with narrow width channels, and very strong with semi-packed channels, making a thickness value hardly accurately definable, especially with semi-packed columns. Given that stationary phase was only deposited on the ¾ of channel circumference (Pyrex was uncovered), and that retention is expected to be ensured only by side walls, stationary phase film thickness might not be the most appropriate parameter for column behavior interpretation and modeling. In Chapter IV, displayed thicknesses will correspond to the thickness measured at the middle of the channel side walls, and will be accompanied by column phase ratio values β (mobile phase / stationary phase volume ratio).

After stationary phase sputter-deposition, Pyrex bonding, and wafer dicing, columns were made ready for evaluation by adding fluidic and electrical connections. These steps are described in next paragraph.

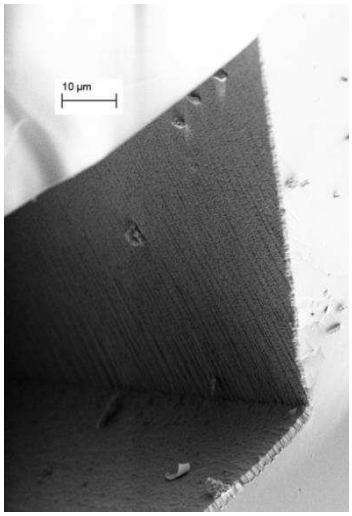


*Fig. 53: ¾ view of a (100 µm)² regular channel with sputter-deposited magnesia (562.5 min)*

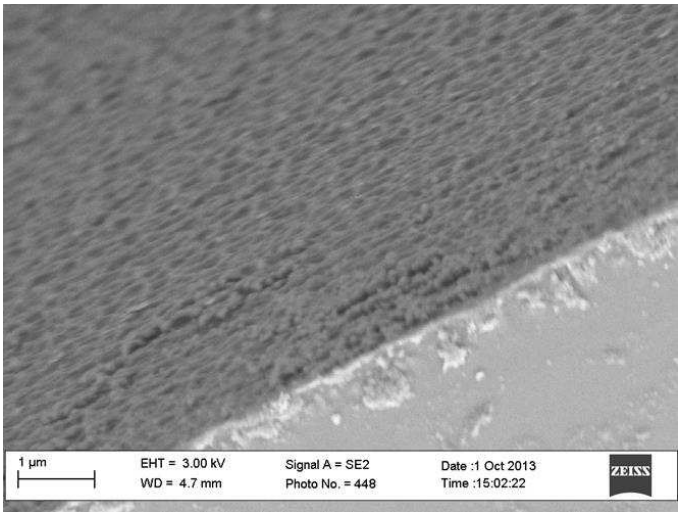


*Fig. 54: surface view of the side wall top of a regular channel before bonding, with sputter-deposited titania (600 min)*

## III.A.4. Bench completion

Bench completion was carried out at MEMS TC. It included fluidic connections (fused-silica capillaries) and electrical connections (conventional wires) gluing.

### *III.A.4.01 Capillary gluing*

After dicing, the chips were taped to a bench with conventional adhesive tape (figure 55a, left); the tape was carefully put on the corners of the chips, to avoid any adhesion of the platinum filaments to the tape (which would result in the adhesion of the filaments on the tape rather than on the chip).

Two 5 cm-long capillaries per chip were cut from a 20 m-long capillary tubing by Polymicro Technologies (fused silica, inner diameter 100 µm, outer diameter 360 µm, reference TSP100375, figure 55a, right). The capillaries were plugged into the two 300 µm deep central holes of each chip (figure 55d, left).

1 cm of each component of a gastight epoxy resin (Hysol 1C by Loctite) were poured on a sheet and mixed with a wooden stick (figure 55b). The mixing lasted at least 1 minute, and was energetic and entropic.

Using an extra capillary as a nib, drops of glue were applied to the base of the capillary to be glued (figure 55c). The glue was applied all around the plugs of the capillaries, while holding the capillaries with the fingers. The capillaries were very slowly and carefully released (after the gluing extra capillary was taken away from the gluing point).

Only one of the two capillaries was first glued on each chip (figure 55d). The glue was left drying at ambient air for 3 hours. The second capillary was then glued on each chip. Again, the glue was left drying at ambient air for 3 hours. Finally, the chips were put in an oven at 110°C for 1 hour for annealing.

### *III.A.4.02 Wire gluing*

Conventional stain soldering could unfortunately not be performed to connect electrical wires to the bonding tracks of the chip filaments. Indeed, stain poorly wetted platinum (balls forming). At the very end of the thesis, two solutions were found, experimented, and validated: chip heating at 220°C while soldering enabled conventional soldering on a specific heating station, and a vertical screws system (in contact with bonding tracks and connected to electric wires) was suggested to and chosen by GeoServices for prototype development (see III.D.2.). However, an alternative process was used during the main part of the research work.

Following the same process as for capillary gluing, the 1 mm stripped extremities of 1 cm long usual electrical wires were glued on the bonding tracks of the filaments with a conductive (silver-doped) two-component epoxy resin (CW2400 by CircuitWorks, figure 56).

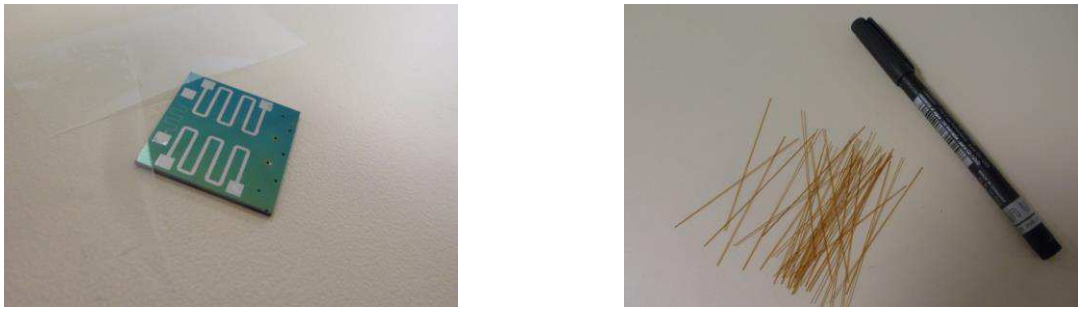

*Fig. 55a: capillary gluing preparation (left: taped chip, right: cut capillaries)*

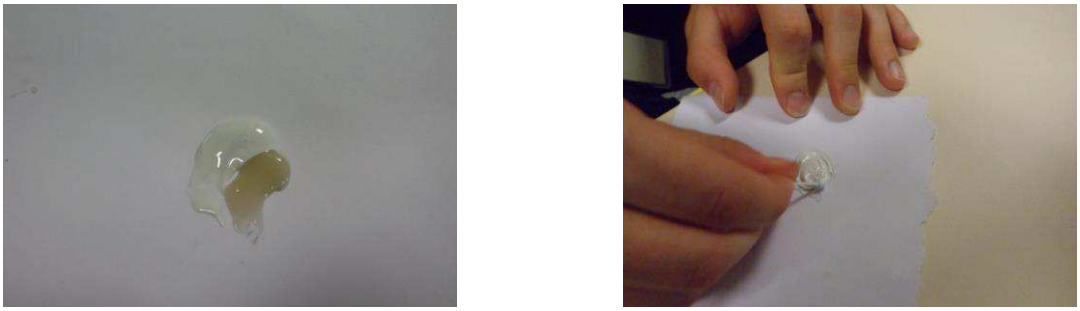

*55b: two-component gastight epoxy resin, before (left) and after (right) mixing*

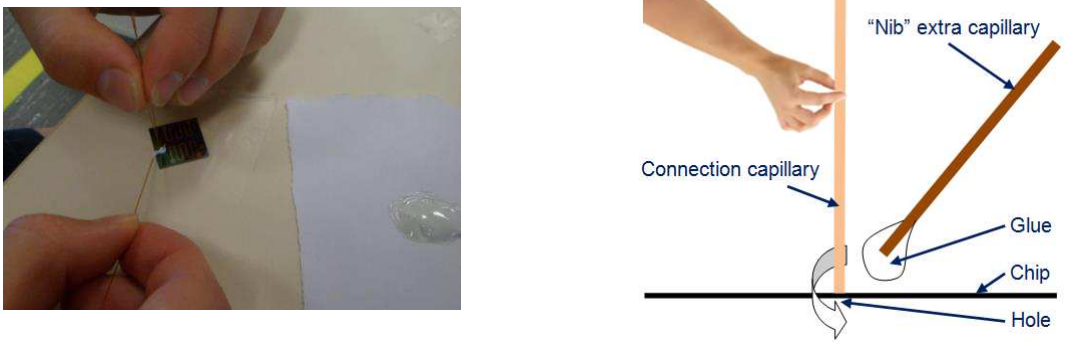


*55c: gluing of the capillary on the chip*

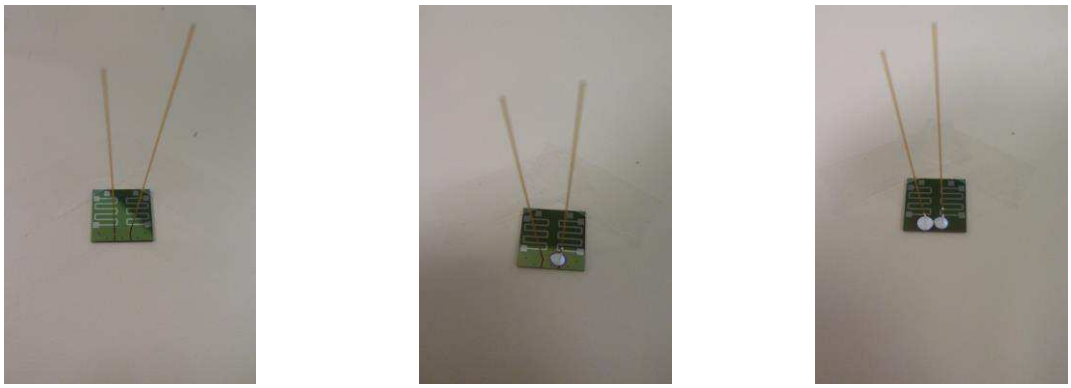

*Fig. 55d: bench (top) and zoom on one chip (bottom) before gluing (left), after gluing one capillary on each chip (middle), and after gluing two capillaries on each chip (right)*

*Fig. 55: capillary gluing*

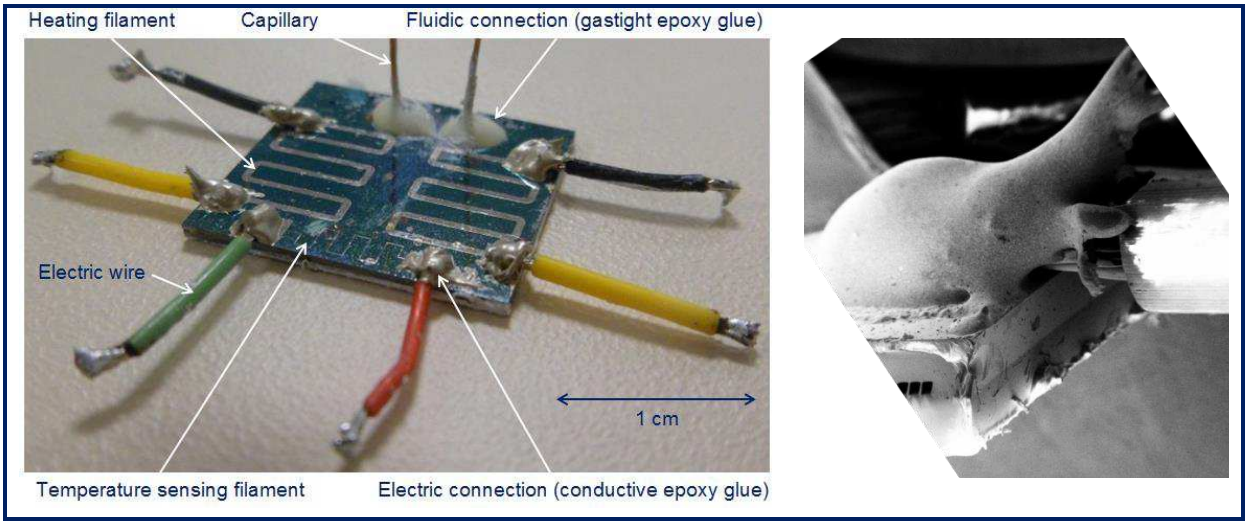


*Fig. 56: electrical connections*
*(left: chip with 6 wires, right: SEM image, zoom on one connection)*

## III.A.5. Troubleshooting inventory

This paragraph consists of a summary of the different limits or failures experienced during columns fabrication, both concerning stationary phase deposition at MEMS TC clean room and chip fabrication at the ESIEE.

### *III.A.5.01 Stationary phase sputtering deposition*

A first limit was due to the number of RF power supply in the existing sputtering machine, which was unique. Although the machine contained four different places (and could thus contain up to four different targets), only one RF-sputterable target could be placed inside the machine at a time. Placing all different RF-sputterable inside the machine and changing RF power supply place when necessary was considered to present far more difficulties than the chosen alternative, which consisted in keeping the RF power supply at the same place and changing targets when necessary. As 4 different oxide targets were used throughout the study, target changing was operated 6 times in less than 3 years (and 4 times within 4 months). This barely corresponded to usual compliance of such equipment (so were deposited thicknesses).

This was accompanied by changes in MEMS TC clean room and sputtering machine status over the research work: initially used and considered as production equipment (with corresponding funding, standards, and maintenance), they were then turned into pure research instruments (with corresponding advantages in terms of freedom of use and drawbacks in terms of maintenance); clean room actual cleanliness and sputtering machine state was constantly decreased throughout the study. Frequent openings and long period shutdowns of the machine, as well as half-solved breakdowns, naturally damaged process quality.

Pollution of the inside of the machine was a strong limitation observed in the utilization of machine (figure 57a) and had three main origins:

- very thick layers deposition layers resulted in the flaking of collaterally deposited materials (on the walls of the machine, under the movable cover, and on the substrate holder); this flaking phenomenon was worsened by vacuum absence in the machine during long period shutdowns;

- the successive use of several targets on the same place, and the use of graphite (relatively dirty material in terms of flaking), probably led to cross-polluting of target places, in spite of frequent cleanings; pieces cleanings were carried out with ethanol-wetted tissues and usual vacuum cleaner, whereas sandblasting cleaning should be mandatory in these cases;

- the absence of clean room maintenance induced increasing presence of dusts and decreased process quality;

A last illustration of decreasing process quality is substrate temperature evolution throughout the study: the substrate cooling circuit chiller broke down in the middle of the research work and could luckily be replaced, but only by an already present and available chiller, which did not perfectly match the requirements for the use of ambient temperature sputtering; this resulted in a slight but non-controlled increase of substrate temperature during sputtering.

Of course, such difficulties would not occur in a production context and should not be taken as strong limitations for industrial development, but they probably deteriorated quality and accuracy of this preliminary research work.

### *III.A.5.02 Chip fabrication*

Most problematic issue encountered during the rest of chip fabrication stemmed from the previous ones and concerned photoresist removal (between sputtering and Pyrex bonding): due to long deposition times, to large deposited thicknesses, to substrate heating while sputtering (in the latest moments of the study) and to the presence of polluting particles during sputtering, photoresist removal could not always be perfectly operated. This problem was rare or inexistent at the beginning of the research and silica, alumina or graphite sputtering coated wafers could be easily photo-resist removed and Pyrex-bonded; semi-packed sputtering magnesia-coated wafers and all titania wafers fabrication failed due to the impossibility to remove photoresist layer with usual processes. Latest-fabricated silica columns (purported to serve as probes for precision studies, cf. III.C.3.02) showed a dramatic failure rate of 5 columns out of 18 only due to this aspect.

The main consequence of flawed photoresist removal was irregular Pyrex bonding, as shown on figure 57b. Defaults in Pyrex bonding could be either benign (when not located on column channels) either serious; in this case, chromatographic properties of the corresponding column was clearly damaged, if not completely annihilated.

Other marginal issues were encountered and solved:

- very narrow columns (width smaller than 30 µm) showed a higher jamming rate than other columns; small section columns were then fabricated by reducing channel depth along with channel width (which also enhanced deposition homogeneity at the same time);

- 50 µm-deep columns etched in 400 µm-thick wafers implied an etching depth of 350 µm for connections holes, and such wafers were observed to be more fragile than wafers with 300 µm-deep holes (and 100 µm-deep columns); 500 µm-thick wafers were then used instead, which solved the problem;

- platinum filaments adhesion, which occasionally presented some flaws (figure 57b), was enhanced and made compliant with industrial requirements at the very end of the study by intercalating a thin titanium layer bond between surface silicon dioxide of the chip and platinum filament.

*Fig. 57a: illustrations of sputtering machine pollution issues encountered on the silica target (left) and over the covers (middle) due to flaking phenomenon and a long absence of vacuum, and impact on a wafer after 120 minutes silica sputtering (right).*


*Fig. 57b: illustrations of fabrication issues encountered: benign irregularity (left) and serious default (middle) of Pyrex bonding, and platinum filaments partial tearing (right).*

*Fig. 57: failures and problems in columns fabrication*

### *III.A.5.03 Conclusion*

To save as much time as possible, a logical protocol was followed after each new wafer delivery: filaments resistance values were first checked, then capillaries were glued only on electronically functional columns, which were chromatographically tested. Finally, electric wires were glued only on both electrically and chromatographically functioning columns. The average number of fully functional columns on each wafer was around 5 (out of 9) at the end of the study.

This number was rather around 8/9 at the beginning of the study when chips were not equipped with filaments, and when clean room and sputtering machine grade were maximal, and filaments failure origin was corrected, which suggested that failure ratio could finally be easily brought close to zero in the future industrial developments (one target per place, qualified and dedicated machine, standard clean room grade etc.). This number was 9/9 for the two lasts wafers fabricated at the very end of this writing (November 2013), thus partially confirming the hypothesis of 0% failure ratio under standard use for production.

The last point which could possibly remain a problem was the thickness of the deposited layer, although proofs could not be given to decide whether it was a critical limit in terms of photoresist removal or not.

Next section is dedicated to the building of the appropriate chip temperature-programming system.

## III.B. Temperature programming engineering

To enable controlled heating and cooling of the chip, 4 elements were necessary:

- a column block, including:
  - real-time temperature sensing system, based on the instantaneous measure of the sensing filament resistance value;
  - resistive heating system, based on the application of an appropriate voltage to the heating filament;
  - chip cooling system, with specific requirements and constraints;
- appropriate power supplies;
- an electrical hardware, to link column block, power supplies and computer.
- a software for user inputs and values display;

A whole system was elaborated by the author at the end of 2010, and was constantly improved during the thesis. This section is dedicated to a synthetic description of the last version of the system, used in the production of most chromatographic results presented in chapter IV.

## III.B.1. Temperature sensing

To insert the sensing resistor in the appropriate electrical circuit, it was necessary to estimate the range of variation of the resistance in the targeted range of temperatures. To this purpose, resistance-temperature coefficient (RTC, or α) of platinum filaments was measured with the following experiment: a chip was placed in a conventional oven, the sensing resistor was connected to an ohmmeter, two thermocouple probes of a thermometer (HH306A by Omega) were tied to the chip, and contact between chip and probes was enhanced with thermal paste (2265931 by Dow Corning); oven temperature was increased from ambient to 130°C, by steps of 10°C; at each step, after both oven and chip temperature stabilization, the value of the resistance and the mean value of the two chip temperatures displayed were picked up; this experiment was carried out with two different chips. The resulting plots are displayed on figure 58.

The relation $\Delta R/R_0=f(\Delta T)$ was expectedly found linear in the range 33°C-138°C (correlation coefficients higher than 0.999), and α values for two different chips were found very close (0.248%/°C and 0.246%/°C).

To enable a posteriori adjustment of heating resistance nominal value without changing filament mask (only by adjusting deposition thickness), the targeted range of heating resistances at the ambient temperature was roughly considered to be 3Ω-20Ω, with a first chosen value of 10Ω (see III.A.1.03). Thus, targeted range of sensing resistances at the ambient temperature was roughly considered to be 50Ω-300Ω, with a first chosen value of 135Ω (see also III.A.1.03). Taking account of the targeted range of temperatures (roughly and largely considered 0°C-250°C), and of the calculated values of α, the range of variation of the sensing resistances under temperature programming was considered to be 44Ω-564Ω. This range was essential for the development of the electronic hardware described in III.B.4.

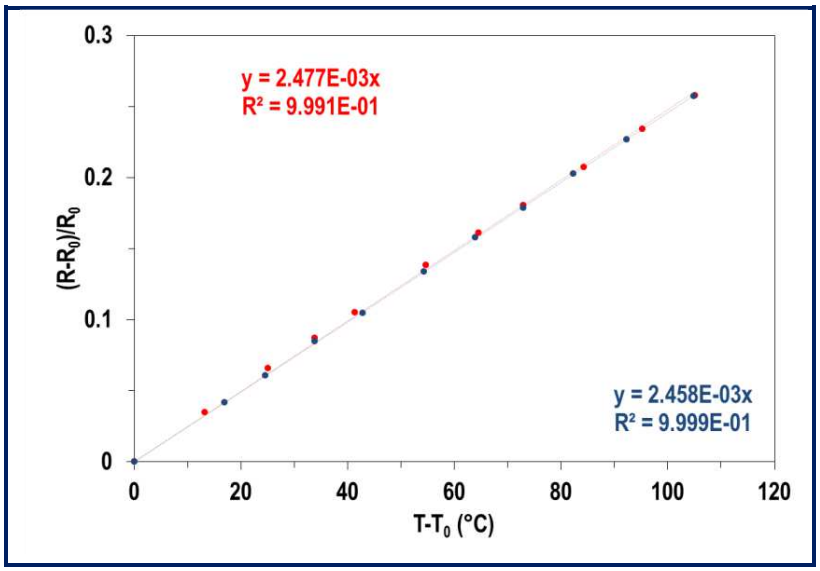


*Fig. 58: resistance-temperature plots of the sensing filaments from two different chips (red and blue)*

## III.B.2. Resistive heating through Pulse Width Modulation

After investigations, pulse width modulation (PWM, cf. example on figure 59) was the method chosen to provide linear temperature ramps to the chip through resistive heating. First order pulse width modulation of a constant voltage consisted in setting a constant voltage to the heating filament, and to open and close the circuit depending on the instantaneous temperature of the chip, measured through the sensing filament: at each sampling instant, the system compared chip actual temperature to the temperature of reference ideal ramp (user input); if the actual temperature was found lower, a switch closed the circuit, power was delivered to the chip by Joule effect, and chip temperature increased; if the actual temperature was found higher, the switch opened the circuit, and temperature chip decreased. Linear-like temperature increase was then ensured thanks to a high sampling frequency.

This method showed two crucial advantages: first, no variation of input voltage was required from power supply, which could be harder to implement than constant voltage, especially in already existing systems (such as the XXXXXXXXXXX described in III.D., which had for instance an available constant voltage supply of 24 V); second, circuit opening and closing could very simply be implemented through the insertion of basic digital solid state relays (SSR) between the power supply and the heating filament.

General functioning of the whole system is summarized in the electronics paragraph (III.B.4), and additional details are given in appendix C.

## III.B.3. Thermoelectric cooling

After investigations, thermoelectric cooling of the chip was chosen to be provided by Peltier module. Peltier module (MCHPE-128-10-05-E by Multicomp) was put on a heat sink, and two fans (Sunon - MC35100V2-0000-A99) were glued to the side of the heat sink with the same glue used for capillaries (see figure 60a). Thermal contacts between chip and Peltier module, and between Peltier module and heat sink were enhanced using the thermal paste previously reported.

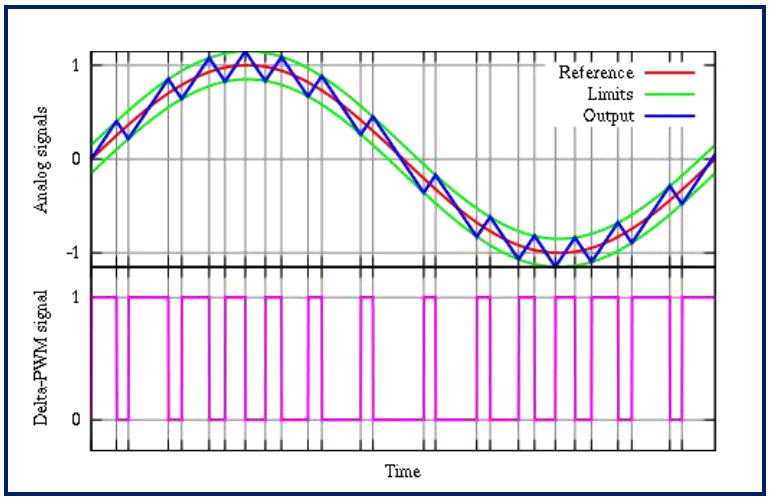


*Fig. 59: PWM technique: sinusoidal-like signal (top) created through PWM of a constant signal of value 1 (bottom)*

At the end of the thesis, an internship mission, carried out by Emna Zoghlami and supervised by the author, partially focused on the research of the most appropriate cooling system, and provided significant improvements in cooling performances. Additional details on this comparison are provided in appendix C. Finally chosen system consisted of an assembled Peltier kit (module with adapted heat sink, fan, and contacts, UEPT-KIT3 by Uwe Electronics, figure 60b).

## III.B.4. Electronics

Column block (figures 60 a&b) outputs (sensing resistor, heating resistor, Peltier module and fans connections), corresponding power supplies (figure 60c), and computer (see III.B.6) were linked together through two electronic boards (figures 60 d&e).

Figure 61 displays the electronic circuit designed and developed for temperature programming. Basic functioning principle was as follows:

- Column block and power supplies were connected to a self-made electronic board (figure 60d): heating resistor, Peltier module and fans power supply lines were sent to corresponding lines toward column block through solid state relays; sensing resistor line was inserted in a voltage divider bridge, to convert resistance changes into voltage changes; raw signal thus obtained was sent to a processing unit, to shift, center, and amplify raw voltage, so that the 44Ω - 464Ω range for sensing resistor reported in III.B.1. corresponded to the +10 V / - 10 V range accepted by the analogical input of the data acquisition module (cf. below).

- A low-cost multifunction data acquisition module (National Instruments OEM 6008 USB, 12-Bit, 10 kS/s) was purchased and connected on one side to a conventional computer ran with Labview (figure 60). On the other side (towards self-made board), one analogical input was connected to the processed temperature sensing signal, three digital outputs were connected to the solid state relays to control power circuits closing and opening.

## III.B.5. Calibration

The relationship between the analogical voltage received by the DAQ board and the computer from sensing filament circuit had to be obtained for each tested chip, according to the following protocol: the temperature probe of the thermometer was put in thermal contact with the chip as previously described (III.B.1.), and different input voltages were directly and successively applied to the heating filament. For each input voltage, chip temperature was waiting to be stabilized, and both chip temperature displayed by the thermometer and analogical voltage displayed by the Measurement and Automation Explorer (furnished by National Instruments) were recorded. Calibration curves were obtained from the resulting plot and fit with a linear regression (figure 62).

Correlation coefficients were generally found very good (higher than 0.995) and fit parameters (slopes in °C/V and intercepts in °C) were used as inputs in the self-made software described in next paragraph.

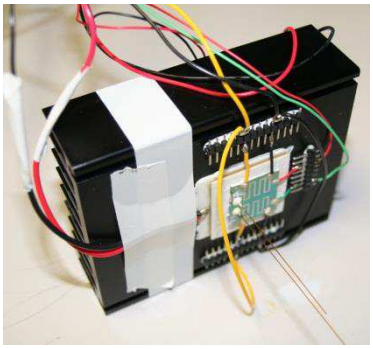

*Fig. 60a: self-assembled column block*

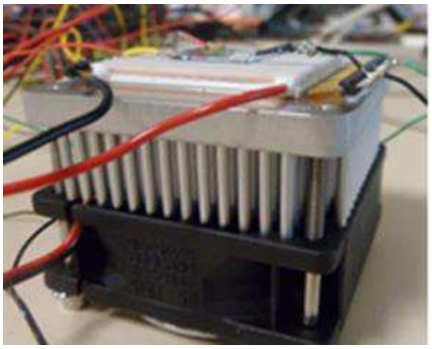

*Fig. 60b: industrial assembled Peltier kit (Uwe Elec.) with chip*

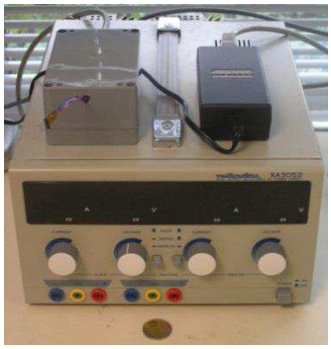

*Fig. 60c: power supplies (OA, fans, heater + Petlier)*

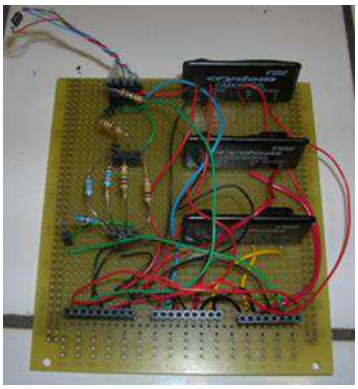

*Fig. 60e: self-made eletronic board, with signal processing circuit (left), SSR (right), and bus connection (bottom)*

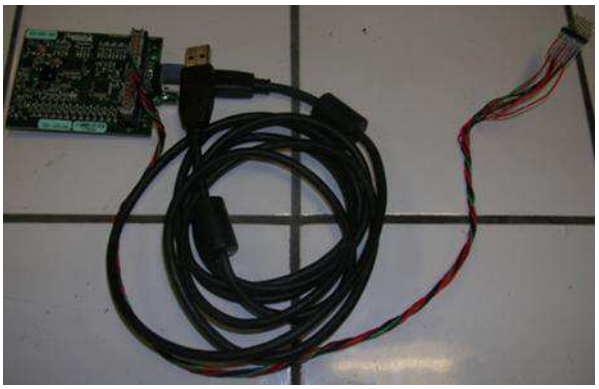

*Fig. 60d: data acquisition module by National instruments, with bus connections*

*Fig. 60: pictures of the 3 hardware components of the temperature programming system*

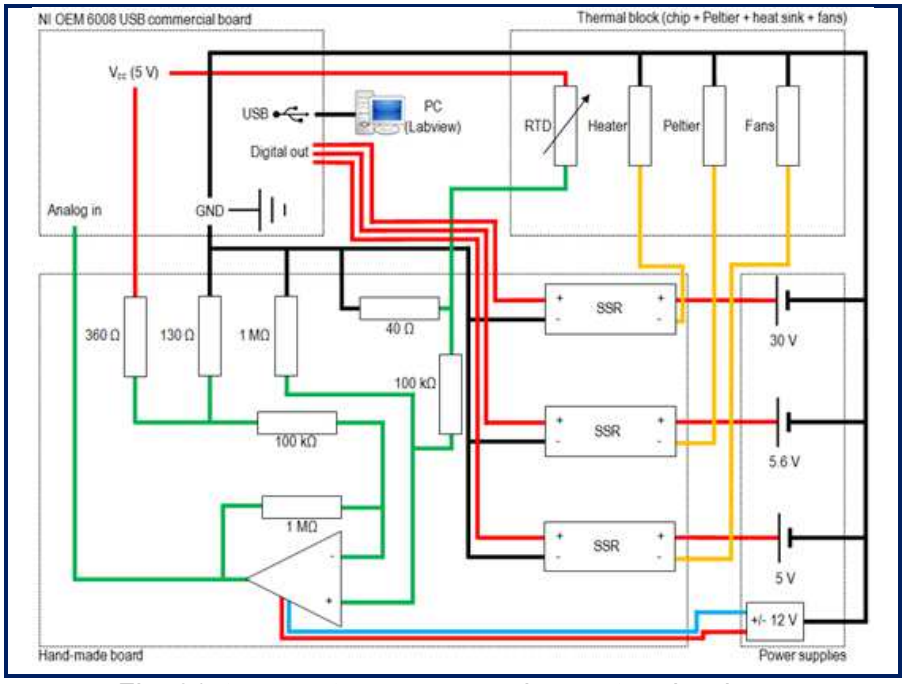


*Fig. 61: temperature programming system hardware*

## III.B.6. Software

A Labview software was developed for temperature programming (figure 63).

User inputs included ramp parameters (start temperature, ramp value in °C/s, stop temperature), calibration parameters obtained as described above, two switches (standby / prepare to initial temperature and ramp on / off), and temperature log save option.

Software displays included mainly real time chip temperature, but also analogical voltage and heating and cooling circuits states, for troubleshooting.

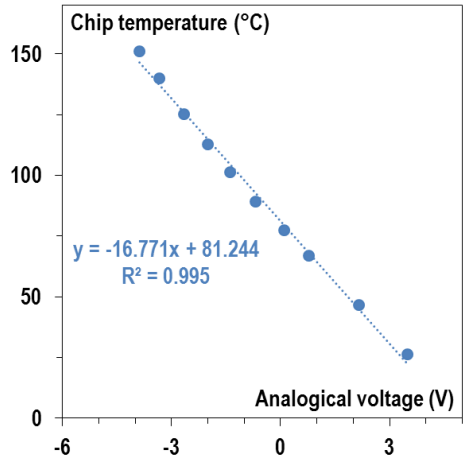


*Fig. 62:*
*typical chip calibration curve*
*(temperature from 26 to 151°C,*
*input voltages:*
*0, 4, 8, 11.5, 14.5, 17, 18.5, 19.5 , 20, 20.3 V)*

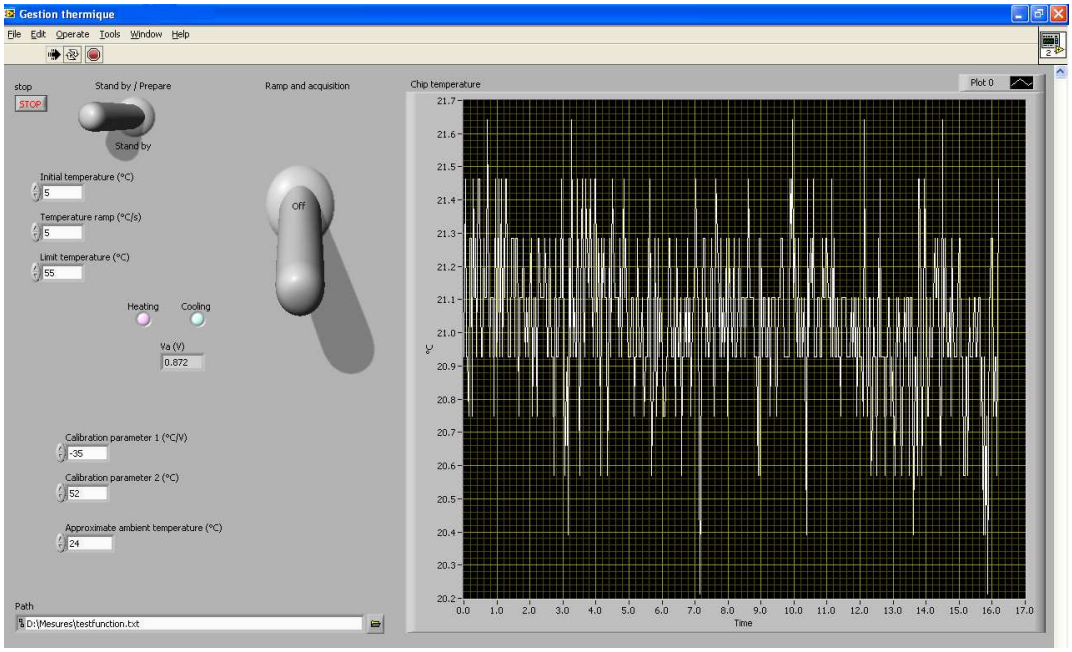


*Fig. 63: screenshot of Labview software developed for temperature programming*

## III.B.7 Conclusion

Hard- and software were designed, developed, and continuously improved to enable chip temperature programming. Four temperature programming systems were fabricated, two for MEMS TC laboratory (one first and one recent version), one for ESPCI LSABM, one for GeoServices. Thermal management enabled by the developed system is later described in the results and discussion chapter, but a few observed limitations of the use of this system should be mentioned here:

- temperature programming system utilization required a tedious step of temperature – voltage calibration for each chip and each setup;
- no accurate evaluation of the error on command temperature was carried out; it could be reasonably considered within 1°C near ambient temperature and within 5°C at highest temperatures;
- a crash test chip was used to roughly estimate high limit temperature in temperature programming; it was concluded that frequently bringing chip at temperatures higher than 220°C could damage capillaries and wires glued connections; at 250°C, platinum filaments were observed to be smoking just before the chip was broken down in two due to excessive heating; a limit temperature of 200°C was therefore respected during temperature-programmed chromatographic experiments;
- although initial temperatures below 0°C (at a room temperature of 30°C) could be obtained with the best cooling system tested in this project, a low limit temperature of 0°C was chosen to avoid any water condensation issues.

Further details on temperature programming are described in appendix C. Next section is dedicated to the description of the gas chromatographic equipment and samples used in this study, and of the method followed for column evaluation.

# III.C. Gas chromatography

## III.C.1. Equipment

Columns were connected to conventional GC apparatuses using universal press-fit connectors (Restek). Experiments were mainly carried out at MEMS TC, but also occasionally at the ESPCI.

### *III.C.1.01 Equipment at MEMS TC*

Helium was purchased from Air Liquide (grade Alphagaz 1) and used as carrier gas. In a specific experiment, nitrogen (Praxair 2.0) was used as carrier gas, to compare kinetic performances of both carrier gases and to evaluate the possibility to use air instead of helium, as it is the case in XXXXXXXXXXX.

Experiments were carried out on a Varian 3800 run with Galaxy software (figure 64a). The chromatograph was equipped with a 1079 split-splitless injector set at 200°C and a flame

ionization detection (FID) system set at 300°C. Hydrogen was obtained from an F-DBS NMH2 250 hydrogen generator. A compressor with F-DBS GC 1500 air generator and Donaldson filters were used for the air gas source. Makeup gas (helium) flow rate was set at 30 mL.min$^{-1}$, hydrogen flow rate at 30 mL.min$^{-1}$, and air flow rate at 300 mL.min$^{-1}$.

An alternative GC system (figure 64b) with the micro machined thermal conductivity detector and the micro mechanical injector developed at MEMS TC was also, to check for air-methane separation on the different columns prior to thermodynamic and kinetic evaluations. A few other specific tests carried out with this setup are detailed in appendix A. Helium was as well used carrier gas (same reference), and detector signal was hard- and software processed by adequate tools developed at MEMS TC.

### *III.C.1.02 Equipment at the ESPCI*

Experiments were carried out on an Agilent 7820A run with ChemStation software (figure 64c). The chromatograph was equipped with a split-splitless injector set at 40°C and a flame ionization detection (FID) system set at 300°C. Hydrogen was purchased (grade HG by Air Liquide) and compressed air from the lab network was used for the air gas source. Makeup gas (helium) flow rate was set at 60 mL.min$^{-1}$, hydrogen flow rate at 30 mL.min$^{-1}$, and air flow rate at 300 mL.min$^{-1}$.

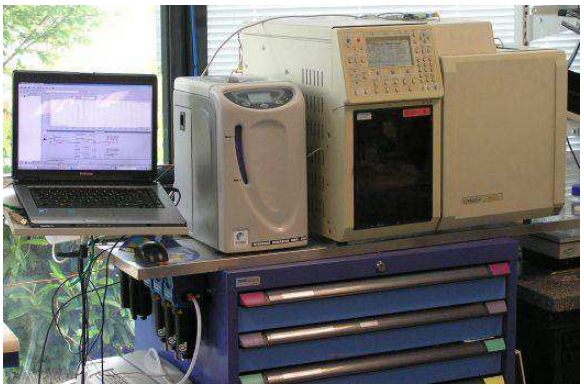

*Fig. 64a: GC Varian 3800 setup at MEMS TC, before (left) and after (right) moving*

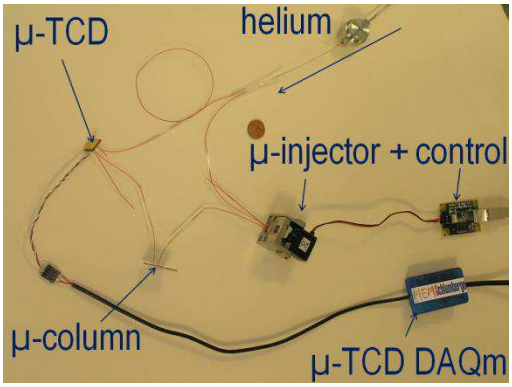


*Fig. 64b: micro thermal conductivity detector and micro mechanical injector setup at MEMS TC*

*Fig. 64c: GC Agilent 7820 setup at the LSABM of the ESPCI*

*Fig. 64: pictures of the different GC setups used in this study.*

- Other compounds separations (alcohols and amines) tests were planned and very briefly and roughly carried out on regular sputter-deposited silica columns, without success.

## III.C.2. Samples

Three types of hydrocarbon gaseous mixtures were used, corresponding to different periods of the study (light alkanes, various hydrocarbons, and GeoServices mixtures); their names, origins, compositions and purposes are summarized in table 10.

Gas samples were prepared by filling a sampling bag (Calibond, Calibration Technologies Inc) with the different mixtures. A 10 µL gas tight glass syringe (Hamilton) was used to sample the gas mixture and inject it into the injector (for both experiments with conventional GC and with µTCD setup).

## III.C.3. Column evaluation

The most important part of this research work focused on column evaluation. Preliminary observations aimed at qualitatively describing which separations could be operated on which columns; very basic precision studies were carried out, and columns thermodynamic and kinetic behaviors were evaluated; finally, a few experiments aimed at partially demonstrating the possibility to use such columns in industrial developments.

### *III.C.3.01 Preliminary observations*

Light saturated hydrocarbon mixtures were injected on the different columns under isothermal conditions to determine which compounds could be separated or not for each stationary phase and column design. As air – methane separation was tested on the µTCD setup long before temperature programming system was achieved and dicing systematical, column cooling (to improve possible separation resolution) was enabled by placing the wafer upon ice cubes in a glass chiller. Preliminary separation tests which did not involve air were naturally carried out on the conventional GC setup.

No specific activation was led before preliminary observations, except for alumina columns (1 hour, 150°C, 5.1 bars helium sweeping), but, for following quantitative evaluations, in order to ensure that all columns were tested in similar temperature and humidity conditions, each column was regenerated with a 30 minutes-long drying at 110°C and 5.1 bars helium sweeping prior to evaluation.

As mentioned in I.G., injected quantities could not be held constant for the different columns evaluated: in the extreme cases, volumes that were not detected on one column could result in overloading for another column, inducing flawed retention and efficiency. Therefore, the smallest volume leading to a signal satisfying enough for accurate post-processing was estimated for each column in the preliminary study and used for its evaluation.

### *III.C.3.02 Precision tests*

Very basic preliminary studies were led with the following approach:

- injection repeatability study aimed at assessing standard deviations between several successive injections, within one experiment, with the same column, parameters and user;

- column evaluation precision over short periods, and over user and/or setup change was also estimated on a regular silica column;

- finally, fabrication method precision was evaluated (figure 65), with a column to column (three columns from the same wafer) and a wafer to wafer (four columns from four wafers) precision evaluation, again on regular silica columns, including thermodynamic, kinetic, and temperature-programmed experiments.

| Name | Origin | Compound | Quantity (%) | Purpose |
|---|---|---|---|---|
| C1-C3 | Praxair individual bottles | C1 | ~33 | First tests and characterizations (until 03/2011) |
| | | C2 | ~33 | |
| | | C3 | ~33 | |
| C1-C4 | Air Liquid mixture | C1 | 25 | Advanced tests and characterizations (from 03/2011) |
| | | C2 | 25 | |
| | | C3 | 25 | |
| | | C4 | 25 | |
| C1-C5 | C1-C4 | C1-C4 | ~20 each | Occasional tests |
| | VWR flask headspace | C5 | ~20 | |
| C1-C9 | C1-C4 | C1-C4 | ~11 each | |
| | VWR individual flasks headspace | C5 | ~11 | |
| | | C6 | ~11 | |
| | | C7 | ~11 | |
| | | C8 | ~11 | |
| | | C9 | ~11 | |
| Cyclic hydrocarbons | VWR individual flasks headspace | cC5 | ~50 | |
| | | cC6 | ~50 | |
| Aromatic hydrocarbons | VWR individual flasks headspace | Bnz | ~50 | |
| | | Tol | ~50 | |
| GeoServices 1 | Calibration mixture provided by GeoServices | C1 | 10 | Real mixture separation tests |
| | | C2 | 2.5 | |
| | | C3 | 2.5 | |
| | | iC4 | 1 | |
| | | C4 | 1 | |
| | | iC5 | 0.25 | |
| | | C5 | 0.25 | |
| | | 2iC6 | 0.03 | |
| | | 3iC6 | 0.03 | |
| | | C6 | 0.03 | |
| | | $N_2$ | make up | |
| GeoServices 2 | Calibration mixture provided by GeoServices | πC2 | 0.5 | |
| | | C6 | 0.025 | |
| | | C7 | 0.025 | |
| | | C8 | 0.025 | |
| | | Bnz | 10 | |
| | | Tol | 10 | |
| | | He | 10 | |
| | | $N_2$ | make up | |

*Table 10: mixtures used in this study, quantitative compositions and purposes*

### *III.C.3.03 Thermodynamic evaluation*

Thermodynamic evaluations of the different columns were carried out by quantifying the influence of temperature (Van't Hoff plot), column geometry (section, length, structural design) and stationary phase (nature, deposition time and pressure) on the retention and selectivity of light alkanes separations.

For relatively short columns as those reported in this study, retention factors were corrected to take into account the length of connection capillaries (~2x5 cm for the chip and ~2x15 cm for the GC apparatus, ~40 cm), which was not negligible compared to the length of the column.

Indeed, $k_{app}=(t_R-t_0)/t_0$ was the apparent retention factor; but, if $t_{Rcol}$ was the time effectively spent in the column by a retained compound, and if $t_{0col}$ was the time effectively spent in the column by a non-retained compound, then $t_R=t_{Rcol}+t_{Rcap}$ and $t_0=t_{0col}+t_{0cap}$ ("cap" stands for capillaries), and the real retention factor k was equal to $k=(t_{Rcol}-t_{0col})/t_{0col}=k_{app}$ x $(1+L_{cap}/L_{col})$.

This correction factor was of 1.18 for regular columns, 1.36 for semi-packed columns, and respectively 1.4 and 1.8 for 1 m and 0.5 m short-length columns.

Efforts were provided to model and interpret the observed behavior, according to GC basic theories (cf. I.A.5.): the plot of ln k against $10^3$/RT was expected to provide a linear curve with a positive slope equal to the adsorption heat $|\Delta_rH°|$ (for readability reasons, only the absolute value of the negative standard enthalpy $\Delta_rH°$ was considered); y-intercept of the plot ln k = f($10^3$/RT) then consisted in $\Delta_rS°/R$ - ln β (the range of the values of ln β explored in this study was around 1.5 to 4). ; for readability reasons as well, this y-intercept value of $\Delta_rS°/R$ - ln β was shortened in ln $k^\infty$ (value of ln k at infinite temperature).

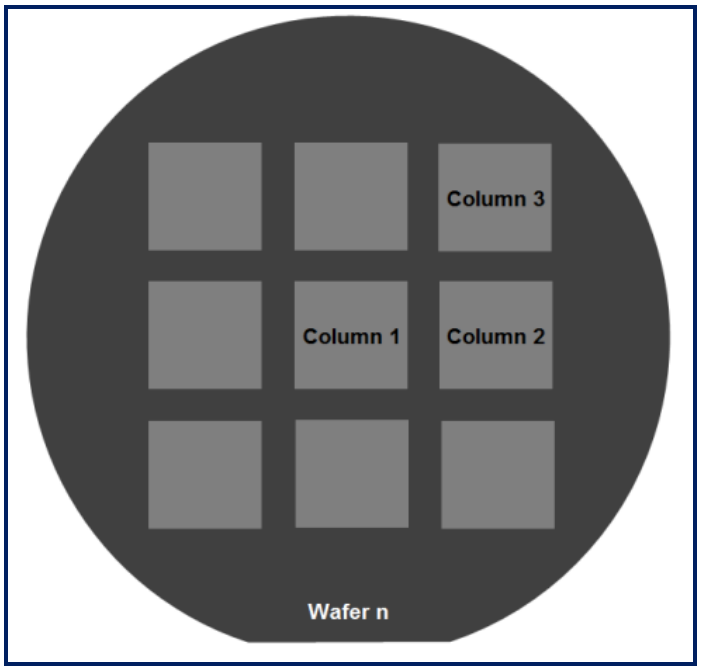


*Fig. 65: illustration of method precision evaluation for column fabrication*

### *III.C.3.04 Kinetic evaluation*

The influence of carrier gas velocity, temperature, column geometry (section, length, structural design) and stationary phase (nature, deposition time and pressure) on the efficiency of light alkanes separations was as well quantitatively evaluated and reported.

Van Deemter experiments were as usually carried out by measuring column theoretical plate number for different carrier gas velocities resulting from changes in input pressure; results modeling by a Van Deemter equation, as well as A, B and C coefficients calculation, were obtained by plotting HETP x u as a function of u, and by fitting the curve with a second order polynomial.

No corrections were brought to carrier gas velocity directly calculated through methane retention time and analytical line total length (column plus connection capillaries). Indeed, as methane could be very slightly retained on a few columns, as column section was not identical to capillary section (which implied different velocities), and as gases were compressible owing to their nature, displayed carrier gas velocity was thus an apparent velocity.

Numbers of plates were directly calculated by Galaxy software (as well as asymmetries and resolutions). In the discussions, emphasis will be not only put on minimal plate heights (for absolute comparisons of columns performances, as usual), but also on numbers of plates. In fact, as miniaturization was the crucial point, and as chip volume was directly linked to column length, total number of plates could be considered as more relevant than plate height, for chip size was the same for all the columns. For instance, if a semi-packed column presented a twice smaller plate height than a regular one, both finally resulted in the same total number of plates present on the chip, because of the channel wide section (and thus short length) required by semi-packed design.

### *III.C.3.05 Potential applications evaluation*

Temperature-programmed separations of C1-C4 (or C5) and of other hydrocarbons on sputter-deposited stationary phase micro columns were attempted. The possibility to use air as carrier gas instead of helium was then evaluated by a chromatographic comparison between helium and nitrogen. Finally, solutions to enable high temperature C1-C2 separation were investigated, and the effect of silica layer hydration on chromatographic properties of the micro column was investigated by injecting and making a 1 µL water droplet percolate through it.

All those experiments aimed at estimating columns versatility towards various requirements, regarding separated compounds, separation time, carrier gas, ambient temperature and humidity. They were carried out at MEMS TC at room temperature (30°C, except for high temperature separations).

The last section of this chapter is dedicated the description of the first attempts of micro column chip and block integration in an existing mini GC developed by GeoServices for the fast monitoring of C1-C5 alkanes as part of XXXXXXXXXXX analyses.

# III.D. Schlumberger confidential section

## III.D.1. Schlumberger confidential paragraph

Schlumberger confidential content – address requests to raphael.haudebourg@gmail.com
Schlumberger confidential content – address requests to raphael.haudebourg@gmail.com
Schlumberger confidential content – address requests to raphael.haudebourg@gmail.com
Schlumberger confidential content – address requests to raphael.haudebourg@gmail.com
Schlumberger confidential content – address requests to raphael.haudebourg@gmail.com
Schlumberger confidential content – address requests to raphael.haudebourg@gmail.com
Schlumberger confidential content – address requests to raphael.haudebourg@gmail.com
Schlumberger confidential content – address requests to raphael.haudebourg@gmail.com

## III.D.2. Schlumberger confidential paragraph

Schlumberger confidential content – address requests to raphael.haudebourg@gmail.com
Schlumberger confidential content – address requests to raphael.haudebourg@gmail.com
Schlumberger confidential content – address requests to raphael.haudebourg@gmail.com
Schlumberger confidential content – address requests to raphael.haudebourg@gmail.com
Schlumberger confidential content – address requests to raphael.haudebourg@gmail.com
Schlumberger confidential content – address requests to raphael.haudebourg@gmail.com
Schlumberger confidential content – address requests to raphael.haudebourg@gmail.com
Schlumberger confidential content – address requests to raphael.haudebourg@gmail.com
Schlumberger confidential content – address requests to raphael.haudebourg@gmail.com
Schlumberger confidential content – address requests to raphael.haudebourg@gmail.com
Schlumberger confidential content – address requests to raphael.haudebourg@gmail.com
Schlumberger confidential content – address requests to raphael.haudebourg@gmail.com
Schlumberger confidential content – address requests to raphael.haudebourg@gmail.com
Schlumberger confidential content – address requests to raphael.haudebourg@gmail.com
Schlumberger confidential content – address requests to raphael.haudebourg@gmail.com

# Conclusion

Various designs of micro machined columns were fabricated (open and semi-packed, different lengths and sections) and 5 different materials were tested as potential stationary phases (silica, alumina, graphite, magnesia, and titania), with different deposition processes. Layer structure was microscopically investigated and described, which both confirmed expectations from literature and prove it very difficult to accurately define deposition thickness and measure specific surface area.

Fabrication of semi-packed magnesia columns and of titania columns could not be achieved for technical reasons. Other difficulties, limitations and failures were encountered and partially solved, and did not jeopardize perspectives expected from the technology presented in this report.

An appropriate thermal management system was developed to enable chip temperature programming, and gas chromatography equipment utilized for column evaluation was accurately described. Chromatographic evaluation methods were as well presented.

First attempts to XXXXXXXXXXXXXXXXXXXXXXXXXXXXXXXXXXXXXXX were finally introduced.

The results of all these evaluations are displayed and discussed in the following chapter. A summary of partially or totally characterized columns is displayed in table 11.

| Stat. phase | Design and dimensions (length x width x depth) | Deposition time | Fabrication achieved? |
|---|---|---|---|
| Silica | Regular 2.2 m x 100 µm x 100 µm | 120 min | v (x 4) |
| | | 300 min (50 mT) | v |
| | Variable width 2.2 m x (100, 75, 50, 30) µm x 100 µm | 30 min | v |
| | | 60 min | v |
| | | 120 min | v |
| | | 180 min | v |
| | | 240 min | v |
| | Small section 2.2 m x 50 µm x 50 µm | 30 min | v |
| | | 240 min | v |
| | Short length (0.5, 1) m x 75 µm x 75 µm | 240 min | v |
| | Semi-packed (early design) 1.1 m x 200 µm x 100 µm | 120 min | v |
| | Semi-packed (late design) 1.1 m x 200 µm x 100 µm | 30 min | v |
| | | 120 min | v |
| Alumina | Regular 2.2 m x 100 µm x 100 µm | 60 min | v |
| | | 120 min | v |
| | Semi-packed (late design) 1.1 m x 200 µm x 100 µm | 120 min | v |
| | Variable width 2.2 m x (100, 75, 50, 30) µm x 50 µm | 240 min | v |
| Graphite | Variable width 2.2 m x (100, 75, 50, 30) µm x 100 µm | 60 min | v |
| | | 200 min | v |
| | Semi-packed (late design) 1.1 m x 200 µm x 100 µm | 60 min | v |
| Magnesia | Regular 2.2 m x 100 µm x 100 µm | 562.5 min | v |
| | Semi-packed (late design) 1.1 m x 200 µm x 100 µm | 280 min | x |
| Titania | Regular 2.2 m x 100 µm x 100 µm | 600 min | x |
| | Semi-packed (late design) 1.1 m x 200 µm x 100 µm | 618 min | x |

*Table 11: summary of fabricated wafers*

# IV. Results and discussions

This chapter displays the most relevant results obtained during the research work. They will first deal with temperature programming system performances, then with columns evaluations, and finally with XXXXXXXXXXX application preliminary tests. Discussions will be proposed along with presented results.

## IV.A. Temperature programming

This section presents a few major results obtained with the temperature programming system, regarding column heating and cooling. Additional technical and justification results are presented in appendix C.

### IV.A.1. Heating

Pulse Width Modulation (PWM) of constant voltage supply of the heating filaments at a work frequency of 21.3 Hz provided linear-like ramps, as shown on figure 67. In this example, a 10°C/s ramp (from 15°C to 215°C, with an ambient temperature of 30°C) was obtained with a voltage of 30 V.

As detailed in appendix C, using high voltages induced noticeable deviations from command temperature ramp, especially at low temperature (beginning of the ramp) and for slow ramps. On the contrary, using low voltages induced strong and irreversible deviation from command temperature ramp, due to insufficient power supply at high temperatures (end of the ramp) or for fast ramps. Second drawback was obviously found more constraining, and the maximum voltage allowed by the power supply (30 V) was chosen in the rest of the study.

Instantaneous power consumption was estimated through Joule law ($P=V^2/R$) and resistance was estimated through resistance temperature relation ($\Delta R/R_0=\alpha\Delta T$, cf. III.B.1). Power consumption for a 10°C/s ramp was between 80 W and 110 W for instantaneous power and between 10 W and 30 W for average power.

In this way, with the limit temperature of 220°C mentioned in III.B.7., it was possible to obtain temperature ramps up to 20°C/s (figure 68).

Infrared video recordings of PWM chip heating were taken for the three designs of heating filaments (figure 69), in order to check for possible heat inhomogeneities, and to choose the best design for mass production (9 identical filaments per wafer). Although no major inhomogeneity was found on the three designs, design 2 was naturally found to provide the most homogeneous heating. The main drawback with this design was the necessity to connect 6 wires (instead of 4 for both other designs). This drawback appeared to be relatively constraining for first manual bench completion, but was expected not to be constraining anymore for further industrial packaging, and design 2 was chosen for 9 identical filaments mask drawing.

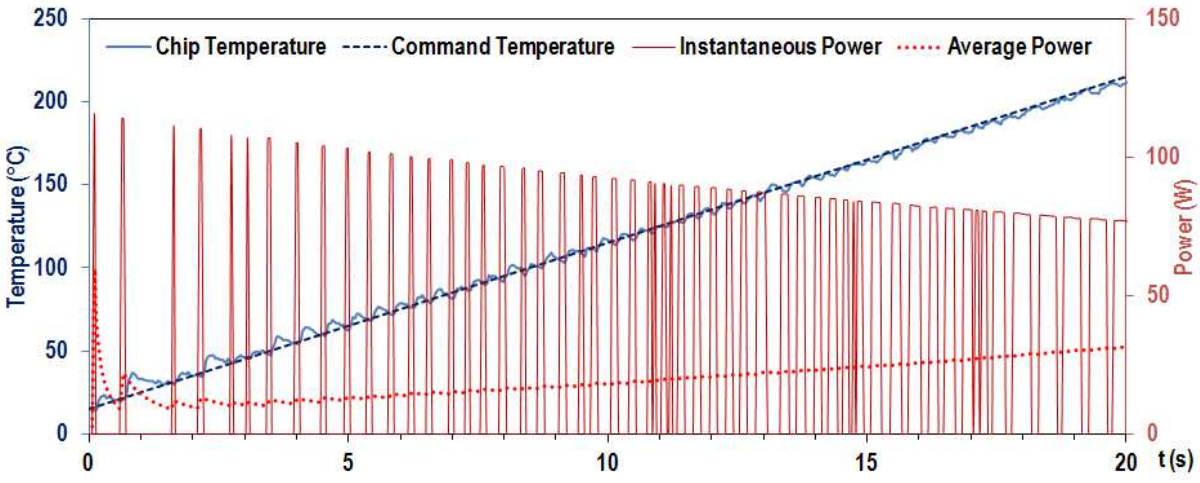


*Fig. 67: illustration of 1st order PWM of a constant voltage (30 V) to obtain a linear temperature ramp (from 15°C to 215°C at 10°C/s), and corresponding power consumption*

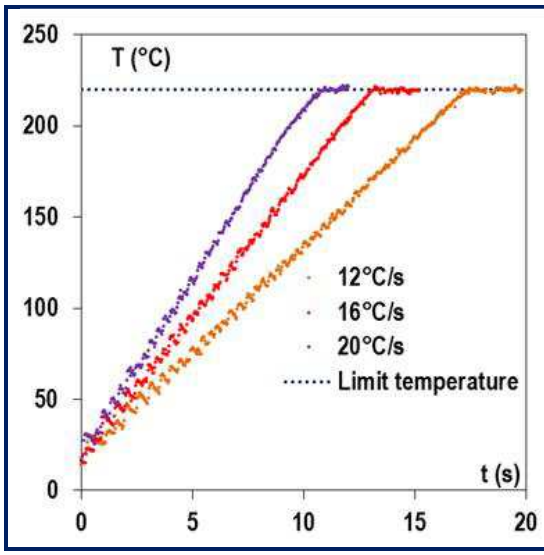


*Fig. 68: temperature ramps of 12°C/s, 16°C/s and 20°C/s, from an initial temperature of 15°C to an final temperature of 220°C.*

*Ambient temperature: 30°C*
*Voltage: 30 V PWM*

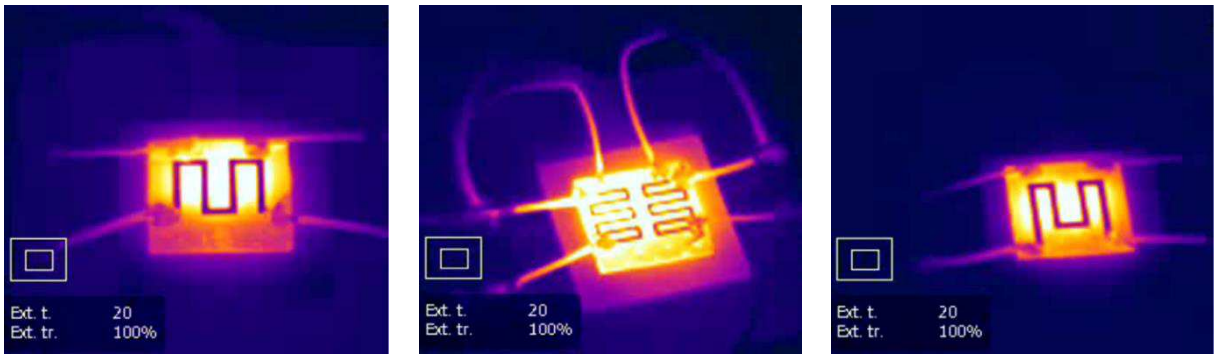


*Design 1* *Design 2* *Design 3*

*Fig. 69: frozen images from infrared video recordings of PWM heating (20°C-100°C at 15°C/s) of chips with the three different designs*

Fast cooling to ramp initial temperature (initially or after a preceding ramp) was performed thanks to the Peltier kit, as described in next paragraph.

## IV.A.2. Cooling

After comparative investigation by Emna Zoghlami under the supervision of the author, an optimized cooling system, as reported in III.B.3., provided fast temperature drops between ramp end temperature and ramp beginning temperature. As it will be shown in the columns evaluation section, those temperatures typically ranged around 120-130°C for end of ramp and 10°C-20°C for start of ramp.

Cooling time from 130°C to 15°C was for instance performed in less than 14 s at an ambient temperature of 30°C, as demonstrated by figure 70a.

Whole cooling system (Peltier and fan) power consumption while working ranged between 10 W and 20 W.

In the real conditions of targeted application (successive and continuous heating and cooling cycles), cooling performances were expectedly slightly lowered, due to capacitive effects (heat storing in column block), compared to isolated cooling performances. Cooling time from 120°C to 20°C increased from less than 10 s to around 14 s in an experiment involving 47 heating and cooling cycles in a row (figure 70b). Nevertheless, cooling time stabilized after 15 cycles to reach a plate.

## IV.A.3. Conclusion

Chip low power fast heating and fast cooling were achieved through the temperature programming system. These results will particularly be called on in the potential application evaluation paragraph of the next section, dedicated to column evaluation.

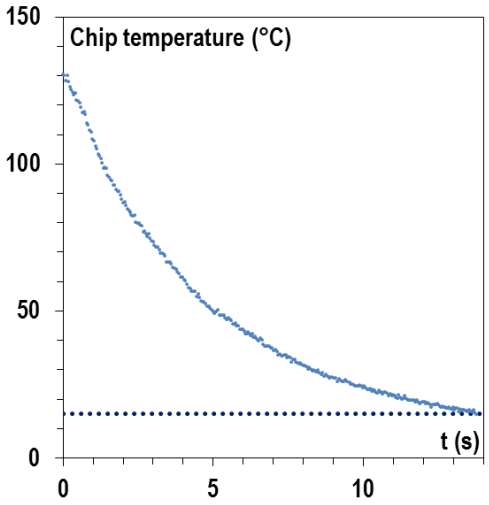


*Fig. 70a: fast temperature drop from 130°C to 15°C in less than 14 s*

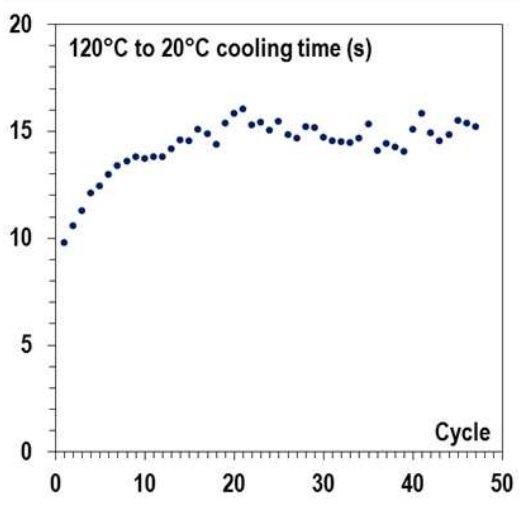


*Fig. 70b: evolution of cooling time (120°C to 20°C) for 47 successive ramps and preparations*

*Fig. 70: cooling system most relevant results (ambient temperature: 30°C)*

## IV.B. Columns evaluations

This section is the heart of the report, from a fundamental point of view, and displays the first chromatographic results ever published of sputter-deposited silica, alumina, graphite and magnesia as stationary phases for micro gas chromatography columns. Preliminary observations will first show which of the light alkanes these columns were able to separate, along with a qualitative evaluation of the separations. Experiments and methods intermediate precisions will allow estimating what credit should be given to the quantitative evaluations which will then follow, namely thermodynamic, kinetic, and real condition behavior of the micro column. A last paragraph will finally summarize the most relevant results obtained in the preceding paragraphs.

### IV.B.1. Preliminary observations

The purpose of this paragraph is to display various relevant examples of light alkanes separations on the different stationary phases and types of column. In order not to overload this report, only one chromatogram for each stationary phase and type of columns is exhibited in this paragraph. Actually, chromatograms shapes were very similar from one column to another with the same design and stationary phase. Quantitative differences will be accurately highlighted in the following paragraphs.

#### *IV.B.1.01 Silica*

Sputter-deposited silica semi-packed and regular micro columns were proven able to separate light alkanes, at room temperature (30°C) and without preliminary treatment (figure 71). Alkanes were baseline resolved (minimal resolution observed: 3.5), and air and methane were even peak summit separated on semi-packed columns ($R_{Air-C1}$=0.7, figure 71a). C1-C5 isothermal separation was performed in 6.5 min on regular columns (figure 71b). A slight peak tailing was observed, as expected (peak asymmetries were 1.7, 2.0, 2.2, 1.8 and 2.0 from C1 to C5), and peak spreading strongly increased along with carbon number (peak base widths of 1 s and 1.3 min for C1 and C5).

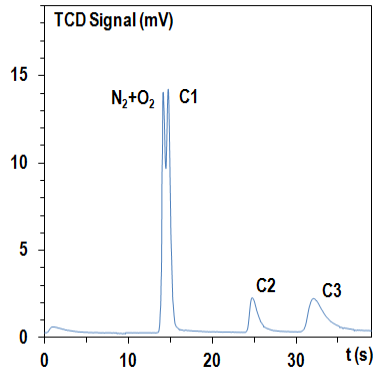


*Fig. 71a: Air-C1-C2-C3 separation (µTCD setup) on a semi-packed column (1.1 m x 200 µm x 100 µm, $e_f$=1 µm) P=7 bar, T=30°C, $V_{inj}$=5 µL*

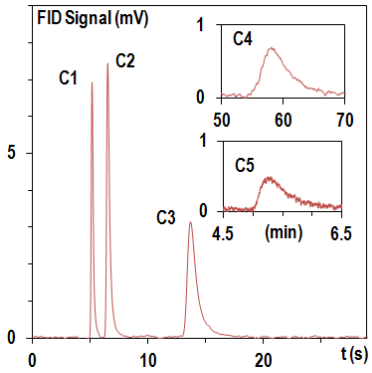


*Fig. 71b: C1--C5 separation (FID setup) on a regular column (2.2 m x 100 µm x 100 µm, $e_f$=2.6 µm) P=1 bar, T=30°C, $V_{inj}$=5 nL*

*Fig. 71: separations on sputter-deposited silica columns*

### *IV.B.1.02 Alumina*

As it was hypothetically suggested by the more dense-looking layer structure (compared to silica), open sputter-deposited alumina columns failed to separate C1, C2 and C3 (only C4 could be resolved from the three first alkanes). Figure 72a displays the corresponding chromatogram, obtained with a regular column. Neither activation, nor fabrication of higher phase ratio columns (thicker film, narrower section) could enable C1-C2-C3 separation. However, C1-C4 separation was possible on semi-packed columns (figure 72b) with a poor C1-C2 resolution (0.7) and a 1.3 min analysis time at room temperature (30°C). Peak tailing (1.1, 2.6, 4.1, and 3.2 from C1 to C4) was as well observed.

### *IV.B.1.03 Graphite*

As expected, graphite provided the strongest retentions (figure 73). Air and methane could be slightly separated ($R_{Air\text{-}C1}$=1.0) on narrow width (30 µm) open columns, with wafer cooling (figure 73a). C1-C4 alkanes could naturally be separated at room temperature (30°C) on regular columns (figure 73b); in this case, peak spreading was very pronounced (peak height decreased from 30 to 4.5 to 0.2 mV from C1 to C3, and C4 was diluted in baseline and could not be detected), as well as peak tailing (C1-C2-C3 peak asymmetries were respectively 2.1, 3.9 and 2.0). These results suggested that graphite was an appropriate stationary phase at higher temperatures. Figure 73c displays the chromatogram corresponding to the same experiment (column, sample, parameters) at 100°C; the C1-C4 mixture could be separated in 4 min, still with pronounced peak asymmetries (2.0, 2.5, 4.4 and 2.7), and tailing.

### *IV.B.1.04 Magnesia*

Similarly to alumina, magnesia was not retentive enough to separate C1 and C2 on open columns (figure 74), but C3 could be resolved from C1+C2 ($R_{(C1+C2)\text{-}C3}$=2.0). Peak asymmetry was also strongly marked for C4 (5.4; 2.0 for C3). Full C1-C4 separation was thus expected on magnesia semi-packed columns, but such columns could not be tested due to process failure (III.A.5.).

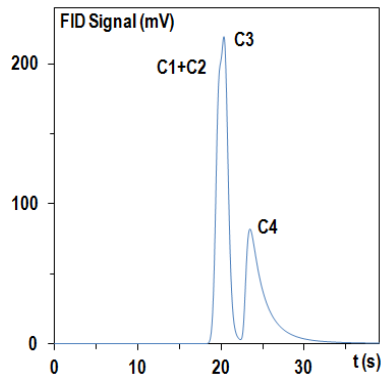


*Fig. 72a: C1-C4 separation on a regular column (2.2 m x 100 µm x 100 µm, $e_f$=1.5 µm) P=0.34 bar, T=30°C, $V_{inj}$=25 nL*

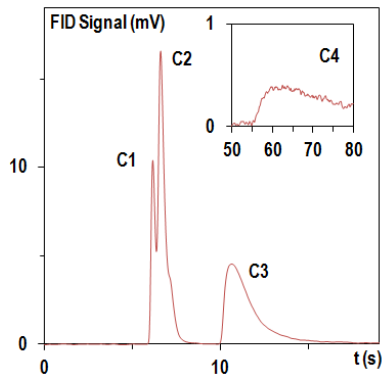


*Fig. 72b: C1-C4 separation on a semi-packed column (1.1 m x 200 µm x 100 µm, $e_f$=1 µm) P=6.75 bar, T=30°C, $V_{inj}$=0.25 µL*

*Fig. 72: separations on sputter-deposited alumina columns*

### *IV.B.1.05 Conclusion*

C1-C4 separation was possible on all types of silica and graphite columns fabricated, and on alumina semi-packed columns, and a very slight air-methane separation could be observed on silica semi-packed columns and on graphite columns. All these columns, plus magnesia open columns, were subject of further thermodynamic and kinetic evaluations. In these evaluations, methane peak served as reference for the measure of dead time.

Such experimental results are preceded by a short precision study, to discriminate between variations actually due to changes in the stationary phase or column design, and variations due to possibly flawed precision.

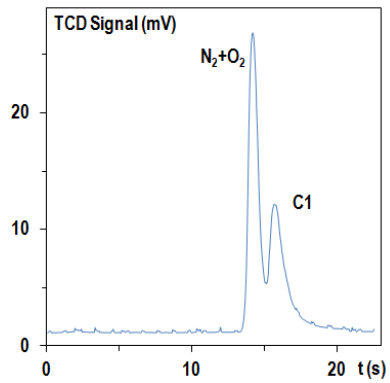


*Fig. 73a: Air-C1 separation on an open column (2.2 m x 30 µm x 100 µm, $e_f$=0.7 µm), P=2 bar, T~0°C, $V_{inj}$=0.5 µL*

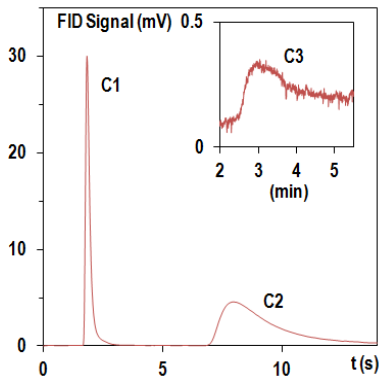


*Fig. 73b: C1-C4 separation on a regular column (2.2 m x 100 µm x 100 µm, $e_f$=1.1 µm), P=5.1 bar, T=30°C, $V_{inj}$=0.1 µL; C4 does not appear*

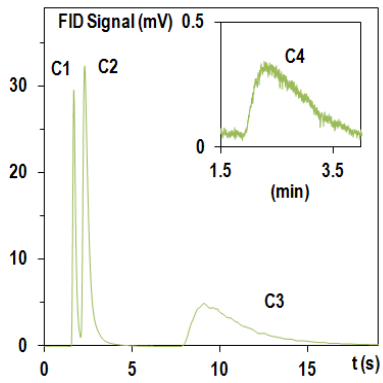


*Fig. 73c: C1-C4 separation on a regular column (same as 73b), P=5.1 bar, T=100°C, $V_{inj}$=0.1 µL*

*Fig. 73: separations on sputter-deposited graphite columns*

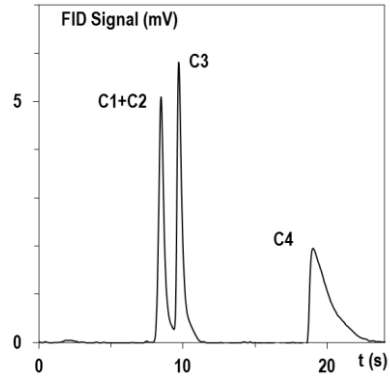


*Fig. 74: C1-C4 separation on a sputter-deposited magnesia regular column (2.2 m x 100 µm x 100 µm, $e_f$=1.2 µm) P=0.7 bar, T=30°C, $V_{inj}$=5 nL*

## IV.B.2. Precision tests

As mentioned in III.C.3.02, the aim of this paragraph is to display preliminary results on injection repeatability (standard deviations between several successive injections), on evaluation precision (over short periods, and over user and/or setup change), and on fabrication method precision (column to column and wafer to wafer precision compared evaluation). All experiments were led at MEMS TC, excepted evaluation precision over GC apparatus.

This paragraph only focuses on deviations due to setup and fabrication process. Thermodynamic and kinetic values will be discussed in the later paragraphs (IV.B.3., 4. & 5.).

### *IV.B.2.01 Injection repeatability*

Consecutive injections of the same sample on the same column under the same conditions provided very similar chromatograms (as for instance displayed on figure 75). Typical relative standard deviations of reference time, of C3 retention time (for Van't Hoff experiments) and of C2 plate height (for Van Deemter experiments) generally ranged below 5% (between 5% and 10% in exceptional cases) for three consecutive injections (see table 12).

In the later experiments, three consecutive injections were proceeded and averaged to obtain each point in the plots.

### *IV.B.2.02 Column evaluation precision*

Column evaluation precision over time and connections was first tested. Main results of two evaluations of the same column one week apart, with connection changes are displayed on figure 76. An expected slight change in carrier gas velocity at identical pressure was observed (for instance 74 and 60 cm/s at 1.7 bars); this was due to unavoidable connection imperfection imprecision, inducing slightly different permeabilities and pressure drops in the system. Nevertheless, this had only a very gentle influence on the thermodynamic behavior of the column (retention factors of 0.34 and 0.33 for C2 and 2.1 for C3), as well as on its kinetic behavior (minimum plate height for C2 of 0.85 and 0.86 mm and optimal velocity of 38 and 36 cm/s).

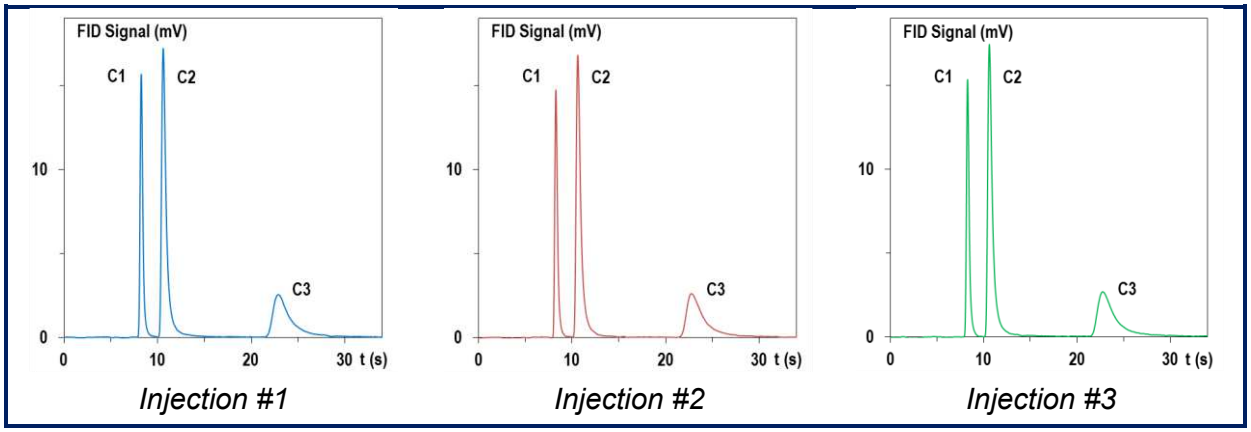


*Fig. 75: C1-C2-C3 separations on a silica regular column*
*(2.2 m x 100 µm x 100 µm, $e_f$=2.6 µm)*
*3 injections in a row P=0.7 bar, T=30°C, $V_{inj}$=5 nL with Varian GC 3800*

| Temperature (°C) | Relative standard deviation for three injections (%) | |
|---|---|---|
| | On $t_0$ | On $t_{R\,C3}$ |
| 30.0 | 0.0 | 1.9 |
| 37.0 | 2.8 | 1.2 |
| 48.0 | 2.8 | 0.0 |
| 68.6 | 1.5 | 1.0 |
| 90.0 | 0.0 | 0.0 |

*Table 12a: for Van't Hoff experiment (C1-C2-C3-C4, P=5 bar, $V_{inj}$=5 nL)*

| Pressure (bar) | Relative standard deviation for three injections (%) | |
|---|---|---|
| | On $t_0$ | On $HETP_{C2}$ |
| 0.34 | 0.00 | 2.89 |
| 0.68 | 0.00 | 2.00 |
| 1.01 | 0.00 | 2.69 |
| 1.35 | 0.00 | 3.38 |
| 1.69 | 0.00 | 3.05 |
| 2.03 | 0.00 | 4.64 |
| 2.36 | 1.32 | 5.20 |
| 2.70 | 2.94 | 2.54 |
| 3.04 | 3.24 | 7.02 |

*Table 12b: for Van Deemter experiment (C1-C2-C3, T=30°C, $V_{inj}$=5 nL)*

*Table 12: relative standard deviations for three consecutive injections on a silica regular column (2.2 m x 100 µm x 100 µm, $e_f$=2.6 µm) with Varian GC 3800*

*Fig. 76 : precision over time (1 week) and connections of column evaluation; silica regular column (wafer 1) (2.2 m x 100 µm x 100 µm, $e_f$=2.6 µm); T=30°C ; P=0.3 to 3 bars (Van Deemter); P=1.7 bars (chromatograms); C1-C2-C3 mixture, $V_{inj}$=5 nL.*

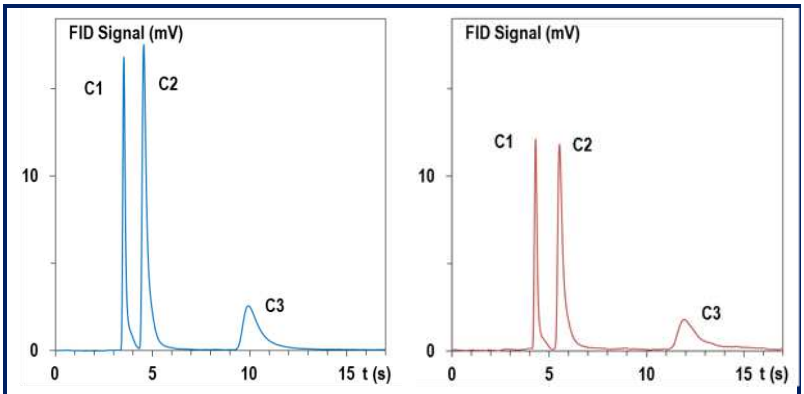


| | | Evaluation #1 | Evaluation #2 |
|---|---|---|---|
| **Fluidics** | $u_{1.7bars}$ | 74 cm/s | 60 cm/s |
| **Thermodynamics** | $k_{C2}$ | **0.33** | **0.33** |
| | $k_{C3}$ | **2.1** | **2.1** |
| **Kinetics (C2)** | $HETP_{min}$ | **0.85 mm** | **0.86 mm** |
| | $u_{opt}$ | 38 cm/s | 36 cm/s |
| | A | -0.62 mm | -0.14 mm |
| | B | 2.6 cm²/s | 1.7 cm²/s |
| | C | 1.8 ms | 1.3 ms |
| | Modeling quality | $R^2$=0.99 | $R^2$>0.995 |

Column evaluation precision over GC apparatus and user was then tested. Main results of two evaluations of the same column on MEMS TC Varian and on ESPCI Agilent GCs by different users are displayed on figure 77. Thermodynamic behavior of the column was found very similar (adsorption heats of 31.8 and 33.5 kJ/mol, entropic-geometric terms of -12.0 and -12.7, for C3). Kinetic behavior showed a more pronounced variation, especially in terms of optimal velocity (33 and 81 cm/s) and curve shape (plate height increased faster at both low and high velocities with Varian GC); minimal plate heights were closer to each other: 0.78 and 0.62 mm. Pronounced variations in terms of kinetic behavior may be due to meaningful differences between both setups regarding dead volumes*, and, therefore, extra column

effects, or regarding carrier gas quality. Other mentionable differences between both setups were injector temperature (220°C for Varian GC, 40°C for Agilent GC), injected quantities (5 and 100 nL), and software for signal processing (Galaxy and Chemstation).

### *IV.B.2.03 Column fabrication intermediate precisions*

A first precision study was early carried out on two columns from the same wafer (W1). At the moment of this preliminary experiment, the only mask to contain open columns was the variable width mask; in this mask, 2.2 m x 100 µm x 100 µm columns were in positions 2 and 3 (cf. figure 65). This first study provided very interesting results, as shown on figure 78. Both thermodynamic and kinetic behaviors were found very similar: retention factors were 0.33 and 0.31 for C2 and 2.1 and 2.0 for C3; minimal C2 plate heights were 0.86 and 0.81 mm and optimal velocities were 36 and 37 cm/s.

*Fig. 77 : precision over GC apparatus and user of column evaluation*

*silica regular column (wafer 2) (2.2 m x 100 µm x 100 µm, $e_f$=2.6 µm);*

*C1-C2-C3-C4 mixture, $V_{inj}$=5 nL (Varian) $V_{inj}$=1 µL (Agilent)*

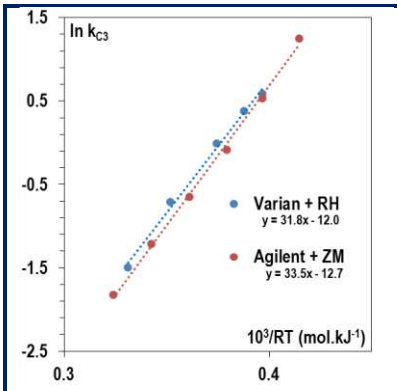


*Van't Hoff plots for C3 ($u=u_{opt}$)*
*Varian: T from 30°C to 90°C*
*Agilent: T from 17°C to 98°C*

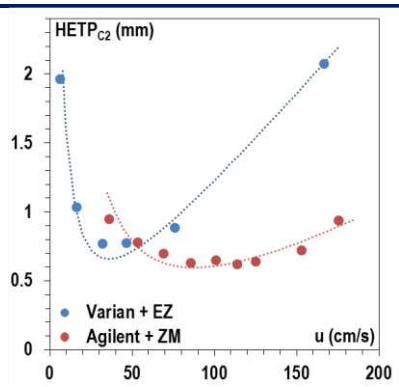


*Van Deemter plots for C2 (T=30°C)*
*Varian: P from 0.1 to 4.1 bars*
*Agilent: P from 0.7 to 4.1 bars*

**Chromatograms**

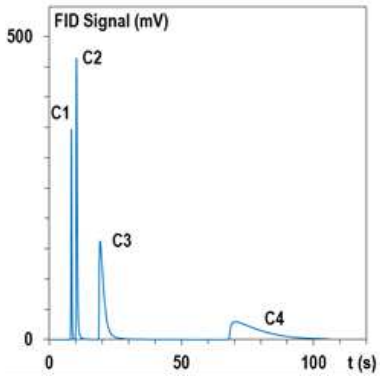


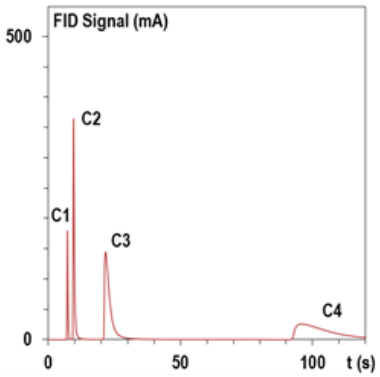


| | | Evaluation at MEMS TC | Evaluation at the ESPCI |
|---|---|---|---|
| **Thermodynamics (C3)** | $\lvert\Delta_r H°\rvert$ | **31.8 kJ/mol** | **33.5 kJ/mol** |
| | ln $k^\infty$ | -12.0 | -12.7 |
| | Modeling quality | $R^2$>0.995 | $R^2$>0.995 |
| **Kinetics (C2)** | $HETP_{min}$ | **0.77 mm** | **0.62 mm** |
| | $u_{opt}$ | 36 cm/s | 88 cm/s |
| | A | -0.33 mm | -0.60 mm |
| | B | 1.8 cm²/s | 5.3 cm²/s |
| | C | 1.4 ms | 0.68 ms |
| | Modeling quality | $R^2$>0.995 | $R^2$=0.98 |

At the end of the research work, when a mask with 9 identical columns was fabricated, a second column to column variation study was led on 3 columns from the same wafer (wafer 3, positions 1, 2 and 3, again according to figure 65). As shown on figure 79, variations were found more important than in the first study, especially regarding kinetic performances: from column 1 to column 3 through column 2, minimal plate height increased from 0.72 to 2.3 mm, while optimal velocity increased from 35 to 69 cm/s. C3 adsorption heats, though in the same order of magnitude, were also significantly dispersed (28.6, 27.1 and 21.5 kJ/mol). Actually, corner column (column 3) showed a relatively strong different behavior than both other columns, as illustrated by entropic-geometrical values, by A, B, and C kinetic values, or more concretely, by modeling correlation coefficients $R^2$. This seemed to stem from inhomogeneities in sputter-deposited layer thickness (~10%, cf. III.A.2.02). Besides, it has to be highlighted that this second study was led after an intense and barely appropriate use of the sputtering machine, including 4 target changes and 2 repairing interventions, with noticeable degradations in clean room status (see III.A.5.).

Gathering results obtained throughout the research work, a wafer to wafer variation study could also be led, on columns in position 2 from 4 different wafers (figure 80). Wafers 1 and 2 were fabricated before clean room and sputtering machine edgy utilization, while wafer 3 and 4 were fabricated after. Standard deviations on 4 values were 20% for C3 retention factor and 30% for C2 minimal plate height. C3 adsorption heats ranged between 25.3 and 31.8 kJ/mol.

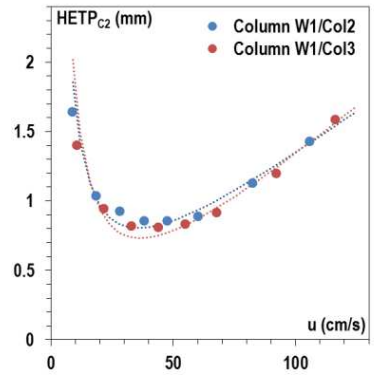


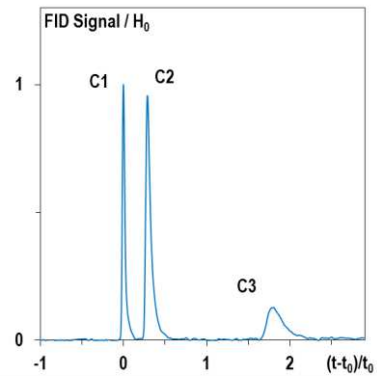


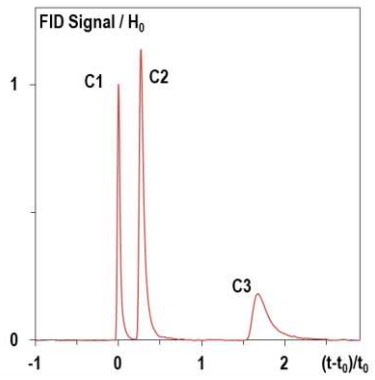


| Van Deemter plots (0.3 to 3 bars) | | Column W1/Col2 | Column W1/Col3 |
|---|---|---|---|
| **Thermodynamics** | $k_{C2}$ | **0.33** | **0.31** |
| | $k_{C3}$ | **2.1** | **2.0** |
| **Kinetics (C2)** | $HETP_{minC2}$ | **0.86 mm** | **0.81 mm** |
| | $u_{opt}$ | 36 cm/s | 37 cm/s |
| | A | -0.14 mm | -0.38 mm |
| | B | 1.7 cm²/s | 2.0 cm²/s |
| | C | 1.3 ms | 1.5 ms |
| | Modeling quality | $R^2$>0.995 | $R^2$>0.995 |

*Fig. 78 : evaluation of fabrication method precision: column to column variability (wafer 1), silica regular columns (2.2 m x 100 µm x 100 µm, $e_f$~2.6 µm), T=30°C, chromatograms P=1.1 bars, C1-C2-C3 mixture, $V_{inj}$=5 nL, normalized axes (by C1 peak height $H_0$ and retention time $t_0$)*

In spite of these quantitative significant variations (column to column and wafer to wafer), columns qualitative behavior in terms of separation and resolution was after all similar, as illustrated in next subparagraph.

*Fig. 79 : evaluation of fabrication method precision: column to column variability (wafer 3)*

*silica regular columns (2.2 m x 100 µm x 100 µm, $e_f$~2.6 µm);*

*C1-C2-C3 mixture, $V_{inj}$=5 nL*

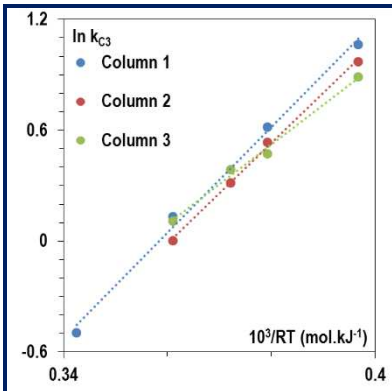


*Van't Hoff plots*
*P=0.3 bars, T from 30°C to 78°C*

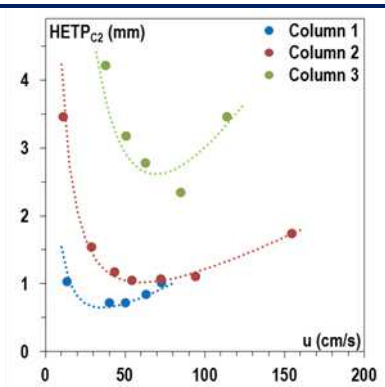


*Van Deemter plots*
*T=30°C, P from 0.3 to 4.1 bars*

| | | Column W3/Col1 | Column W3/Col2 | Column W3/Col3 |
|---|---|---|---|---|
| **Thermodynamics (C3)** | $\|\Delta_r H°\|$ | **28.6** | **27.1** | **21.5** |
| | ln k° | -10.2 | -9.8 | -7.7 |
| | Modeling quality | >0.995 | >0.995 | 0.99 |
| **Kinetics (C2)** | $HETP_{min}$ | **0.72 mm** | **1.1 mm** | **2.3 mm** |
| | $u_{opt}$ | 35 cm/s | 61 cm/s | 69 cm/s |
| | A | -0.35 mm | -0.50 mm | -3.2 mm |
| | B | 1.7 cm²/s | 4.6 cm²/s | 20 cm²/s |
| | C | 1.4 ms | 1.3 ms | 4.2 ms |
| | Modeling quality | $R^2$=0.99 | $R^2$>0.995 | $R^2$=0.95 |

*Fig. 80 : evaluation of fabrication method precision: wafer to wafer variability (column 2)*

*silica regular columns (2.2 m x 100 µm x 100 µm, $e_f$~2.6 µm);*

*C1-C2-C3 mixture, $V_{inj}$=5 nL*

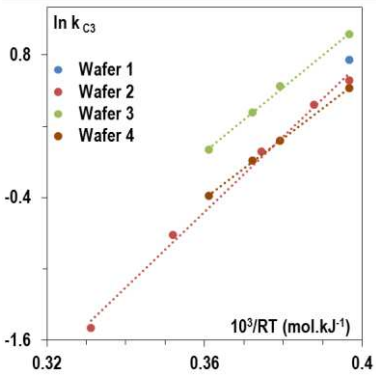


*Van't Hoff plots*
*P=0.3 bars, T from 30°C to 90°C*

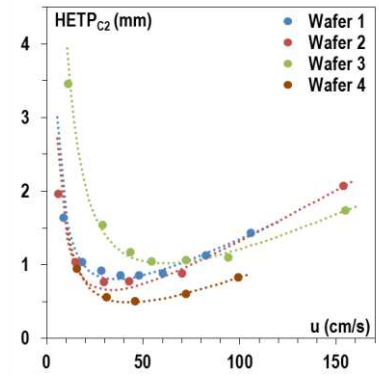


*Van Deemter plots*
*T=30°C, P from 0.3 to 4.1 bars*

| | | Column W1/Col2 | Column W2/Col2 | Column W3/Col2 | Column W4/Col2 |
|---|---|---|---|---|---|
| **Thermodynamics (C3)** | k | **2.1** | **1.8** | **2.6** | **1.7** |
| | $\|\Delta_r H°\|$ | - | 31.8 kJ/mol | 27.2 kJ/mol | 25.3 kJ/mol |
| | ln k° | - | -12.0 | -9.8 | -9.5 |
| | Modeling quality | - | $R^2$>0.995 | $R^2$>0.995 | $R^2$>0.995 |
| **Kinetics (C2)** | $HETP_{min}$ | **0.86 mm** | **0.77 mm** | **1.1 mm** | **0.51 mm** |
| | $u_{opt}$ | 36 cm/s | 36 cm/s | 61 cm/s | 43 cm/s |
| | A | -0.14 mm | -0.33 mm | -0.50 mm | -0.40 mm |
| | B | 1.7 cm²/s | 1.8 cm²/s | 4.6 cm²/s | 1.9 cm²/s |
| | C | 1.3 ms | 1.4 ms | 1.3 ms | 1.0 ms |
| | Modeling quality | $R^2$>0.995 | $R^2$>0.995 | $R^2$>0.995 | $R^2$>0.995 |

### *IV.B.2.04 Temperature-programmed use intermediate precision*

C1-C4 temperature-programmed separations (6°C/s) using the system described in III.B. and IV.A. were evaluated with the three wafer 3 columns and one wafer 4 column above. Figure 81 displays the resulting chromatograms, both on conventional axes and on axes normalized by dead time and C1 peak height for each chromatogram.

Column fabrication and temperature-programming provided just enough precision to obtain specific retentions and absolute peak identification on conventional axes (C1 was eluted between 0 and 4.4 s, C2 between 4.4 s and 5.7 s, C3 between 6.1 and 8.4 s, and C4 between 8.4 and 13 s); on normalized axes, compounds were even more easily identifiable through their retention factors (0.2 to 0.4 for C2, 0.6 to 1.3 for C3, and 1.3 to 2.8 for C4).

### *IV.B.2.05 Conclusions*

Manual injection process was found highly repeatable, and repeatability was even expected to be improved with the use of an automate injection system, as it is the case in XXXXXXXXXXX analysis for instance.

Column evaluation was also found highly reproducible over connections and short periods (such as one week). Precision of column evaluation over GC apparatus was of good quality regarding thermodynamic values, or maximal efficiency, but showed stronger variations regarding other kinetic values. This was probably due to the small volume of the column, inducing much higher influence of GC apparatus dead volumes or carrier gas quality.

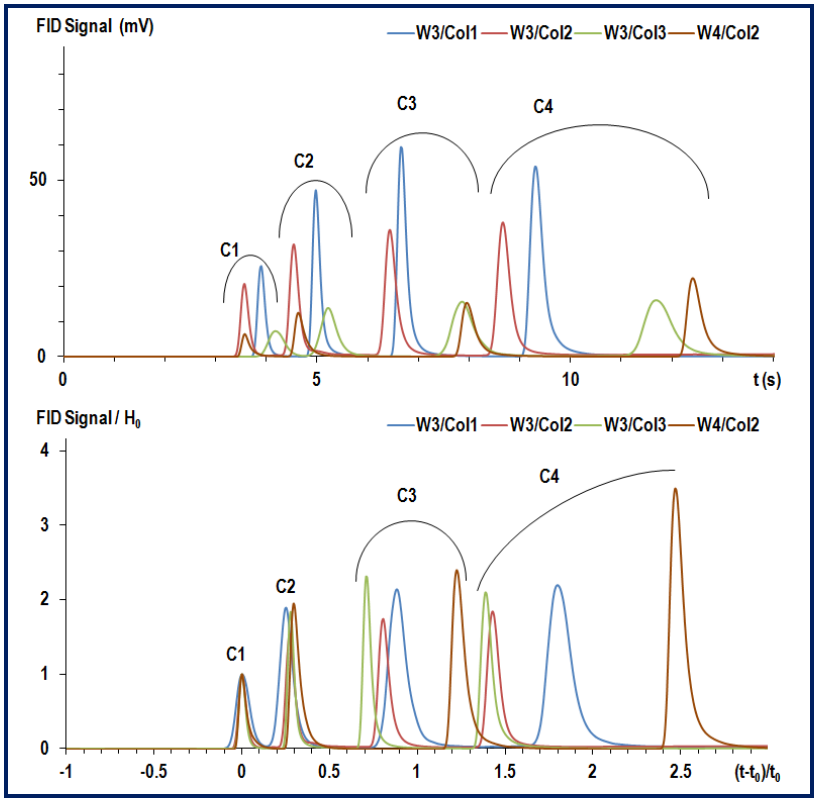


*Fig. 81: temperature-programmed use precision, C1-C4 separations;*

*silica regular columns: 2.2 m x 100 µm x 100 µm, $e_f$~2.6 µm;*

*P=1.7 bars, $V_{inj}$=5 nL, T=17°C to 120°C at 6°C/s;*

*Top: conventional axes*

*Bottom: axes normalized by dead time and C1 peak height for each chromatogram*

The evaluation of column fabrication intermediate precision showed typical variations of 20-30% depending on the considered value. Strongest variations were obtained with corner columns (deposition inhomogeneities) and with columns fabricated in the latest moments of the research work, where sputtering machine use and clean room quality may have been less appropriate.

However, the evaluation of temperature-programmed use precision carried out on late-fabricated columns provided satisfying results, conferring a certain robustness to the chosen method; no dramatic variations in terms of qualitative separation or absolute retention were observed in the different studies.

## IV.B.3. Thermodynamic evaluation

Thermodynamic evaluation consisted of the measure of the variation of retention factor along with chemical compounds (hydrocarbon, stationary phase), with setup parameters (pressure and temperature), and with column layout (design, section, length, stationary phase film thickness). The aim of this evaluation was twofold: pure description of the thermodynamic behavior of sputter-deposited stationary phase micro columns, and modeling attempt.

### *IV.B.3.01 Influence of alkane carbon number*

A first experiment evaluated retention factors for C2-C5 hydrocarbons on silica regular columns. The logarithms of retention factors were plotted against carbon number in an isothermal separation (figure 82 left), and apparent retention factors were plotted against carbon number in a temperature-programmed separation (figure 82 right). Both plots were expectedly found linear ($R^2$>0.995), confirming these micro columns to behave like conventional separation columns, at least for C1-C5 linear saturated hydrocarbons. Physical meaning of slopes is discussed in the section dedicated to Van't Hoff plots (IV.B.3.04).

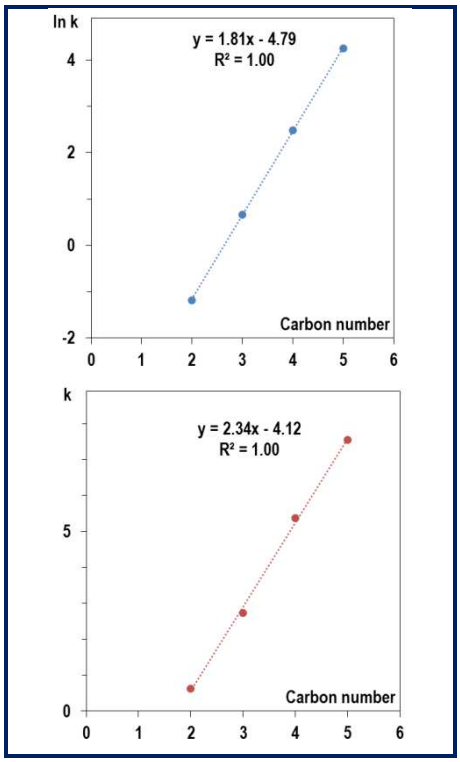


*Fig. 82: retention factors as a function of carbon number for C1-C5 hydrocarbons on silica regular column (2.2 m x 100 µm x 100 µm, $e_f$~2.6 µm);*

*<u>left:</u> isothermal separation at 30°C (see chromatogram on fig. 71b)*

*<u>right:</u> temperature-programmed separation, 13°C - 150°C at 15°C/s (see chromatogram on fig. 105b )*

### *IV.B.3.02 Influence of pressure*

Before proceeding to Van't Hoff plots for the different columns (variation of retention factors along with temperature), it was necessary to evaluate the influence of pressure or carrier gas velocity on retention factors values. Theoretically, retention factors are independent from carrier gas velocity (this is the whole point of the calculation of retention factors, which consists of normalized retention times). Actually, a slight variation (relative standard deviation of 2%) of retention factor due to changes in carrier gas velocity was observed, as shown on figure 83. This variation was smaller than the one observed injection to injection, but was not random, as suggested by the clear increase of retention factor with carrier gas velocity. The hypothesis of a very slight temperature decrease along with carrier gas velocity increase was emitted, but remained unverified. Variation was considered small enough to be ignored in the rest of the thermodynamic study, and carrier gas velocity was chosen according to other criteria.

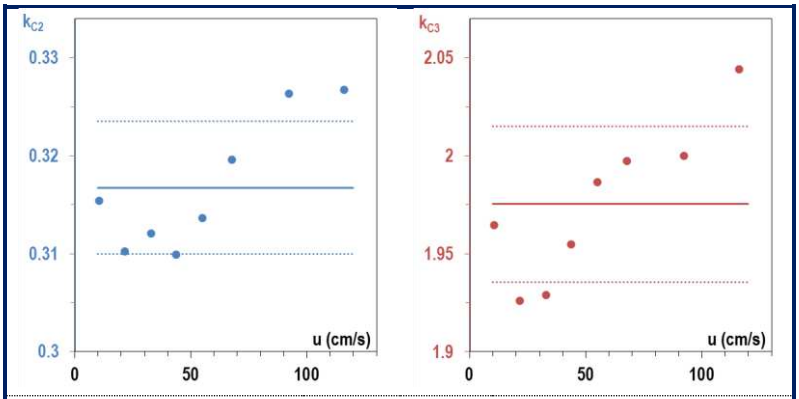


*Fig. 83: retention factors as a function of carrier gas velocity for C2 and C3 hydrocarbons on silica regular column,*

*2.2 m x 100 µm x 100 µm,*
*$e_f$~2.6 µm,*

*evaluation at MEMS TC*
*T=30°C, P=0.3 to 3 bars,*
*$V_{inj}$=5 nL.*

### *IV.B.3.03 Influence of temperature; Van't Hoff plot*

Retention was naturally decreased when temperature increased (see figure 84). On the reference silica regular column, retention factors for C2, C3 and C4 decreased from 0.26, 1.8, and 11, at 30°C, to 0.062, 0.22, and 0.72, at 90°C. The plot of the logarithm of k for C2, C3, and C4, against $10^3$/RT at different temperatures resulted in straight lines, directly indicating adsorption heats in kJ/mol. Obtained values (23.0 kJ/mol, 31.8 kJ/mol and 41.1 kJ/mol for C2, C3, C4) were in full agreement with values expected from literature study (II.D.1.), and suggested sputter-deposited silica as stationary phase to be ranked in the mesoporous category (cf. Kiselev, who obtained 24.9 and 33.1 kJ/mol for C2 and C3 on a mesoporous 720 m²/g silica gel). Moreover, and as suggested in the first subparagraph, the plot of adsorption heat against carbon number for C2-C4 also resulted in a straight line, although only with 3 points. This result was also in agreement with the literature, confirming that adsorption heat was a linear function of hydrocarbon polarizability (which was in turn a linear function of carbon number). Adsorption heats for higher carbon numbers could then be a priori estimated through the obtained relation:

$$|\Delta_r H°| = 9.1\ n_c + 4.7\ \text{kJ/mol}$$

The interpretation of the decrease of the entropic-geometrical term along with carbon number was not as direct. A hypothesis was emitted, stating the decrease of the number of adsorption sites for more bulky hydrocarbons (compared to smaller ones), and thus, the decrease of the entropy of the system, or of the apparent volume of stationary phase available (resulting in an increase of β and in a decrease of - ln β), or both, along with carbon number. The correctness of the relation k=K/β could as well be put in doubt. Anyway, the increase of the retention along with carbon number was confirmed to be entirely enthalpic.

Then, the relative weights of the enthalpy, entropy and geometric contributions in the equation $\ln k = -\Delta_r H°/RT + \Delta_r S°/R - \ln \beta$ for this example could be compared: at 30°C, for propane, and assuming a value of 20.6 for the phase ratio in this column (calculated as described in III.A.3.06), ln k = -(-12.6) + (-8.9) - 3.0.

In this first example as well as in the following, carrier gas velocity was chosen as a compromise between number of points in the plot and experiment time (a velocity close to the optimal velocity for C2 could increase the range of temperatures in which C1 and C2 are separated, but higher velocities could fasten analyses). C3 was used as main probe, but occasionally also C2 for results strengthening and C4 for magnesia evaluation (no C1-C2 separation).

*Fig. 84 : thermodynamic evaluation of a silica regular column, 2.2 m x 100 µm x 100 µm, $e_f$~2.6 µm P=5.1 bars, evaluation at MEMS TC, C1-C2-C3-C4 mixture, $V_{inj}$=5 nL*

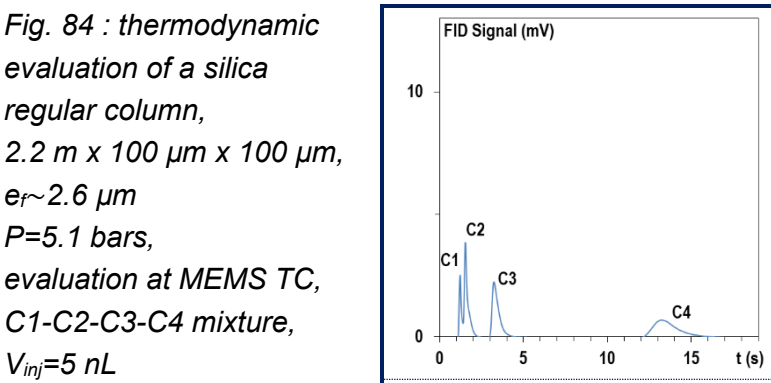


| | | T=30°C | T=90°C |
|---|---|---|---|
| **Chromatograms** | $k_{C2}$ | 0.26 | 0.062 |
| | $k_{C3}$ | 1.8 | 0.22 |
| | $k_{C4}$ | 11 | 0.72 |

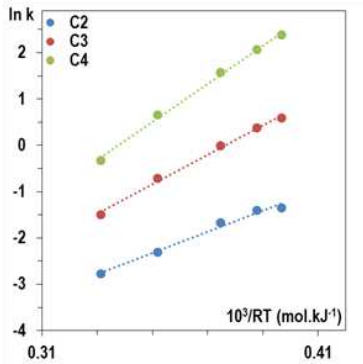


Van't Hoff plots (30 to 90°C)

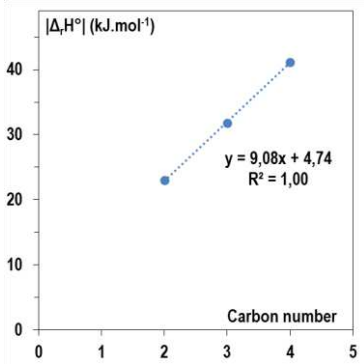


$|\Delta_r H°|$ as a function of carbon number

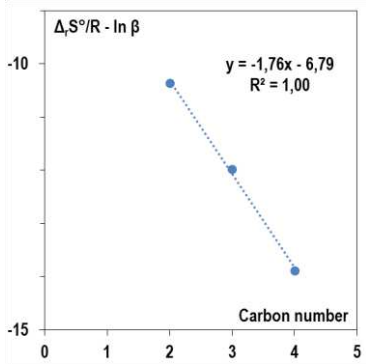


y-intercept as a function of carbon number

| | Compound | C2 | C3 | C4 |
|---|---|---|---|---|
| **Van't Hoff plots** | $\lvert\Delta_r H°\rvert$ | 23.0 kJ/mol | 31.8 kJ/mol | 41.1 kJ/mol |
| | ln k∞ | -10.4 | -12.0 | -13.9 |
| | Modeling quality | $R^2$=0.99 | $R^2$>0.995 | $R^2$>0.995 |

### *IV.B.3.04 Influence of column section*

A first approach was considered to evaluate the variation of retention as a function of phase ratio (volume of mobile phase by volume of stationary phase): using the early variable width mask and a 120 minutes silica sputtering deposition time, 100 µm-, 75 µm-, 50 µm-, and 30 µm-wide and 100 µm-deep columns were fabricated and compared. An additional variable width wafer, etched at a depth of 50 µm, was as well coated with a 120 min-long silica sputtering process, and a 100 µm-wide, 50 µm-deep column was added to the study. Phase ratio was purported to increase with column width (and constant stationary phase film thickness), but due to shadowing effects, deposited layer was also decreased in narrower columns (see also III.A.3.01 and figure 50). Eventually, both mobile and stationary phase volumes decreased with column narrowing, and the five columns thus fabricated presented very similar phase ratios (around 20, see figure 85 left and table).

Phase ratio variation was actually too restrained and phase ratio calculation was too approximate to observe the expected quantitative evolution of retentions factors (figure 85 right). Retention was even found roughly lower for smallest calculated values of β. However, such results were in agreement with the hypothesis according to which floor-deposited layer was not involved in retention process and should not be taken into account in the calculation of stationary phase volume: indeed, 100 µm-deep, 50 µm-wide columns retention was 1.5 time higher than 50 µm-deep, 100 µm-wide retention, with similar mobile phase volume, and similar stationary phase volume in the mentioned hypothesis; if floor-deposited layers had been taken into account, stationary phase volume for the second column would have been even bigger, and as would have been deviation from theory. All in all, C2 and C3 retention was quantitatively reported, but column section on its own was suggested not be the most appropriate parameter to adjust retention.

A second approach to adjust the variation of retention along with phase ratio naturally consisted of the fabrication of identical size column, with different sputter deposition times.

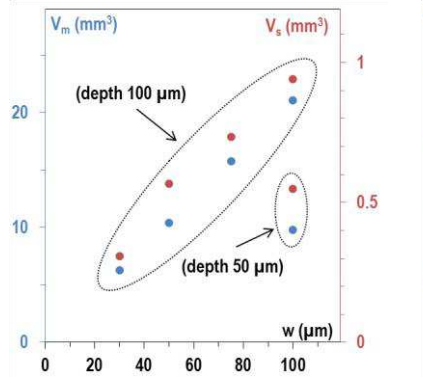


*Mobile and stationary phase volumes, both decreasing with column narrowing.*

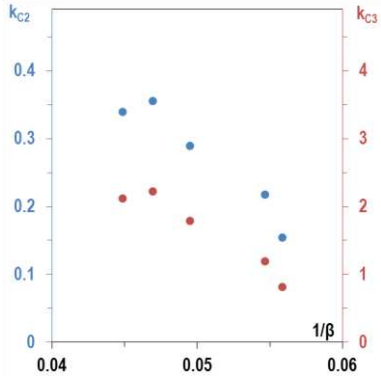


*Retention factors as a function of calculated phase ratios.*

| Depth | 100 µm | 100 µm | 100 µm | 100 µm | 50 µm |
|---|---|---|---|---|---|
| Width | 100 µm | 75 µm | 50 µm | 30 µm | 100 µm |
| Measured thickness | 2.6 µm | 2.4 µm | 2.1 µm | 1.6 µm | 2.8 µm |
| β | 22.3 | 21.3 | 18.3 | 20.2 | 17.9 |
| $k_{C2}$ | 0.34 | 0.36 | 0.22 | 0.29 | 0.15 |
| $k_{C3}$ | 2.1 | 2.2 | 1.2 | 1.8 | 0.82 |

*Fig. 85: influence of column section on retention;*

*sputter-deposited (120 min) silica columns,*

*2.2 m x 100 µm, widths: 100, 75, 50 and 30 µm,*

*and 2.2 m x 50 µm, width 100 µm;*

*evaluation at MEMS TC T=30°C, u~33 cm/s, $V_{inj}$=5 nL.*

### *IV.B.3.05 Influence of stationary phase film thickness*

2.2 m x 75 µm x 100 µm open columns from 5 different wafers with 5 deposition times (30, 60, 120, 180, and 240 minutes) were fabricated and evaluated. SEM observations of 60 and 120 minutes wafers were carried out, and led to the measurement of 1.2 and 2.4 µm layer thicknesses, which were extrapolated to the other wafers (respectively 0.6, 3.6 and 4.8 µm for 30, 180 and 240 min). Mobile phase volume was then calculated by withdrawing measured solid film volume to column volume. Errors made on the calculation of $V_m$, due to layer thickness inhomogeneities, layer porosity, and extrapolation, were supposed to be small (if not negligible) compared to mobile phase volume. According to gas chromatography theory, retention factors k were expected to be inversely proportional to phase ratios β (with distribution factor K as proportionality coefficient), expressed as $V_m/V_s$. In the hypothesis of a stationary phase volume proportional to layer thickness, the plot of $kV_m$ against $T_{depos}$ (figure 84) was expected to be linear, through the theoretical relation:

$$kV_m = KV_s = KL(2w+d)e_f P_{orosity} = KL(2w+d)V_{depos}P_{orosity}T_{depos}$$

where L, w and d are columns length, width, and depth, and where $e_f$ and $P_{orosity}$ are silica layer thickness and bulk porosity in % ($V_s=L(2w+d)e_fP_{orosity}$); $V_{depos}$ and $T_{depos}$ are the deposition rate and time of the silica layer ($e_f=V_{depos}T_{depos}$).

Experimental relation was barely found linear ($R^2$=0.94 for C2 and $R^2$=0.91 for C3), yet strictly increasing, as shown on figure 86. Two hypotheses were emitted to explain this poor linearity:

- low validity of the extrapolation of deposited thicknesses on 30, 180 and 240 minutes wafers; this would mean that layer thickness was not rigorously proportional to deposition time in the range evaluated; however, no trend (acceleration or deceleration of deposition) could be clearly identified from the result.

- low validity of the model k=K/β, which is rather generally valid for liquid films (and retention by dissolution of the analyte in the stationary phase); the extension of this model to inhomogeneous and porous solids would imply to have an accurate evaluation of the porosity of the layer; layer bulk porosity in % could even also depend on layer thickness (less porosity in weakly-columnar structures at short deposition rates?)

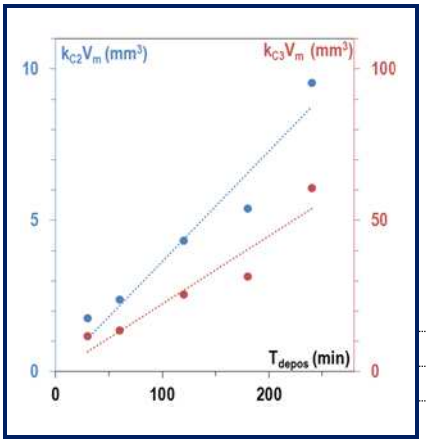


*Fig. 86: retention factors corrected with mobile phase volume as a function of deposition time for C2 and C3 hydrocarbons on silica columns, 2.2 m x 75 µm x 100 µm, evaluation at MEMS TC T=30°C, P=1 bar, $V_{inj}$=5 nL.*

| $T_{depos}$ | 30 min | 60 min | 120 min | 180 min | 240 min |
|---|---|---|---|---|---|
| $k_{C2}$ | 0.11 | 0.15 | 0.29 | 0.38 | 0.70 |
| $k_{C3}$ | 0.72 | 0.86 | 1.7 | 2.2 | 4.4 |

In the latest developments of the research work, 4 other designs of sputter-deposited silica columns were evaluated, including small section (50 µm x 50 µm), short length (1 m and 0.5 m), semi-packed, and high deposition pressure (50 mT). Contrary to variable thickness and variable width columns presented above, the influence of all geometric parameters could not be thoroughly studied; indeed, these developments first aimed at widening the range of explored types of columns, and at finding an appropriate design for industrial developments. Next paragraph is a brief summary of thermodynamic evaluations of these columns.

### *IV.B.3.06 Van't Hoff plots for sputter-deposited silica columns*

These results were mainly provided by Zineb Matouk during a 6 months Master of Science internship. Due to practical constraints, evaluations were led either at the ESPCI, either at MEMS TC, or both, which was demonstrated to have a weak influence on thermodynamic evaluations (see IV.B.1.02 and figure 77).

Figure 87 displays the summary of this thermodynamic evaluation. When qualitatively compared two by two, column retentions were in agreement with expectations: thicker films clearly resulted in higher C3 retentions (semi-packed columns in grey/black and small section columns in greens) in the whole explored temperature range; short lengths columns (1 and 0.5 m, with a thick film of 6 µm, in red/orange) had similar retentions and variation could be attributed to imprecision; it has to be highlighted that, in spite of a thinner film (2 µm), regular column with deposition at 50 mT provided similar (see higher) retention than regular column with deposition at 3 mT with a film of 2.6 µm (blue/purple); this last point may suggest an increase in specific surface area of silica layer (cf. II.C.2.02).

C2 and C3 retentions on latest semi-packed design (displayed in figure 87) were compared to the ones obtained with the early design at identical carrier gas velocities (see III.A.1.01 and table 13): a stronger pressure drop was observed with latest design, while retention was found slightly higher (21% for C2, 16% for C3, compared to early design), but no tangible hypothesis could be formulated to interpret this difference.

Van't Hoff plots were found linear with correlation coefficients higher than 0.97 in the temperature ranges evaluated. In spite of the great diversity of evaluated columns, in terms of deposition pressures, lengths, sections, film thicknesses, and silicon structure, C3 adsorption heats were all found between 20 and 35 kJ/mol. Nevertheless, a standard deviation of 16% was observed within these values, which roughly matched with standard deviations obtained during the preliminary precision study (IV.B.1.03), and could not be accurately related to stationary phase film structure or properties. As foreseen in precision study as well, intercepts values (corresponding to entropic and geometric contributions) could not be directly interpreted. However, a few correlations were found between terms in the 7-points plots: enthropic term $\Delta_r S°/R$ (calculated through $\ln k = -\Delta_r H°/RT + \Delta_r S°/R - \ln \beta$) and enthalpic term $-\Delta_r H°/RT$ (at 30°C) were linked with a (negative) linear correlation of 0.96 and limit retention term $\ln k^{\infty}$ and geometric term $\ln \beta$ were linked with a (positive) linear correlation of 0.94 (>0.995 at 2$^{nd}$ order).

By coupling data displayed in figure 87 and obtained in IV.B.3.04 and IV.B.3.05, a 19-points plot of C3 retention factor measured at 30°C against the invert of calculated values of phase

ratios was drawn (figure 88 left), to evaluate the validity of the relation k=K/β. Although a clear increase of retention along with phase ratio decrease was observed, linear correlation was of very poor quality ($R^2$=0.68, K~30 with forced passage through 0), again owing to the same hypothesis as the ones suggested in the previous subparagraph.

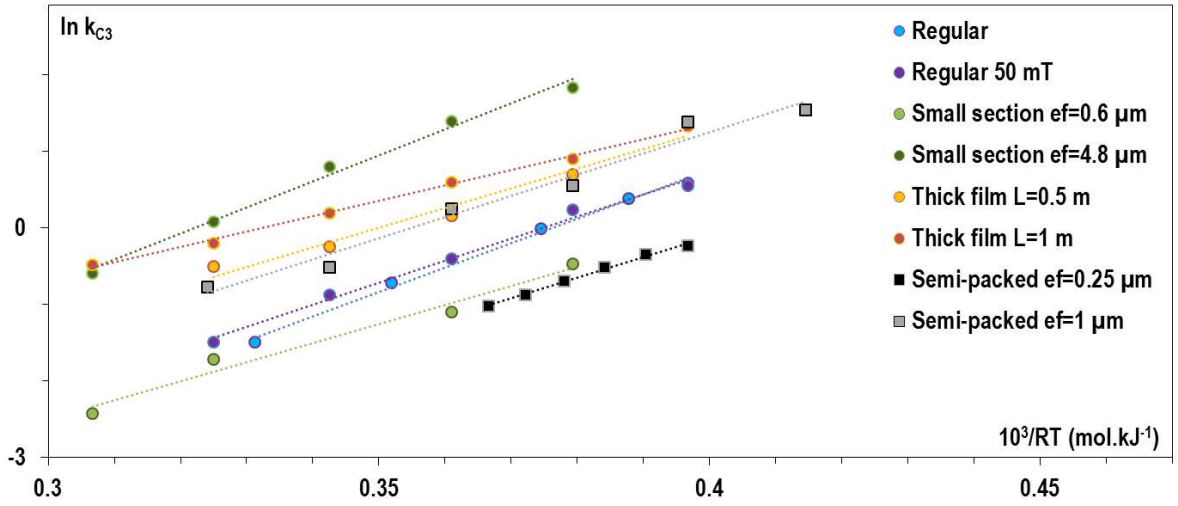


*Fig. 87: summary of a thermodynamic study on sputter-deposited silica micro columns: <u>top:</u> Van't Hoff plots for C3; <u>right:</u> numeric results (adsorption heats for C3, intercepts, and correlation coefficients); <u>bottom:</u> column summary (dimensions, film thickness, calculated phase ratio, and setup parameters); mixture: C1-C2-C3-C4.*

| Column | $\|\Delta_r H°_{C3}\|$ | ln $k^{\infty}_{C3}$ | $R^2$ |
|---|---|---|---|
| Regular | 31.8 kJ/mol | -12.0 | >0.995 |
| Regular 50 mT | 28.8 kJ/mol | -10.8 | 0.99 |
| Thick film L=1 m | 20.1 kJ/mol | -6.7 | >0.995 |
| Thick film L=0.5 m | 25.6 kJ/mol | -9.0 | 0.97 |
| Small section $e_f$=4.8 µm | 34.0 kJ/mol | -11.0 | 0.99 |
| Small section $e_f$=0.6 µm | 24.9 kJ/mol | -10.0 | 0.98 |
| Semi-packed $e_f$=1 µm | 27.8 kJ/mol | -9.8 | 0.99 |
| Semi-packed $e_f$=0.25 µm | 26.8 kJ/mol | -10.8 | 0.99 |

| Column | Length | Width x depth | Film thickness | β | Evaluation | Temperatures | Pressure | $V_{inj}$ |
|---|---|---|---|---|---|---|---|---|
| Regular | 2.2 m | 100 µm x 100 µm | 2.6 µm | 20.6 | MEMS TC | 30°C-97°C | 5.1 bars | 5 nL |
| Regular 50 mT | 2.2 m | 100 µm x 100 µm | 2.0 µm | 24.0 | MEMS TC | 30°C-97°C | 1.0 bars | 5 nL |
| Thick film L=1 m | 1.0 m | 75 µm x 75 µm | 6.0 µm | 5.25 | ESPCI | 30°C-119°C | 1.0 bars | 0.1 µL |
| Thick film L=0.5 m | 0.5 m | 75 µm x 75 µm | 6.0 µm | 5.25 | ESPCI | 30°C-97°C | 1.0 bars | 0.1 µL |
| Small section $e_f$=4.8 µm | 2.2 m | 50 µm x 50 µm | ~4.8 µm | 4.21 | ESPCI | 44°C-119°C | 4.1 bars | 0.1 µL |
| Small section $e_f$=0.6 µm | 2.2 m | 50 µm x 50 µm | ~0.6 µm | 40.1 | ESPCI | 44°C-119°C | 2.9 bars | 0.1 µL |
| Semi-packed $e_f$=1 µm | 1.1 m | 200 µm x 100 µm | 1.0 µm | 6.50 | MEMS TC | 17°C-98°C | 4.1 bars | 10 nL |
| Semi-packed $e_f$=0.25 µm | 1.1 m | 200 µm x 100 µm | 0.25 µm | 26.0 | MEMS TC | 30°C-55°C | 2.4 bars | 5 nL |

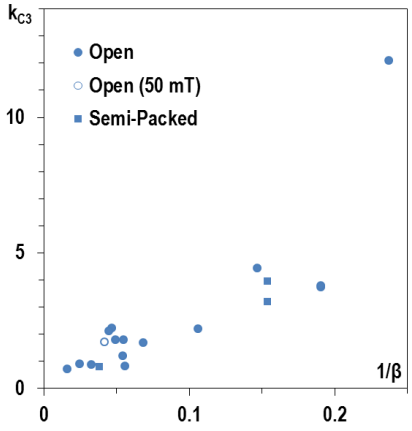


*Fig. 88: data gathering (IV.B.3.04, 05 and 06): plot of C3 retention factor against inverted phase ratio (T=30°C)*

*Table 13: C2 and C3 retentions on the two different semi-packed column designs (1.1 m x 200 µm x 100 µm, 1 µm silica sputtering time 120 min, u=5.0 cm/s, T=30°C)*

| | Early design | Latest design |
|---|---|---|
| $V_{inj}$ | 200 nL | 20 nL |
| Mixture | C1-C2-C3 | C1-C2-C3-C4 |
| Pressure | 2 bars | 5.1 bars |
| **$k_{C2}$** | **0.49** | **0.62** |
| **$k_{C3}$** | **3.2** | **3.8** |

No hypothetical evolution of adsorption heats along with any column parameter could be demonstrated, and deviations were attributed to column fabrication and evaluation imprecision. A last attempt of thermodynamic modeling, concerning selectivity, and including other stationary phases than silica, will be displayed in the conclusion of this paragraph.

### *IV.B.3.07 Other stationary phases*

- Sputter-deposited alumina was only able to separate C1 to C4 linear hydrocarbons on semi-packed design, with a very low C2 retention (<0.1 at 20°C). C2 could not be resolved from C1 above 30°C. C4 peak was very wide spread in isothermal conditions, especially at low temperatures or pressures. Only C3 retention could be evaluated on 1 µm alumina semi-packed columns, and was found similar to C3 retention on 0.25 µm silica semi-packed columns (figure 89a). The measured adsorption heat was 30.2 kJ/mol, which was within the range of variation for silica, above the mean value (27.5 kJ/mol), and above the value found for the same design and thickness (27.8 kJ/mol, see figure 87). In spite of the mentioned limitations, the evolution of retention factors along with carbon number under temperature-programmed conditions was as well found linear with alumina for C2-C4 hydrocarbons (figure 89b).

- Retention was expectedly found higher on graphite than on both silica and alumina. C3 adsorption heat on semi-packed design (figure 89e) was evaluated at 34.9 kJ/mol (27.3 for silica and 30.2 for alumina). C2 and C3 adsorption energies on open designs were evaluated at 31.7 and 44.3 kJ/mol with a 2.7 µm film (23.0 and 31.8 kJ/mol for a silica film of 2.6 µm). A slightly different value (39.1 kJ/mol) was observed for a thin film of 0.8 µm (figure 89e). These values were in very good agreement with the ones expected from the literature (II.D.1.). As well as on silica and alumina, temperature-programmed separation of C1-C4 mixture led to a linear plot for retention factor against carbon number (figure 89c). The relation between adsorption energy and carbon number for regular columns with 2.7 µm thick film was also found linear (figure 89d), as follows: $|\Delta_r H°|=13.6n_c+4.3$ kJ/mol (it was $9.1n_c+4.7$ kJ/mol for regular columns with silica 2.6 µm thick film); in this plot, C4 adsorption heat was estimated only through 2 points (at 100°C and 150°C): at lower temperatures (and in spite of a backpressure of 4.1 bars), retention and spreading were so strong that C4 peak could not be accurately separated from baseline noise. Finally, the same decrease of the entropic-geometrical term along with carbon number was observed on graphite, as it was the case for silica.

- As mentioned in IV.B.1.04, magnesia open columns could only separate C1+C2, C3 and C4. Retained alkanes (C3 and C4) adsorption energies were evaluated at 20.1 and 22.7 kJ/mol (figure 89f), making this stationary phase the most weakly retentive reported in this study.

*Remark: as well as for silica, a study on variable width design was led with graphite as stationary phase (see table 14). For the same reasons, retention was not directly correlated to column width. Graphite layers were expectedly found much more retentive than silica, even with a thinner thickness (0.5-0.8 µm instead of 1.6-2.6 µm for silica), but the ratio between silica and graphite retention presented a strong and unexpected variation (17, 4, 6 and 2 from 30 µm to 100 µm).*

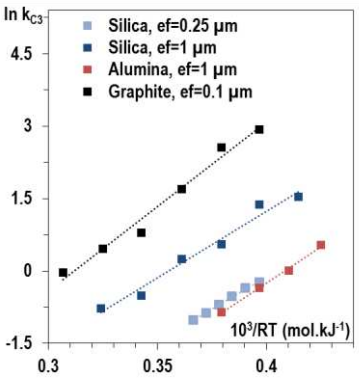


*Fig. 89a: Van't Hoff plots for C3 on semi-packed columns (see table below)*

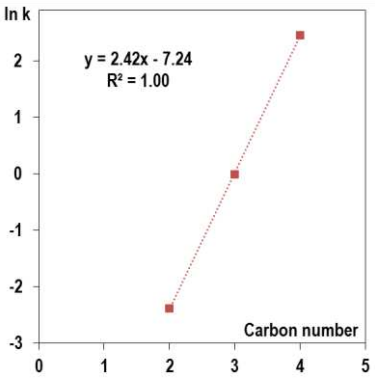


*Fig. 89b: k=f(n$_c$) for a temperature-programmed separation on an alumina semi-packed column (see figure 104)*

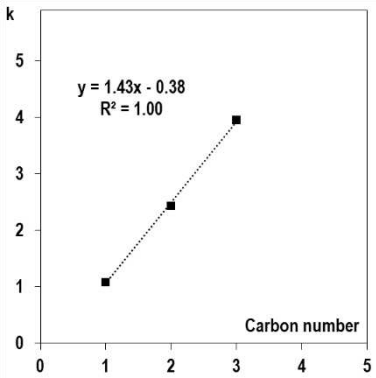


*Fig. 89c: k=f(n$_c$) for a temperature-programmed separation on a graphite semi-packed column (see figure 103b)*

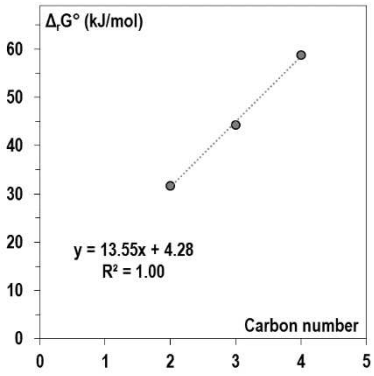


*Fig. 89d: adsorption energies on a regular graphite column (see table below)*

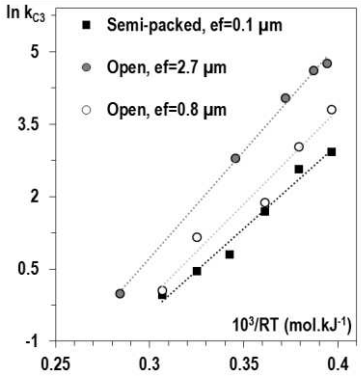


*Fig. 89e: Van't Hoff plots for C3 on graphite columns (see table below)*

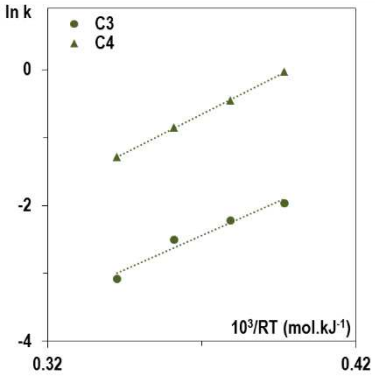


*Fig. 89f: Van't Hoff plots for C3 and C4 on magnesia columns (see table below)*

| Stationary phase | Design | Film thickness | Temperatures | Pressure | $V_{inj}$ | $\|\Delta_r H°\|$ (kJ/mol) | ln k∞ | $R^2$ |
|---|---|---|---|---|---|---|---|---|
| Alumina | Semi-packed | 1 µm | 10°C-44°C | 6.8 bars | 50 nL | **30.2 (C3)** | -12.3 (C3) | >0.995 |
| Graphite | Semi-packed | 0.1 µm | 30°C-119°C | 6.8 bars | 1 µL | **34.9 (C3)** | -10.9 (C3) | 0.98 |
| | Regular | 0.8 µm | 32°C-150°C | 6.8 bars | 10 nL | **39.1 (C3)** | -11.9 (C3) | 0.97 |
| | Regular | 2.7 µm | 30°C-119°C | 4.1 bars | 10 nL | **31.7 (C2)** | -11.0 (C2) | >0.995 |
| | | | | | | **44.3 (C3)** | -12.5 (C3) | >0.995 |
| | | | | | | **58.8 (C4)** | -14.4 (C4) | (>0.995) |
| Magnesia | Regular | 1.2 µm | 30°C-90°C | 0.8 bars | 5 nL | **20.1 (C3)** | -9.9 (C3) | 0.96 |
| | | | | | | **22.7 (C4)** | -9.2 (C4) | 0.99 |

*Fig. 89: summary of a thermodynamic study on sputter-deposited micro columns with other stationary phases than silica: alumina, graphite, and magnesia; mixture: C1-C2-C3-C4, evaluation at MEMS TC*

### *IV.B.3.08 Conclusions*

Thermodynamic behavior of sputter-deposited stationary phase micro columns could be partially modeled: linear relations of retention factors with carbon number and temperature were exhibited; retention roughly increased with phase ratio decrease, and from magnesia to graphite through alumina and silica.

However, the basic relation k=K/β poorly modeled the quantitative evolution of retention factors: contrary to slopes, Van't Hoff plots intercepts could not be interpreted, and the observed variations of adsorption energies within one stationary phase (~16%) were covered by fabrication imprecision. Stationary phase volumes, evaluated through retention factors, distribution coefficients, and mobile phase volumes, were not clearly proportional to deposited thicknesses. Hypotheses concerning model validity and layer bulk porosity (non-constant with film thickness) were emitted.

The study of columns selectivity offered the possibility to get rid of the issues caused by the errors possibly made on phase ratio calculations. Figure 90 displays C2-C3 selectivity for all the columns quantitatively evaluated in this study (excepted magnesia columns), plotted against film thickness. Selectivity was expectedly confirmed to increase from silica (6.5∓20%) to graphite (15∓7.2%) through alumina (8.6, one data point). Results obtained with silica showed a slight trend suggesting that selectivity may have been increased with stationary phase film thickness, but neither with deposition pressure nor semi-packed design (standard deviation was 20% when considering all thicknesses, while it was 8.5% when considering thicknesses below 4 µm). This might have stemmed from changes in overall bulk porosity and specific surface area with stationary phase film thickness.

The same approach was then used to evaluate kinetic performances on the same columns.

*Table 14: C2 retentions on the variable width column designs (2.2 m) with graphite as stationary phase (sputtering time 60 min, u~40 cm/s, T=30°C, mixture C1-C2-C3, $V_{inj}$=1 µL)*

| Width x Depth (µm²) | 30 x 100 | 50 x 100 | 75 x 100 | 100 x 100 |
|---|---|---|---|---|
| Film thickness (µm) | ~0.5 | ~0.6 | ~0.7 | 0.8 |
| Pressure | 4.7 bars | 2 bars | 1 bar | 1.4 bar |
| **$k_{C2}$** | **5.0** | **0.94** | **2.1** | **0.76** |
| ($k_{C2}$ $SiO_2$ 120 min) | (0.29) | (0.22) | (0.36) | (0.34) |

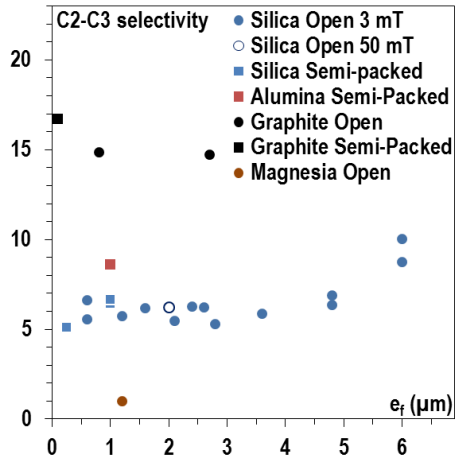


*Fig. 90: C2-C3 selectivity calculated at 30°C for all columns evaluated throughout the study.*

## IV.B.4. Kinetic evaluation

### *IV.B.4.01 Influence of carbon number*

A short preliminary study was carried out on silica regular columns, to evaluate the influence of carbon number on separation efficiency (figure 91).

Plate height (efficiency invert) increased with carbon number at fixed temperature and pressure (figure 91 left); plate height is generally expected to be roughly constant for homologous compounds (such as linear saturated hydrocarbons) for retention factor higher than ~3, and to decrease along with retention factor for smaller values; in this example, C1, C2 and C3 had retention factors lower than 2, whereas C4 and C5 retention factors were higher than 10 (see also figure 82), which could explain plot shape (increase and stabilization). This interpretation was tempered by the fact that peak asymmetries strongly increased from C1 to C5, which could induce increasing efficiency overestimation from C1 to C5.

Minimal plate height obtained in Van Deemter experiments was also observed to increase along with carbon number (0.38, 0.65 and 1.1 mm for C2, C3 and C4, for a silica 2 µm (50 mT) regular column, as shown on figure 91 right), while optimal velocity remained stable (around 40 cm/s in this example). Modeling quality of Van Deemter plot with HETP=A+B/u+Cu was as well decreased with increasing carbon number ($R^2$ was higher than 0.995 for C2, 0.98 for C3, and 0.92 for C4).

### *IV.B.4.02 Influence of temperature*

The influence of temperature (between 30 and 90°C) on separation efficiency was studied with C1-C4 separation on a silica 2.6 µm regular column.

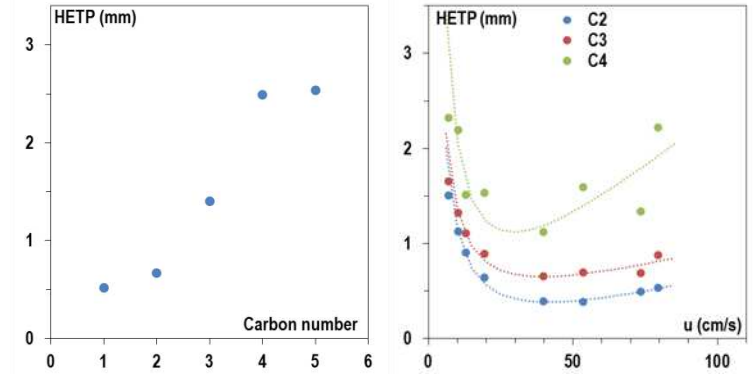


| Compound | C2 | C3 | C4 |
|---|---|---|---|
| A | -0.26 mm | 0.020 mm | -0.37 mm |
| B | 1.3 cm²/s | 1.3 cm²/s | 2.2 cm²/s |
| C | 0.78 ms | 0.80 ms | 25 ms |
| Modeling quality | $R^2$>0.995 | $R^2$=0.98 | $R^2$=0.92 |
| $HETP_{min}$ | **0.38 mm** | **0.65 mm** | **1.1 mm** |
| $u_{opt}$ | 41 cm/s | 39 cm/s | 40 cm/s |
| Peak asymmetry at $u_{opt}$ | 1.6 | 2.2 | 2.3 |

*Fig. 91: influence of carbon number on separation efficiency for silica columns, evaluation at MEMS TC, T=30°C, $V_{inj}$=5 nL: top left: silica 2.6 µm regular column, 2.2 m x 100 µm x 100 µm, P=1.7 bar, C1-C5 mixture top right: Van Deemter plots (1.0 to 6.4 bars), silica 2 µm (50 mT) regular column, 2.2 m x 100 µm x 100 µm, C1-C4 mixture bottom: data corresponding to Van Deemter plots*

Efficiency increased along with temperature, as shown on figure 92 (left). Initially at 3.7, 4.4, and 5.6 mm for C2, C3, and C4 at 30°C, plate height converged towards around 0.8 mm at 90°C. Retention factors and diffusion coefficients decreases along with temperature increase were responsible for this expected behavior, according to gas chromatography theory at high velocities (5.1 bars were used as input pressure; at low velocities, the evolution may have been less clear).

It has to be highlighted here that carrier gas velocity underwent strong variations at fixed pressure and changing temperature, as shown on figure 92 (right). Carrier gas velocity, around 210 cm/s between 30 and 50°C, dropped to 111 and 43 cm/s at 70°C and 90°C. Due to helium viscosity increase along with temperature, this carrier gas speed drop was also responsible for the increase of efficiency, by bringing velocity closer to optimal velocities, as exhibited in next subparagraph.

By providing highest values and lowest deviations of efficiency, C2 was used as probe for the rest of kinetic evaluation, as well as an ambient temperature of 30°C.

### *IV.B.4.03 Demonstration of the influence of carrier gas velocity*

In order to provide an illustration of the influence of carrier gas velocity on efficiency (mostly intended to non-chromatographists), C2 retention times, half-height peak widths, and number of plates were measured on a sputter-deposited silica column (see figure 93).

Both retention time and half-height peak widths were naturally decreased with carrier gas velocity increase (figure 93a). The ratio between these two values, basis of plate number calculation, passed through a maximum at an optimal carrier gas velocity of 42 cm/s (figure 93b). Numbers of plates were directly calculated and displayed by Galaxy software, and plate height value was plotted against carrier gas velocity, showing a minimum at the optimal velocity (figure 93c). Modeling quality of the Van Deemter equation was higher than 0.995.

The utility of such experiments was explained in I.A.6., and kinetic evaluations of all columns fabricated throughout the study were carried out, as well as thermodynamic evaluations.

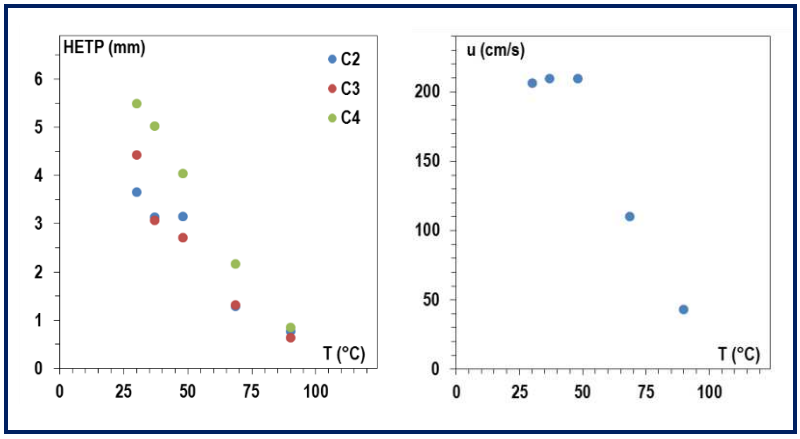


*Fig. 92: influence of temperature on kinetic performances of a silica 2.6 µm regular column, 2.2 m x 100 µm x 100 µm, evaluation at MEMS TC, T=30°C to 90°C, P=5.1 bars, $V_{inj}$=5 nL, C1-C4 mixture*
*left: C2, C3 and C4 efficiency*
*right: carrier gas velocity*

### *IV.B.4.04 Influence of column section*

Efficiency evolution along with column section (at constant deposition time) is displayed on figure 94. Modeling qualities were of good to very good quality ($R^2$ between 0.98 and 1.00), but no clear trend of Van Deemter coefficients could be observed, neither along with raw columns parameters, nor along with retentions measured in the previous paragraph.

Concerning variable width design with 120 minutes deposition time (figure 94a), highest efficiency was provided by the 50 µm-wide column (3860, $HETP_{minC2}$=0.57 mm), while smallest was provided by the 30-µm wide column. 50 µm-deep and 100 µm-wide column (2256) was thus found less efficient than 50 µm-wide and 100 µm-deep column; higher stationary phase film thickness (at constant deposition time, due to shadowing effects) could be held responsible of this specific observation.

The comparison between 100 µm x 75 µm and 50 µm x 50 µm sections (at a 240 minutes deposition time, figure 94b, or 30 minutes, figure 94c) led to the same conclusion, namely small sections provided less efficient separations than bigger sections. Experiments were not led on the same apparatus, but this was expected not to have a crucial influence on maximal efficiency (cf. IV.B.1.02: 0.77 mm and 0.62 mm for the same column). A high efficiency of 5517 plates was measured on a 0.6 µm silica 2.2 m x 100 µm x 75 µm column.

### *IV.B.4.05 Influence of column length*

1 m-long and 0.5 m-long columns (75 µm x 75 µm, silica 6 µm) were compared (figure 95a): both columns expectedly showed comparable relative efficiencies ($HETP_{minC2}$=0.63 and 0.59 mm, respectively). A stabilization of plate height at high velocities due to turbulences apparition could be observed at the ESPCI on the 0.5 m column (figure 95b), which suggested that such columns could be used at high flow rates (to shorten analysis time) without dramatic loss of efficiency.

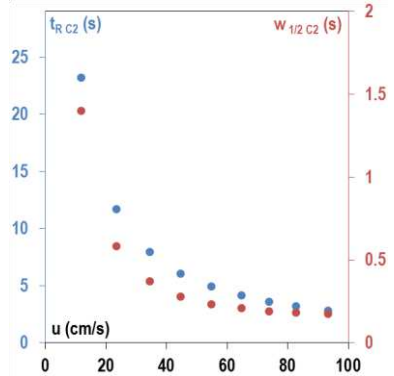


*Fig. 93a: C2 retention time and half-height peak width*

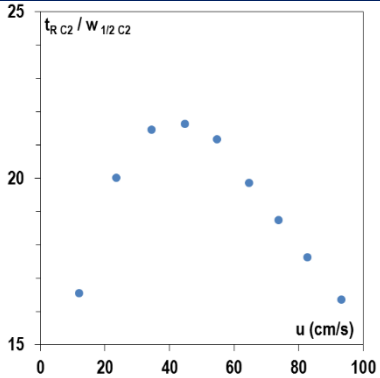


*Fig. 93b: retention time on half-height peak width*

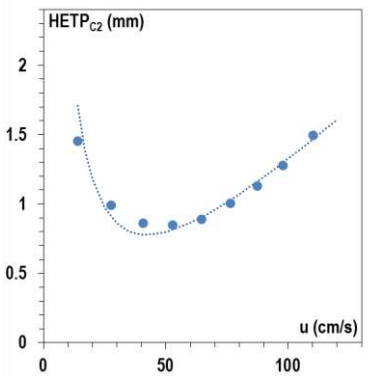


*Fig. 93c: HETP (N provided by Galaxy, fit $R^2$>0.995)*

*Fig. 93: illustration of the influence of carrier gas velocity on efficiency (2.4 µm silica column,2.2 m x 75 µm x 100 µm), evaluation at MEMS TC, T=30°C, P from 5 to 45 bars, $V_{inj}$=5 nL, C1-C2-C3 mixture*

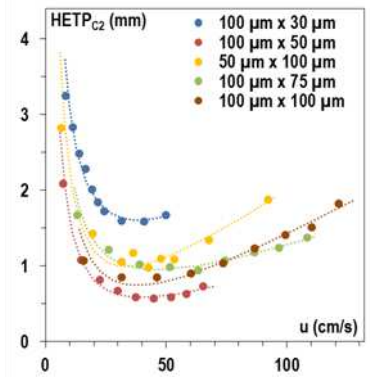


Fig. 94a: 120 min

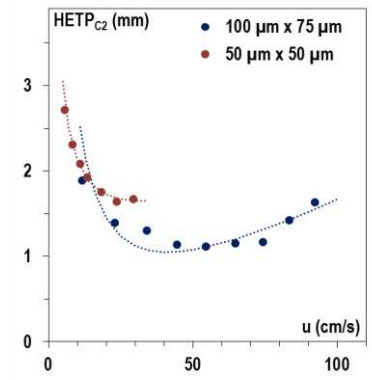


Fig. 94b: 240 min

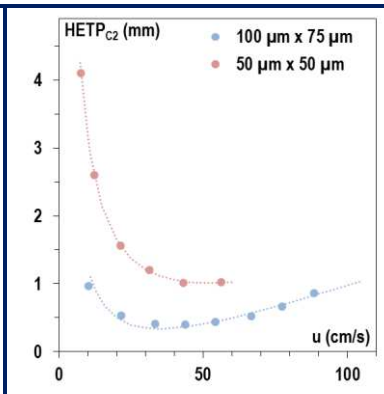


Fig. 94c: 30 min

| Depth x width (µm²) | 100 x 30 | 100x 50 | 50 x 100 | 100 x 75 | 100 x 100 | 100 x 75 | 50 x 50 | 100 x 75 | 50 x 50 |
|---|---|---|---|---|---|---|---|---|---|
| Dep. time (min) | 120 | 120 | 120 | 120 | 120 | 240 | 240 | 30 | 30 |
| Film thickness (µm) | 1.6 | 2.1 | ~2.8 | 2.4 | 2.6 | ~4.8 | ~4.8 | ~0.6 | ~0.6 |
| Pressure (bars) | 1-6.8 | 0.3-3 | 0.3-5.7 | 0.3-3 | 0.3-3 | 0.3-3 | 0.7-4.1 | 0.3-2.7 | 0.7-4.1 |
| $V_{inj}$ | 1 µL | 5 nL | 20 nL | 5 nL | 5 nL | 20 nL | 0.1 µL | 10 nL | 0.1 µL |
| Mixture | C1-C3 | C1-C3 | C1-C3 | C1-C3 | C1-C3 | C1-C3 | C1-C4 | C1-C3 | C1-C4 |
| Evaluation | MEMS TC | MEMS TC | MEMS TC | MEMS TC | MEMS TC | MEMS TC | ESPCI | MEMS TC | ESPCI |
| $N_{maxC2}$ | **1387** | **3860** | **2256** | **2331** | **2597** | **1988** | **1318** | **5517** | **2229** |
| $HETP_{minC2}$ (mm) | **1.6** | **0.57** | **0.98** | **0.94** | **0.85** | **1.1** | **1.7** | **0.40** | **1.02** |
| $u_{optC2}$ (cm/s) | 39 | 45 | 33 | 46 | 38 | 54 | 33 | 35 | 52 |
| A (mm) | 0.21 | -0.32 | -0.52 | -0.08 | -0.61 | -0.41 | 1.1 | -0.70 | -0.25 |
| B (cm²/s) | 2.7 | 1.8 | 2.5 | 2.6 | 2.6 | 3.0 | 0.97 | 2.1 | 3.3 |
| C (ms) | 1.8 | 1.1 | 2.3 | 1.8 | 1.8 | 1.8 | 0.91 | 1.5 | 1.2 |
| Modeling quality | 0.99 | 0.98 | 0.99 | >0.995 | >0.995 | >0.995 | >0.995 | 0.99 | >0.995 |

Fig. 94: influence of column section (at identical deposition times) on kinetic performances for 2.2 m-long open silica columns, T=30°C

Fig. 95: influence of column length on kinetic performances: 6 µm silica open columns, section 75 µm x 75 µm, T=30°C

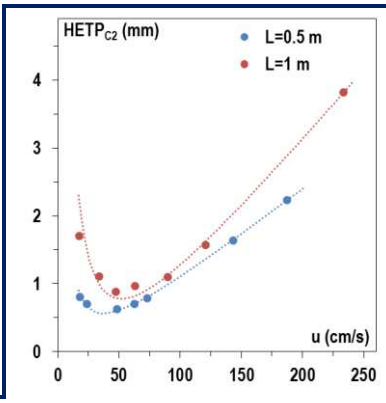


Fig. 93a: compared evaluation (MEMS TC)

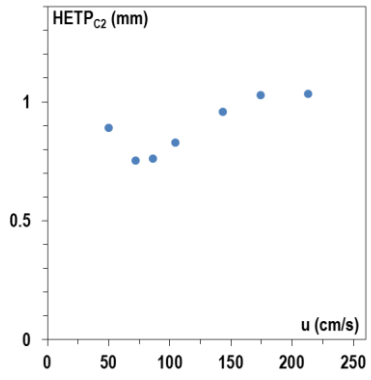


Fig. 94b: turbulences at high velocities (ESPCI)

| Length | 0.5 m | 1 m | 0.5 m |
|---|---|---|---|
| Evaluation | MEMS TC | MEMS TC | ESPCI |
| Pressure (bars) | 0.3-4.1 | 0.3-6.8 | 0.3-4.1 |
| $V_{inj}$ | 20 nL | 20 nL | 0.2 µL |
| $N_{maxC2}$ | **799** | **1137** | **665** |
| $HETP_{minC2}$ (mm) | **0.63** | **0.59** | **0.75** |
| $u_{optC2}$ (cm/s) | 37 | 51 | 72 |
| A (mm) | -0.47 | -1.4 | - |
| B (cm²/s) | 1.9 | 5.7 | - |
| C (ms) | 1.4 | 2.1 | - |
| Modeling quality | $R^2$>0.995 | $R^2$>0.995 | - |

### *IV.B.4.06 Influence of column structure*

As shown on figure 96, maximal efficiencies obtained on semi-packed columns (1 µm silica) were similar to the ones obtained on open regular columns (2.6 µm silica) at constant deposition time (120 minutes). They precisely reached 2663 plates for early semi-packed design (shifted pillars), 2344 for latest semi-packed design (non-shifted pillars), and 2597 for regular design. As column length was twice shorter for semi-packed designs (1.1 m) than for regular design (2.2 m), plate height was significantly improved (0.41 and 0.47 mm for semi-packed designs and 0.85 mm for regular design).

Optimal velocity was barely reached on first semi-packed design, and not at all on second one, which suggested than even higher efficiencies could be obtained on such columns, by using higher pressures than 6.8 bars.

Concerning both semi-packed designs comparison, pressure drop was found twice bigger on latest design, while minimal plate height was found 13% higher (which was probably due to the higher retention observed on the latest design, see IV.B.3.06).

### *IV.B.4.07 Influence of stationary phase film thickness*

Kinetic performances comparisons between identical designs with different silica deposition times were led on open 2.2 m x 75 µm x 100 µm columns (figure 97a), on open 2.2 m x 50 µm x 50 µm columns (figure 97b), and on semi-packed columns (latest design, figure 97c).

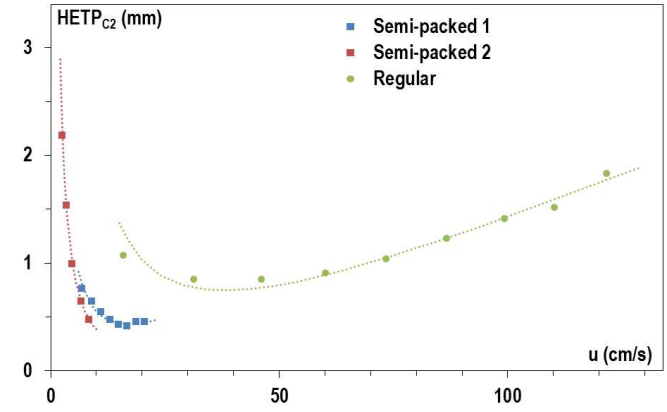


*Fig. 96:*
*influence of column structure on kinetic performances:*
*120 min silica sputter-deposition time on semi-packed columns (early and late design) and open regular columns;*
*evaluation at MEMS TC, T=30°C.*

| Structure | Semi-packed 1 | Semi-packed 2 | Open regular |
|---|---|---|---|
| **Dimensions (length (m) x width x depth (µm²))** | 1.1 x 200 x 100 | 1.1 x 200 x 100 | 2.2 x 100 x 100 |
| **Film thickness (µm)** | 1 | 1 | 2.6 |
| **Pressure (bars)** | 2-6.8 | 1.7-6.8 | 0.3-3.0 |
| **$V_{inj}$** | 0.2 µL | 20 nL | 5 nL |
| **$N_{maxC2}$** | **2663** | **2344** | **2597** |
| **$HETP_{minC2}$ (mm)** | **0.41** | **0.47** | **0.85** |
| **$u_{optC2}$ (cm/s)** | 17 | 16 | 38 |
| **A (mm)** | -0.38 | -0.54 | -0.61 |
| **B (cm²/s)** | 0.69 | 0.68 | 2.6 |
| **C (ms)** | 2.4 | 2.5 | 1.8 |
| **Modeling quality** | $R^2$=0.96 | $R^2$=0.99 | $R^2$>0.995 |

The same evolution was observed on open 50 µm x 50 µm and on semi-packed columns. Optimal velocity could hardly be reached on both designs, and even higher efficiencies could probably be obtained. It should be highlighted here that silica 30 minutes deposition semi-packed column provided the smallest plate height among silica columns in this study (0.28 mm).

### *IV.B.4.08 Influence of stationary phase deposition pressure*

Two different pressures (3 mT and 50 mT) were used in the deposition of silica layers and compared on regular columns. A strong difference was observed in their kinetic performances, as shown on figure 98. Minimal plate height was more than twice smaller on 50 mT-deposition column than on 3 mT-deposition column, which could neither be attributed to very different retentions (which were very close, according to IV.B.3.06), nor to the difference in stationary phase film thickness (respectively 2 and 2.6 µm), according to previous subparagraph. An hypothesis was emitted, according to which 50 mT-deposited layer structure was more favorable to mass transfer than 3 mT-deposited layer structure.

The 300 minutes 50 mT silica deposition regular column provided the highest number of plates reported in the whole study (5731).

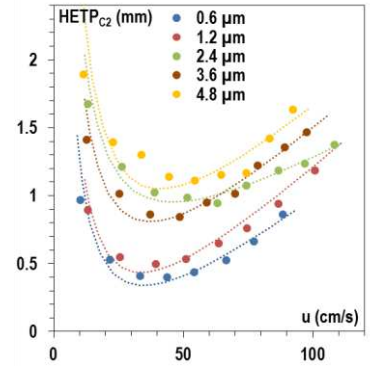


*Fig. 97a: open 100 x 75 µm²*

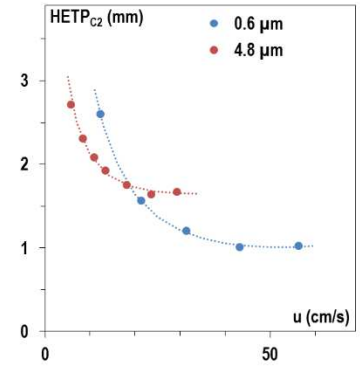


*Fig. 97b: open 50 x 50 µm²*

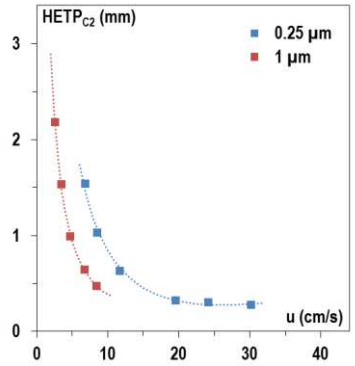


*Fig. 97c: semi-packed*

| | | | | | | | | | |
|---|---|---|---|---|---|---|---|---|---|
| **Dep. time (min)** | 30 | 60 | 120 | 180 | 240 | 30 | 240 | 30 | 120 |
| **Film thickness (µm)** | **~0.6** | **1.2** | **2.4** | **~3.6** | **~4.8** | **~0.6** | **~4.8** | **0.25** | **1** |
| **Depth x width (µm²)** | 100 x 75 | 100 x 75 | 100 x 75 | 100 x 75 | 100 x 75 | 50 x 50 | 50 x 50 | 100 x 200 | 100 x 200 |
| **Pressure (bars)** | 0.3-2.7 | 0.3-2.7 | 0.3-3 | 0.3-3 | 0.3-3 | 0.7-4.1 | 0.7-4.1 | 1-6.4 | 1.7-6.8 |
| **$V_{inj}$** | 20 nL | 20 nL | 5 nL | 5 nL | 20 nL | 0.1 µL | 0.1 µL | 10 nL | 20 nL |
| **Mixture** | C1-C3 | C1-C3 | C1-C3 | C1-C3 | C1-C3 | C1-C4 | C1-C4 | C1-C4 | C1-C4 |
| **Evaluation** | MEMS TC | MEMS TC | MEMS TC | MEMS TC | MEMS TC | ESPCI | ESPCI | MEMS TC | MEMS TC |
| **$N_{maxC2}$** | **5517** | **4425** | **2331** | **2616** | **1988** | **2229** | **1318** | **3945** | **2344** |
| **$HETP_{minC2}$ (mm)** | **0.40** | **0.50** | **0.94** | **0.84** | **1.1** | **1.0** | **1.7** | **0.28** | **1.0** |
| **$u_{optC2}$ (cm/s)** | 35 | 34 | 46 | 37 | 54 | 52 | 33 | 26 | 16 |
| **A (mm)** | -0.70 | -0.75 | -0.08 | -0.48 | -0.41 | -0.25 | 1.1 | -0.85 | -0.54 |
| **B (cm²/s)** | 1.8 | 2.0 | 2.4 | 2.4 | 3.0 | 3.3 | 0.97 | 1.5 | 0.68 |
| **C (ms)** | 1.5 | 1.8 | 1.1 | 1.7 | 1.8 | 1.2 | 0.91 | 2.2 | 2.5 |
| **Modeling quality** | 0.99 | >0.995 | >0.995 | >0.995 | 0.98 | >0.995 | >0.995 | 0.92 | 0.99 |

*Fig. 97: influence of deposition time (at identical sections) for silica columns, T=30°C*

### *IV.B.4.09 Stationary phase comparison*

Maximal efficiencies obtained on silica, alumina, and graphite semi-packed columns were observed to be sorted by retentions measured in IV.B.3.07. As shown on figure 99, maximal plate numbers were respectively 2344, 4479 and 959. The 120 minutes alumina deposition semi-packed column provided the smallest plate height reported in the whole study (0.25 mm). Higher efficiencies could probably be reached at higher pressures.

*Fig. 98: influence of deposition pressure for regular silica columns, 2.2 m x (100 x 100) µm², evaluation at MEMS TC, T=30°C*

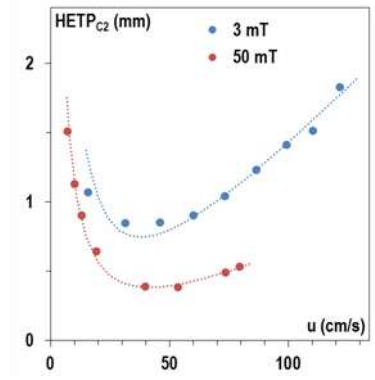


| Deposition pressure | 3 mT | 50 mT |
|---|---|---|
| Deposition time | 120 min | 300 min |
| Film thickness (µm) | 2.6 | 2 |
| Pressure (bars) | 0.3-3 | 1-6.4 |
| $V_{inj}$ | 5 nL | 20 nL |
| $N_{maxC2}$ | **2597** | **5731** |
| $HETP_{minC2}$ (mm) | **0.85** | **0.38** |
| $u_{optC2}$ (cm/s) | 38 | 41 |
| A (mm) | -0.61 | -0.26 |
| B (cm²/s) | 2.6 | 1.3 |
| C (ms) | 1.8 | 0.78 |
| Modeling quality | R²>0.995 | R²=0.99 |

*Fig. 99: influence of target material chosen for stationary phase sputtering deposition : silica, alumina, and graphite; semi-packed columns (late design); evaluation at MEMS TC, T=30°C.*

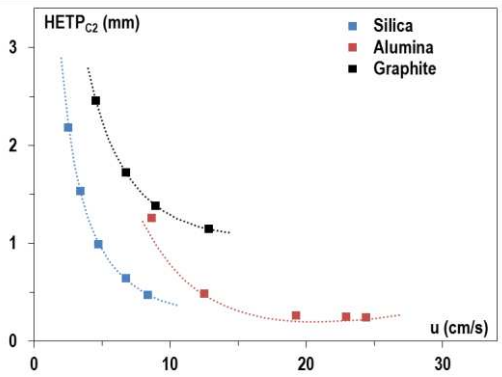


| Stationary phase | Silica | Alumina | Graphite |
|---|---|---|---|
| Deposition time (min) | 120 | 120 | 60 |
| Film thickness (µm) | 1 | 1 | 0.1 |
| Pressure (bars) | 1.7-6.8 | 2-6.8 | 3-6.8 |
| $V_{inj}$ | 20 nL | 0.1 µL | 2 µL |
| $N_{maxC2}$ | **2344** | **4479** | **959** |
| $HETP_{minC2}$ (mm) | **0.47** | **0.25** | **1.1** |
| $u_{optC2}$ (cm/s) | 16 | 21 | 17 |
| A (mm) | -0.54 | -1.9 | -0.24 |
| B (cm²/s) | 0.68 | 2.2 | 1.2 |
| C (ms) | 2.5 | 5.0 | 3.8 |
| Modeling quality | R²=0.99 | R²=0.95 | R²>0.995 |

Sputter-deposited graphite as stationary phase was far less efficient than sputter-deposited silica, but showed similar evolutions regarding column structure and stationary phase film thickness (figure 100 and table 15): semi-packed design significantly increased efficiency (959 plates instead of 256 at 30°C); no direct correlation between column width and maximal efficiency was found with the variable width design, and maximal efficiencies varied between 134 and 256 plates; thicker graphite film (2.7 µm instead of 0.8 µm) provided smaller maximal efficiency (83 plates), but this maximal efficiency could be raised to 946 plates by

bringing the column to 100°C; this last aspect suggested that graphite columns could be used at high temperatures, where silica may not be retentive enough to separate lightest hydrocarbons (see IV.B.5.04).

In spite of the inability of sputter-deposited magnesia to separate C1 and C2 (even with 562.5 minutes deposition, and even at optimal velocity and ambient temperature), maximal efficiency of C3 separation was found higher than on 50 mT 300 min sputter-deposited silica column of the same dimensions (4393 plates instead of 3352, see figure 101).

*Fig. 100: graphite as stationary phase, kinetic comparison: - semi-packed (late) 1.1 m x (200 x 100) µm² - open regular 2.2 m x (100 x 100) µm², evaluation at MEMS TC, T=30°C.*

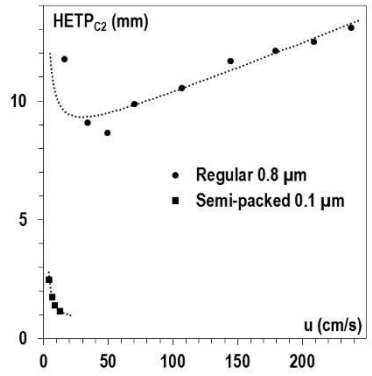


| Design | Regular | Semi-packed |
|---|---|---|
| Symbol | ● | ■ |
| Deposition time | **60 min** | **60 min** |
| Film thickness | 0.8 µm | 0.1 µm |
| Pressure (bars) | 1-6.4 | 3-6.8 |
| $V_{inj}$ | 1 µL | 2 µL |
| $N_{maxC3}$ | **256** | **959** |
| $HETP_{minC3}$ (mm) | **8.6** | **1.1** |
| $u_{optC3}$ (cm/s) | 30 | 17 |
| A (mm) | 8.0 | -2.4 |
| B (cm²/s) | 1.9 | 1.2 |
| C (ms) | 2.2 | 3.8 |
| Modeling quality | R²=0.98 | R²>0.995 |

| Design | Open | | | | | | Semi-packed |
|---|---|---|---|---|---|---|---|
| Length (m) | **2.2** | | | | | | **1.1** |
| Width x Depth (µm²) | **30 x 100** | **50 x 100** | **75 x 100** | **100 x 100** | | | **200 x 100** |
| Deposition time (min) | 60 | 60 | 60 | 60 | 200 | | 60 |
| Film thickness (µm) | **0.5** | **0.6** | **0.7** | **0.8** | **2.7** | | **0.1** |
| Pressure (bars) | 1.4-5.7 | 0.3-5.7 | 0.3-5.7 | 1-6.4 | 2.4-6.8 | 0.3-2.7 | 3-6.8 |
| $V_{inj}$ | 1 µL | 1 µL | 1 µL | 1 µL | 0.1 µL | 1 µL | 2 µL |
| Mixture | C1-C2-C3 | C1-C2-C3 | C1-C2-C3 | C1-C2-C3 | C1-C2-C3-C4 | C1-C2-C3 | C1-C2-C3-C4 |
| T (°C) | 30 | 30 | 30 | 30 | 30 | 100 | 30 |
| $N_{maxC2}$ | **172** | **224** | **134** | **256** | **83** | **946** | **959** |
| $HETP_{minC2}$ (mm) | **13** | **9.8** | **16** | **8.6** | **26.5** | **2.3** | **1.1** |
| $u_{optC2}$ (cm/s) | 23 | 44 | 74 | 30 | 17 | 99 | 17 |
| A (mm) | 14 | 14 | 14 | 8.0 | - | 0.80 | -2.4 |
| B (cm²/s) | 0.76 | 6.8 | 6.5 | 1.9 | - | 4.3 | 1.2 |
| C (ms) | 3.0 | 0.96 | 1.7 | 2.2 | - | 1.3 | 3.8 |
| Modeling quality | R²=0.98 | R²=0.98 | R²>0.995 | R²=0.98 | - | R²>0.995 | R²>0.995 |

*Table 15: summary of kinetic evaluations of graphite columns*

*Fig. 101: influence of target material chosen for stationary phase sputtering deposition : silica and magnesia; open regular columns 2.2 m x (100 x 100) µm², evaluation at MEMS TC, T=30°C.*

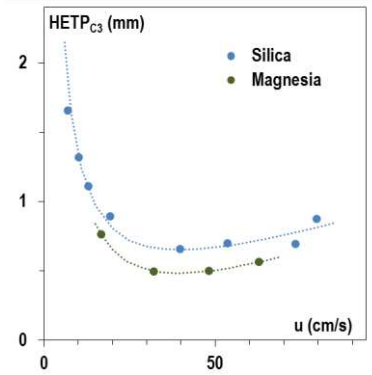


| | Silica | Magnesia |
|---|---|---|
| Deposition pressure | **50 mT** | **22.5 mT** |
| Deposition time | **300 min** | **562.5 min** |
| Film thickness (µm) | 2 | 1.2 |
| Pressure (bars) | 1-6.4 | 0.3-1.4 |
| $V_{inj}$ | 20 nL | 10 nL |
| $N_{maxC3}$ | **3352** | **4393** |
| $HETP_{minC3}$ (mm) | **0.66** | **0.50** |
| $u_{optC3}$ (cm/s) | 39 | 39 |
| A (mm) | -0.020 | -0.23 |
| B (cm²/s) | 1.3 | 1.4 |
| C (ms) | 0.80 | 0.91 |
| Modeling quality | R²=0.98 | R²>0.995 |

### *IV.B.4.10 Conclusions*

Maximal efficiencies provided by micro columns with sputter-deposited solid stationary phases were expectedly not found better (roughly lower or comparable) than those obtained with PDMS and reported in the literature (II.B.8.). However, they rank in the most efficient gas-solid chromatography micro columns (see appendix B).

Separation efficiency was increased by adjusting carrier velocity, by increasing temperature, by stationary phase film thinning, by higher pressure sputtering (50 mT instead of 3 mT for silica) and by using oxide stationary phases (silica, alumina, magnesia) rather than graphite; semi-packed designs provided smaller plate heights than open columns, but comparable number of plates. Highest efficiency of this study was provided by a regular column with 50 mT sputter-deposited 2 µm-thick silica layer: 5731 plates, also corresponding to 955 plates per second, which was close to the limit of 1000 plates per second established in the literature for capillary columns; smallest plate height was provided by a semi-packed column with sputter-deposited 1 µm-thick alumina layer (0.25 mm).

Columns kinetic behavior along with carrier gas velocity variations could be described by Van Deemter equation with good accuracy, but quantitative evolution of A (expected null, often found negative, B, C terms and of minimal plate height and optimal velocity could not be simply modeled, in spite of strong efforts. Indeed, contrary to gas-liquid chromatography, gas-solid chromatography on porous layer columns kinetic theory was not simple and robust enough to provide accurate predictions and modeling.

The last paragraph of this section is dedicated to real conditions micro columns use.

## IV.B.5. Potential application evaluation

In this paragraph, temperature-programmed separations of C1-C4 (or C5) and of other hydrocarbons on sputter-deposited stationary phase micro columns will be exhibited. The possibility to use air as carrier gas instead of helium will be evaluated by a chromatographic comparison between helium and nitrogen. Approaches to enable C1-C2 separation at high temperatures will then be demonstrated. Finally, the effect of silica layer hydration on chromatographic properties of the micro column will be reported.

All those experiments aimed at estimating columns versatility towards various requirements, regarding separated compounds, separation time, carrier gas, ambient temperature and humidity. They were carried out at MEMS TC at room temperature (30°C, except for high temperature experiment).

### *IV.B.5.01 C1-C4 (or C5) temperature-programmed separations*

Figure 102 displays temperature-programmed separations of light linear alkanes on sputter-deposited silica micro columns.

Using the self-made temperature programming system described in this report, and a temperature ramp of 15°C/s, C1-C5 separation could be performed in 9 seconds on an open regular column (figure 102a). To increase separation speed, an input pressure of 6.1 bars was used, which induced an apparent carrier gas velocity of 226 cm/s (velocity varied with

temperature, cf. IV.B.4.02): this was 6 times higher than isothermally measured C2 optimal velocity for such columns (around 38 cm/s, cf. IV.B.4.07), and, in order to preserve C1-C2 separation at such a high velocity, an initial temperature of 15°C was necessary. Data processing of this chromatogram led to the calculation of high separation numbers* (4 between C1 and C2, 11 between C2 and C3, 12 between C3 and C4, and 9 between C4 and C5), and separation time was expected to be improvable by building the appropriate set of parameters (flow rate, initial temperature, ramp intensity). Combined with cooling performances shown in IV.A.2. (from 130°C to 15°C in less than 14 seconds), this result suggests the possibility to perform C1-C5 analyses in 9+14=23 seconds cycles.

Non-optimized temperature-programmed C1-C4 separations were also carried out on short length column (balanced with a low β) in 10 seconds (figure 102b) or on semi-packed column in 50 seconds. In those cases, an initial temperature of 30°C (room temperature) was sufficient to obtain a full C1-C2 separation.

This was also naturally the case for temperature-programmed separations on graphite columns (figure 103, non-optimized again): C1 to C4 hydrocarbons were separated in 13 seconds on an open regular column (figure 103a) and in 55 s seconds on a semi-packed column (figure 103b).

Finally, C1-C4 hydrocarbons (with C4 isomers) were separated in 60 seconds on an alumina semi-packed column with an initial temperature of 10°C to ensure C1-C2 separation resolution (figure 104).

C1-C9 linear alkanes were separated in less than 15 seconds thanks to a temperature ramp of 15°C/s and an initial temperature of 13°C, for the same reasons than in previous subparagraph (figure 105a). Resolution between peaks was higher than 2.4. Neither equivalent nor close result was found in the literature.

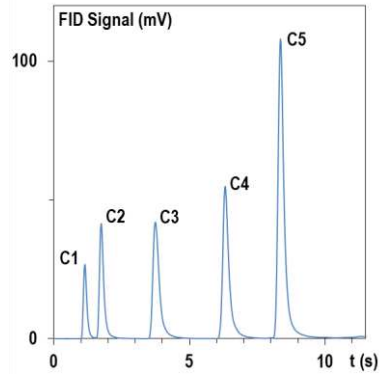


*Fig. 102a: C1-C5, open regular column*
*(2.2 m x (100x100) µm², $e_f$=2.6 µm), P=6.1 bars, $V_{inj}$=50 nL, T=15°C-200°C at 15°C/s.*

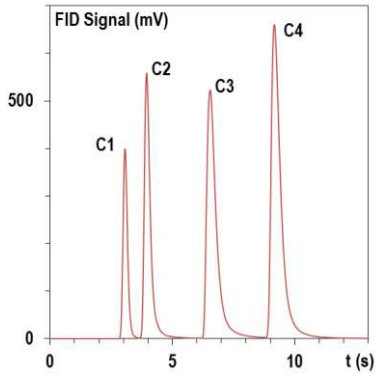


*Fig. 102b: C1-C4, open column*
*(1 m x (75x75) µm², $e_f$=6 µm), P=1 bar, $V_{inj}$=20 nL, T=30°C-90°C at 6°C/s.*

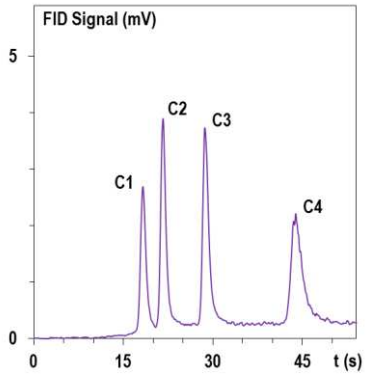


*Fig. 102c: C1-C4, semi-packed column*
*(1.1 m x (200x100) µm², $e_f$=1 µm), P=6.8 bar, $V_{inj}$=20 nL, T=30°C-130°C at 6°C/s.*

*Fig. 102: Temperature-programmed separations of light linear alkanes on sputter-deposited silica micro columns*

Such a separation was again expected to be improvable, due to the high separation numbers* observed: 4 between C1 and C2 or C8 and C9, and up to 12 between C3 and C4. Moreover, C8 and C9 were partially eluted in isothermal conditions (ramp stopped at 12.5 seconds when chip limit temperature was reached), which probably damaged last eluting peaks shapes and increased separation time; these limitations should be overcome with the same method as mentioned in previous subparagraph).

C1-C6 alkanes with isomers were also separated in 15 s (figure 105b) with the same temperature program (limit temperature excepted). Although C6 had to be partially eluted in isothermal conditions, again, resolution between isomers was 1.3 for C4, 0.9 for C5, and 0.8 and 2.8 for C6. The sample was a test mixture by GeoServices, and this preliminary result suggested a good adaptability of the column to the mentioned problem of XXXXXXXXXXX application.

### *IV.B.5.02 Other hydrocarbons separations on sputter-deposited silica*

An open regular silica (2.6 µm) column was used to test separations of other hydrocarbon compounds (figure 105).

Aromatics (benzene and toluene) could be separated (figure 105c), and a second test mixture by GeoServices, with unsaturated (ethene), saturated (C6-C7-C8) and aromatic (benzene and toluene) hydrocarbons, could as well be analyzed with a resolution higher than 1.7 (figure 105d). Aromatics were expectedly eluted after identical carbon number alkanes; although it could not be directly verified, chromatograms suggested that ethene would be eluted between C2 and C3.

Cyclopentane and cyclohexane were also naturally separated, as shown on figure 105e.

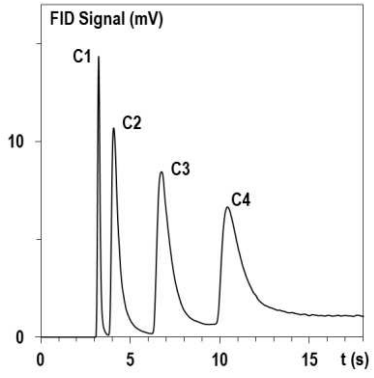


*Fig. 103a: C1-C4, open regular column (2.2 m x 100 µm x 100 µm, $e_f$=0.8 µm), P=6.8 bars, $V_{inj}$=20 nL, T=30°C-120°C at 10°C/s.*

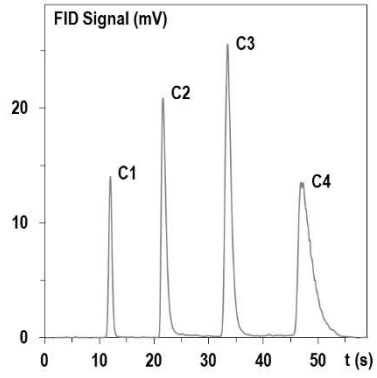


*Fig. 103b: C1-C4, semi-packed column (1.1 m x 200 µm x 100 µm, $e_f$=0.1 µm), P=6.8 bar, $V_{inj}$=2 µL, T=30°C-120°C at 3°C/s.*

*Fig. 103: on sputter-deposited graphite micro columns*

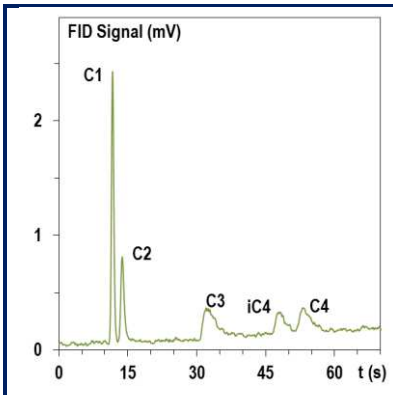


*GeoService1, semi-packed column (1.1 m x 200 µm x 100 µm, $e_f$=1 µm), P=6.8 bar, $V_{inj}$=2 µL, T=10°C-120°C at 6°C/s.*

*Fig. 104: on sputter-deposited alumina micro column*

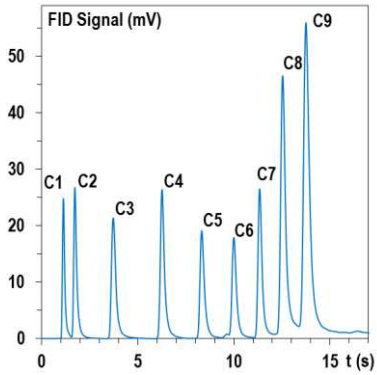


*Fig. 105a: linear alkanes C1-C9*
*P=6.1 bars, $V_{inj}$=20 nL,*
*T=13°C-200°C at 15°C/s*

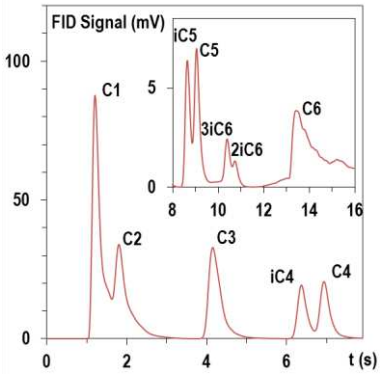


*Fig. 105b: isomeric alkanes C1-C6*
*(GeoServices 1 mixture)*
*P=6.1 bars, $V_{inj}$=1 µL,*
*T=13°C-180°C at 15°C/s*

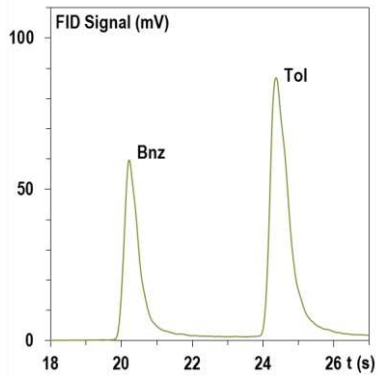


*Fig. 105c: aromatics*
*(benzene and toluene)*
*P=6.1 bars, $V_{inj}$=0.1 µL,*
*T=50°C-200°C at 5°C/s*

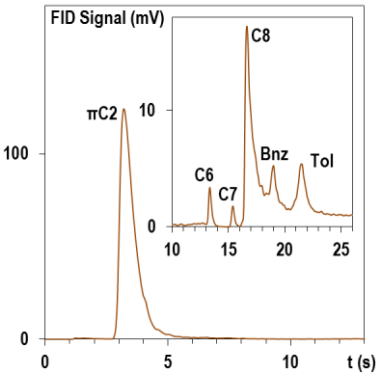


*Fig. 105d: saturated and unsaturated*
*(GeoServices 2 mixture)*
*P=6.1 bars, $V_{inj}$=1 µL,*
*T=40°C-190°C at 10°C/s*

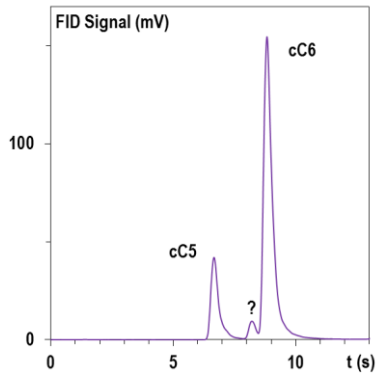


*Fig. 105e: cyclic alkanes (cC5 and cC6)*
*P=6.1 bars, $V_{inj}$=20 nL,*
*T=50°C-200°C at 10°C/s*

*Fig. 105: Temperature-programmed separations of other hydrocarbons on sputter-deposited silica open regular column (2.2 m x 100 µm x 100 µm, $e_f$=2.6 µm)*

### *IV.B.5.03 Use of nitrogen as carrier gas*

Nitrogen was compared to helium as carrier gas to preliminary estimate the feasibility of finally using air as carrier gas (which is generally mandatory in the aim of portability and in-situ analyses); corresponding results are gathered in figure 106.

No major changes were observed in terms of carrier gas velocity (at identical input pressure) and retention (figure 106a); C3 retention was found very slightly higher with nitrogen (2.4 instead of 2.3). FID signal was importantly disturbed, possibly due to the use of unpurified nitrogen. Optimal velocity for C2 obtained from Van Deemter experiments was found lower with nitrogen than with helium (respectively 26 and 50 cm/s), which was in agreement with acknowledged kinetic theory (figure 106b); nevertheless, efficiency was clearly improved with nitrogen (4329 plates instead of 3140) which was less expected and remained unexplained.

Temperature-programmed C1-C5 fast separation could as well be obtained with nitrogen in 11 seconds (figure 106c).

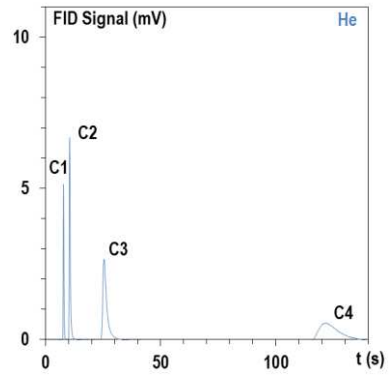


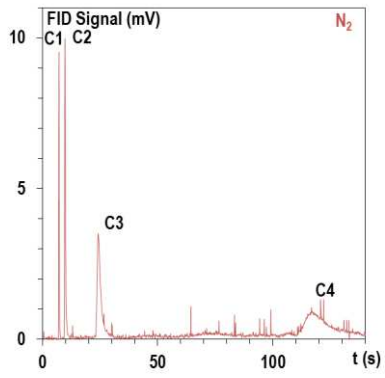


*Fig. 106a: isothermal C1-C4 separation with helium (left, $V_{inj}$=5 nL) and nitrogen (right, $V_{inj}$=10 nL) as carrier gas (P=0.7 bars, u=35 cm/s, T=30°C); $k_{C3,He}$=2.3, $k_{C3,N2}$=2.4.*

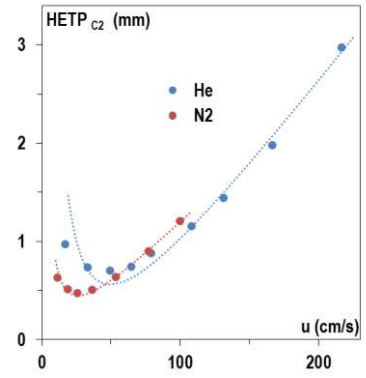


*Fig. 106b: Van Deemter plots (T=30°C)*

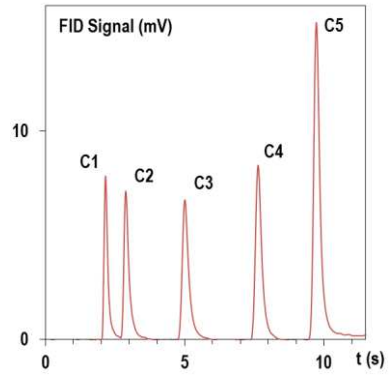


*Fig. 106c: temperature-programmed separation of linear alkanes C1-C5 with nitrogen as carrier gas, P=2.5 bars, $V_{inj}$=10 nL, T=30°C-185°C at 16°C/s*

*Fig. 106: comparison between helium and nitrogen as carrier gas on sputter-deposited silica open regular column (2.2 m x 100 µm x 100 µm, $e_f$=2.6 µm)*

| | He | $N_2$ |
|---|---|---|
| **P (bars)** | **0.3-5.1** | **0.2-2** |
| **$V_{inj}$ (nL)** | **5** | **10** |
| **$N_{maxC2}$** | **3140** | **4329** |
| **$HETP_{minC2}$ (mm)** | **0.70** | **0.51** |
| **$u_{optC2}$ (cm/s)** | **50** | **26** |
| **A (mm)** | -1.3 | -0.27 |
| **B ($cm^2/s$)** | 4.5 | 0.9 |
| **C (ms)** | 1.8 | 1.4 |
| **Modeling quality** | $R^2$>0.995 | $R^2$>0.995 |

*Results from Van Deemter plots*

### *IV.B.5.04 High temperature C1-C2 separations*

C1-C2 separation was understood to be crucial in most targeted applications. In the case of strong ambient conditions constraints (ambient temperature higher than 30°C, such as in the desert, or downhole), a ramp initial temperature of 15°C would be hardly reachable, and C1-C2 separation could be damaged: at 100°C and 2 bars, C1-C2 resolution was found as low as 0.8 on 2.6 µm silica open regular column (figure 107 left). Solutions were proposed to meet this specific requirement, by changing stationary phase or phase ratio.

C1 and C2 separation at the same high ambient temperature (100°C) was evaluated on a graphite (2.7 µm) regular column, at a similar carrier gas velocity (88 instead of 98 cm/s). Graphite provided a fully resolute separation ($R_{C1-C2}$=2.0 at 100°C, see figure 107 middle, and $R_{C1-C2}$=0.7 at 150°C).

Using silica as stationary phase, C1-C2 separation at high temperature (97°C) could also be enabled on a 4 times narrower column (section 50 µm x 50 µm) and a twice longer deposition time (thickness 4.8 µm), with 4.1 bars as input pressure (and 32 cm/s as carrier gas velocity): a resolution of 2.3 was obtained (1.4 at 119°C, see figure 107 right).

Depending on the rest of the possible requirements (separation speed, peak symmetry, low input pressure etc.), one or the other of these approaches could be followed.

### *IV.B.5.05 Effect of silica layer hydration*

The effect of silica layer hydration on thermodynamic and kinetic properties of a regular column was evaluated. After recording reference chromatograms, a droplet of water was percolated through the column and spontaneous evolution of the column was monitored by continuous recordings of chromatograms (figure 108). After 2 hours, verifications were carried out by twice drying the column and twice de- and reconnecting it.

A strong drop (from 0.3 to 0.1) in C2 retention factor was observed after hydration, as well as an increase of plate number (2400 to 3600, probably due to retention decrease). As the most significant (both thermodynamic and kinetic quantity), corresponding C1-C2 resolution was measured: a drop from 3.7 to 1.3 was observed.

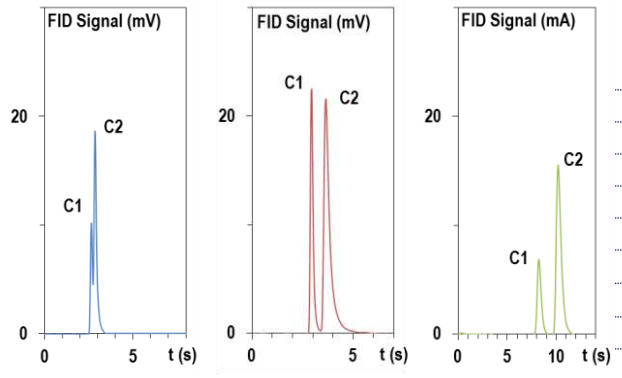


| | Left (ref) | Middle | Right |
|---|---|---|---|
| Width (µm) x Depth (µm) | **100x100** | **100x100** | **50x50** |
| Stationary phase | **Silica** | **Graphite** | **Silica** |
| Deposition time | **120 min** | **200 min** | **240 min** |
| Thickness (µm) | **2.6** | **2.7** | **4.8** |
| $V_{inj}$ (nL) | 5 | 10 | 200 |
| GC apparatus | Varian | Varian | Agilent |
| P (bars) | 2 | 1.4 | 4.1 |
| u (cm/s) | 98 | 88 | 32 |
| T (°C) | **100** | **100** | **97** |
| $R_{C1-C2}$ | **0.8** | **2.0** | **2.3** |

*Fig. 107: high temperature (~100°C) C1-C2 separations enabling (open columns 2.2 m, mixture C1-C4)*

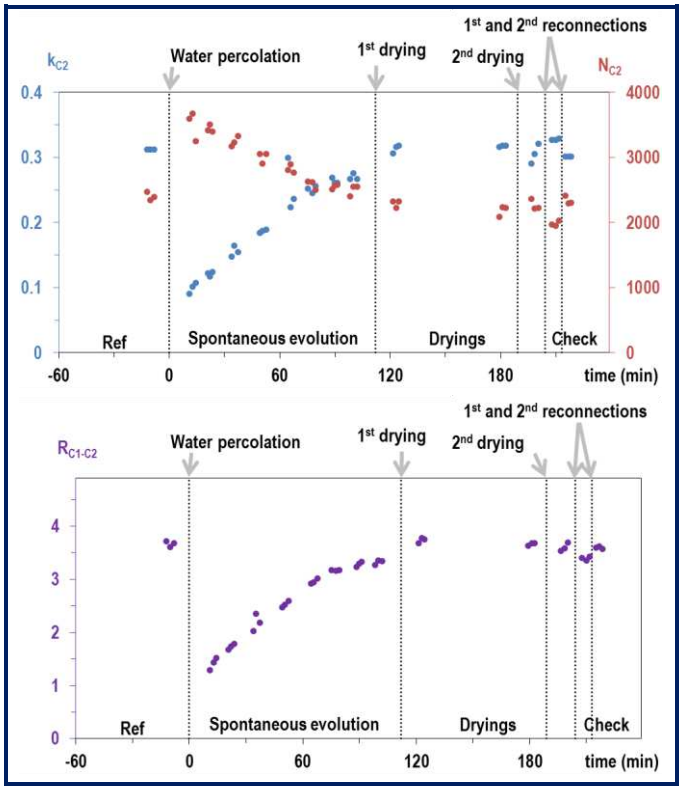


*Fig. 108: effect of water percolation on thermodynamic and kinetic properties of C2 retention;*

*regular column (2.2 m x 100 µm x 100 µm), 2.6 µm sputter-deposited silica;*

*T=30°C, C1-C3 mixture, $V_{inj}$=5 nL, P=0.9 bars ;*

*top: evolution of C2 retention factor (blue) and number of plates (red);*

*bottom: evolution of C1-C2 resolution*

Then, system spontaneous evolution brought back retention factor, efficiency, and resolution to their initial values within around 2 hours, only thanks to the continuous sweeping of the carrier gas (less than 1 bar of input pressure) at ambient temperature (30°C). Final values remained naturally unchanged neither by column dryings nor by column reconnections.

These results suggested that such columns could work in environments with high humidity or bulk water presence, especially with temperature-programmed use, which would as well contribute to water desorption from silica layer and elution out of the column.

### *IV.B.5.06 Conclusions*

These few preliminary results concerning columns use in potential real conditions were very promising. Very fast C1-C5 separations were obtained (9 seconds), as well as other hydrocarbons fast separations (C1-C9, isomers, unsaturated, aromatic and cyclic). Columns versatility towards carrier gas change (nitrogen), higher ambient temperature (100°C), and water presence was demonstrated.

## IV.B.6 Conclusions

To close this most important section on columns evaluations, the following summary is proposed:

- open and semi-packed columns with sputter-deposited silica and graphite, and semi-packed columns with alumina, were fabricated, evaluated, and proven able to separate C1-C4 (or C1-C5) mixtures; open magnesia columns provided separations only between C1+C2, C3 and C4; resolutions were sufficient in most operating conditions, in spite of more or less pronounced peak asymmetries;

- intermediary precisions (injection, evaluation, fabrication, temperature-programmed use) were roughly estimated; fair to excellent precisions were observed, and promising results were obtained (especially in terms of real condition use after calibration), but they remained insufficiently precise for thorough and accurate modeling; the difficulty to exactly define layer thickness or stationary phase volume was partially responsible for this lack;

- thermodynamic studies of the fabricated columns were quantitatively reported (specific retention factors measures or Van't Hoof plots), and led to the conclusions that retention qualitatively increased with phase ratio decrease, and from magnesia to graphite through alumina and silica, with adsorption energies in agreement with the literature;

- kinetic studies were as well reported, and although kinetic behavior could easily be modeled with Van Deemter equation, kinetic performances were hardly predictable (excepted evolution with stationary phase film thickness); highest efficiency was provided by a regular column with 50 mT sputter-deposited 2 µm-thick silica layer (5731 plates), and smallest plate height was provided by a semi-packed column with sputter-deposited 1 µm-thick alumina layer (0.25 mm);

- anticipation tests on real condition use exhibited a fast C1-C5 separation in 9 seconds on silica open regular columns, and interesting versatility properties of these columns were demonstrated.

A summary of thermodynamic and kinetic results obtained throughout this study is proposed in table 16. As a simultaneously thermodynamic and kinetic quantity, and as a crucial requirement in most applications, C1-C2 resolution was indicated for each column, at 30°C and C2 optimal velocity. Excepted a few particular cases (very thin layers of silica, use of alumina), resolutions were higher than the reference value of 1.25 usually required for quantitative analyses. High resolution columns (low phase ratio columns, graphite columns) could be either used at high temperature as demonstrated, either be shortened to the minimal length so that resolution remains above 1.25; in a first approximation, resolution is roughly proportional to $\sqrt{L}$, which means that the 2.2 meters-long regular column (silica 2.6 µm) enabling a resolution of 3.9 could enable a resolution of 1.25 within 23 cm… In this way, analysis time could be drastically decreased, as well as chip size.

Cooling time should also be decreased by using smaller temperature windows, which is possible by using a higher start temperature (with a high resolution column) and/or by using a lower stop temperature (with a low retention column). 50 mT (open column) and 30 minutes (semi-packed) silica deposition may be appropriate methods to solve this apparent antagonism. Cooling time could also be decreased by using smaller chips (with shorter columns), owing to a lower heat capacity.

The last section of this results and discussion chapter is dedicated to the first steps of the development of this discovery at GeoServices, for XXXXXXXXXXX application.

| Design | Length (m) | Section (µm²) | Stat. phase | Deposition time (min) | $k_{C3}$ | $\lvert\Delta_r H°_{C3}\rvert$ (kJ/mol) | $\alpha_{C2\text{-}C3}$ | $N_{maxC2}$ | $N_{maxC2}$ (/m) | $HETP_{minC2}$ (mm) | $R_{C1\text{-}C2}$ |
|---|---|---|---|---|---|---|---|---|---|---|---|
| Open | 2.2 | 100x100 | Silica | 300 (50 mT) | 1.7 | 28.8 | 6.2 | **5731** | **2605** | **0.38** | 3.9 |
| | | | | 120 | 2.1 | 31.8 | 6.2 | 2597 | 1180 | 0.85 | 3.5 |
| | | 75x100 | | | 2.2 | - | 6.3 | 2331 | 1060 | 0.95 | 3.3 |
| | | 50x100 | | | 1.2 | - | 5.5 | 3860 | 1755 | 0.57 | 2.8 |
| | | 100x50 | | | **0.8** | - | 5.3 | 2256 | 1025 | 0.98 | 1.8 |
| | | 30x100 | | | 1.8 | - | 6.2 | 1387 | 630 | 1.6 | 2.0 |
| | | 50x50 | | 240 | 6.2 | 34.0 | 5.6 | 1318 | 599 | 1.7 | **6.6** |
| | | 50x50 | | 30 | 0.62 | 24.9 | 6.9 | 2229 | 1013 | 1.0 | 0.88 |
| | | 75x100 | | | **0.7** | - | 6.6 | **5517** | 2508 | 0.40 | 1.7 |
| | | | | 60 | 0.9 | - | 5.7 | 4425 | 2011 | 0.50 | 2.0 |
| | | | | 180 | 2.2 | - | 5.9 | 2616 | 1189 | 0.84 | 4.0 |
| | | | | 240 | 4.4 | - | 6.4 | 1988 | 904 | 1.1 | **5.5** |
| | 1 | 75x75 | | | 3.7 | 20.1 | 8.7 | 1137 | 1137 | 0.59 | 2.2 |
| | 0.5 | | | | 3.8 | 25.6 | 10.1 | 799 | 1598 | 0.63 | 1.3 |
| SP(1) | 1.1 | 200x100 | | 120 | 3.9 | - | 6.4 | 2663 | 2421 | 0.41 | 4.1 |
| SP(2) | | | | | 3.2 | 26.8 | 6.7 | 2344 | 2131 | 0.47 | 4.4 |
| | | | | 30 | **0.8** | 27.8 | 5.1 | 3945 | **3586** | **0.28** | 3.3 |
| | | | Alumina | 120 | 0.7 | 30.2 | 8.6 | **4479** | **4072** | **0.25** | 0.96 |
| | | | Graphite | 60 | 12.0 | 34.9 | 16.7 | 959 | 872 | 1.1 | **6.3** |
| Open | 2.2 | 30x100 | | 60 | - | - | - | 172 | 78 | 13 | 4.7 |
| | | 50x100 | | 60 | - | - | - | 224 | 102 | 9.8 | 2.5 |
| | | 75x100 | | 60 | - | - | - | 134 | 61 | 16 | 2.9 |
| | | 100x100 | | 60 | 11.4 | 39.1 | 14.9 | 256 | 116 | 8.6 | 1.8 |
| | | | | 200 | 117 | 44.3 | 14.7 | 83 | 38 | 27 | 3.9 |
| | | | Magnesia | 562.5 | 1.0 | 20.1 | - | - | - | - | - |

*Table 16: summary of thermodynamic and kinetic evaluation of fabricated columns; retention factors and resolutions are the ones obtained at 30°C and optimal velocities; three best values of efficiency and resolution appear in red, and three lowest retention values with R>1.25 appear in green.*

## IV.C. Schlumberger confidential section

Schlumberger confidential content – address requests to raphael.haudebourg@gmail.com
Schlumberger confidential content – address requests to raphael.haudebourg@gmail.com
Schlumberger confidential content – address requests to raphael.haudebourg@gmail.com

### IV.C.1. Schlumberger confidential paragraph

Schlumberger confidential content – address requests to raphael.haudebourg@gmail.com
Schlumberger confidential content – address requests to raphael.haudebourg@gmail.com
Schlumberger confidential content – address requests to raphael.haudebourg@gmail.com
Schlumberger confidential content – address requests to raphael.haudebourg@gmail.com

### IV.C.2. Schlumberger confidential paragraph

Schlumberger confidential content – address requests to raphael.haudebourg@gmail.com
Schlumberger confidential content – address requests to raphael.haudebourg@gmail.com
Schlumberger confidential content – address requests to raphael.haudebourg@gmail.com
Schlumberger confidential content – address requests to raphael.haudebourg@gmail.com
Schlumberger confidential content – address requests to raphael.haudebourg@gmail.com
Schlumberger confidential content – address requests to raphael.haudebourg@gmail.com
Schlumberger confidential content – address requests to raphael.haudebourg@gmail.com
Schlumberger confidential content – address requests to raphael.haudebourg@gmail.com

## Conclusion

Although the last chapter of this report will be dedicated to a general conclusion of this research work (including summary and perspectives), the major key points of this chapter should be highlighted here:

- thanks to low thermal mass on-chip columns, and the appropriate temperature-programming system (including thermal elements, hardware and software), pseudo-linear temperature ramps up to 20°C/s could be obtained, as well as fast cooling of the chip, with low power consumption;

- sputter-deposited silica, alumina, graphite and magnesia as stationary phase were evaluated for the separation of light hydrocarbons; sputter-deposited stationary phase micro columns were proven to partially or fully fill various requirements, in terms of collective and reproducible fabrication, volatile hydrocarbons separations, thermodynamic and kinetic modeling, and targeted applications (in-situ fast monitoring);

- the integration of a sputter-deposited silica micro column in a XXXXXXXXXXX by GeoServices and the first tests carried out provided very encouraging results, by partially demonstrating the possibility to multiply by a factor at least 2.3 analysis throughput.

# V. Conclusions and perspectives

## V.A. Improvements

### V.A.1. In micro gas chromatography

A totally new stationary phase deposition process for micro gas chromatography columns was invented and patented. It was fully compatible with collective production, and could be integrated in a standard clean room process flow. Whereas only carbon nanotubes had been the only untreated and collectively-deposited solid material used as stationary phase in micro columns so far, sputtering enabled deposition of various solid stationary phases such as silica, alumina, graphite and magnesia, and the collective fabrication of PLOT-like columns.

These columns were intended to serve as the separating element for oilfield analyses, and low-power fast separations of light hydrocarbons were successfully obtained on different columns types and stationary phases. Thermodynamic, kinetic, and temperature-programmed behavior of these columns towards light hydrocarbons separation was investigated and quantitatively reported. In particular, measured efficiencies reached 5730 plates in 2 cm x 2 cm x 1 mm chip, and plate heights down to 250 µm were obtained. The small loss of efficiency compared to conventional PDMS micro columns was a very gentle compromise to enable fast but full targeted separations (for instance C1-C9 in less than 15 seconds).

The interest of the scientific community for this finding was demonstrated in many occasions (publications in top-rated analytical chemistry journals, rewarded communications, see page 171).

### V.A.2. In oilfield applications

Similarly, the interest of the oilfield industry for the finding was demonstrated not only by the launching of a 4 years (2010-2014) research project reported in this manuscript, but also by the joining of GeoServices in 2012.

# V.B. Limitations

## V.B.1. In column evaluation

Qualitative predictions of micro columns behavior were generally confirmed, but quantitative modeling was often difficult. This was due to two main reasons: the first one was the complex structure of stationary phase layer; indeed, 3 square sides out of 4 were covered with stationary phase, layer structure depended on the side (floor or wall), observed porosity could not be accurately measured, and layer thickness was not homogeneous; the second one was the conclusion of the short precision study: method general precision (from fabrication to temperature-programmed separations) was only partially investigated on a very few amount of samples, and provided mitigated results, which naturally but temporarily limited the impact of the discovery.

Moreover, no study on column overloading or sample capacity could be relevantly reported, extra column effects were not evaluated (and probably led to an underestimation of micro columns efficiencies), and the few attempts to separate other compounds than hydrocarbons failed, probably rather due to the inappropriateness of the chosen protocol than to columns properties themselves.

## V.B.2. In industrial developments

Most of the limitations and failure experienced in columns fabrication could be overcome within the research project. The rest of them were due to the context of the production (low-funded research work) and were reasonably expected to be as well overcome in an industrial development.

For XXXXXXXXXXX analyses, doubts could still be emitted regarding general method precision (again, from fabrication to temperature-programmed separations), pending exhaustive precision studies. No accurately defined method for this application (column dimensions and handling) was set at the moment of this writing.

For whole GC system miniaturization, the three different micro machined components (injector, column and detector) were eventually reported, but only a few non-temperature-programmed specific experiments have been carried out so far with the three components together.

# V.C. Perspectives

## V.C.1. Column fabrication

Numerous perspectives are now opened to improve or diversify columns fabrication.

Although failure rates should tend towards 0% only by respecting appropriate production standards, two other suggestions to solve residual photoresist removal problems can be formulated: first, a solution consisting in using much shorter deposition times (i.e. thinner stationary phase films) can be investigated (for instance 100 – 500 nm instead of 600 nm – 5 µm used so far); in this case, retention should be retrieved either by column length

extending, either by column section narrowing, either both; section narrowing also should increase space available on the chip for length extension, so that chip size could remain the same (see lower); and second, an alternative sputtering mode, consisting in using reactive metal sputtering in the presence of oxygen to form the oxide layer (which is expected to decrease deposition time) can be attempted.

This alternative approach could also be used to widen the range of sputter-deposited stationary phase micro columns, to improve columns chromatographic performances and target diversified industrial applications. The influence of sputtering mode (direct oxide deposition or reactive metal-oxygen deposition), of sputtering pressure (which was only slightly but relevantly studied in this report), and of sputtering material are all interesting studies to carry out.

Although silica and graphite were evaluated in numerous layouts in this study, alumina, magnesia and titania could not be as thoroughly evaluated, but should be in further research work. Other materials than those studied in this report could for instance consist of other pure oxides, of oxide alloys, of silicon carbide, of polymers.

Finally, other channel layouts could be experimented, such as semi circular or triangle shape open channels, or sputter-covered wafers bonding (to form 4-sides covered channels), or various semi-packed designs…

A last, but not least, aspect of column fabrication which should be improved is fluidic connections, as capillary gluing used so far remains poorly compatible with mass production and robust product definition.

## V.C.2. Column handling and evaluation

Exhaustive precision evaluations will be carried out at GeoServices in 2014 for a specific application, but could as well be led in a general context (such as processed in this study, but for a much larger amount of samples).

Extra-column effects, sample capacity, and non-oilfield-related compounds separations should as well be evaluated in further developments of this technology. Depending on the targeted application, accurate methods for column handling should be defined (injection volume, flow rate, initial temperature, ramp start time, ramp intensity and ramp stop time or stop temperature, cooling system…).

## V.C.3. Schlumberger confidential paragraph

## V.C.4. Low-cost pocket gas chromatography

Total integration of micro column block (including temperature-programming system) with the micro injector and micro detector, along with all other essential components (sample and carrier gas inlet, flow controllers, fluidic connections, electronic hardware and user interface) could finally lead to a new generation of micro gas chromatograph, presenting all advantages mentioned above, in terms of collective clean room-compatible fabrication and versatile utilization.

Other applications than oilfield services could as well be imagined, such as environmental monitoring of volatile organic compounds*.

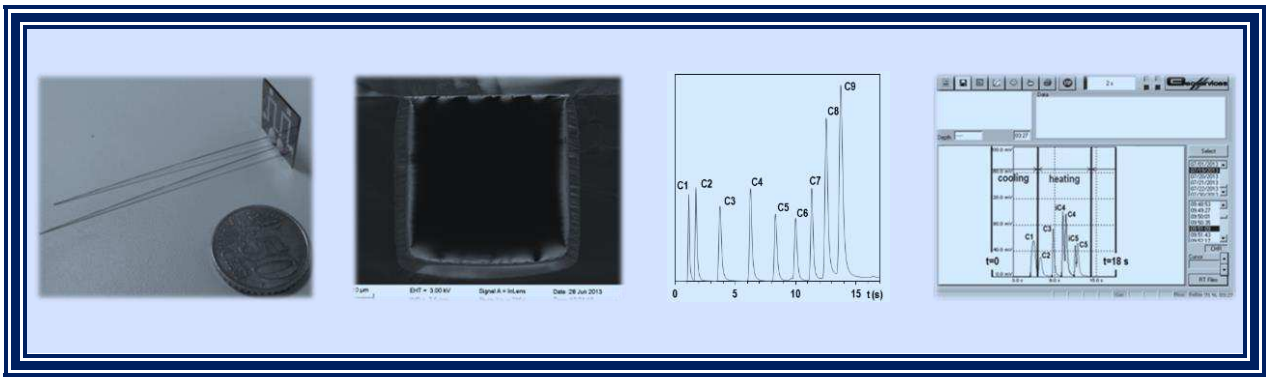

# Appendices

Three appendices are proposed to the reader to deepen a few technical aspects of this research work and to finally improve its general understanding. A first appendix is dedicated to compared physical and chromatographic studies of the micro thermal conductivity detector developed at MEMS TC and introduced and used in this report; then, a second appendix deals with the separations and limitations observed at MEMS TC with other stationary phases in micro columns, just before the discovery presented in this report; finally, a last appendix provides technical details on the temperature programming system which were not crucial enough to be placed in the body of this report.

## Appendix A: micro thermal conductivity detector evaluation

The first purpose of the studies displayed in this appendix dedicated to the evaluation of the µ-TCD was to estimate by two different means the order of magnitude of its detection limit. The second one was to evaluate its sensitivity to flow rate. The last one was to estimate its linearity.

### Apdx A.1. Detection limit

The order of magnitude of µTCD detection limit was estimated by two totally independent approaches: a first one consisting in evaluating the sensitivity of the platinum filaments (and, thus, of the Wheatstone bridge) to changes in gas thermal conductivity, and to obtain an approximate value of $dS_{\mu TCD}/dc$, where $S_{\mu TCD}$ is the final µTCD signal displayed on the computer and c is the concentration of an analyte in the carrier gas; the second approach consisted in a conventional chromatographic experiment, where a sample was gradually enriched with the analyte, and where corresponding chromatographic peaks characteristics were plotted against estimated concentration.

#### *Apdx A.1.01 Physical evaluation*

TCD general operating principle was described earlier (II.B.4.02, see also figure 110a below).

The expression of $dS_{\mu TCD}/dc$ to be estimated was split down into the four following terms:

$$\frac{dS_{\mu TCD}}{dc} = \frac{dS_{\mu TCD}}{dV_{outTCD}} x \frac{dV_{outTCD}}{dR_{PF}} x \frac{dR_{PF}}{d\lambda} x \frac{d\lambda}{dc}$$

where:

- $V_{outTCD}$ was the raw analogical voltage at the output of the Wheatstone bridge as displayed on figure 110b ($V_{inTCD}$ was the input voltage of the Wheatstone bridge provided by USB, $V_{inTCD}$=5 V);

- $R_{PF}$ was the value of the resistance of one platinum filament in the analytical channel with voltage supply (figure 110b); $R^0_{PF}$ was the reference value of the resistance of one platinum filament without voltage supply;

- λ was the thermal conductivity of the gas in the measure channel.

$dS_{\mu TCD}/dV_{outTCD}$ was measured by using arbitrary-generated triangle waves of different amplitudes as the input of the electronic module of the μTCD (see also figure 64b). The amplitude of the numeric signal displayed on the computer was plotted against the analogical amplitude of the triangle waves, and a linear gain of $9.4x10^9$ $V^{-1}$ was observed (figure 110d).

A usual Wheatstone bridge calculation and the first order approximation on $R_{PF}$ resulted in:

$$\frac{dV_{outTCD}}{dR_{PF}} \approx \frac{V_{inTCD}}{2R_{PF}}$$

To study the value of $R_{PF}$ (including $R^0_{PF}$), one of the two analytical platinum filaments was disconnected from the circuit of a purposely manufactured μTCD; it was then connected to both a voltage divider bridge (with a load to mass resistance of 269 Ω) and to a National Instruments Data Acquisition PAD ran with Labview, to simultaneously record the variations of $R_{PF}$ and of $V_{PF}$ (the input voltage applied to the platinum filament through the DAQ-PAD). Acquisition frequency was 100 Hz. As a reminder, $V_{PF}$ was purported to vary around 2.5 V ($V_{inTCD}/2$) in operating conditions.

Thanks to this setup, the influence of gas thermal properties, of gas flow rate, and of input voltage, on the value of $R_{PF}$ could be quantitatively studied. Four different gases (helium and carbon dioxide, by Air Liquide, and nitrogen and ethane, by Praxair) were used.

A first experiment consisted in measuring $R_{PF}$ variations along with $V_{PF}$ for different gases (without flow rate, at ambient temperature); corresponding result is displayed on figure 110e. A first qualitative observation was the increase of the difference between $R_{PF}$ values for different gases along with $V_{PF}$ increase: for instance, at $V_{PF}$ = 1 V, $(R_{PF\ C2} - R_{PF\ He})/R_{PF\ He}$ = 14 %, whereas at $V_{PF}$ = 2.5 V, this value was 28 %. Thus, working at even higher input voltage should increase detector sensibility. A second quantitative observation was the reading of $R_{PF}$ near operating point (2.5 V in helium): $R_{PF} \approx 326$ Ω. An approximate value of $dV_{outTCD}/dR_{PF}$ of 7.7 mA was therefore obtained.

To estimate the value of $dR_{PF}/d\lambda$, an energy balance equation was first considered:

$$P_{\text{electrical power dissipated by Joule effect in the platinum filament}} = P_{\text{thermal poser transferred to surrounding gas}}$$

$$\frac{V_{PF}^2}{R_{PF}} = G(\lambda) x \Delta T$$

where G(λ) was the thermal conductance of heat flow from platinum filament towards surrounding gas, and therefore depended on gas nature and thermal conductivity, and where ΔT was the temperature difference between platinum filament and surrounding gas. To estimate ΔT in this equation, the resistance temperature coefficient of the platinum filament

was estimated through the exact same experiment as the one described in III.B.1. A linear plot was obtained ($R^2$>0.999) and a resistance-temperature coefficient α=0.24%/°C was measured (figure 110f). With the relation $\Delta T=\Delta R/R_0/\alpha$, the energy balance equation could be rewritten as:

$$\frac{R_{PF}^0}{R_{PF}x(R_{PF}-R_{PF}^0)}=\frac{G(\lambda)}{\alpha V_{PF}^2}$$

Data from figure 110e were rearranged to plot the left term of the equation above against $1/V_{PF}^2$ for the four different gases (figure 110g).

Corresponding slopes of the linear curves ($R^2$>0.99, except for C2, $R^2$=0.96) were divided by the measured values of α and plotted against thermal conductivities of the different gases found in the literature (figure 110h) [1]. A few limitations of the approach should be mentioned here:

- this first order modeling did not consider slight but acknowledged variations of thermal conductivities with temperature;
- thermal conductivities of nitrogen, carbon dioxide and ethane were very close, and the plot was closer to a 2-points plot (with a ¾ weight for the low λ point) than to a 4-points plot;
- thermal transfer from the filament to the gas was probably due to at least two phenomena (conduction and convection): no study on the respective weights of these two mechanisms was carried out; but convection transfer is generally ruled by a similar equation (P=hΔT), and the quantity λ can be considered as a global value;
- the plot of G(λ) was far from passing through (0;0), which was probably due to heat losses in the solid structure (heat conduction in the $Si_3N_4$ supporting structure and in the platinum connection tracks); total conductance could be considered as $G_{tot}=g_{gas}\lambda+G_{sol}$, with $g_{gas}$=0.99 mm and $G_{sol}$=17 µW/K/m; the relative weights of these losses $G_{sol}/G_{tot}$ were 11% for helium, 42% for nitrogen, 53% for carbon dioxide and 49% for ethane; however, in operating conditions, λ value remains usually very close to $\lambda_{He}$.

The rewritten energy balance equation was then differentiated by λ:

$$\frac{d}{dR_{PF}}\left[\frac{R_{PF}^0}{R_{PF}x(R_{PF}-R_{PF}^0)}\right]x\frac{dR_{PF}}{d\lambda}=\frac{dG(\lambda)}{d\lambda}\frac{1}{\alpha V_{PF}^2}$$

With $dG(\lambda)/d\lambda=g_{gas}$, the value of $dR_{PF}/d\lambda$ could finally be expressed as:

$$\frac{d\,R_{PF}}{d\,\lambda}=-\frac{g_{gas}}{\alpha V_{PF}^2}\frac{R_{PF}^2}{R_{PF}^0}\frac{(R_{PF}-R_{PF}^0)^2}{2R_{PF}-R_{PF}^0}$$

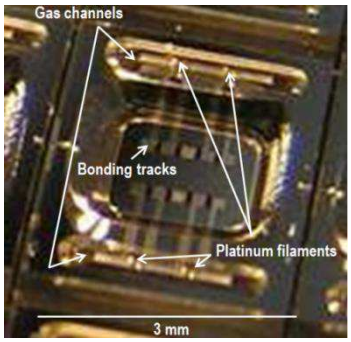


*Fig. 110a: picture of µTCD chip (before wire bonding and capillary gluing);*

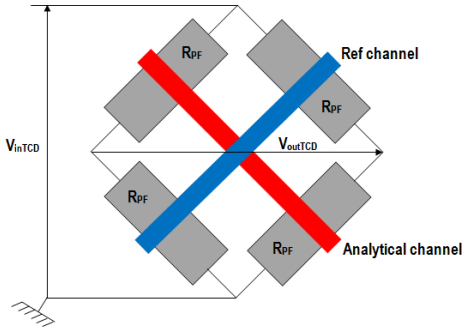


*Fig. 110b: platinum filaments layout in a Wheatstone bridge;*

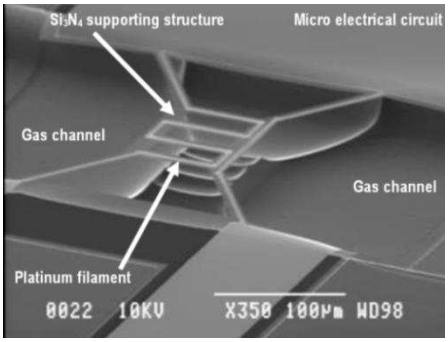


*Fig. 110c: SEM picture of one platinum filament hanging in one of the gas channels;*

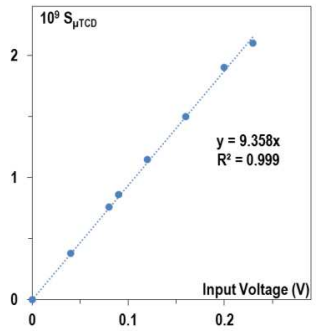


*Fig. 110d: analogical to numerical conversion plot for the µTCD*

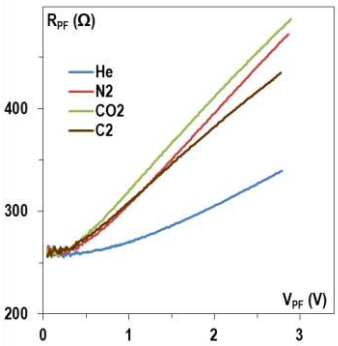


*Fig. 110e: influence of gas nature and applied voltage on the resistance of one platinum filament;*

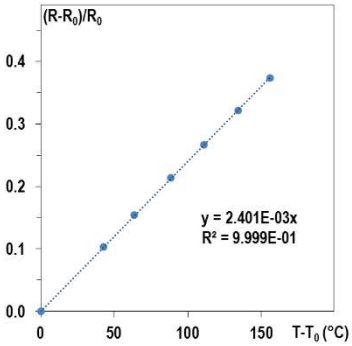


*Fig. 110f: resistance-temperature characterization of one platinum filament; $T_0$=30°C; $\alpha_{measured}$=0.24%/°C;*

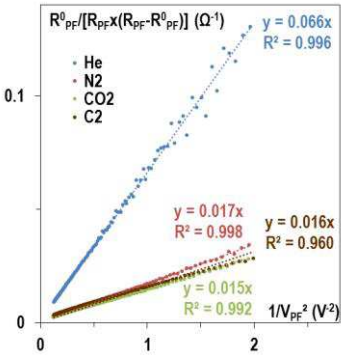


*Fig. 110g: indirect plots from energy conservation law; slopes=G(λ)/α;*

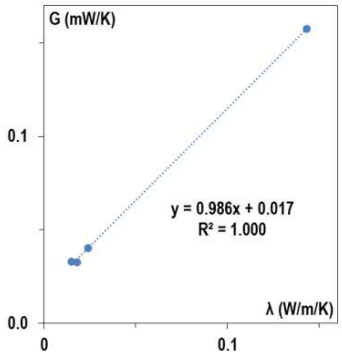


*Fig. 110h: conductance value as a function of gases thermal conductivities*

*Fig. 110: µTCD platinum filaments description and characterization*

In a first order approximation, a $R^0_{PF}$ value in helium without voltage supply of 256 Ω was extracted, and the same $R_{PF}$ value of 326 Ω was considered (helium at $V_{PF}$=2.5 V). With $V_{PF}$=2.5 V, the approximation of $dR_{PF}/d\lambda$=-338 ΩmK/W was obtained.

At last, to estimate the value of dλ/dc, Wassilijewa-Saxena-Mason mixing rule [2] was used in the example of a very diluted mixture of propane in helium: if $x_{C3}$ is the molar fraction of propane in helium and if $x_{C3}$<<1, then $\lambda = x_{C3}\,\lambda_{C3}/0.23 + (1- x_{C3})\,\lambda_{He}/0.35$, and $d\lambda/dx_{C3}$=-0.34 W/m/K. For very diluted mixtures, and in the ideal gas hypothesis, molar and volume fraction and particle concentration (in ppm for instance) were considered equal and dλ/dc=-3.4x10$^{-7}$ (W/m/K)/ppm.

Finally, detector sensitivity, in the example considered (propane in helium) and with detailed approximations, could be expressed as:

$$\frac{dS_{\mu TCD}}{dc} = \frac{dS_{\mu TCD}}{dV_{outTCD}} x \frac{dV_{outTCD}}{dR_{PF}} x \frac{dR_{PF}}{d\lambda} x \frac{d\lambda}{dc}$$

$$\frac{dS_{\mu TCD}}{dc} = 9.3x10^{9}\ x\ 7.7x10^{-3}\ x\ 3.4x10^{2}\ x\ 3.4x10^{-7} = 8.3x10^{3}\ /ppm$$

A very basic definition of detection limit was chosen: concentration below which signal to noise ratio becomes less than twice baseline noise level. According to the previously calculated µTCD signal sensibility (8300/ppm) and to the signal baseline monitoring displayed on figure 111 (noise level 1.5x10$^5$), roughly predicted detection limit of propane in helium was 2x150/8.3=36 ppm.

A chromatographic experiment was then carried out to challenge this calculation.

### *Apdx A.1.02 Chromatographic evaluation*

For this test, a column was placed upstream of the detector, so that propane could be separated from air (test could not be carried out with air only because of its hardly controllable quantity). The column used was a high efficiency PDMS micro column fabricated at MEMS TC (see appendix B).

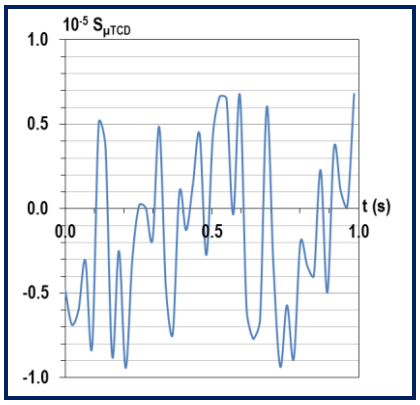


*Fig. 111: baseline monitoring of µTCD signal;*

*carrier gas helium, P=2 bars, T=30°C;*

*noise level was considered to be 1.5x10$^5$.*

An unused 2L gas tight Tedlar bag was first filled with helium (Air Liquide). The input of the sample micro fluidic circuit consisted in a capillary immerged directly inside the bag (the capillary was passed through the integrated septum of the bag). The output consisted of an electric micro pump in traction mode, which allowed a regular flow of the gas from the bag through the sampling loop. Injections were effectuated thanks to the electrical mechanical injector ($V_{inj}$=1 µL) fabricated at MEMS TC. Increasing and accurate propane volumes were successively sampled from another identical bag containing propane (Praxair), and injected in the measure bag through the septum, using a syringe adapted to the propane volume added (added volumes varied from 10 µL to 1 mL). After each addition of propane, the bag was softly shaken (to homogenize the mixture), an injection was processed, and a chromatogram was recorded. 46 chromatograms were taken in all, and total propane volume in the measure bag varied from 0 to 2.5 mL. At the end of the experiment, the final volume of the measure bag was assessed thanks to a simple in-water degassing ($V_{end}$ = 1.860 L): thus, estimated concentration of propane in helium varied from 0 to 1330 molar or volume ppm. This setup was the most reliable in terms of control of quantities (fidelity of the volume injected by the injector, accuracy of propane concentration, limitation of the presence of air in the circuit…).

Three examples of chromatograms obtained are displayed on figure 112. Air presence was limited and a full air-propane separation was observed. Concentration below which signal to noise ratio became less than twice baseline noise level was 33 volume ppm, which was surprisingly in excellent agreement with the value predicted physically (36 volume ppm), in spite of all the approximations operated.

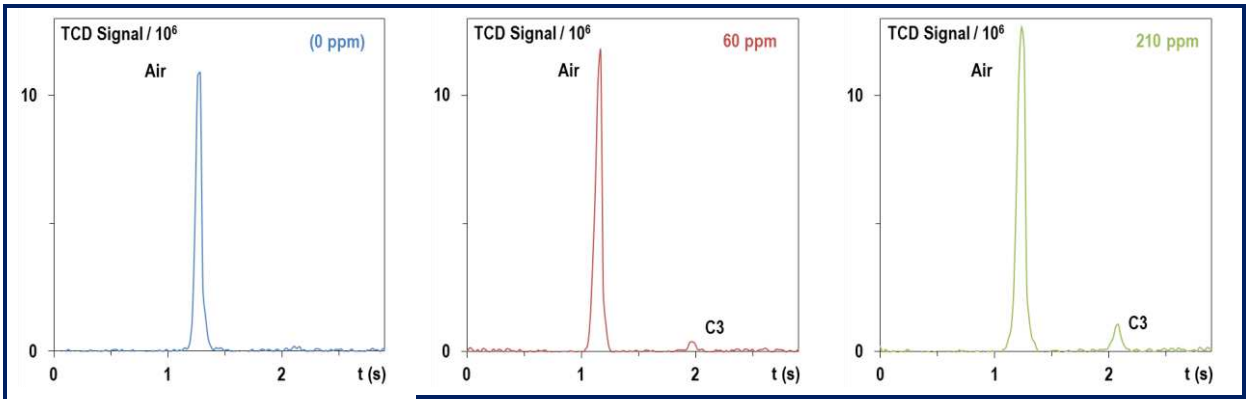


*Fig. 112: µTCD detection limit chromatographic evaluation: C3 in helium mixture; micro machined PDMS column; $V_{inj}$=1 µL (micro machined mechanical injector); carrier gas helium, P= 2 bars; top: examples of chromatograms at different volume concentrations of propane in helium; bottom left: signal to noise ratio of propane peak as a function of estimated propane volume concentration in helium (three last points between 250 and 1330 are not displayed).*

## Apdx A.2. Sensitivity to flow rate

The experiment described in Apdx A.2.01 was carried out at different input pressures. Flow rates were measured thanks to a flow meter (ADM 2000 by Agilent). Variation of platinum filament resistance along with flow rate is displayed on figure 113, in the operating zone of platinum filament voltage supply (2.5 V). A variation of $dR_{PF}/dD$=-6.2/15.3=-0.41 Ω/(mL/min) was observed, which for instance roughly corresponded to a signal variation of 3500 ppm in the concentration of propane in helium. Detector was therefore expectedly found flow rate sensitive, and a very particular attention should be paid to input pressure while using micro thermal conductivity detector.

## Apdx A.3. Detector linearity

A few direct approaches were attempted to evaluate µTCD linearity, in various concentration ranges. However, a strong limitation was experienced concerning the accurate measures and calculations of concentration in a conventional S=f(c) plot. The most relevant result of this series of experiments consisted of a compared study of TCD and FID signal for the same injection in a TCD-FID series setup.

The same PDMS column as in previous paragraph was used to separate C3 from air. The non-destructive µ-TCD was inserted between column outlet and FID inlet. 1 µL injections were made with a 10 µL gas tight SGE© syringe through GC Varian 3800© injector. Three different gas tight Tedlar© bags were used: a pure C3 bag, a pure helium bag, and an initially pure helium bag, which was gradually enriched with propane as in previous paragraph. Low concentration samplings (from ≃0.1% to ≃1% molar) were made with this third bag, while intermediate concentration samplings (from ≃1% to ≃5% molar) were then made by mixing different quantities from this enriched bag and from the pure propane bag; high concentrations (from 5 % to 95 % molar) were then made by mixing different quantities from the pure propane bag and from the pure helium bag, and pure propane was finally injected.

This experiment did not provide an absolute linearity characterization, because accurate quantities were not taken into account, but it exhibited an exact relative characterization of µ-TCD response compared to FID response, which was known to have a very wide range of linearity, with an excellent linearity, and a very low detection limit [3].

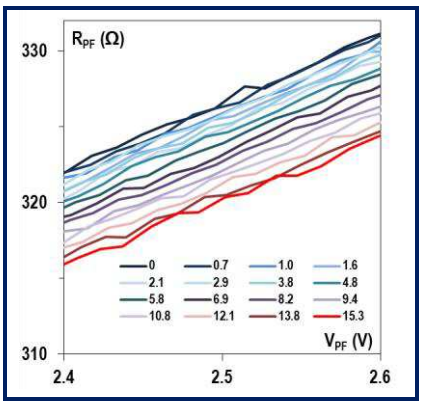


*Fig. 113: sensitivity of platinum filament resistance to carrier gas flow rate;*

*zoom on operating zone of $V_{PF}$ (near 2.5 V);*

*carrier gas: helium; P from 0 to 8 bars; corresponding flow rates are displayed on the legend (0 to 15.3 mL/min)*

Relationship between TCD and FID responses over 3 orders of magnitude of propane concentration was found linear with a very good correlation coefficient ($R^2$=0.992, figure 114). Forced passage through (0;0) did not change correlation coefficient but slightly changed the slope ($9.4x10^{-3}$ instead of $9.3x10^{-3}$). TCD response was thus concluded to be comparable for C3 peak area in the range 0.1% volume to pure.

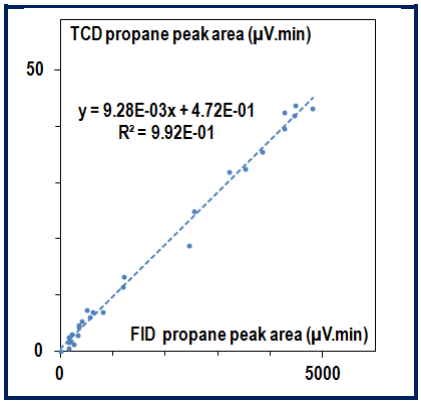


*Fig. 114: plot of propane peak area for TCD against same quantity for FID in a TCD-FID series setup;*

*C3 concentration range: from around 1000 volume ppm to pure;*

*P= 1.4 bars, $V_{inj}$=1 µL, T=30°C.*

## Apdx A.4. Conclusion

Many other studies were carried out in the µTCD but were of lower relevance in this appendix, whose purpose was to present the 3 previous major results: a predicted and experimentally confirmed detection limit of around 30 ppm, a certain sensitivity to flow rate, and a linearity comparable to a FID in the range 0.1% to pure.

A few improvements could still be performed on µTCD, especially in terms of detection limit: for instance in the design of the filaments to increase dR/dλ term or to decrease sensitivity to flow rate, or in the electronic unit to implement a noise removal unit. However, the feasibility of a fully miniaturized GC including micro injector, micro column and micro detector, all three developed at MEMS TC, was demonstrated, and an integrated USB-supplied demonstration prototype was built up (figure 115). This prototype could not perform temperature-programmed separations at the moment of this writing (USB 2.0 maximal power supply is 2.5 W), but showed automate Air-C3-C4 separations.

## Apdx A.5. References

[1] encyclopedia.airliquide.com
[2] http://www.chem.agilent.com/en-S/Newsletters_old/einspirations/archives/Pages/oct09techtip.aspx
[3] Book by Tranchant, cf. reference [1] from chapter II (bibliography)

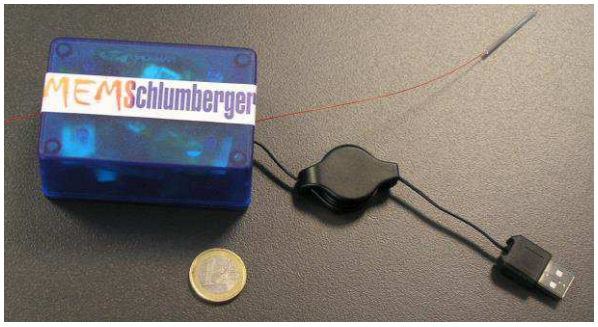


*Fig. 115: integrated "USB-GC"*

# Appendix B: limitations of other solid stationary phases

The approach and results displayed in this appendix WERE NOT the author's production: they were obtained just before the beginning of the research work on sputter-deposited stationary phase micro columns. Thus, they are displayed here rather as an appendix to bibliographical chapter, than as an appendix to the results and discussion chapter. The purpose is twofold: give credit to the context and the position of the problem stated in the introduction, and to reward the research work led before this one, which too much consisted of a limitation demonstration to be published, but was actually a work of the highest interest.

This appendix shortly reports the 6 materials attempted to serve as stationary phase in micro columns (for the separation of light hydrocarbons), as designed and developed at MEMS TC: PDMS, conventional packing powders (silica gel, activated alumina, black graphitized carbon and molecular sieve), and in-situ synthesized carbon nanotubes. Insertion processes are briefly described, thermodynamic and kinetic performances are summarized and illustrated with typical chromatograms, and results are discussed.

## Apdx B.1. Stationary phase insertion processes

- *PDMS coating:* PDMS (type: OV-1) was dissolved in pentane (approximate mass ratio: 1/40) and pushed into the column (regular type) thanks to a syringe plunger. The solvent was then evaporated by heating (10 minutes at 70°C), and thus the 4 inner walls of the channel were coated with a ~1.2 µm thick PDMS layer all along the column.

- *Graphite, molecular sieve, alumina and silica gel packing:* these materials were purchased in the form of powders. Silica gel consisted in Hayesep, type Davisil grade 634 (mesh 100/200, surface area 480 m²/g, pore size 60 A / 0.75 $cm^3$/g) by Sigma-Aldrich. Alumina consisted in activated neutral alumina, type Brockmann I (mesh 150, surface area 155 m²/g; pore size 58 A) by Sigma-Aldrich. Black graphitized carbon consisted in Carbotrap / Carbopack, type Carbopack X (mesh 120/400, surface area 240 m²/g, pore size 100 A / 0.62 $cm^3$/g) by Supelco; molecular sieve consisted in zeolite, type 13 X (mesh 100/120, pore size 13 A) by Supelco. Before gluing the connection capillaries to the in- and outlet holes, the column ("to-pack" type) was filled with the powder (see figure 116a). To help the packing to reach the middle of the column and to be homogeneous, softly tapping the column was necessary. Overall packing operation time was between 1 and 4 hours.

- *CNTs' in-situ growth:* nickel or kanthal (alloy of iron, aluminum and chromium, with traces of cobalt) was sputtered in the uncovered channels (variable width type) of the diced column to form a thin catalyst layer. CNTs were then grown (see figure 116b) by chemical vapor deposition (CVD) using a 4-step process: the system was flushed with an argon flow first at room temperature, then at 800°C; still at 800°C, the argon flow was then changed into a argon, hydrogen and ethylene mixture flow (5 minutes); finally, the

system was cooled down while flushed by the argon flow. The column was then bonded to the Pyrex lid.

Both first insertion processes were not collective and induced strong (yet not quantitatively evaluated) imprecision in the fabrication of the micro columns. For solid packings, irregularities and inhomogeneities in the filling of the columns were visible with bare eyes through the Pyrex cover.

Last insertion process was collective, although no quantitative evaluation of the deviation in the thickness of the carbon nanotubes was led. Besides, such a process required much higher standards in terms of clean room grade and processer safety than sputtering.

## Apdx B.2. Chromatographic evaluation

Columns were evaluated following roughly the same method than in Chapter III: air methane separation was evaluated on the µTCD setup, and C1-C4 separation on the Varian FID setup. Retention factors and maximal efficiencies for the first retained alkane obtained with each column are displayed in table 17, and typical chromatograms on figure 117.

PDMS regular column expectedly provided the highest efficiency (9900 plates, plate height 0.22 mm), but could not separate ethane from methane, although C4 isomers could be baseline-separated (figure 117a).

Packed columns provided less plates (around 1000, plate height around 0.40 mm), but were all able to separate methane from air. Methane-ethane separations were of excellent quality, but high retention factors resulted in very long C4 elution times (figure 117b,c,d,e).

Carbon nanotubes expectedly provided strong retention, with long separation time, pronounced peak asymmetry, and high plate height (1.4 mm, figure 117f).

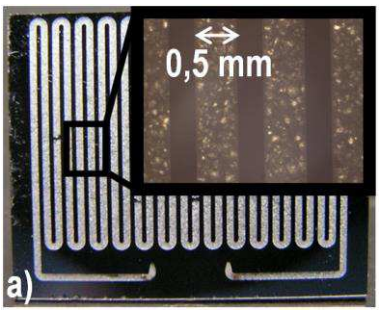


*Fig. 116a: micro column directly packed with commercial conventional powder (here : molecular sieve 13X); other packed columns had basically the same outlook (except for Carbopack X which color was black);*

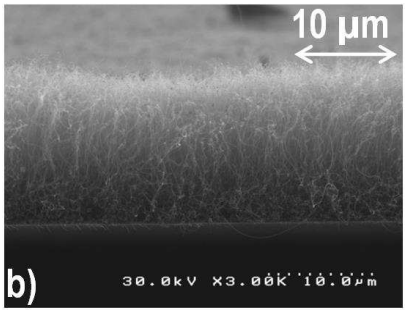


*Fig. 116b: SEM picture of micro column channel floor with in-situ-synthesized CNTs.*

*Fig. 116: pictures of micro columns developed at MEMS TC with other stationary phases*

## Apdx B.3. Conclusion

All these attempts presented strong drawbacks in the targeted application (mass produced micro columns for fast C1-C5 separations), in terms of non-collective fabrication (PDMS and packed columns), of separation (PDMS columns), of strong retentions and long analysis times (packed and CNTs columns). The will to overcome these drawbacks then led to the birth of the research work on sputter-deposited stationary phases.

| Stationary phase | Pattern | T (°C) | First retained alkane | k | $N_{max}$ ($HETP_{min}$, mm) |
|---|---|---|---|---|---|
| **PDMS** | Regular | 30 | Propane | **0.51** | **9900** (0.22) |
| **Silica gel** | To-pack | 30 | Methane | **0.36** | **1056** (0.42) |
| **Alumina** | To-pack | 60 | Methane | **0.29** | **1199** (0.37) |
| **Carbopack X** | To-pack | 60 | Methane | **0.59** | **1102** (0.40) |
| **Molecular sieve** | To-pack | 60 | Methane | **1.8** | **964** (0.46) |
| **Carbon nanotubes** | Variable width 30 µm | 100 | Ethane | **0.64** | **1543** (1.4) |
| *Sputter-dep.silica 2 $\mu m_{50mT}$* | *Regular* | *30* | *Ethane* | *0.28* | *5731 (0.38)* |
| *Sputter-dep. silica 1 µm* | *Semi-packed* | *30* | *Ethane* | *0.60* | *2663 (0.41)* |
| *Sputter-dep. alumina 1 µm* | *Semi-packed* | *30* | *Ethane* | *0.07* | *4479 (0.25)* |
| *Sputter-dep. graphite 2.7 µm* | *Regular* | *100* | *Ethane* | *0.35* | *946 (2.3)* |
| *Sputter-dep. graphite 0.1 µm* | *Semi-packed* | *30* | *Ethane* | *0.72* | *959 (1.1)* |
| *Sputter-dep. magnesia 1.2 µm* | *Regular* | *30* | *Propane* | *0.14* | *4393 (0.5)* |

*Table 17: retention factors (k), highest numbers of theoretical plates ($N_{max}$), and minimal heights equivalent to a theoretical plate ($HETP_{min}$) of the first retained alkane obtained with the different stationary phases; PDMS: P=3.4 bars, $V_{inj}$=1 µL; silica gel: P=2.4 bars, $V_{inj}$=0.2 µL (TCD setup: 2 bars); alumina: P=4.7 bars, $V_{inj}$=0.2 µL (TCD setup: 5.1 bars); Carbopack X: P=6.8 bars, $V_{inj}$=0.2 µL (TCD setup: 8.1 bars); molecular sieve 13X: P=2.4 bars, $V_{inj}$=0.2 µL (TCD setup: 2.5 bars); CNTs: P=6.8 bars, $V_{inj}$=0.1 µL; sputter-deposited stationary phases: reminders from report body; carrier gas: helium; detector: FID; for TCD setup, $V_{inj}$=0.5 µL, T=30°C.*

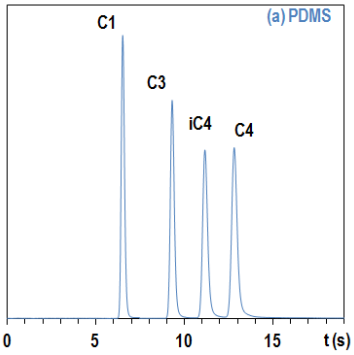


*Fig. 117a: PDMS, P=3.4 bars, $V_{inj}$=1 µL, T=27°C;*

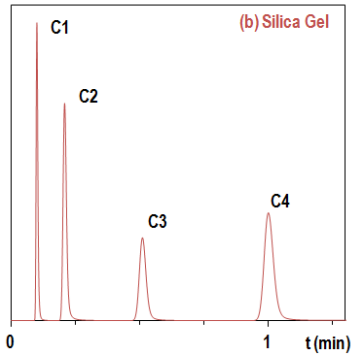


*Fig. 117b : silica gel, P=2.4 bars, $V_{inj}$=0.2 µL, T=30°C (12 s), then 1°C/s to 200°C;*

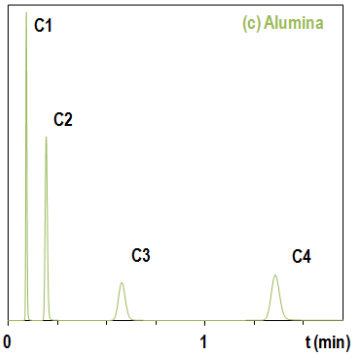


*Fig. 117c: activated alumina, P=4.7 bars, $V_{inj}$=0.2 µL, T=60°C (30 s), then 1°C/s to 200°C;*

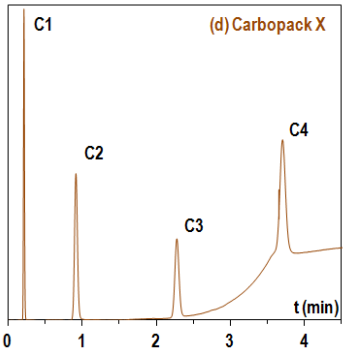


*Fig. 117d: Carbopack X, P=6.8 bars, $V_{inj}$=0.2 µL, T=60°C (18 s), then 1°C/s to 250°C;*

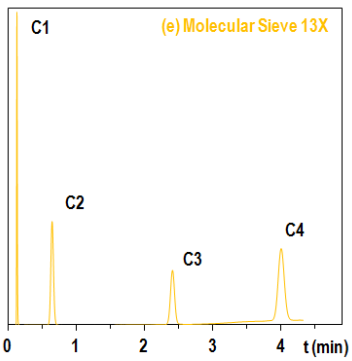


*Fig. 117e: molecular sieve 13X, P=2.4 bars, $V_{inj}$=0.2 µL, T=60°C (1 min), then 1°C/s to 200°C;*

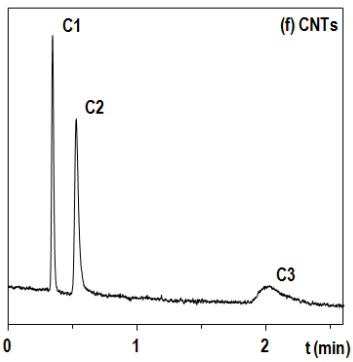


*Fig. 117f: in-situ-synthetized CNTs, P=6.8 bars, $V_{inj}$=0.1 µL, T=100°C;*

*Fig. 117: typical chromatograms obtained with the different stationary phases inserted in the micro columns; temperature programming was provided by Varian GC 3800 oven; arbitrary units on Y-axis*

# Appendix C: details on self-made temperature-programming system development

The purpose of this appendix is to provide a few technical details on the development of the electronic board, of the heating and cooling systems, and of the software.

## Apdx C.1. Electronic components references

- NI OEM 6008 USB (12-Bit, 10 kS/s Low-Cost Multifunction DAQ): National Instruments 202751
- Resistors Philips Metal Film MRS25
- SSR (Solid-state relay): CRYDOM CMX60D5
- Operational Amplifier: INTERSIL - ISL55001IBZ
- +/- 12 V power supply (for operational amplifier): TRACOPOWER - TML 20212C
- 30 V/5.6 V/5 V power supply (for thermal block): EA ELEKTRO-AUTOMATIK - EA-PS 2342-10B
- Conventional wires and prototype blank boards.

## Apdx C.2. Influence of input voltage

First attempts to enable chip temperature programming through pulse width modulation of a constant voltage signal were carried out with a voltage of 16 V. To check for system limits, different ramps between 15°C and 200°C with increasing intensity were set and the deviation of actual chip temperature from set was measured (figure 118a). Only a ramp of 2°C/s could reach end-of-ramp temperature without major deviation from set (less than 5%), and for a 10°C/s ramp set, temperature deviated of more than 5% from set as soon as 130°C were reached. This was due to the inability of the system to provide enough power to follow set ramp.

The deviation from a set ramp of 10°C/s between 15°C and 200°C was therefore measured for different input voltages (between 12 and 24 V, see figure 118b). In this case, only the 24 V voltage supply provided enough power not to deviate from set of more than 5% until the end of the ramp. Thus, this first experiment suggested using the highest voltage possible.

Nevertheless, as it was already visible on figure 68, and as it is clearly shown on figure 118c, using the highest voltage possible may not be the most appropriate method for relatively low intensity ramps (5°C/s in this example). Indeed, in such cases, and especially at the beginning of the ramp, excesses of energy provided by a high voltage supply induced pronounced deviation from ideality (for instance chip temperature actually decreased during more than 1.5 second between 16.5 and 18 seconds). Such temperature decreases should be carefully avoided for chromatographic applications, for they may strongly damage peak shapes. Such strong deviations were avoided by using a lower voltage (16 V instead of 30 V).

Moreover, average power consumption during the 20 seconds necessary to raise chip temperature from 15°C to 115°C at 5°C/s was proven to be very similar with both voltages (11 W with 16 V and 13 W with 30 V).

Thus, the second conclusion was that voltage supply should be carefully chosen in agreement with an accurately defined application and temperature-programmed method.

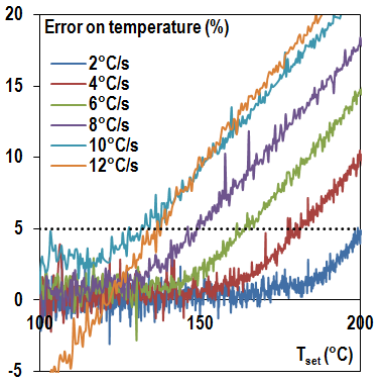


*Fig. 118a: relative deviation of chip actual temperature from set ramp temperature, for different ramps (from 2°C/s to 12°C/s) between 15°C and 200°C, with an input voltage of 16 V;*

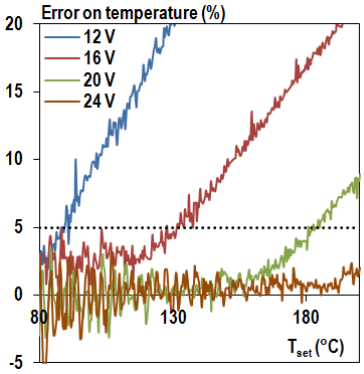


*Fig.118b: relative deviation of chip actual temperature from set ramp temperature, for different input voltages and a ramp set of 10°C/s between 15°C and 200°C/s;*

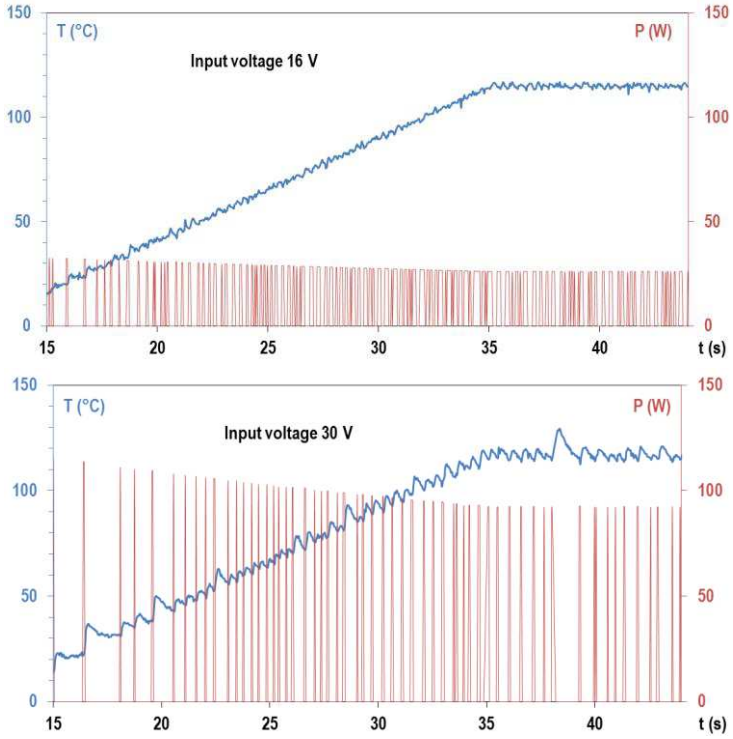


*Fig. 118c: chip temperature and power consumption for a low intensity ramp of 5°C/s between 15°C and 115°C:*

*top: input voltage 16 V, total energy provided: 230 J, average power: 11 W;*

*bottom: input voltage 30 V, total energy provided: 250 J, average power: 13 W;*

*Fig. 118: illustration of the influence of input voltage choice for chip heating; $T_{amb}$=30°C.*

## Apdx C.3. Cooling system optimization

Results detailed in this paragraph were provided by Emna Zoghlami. A short state-of-the-art review on existing cooling methods (mainly through a gaseous or liquid heat transfer medium or through thermoelectric heat transfer) led to the conclusion that Peltier modules best matched requirements in terms of targeted application (hot chip fast cooling in cycles) and of implementation ease and cost.

As Peltier module surface increased with cooling power, only one model of Peltier (MULTICOMP - MCHPE-128-10-05-E) from usual supplier matched both requirements in terms of size (Peltier module had to have comparable dimensions with the chip) and in terms of power (Peltier module had to work at the highest power possible). It was integrated with a heat sink and two fans (SUNON - MC35100V2-0000-A99) as described in III.B.3., and served as reference for improvements. Table 18 summarizes most relevant results obtained in this study: minimal temperature reached with the different systems evaluated are displayed, as well as cooling time necessary to decrease temperature from 150°C to 30°C and from 150°C to 15°C. Indeed, 15°C-150°C was the temperature range used for C1-C5 separation in 9 seconds at 15°C/s as shown on figure 102. With this reference system, a lowest temperature of 6°C could be reached, and 10 and 15 seconds were respectively necessary to reach 30°C and 15°C from 150°C.

First attempted improvements were self-made and consisted in adding an air blast from the outlet of a pressurized air tubing. Indeed, pressurized air outlets are available in most gas chromatographic apparatuses (such as GeoServices mini GC). Air blasting on its own was able to decrease chip temperature from 150°C to 30°C in 14 s, but could obviously not decrease temperature below 27°C. Reference system with addition of air blasting could reach 17°C, and 30°C in 8 seconds.

Other self-made attempts consisted in putting two identical Peltiers in cascade (in series), or two different Peltiers in cascade and series as well, with the reference Peltier underneath a smaller Peltier with the exact same dimensions than the chip. Although it improved the equilibrium of the system (temperatures below 0°C were reached), this did not improve the dynamics of the system.

| Fabrication | Name | Description | $T_{min}$ reached | $\Delta t_{150°C>15°C}$ | $\Delta t_{150°C>30°C}$ |
|---|---|---|---|---|---|
| Self-made | Reference | First system as described in III.B.3. | 6°C | 15 s | 10 s |
| | (Air blasting) | Pressurized air D~20 $m^3$/min | 27°C | - | 14 s |
| | Reference + air blasting | First system with air blasting | 17°C | - | 8 s |
| | 2-stage block cascade | Two identical Peltier superimposed | <0°C | 16 s | 11 s |
| | 2-stage pyramid cascade | Two different Peltier superimposed | <0°C | 22 s | 17 s |
| Industrial | 2-stage pyramid cascade | Two different Peltier superimposed | <0°C | 27 s | 20 s |
| | 3-stage pyramid cascade | Three different Peltier superimposed | <0°C | 33 s | 23 s |
| | Peltier for cycle handling | Specific Peltier | 25°C | - | 30 s |
| | Peltier kit | Integrated Peltier+sink+fan kit | 2°C | 18 s | 13 s |
| | Peltier kit + air blasting | Peltier kit with air blasting | 10°C | 14 s | 8 s |

*Table 18: summary of the different Peltier-based cooling systems evaluated; best results appear in red*

Industrial Peltier modules (pyramidal two- or three stages cascades, cycle handling-dedicated, and a Peltier kit) were then bought at Uwe Electronics and evaluated. The system Peltier kit (described in III.B.3.) with air blasting provided the best results for the targeted application, namely a minimal temperature of 10°C, and 8 and 14 seconds as cooling times from 150°C to respectively 30°C and 15°C.

## Apdx C.4. Labview software block diagram

Block diagram of the Labview software used for temperature programming is displayed on figure 119.

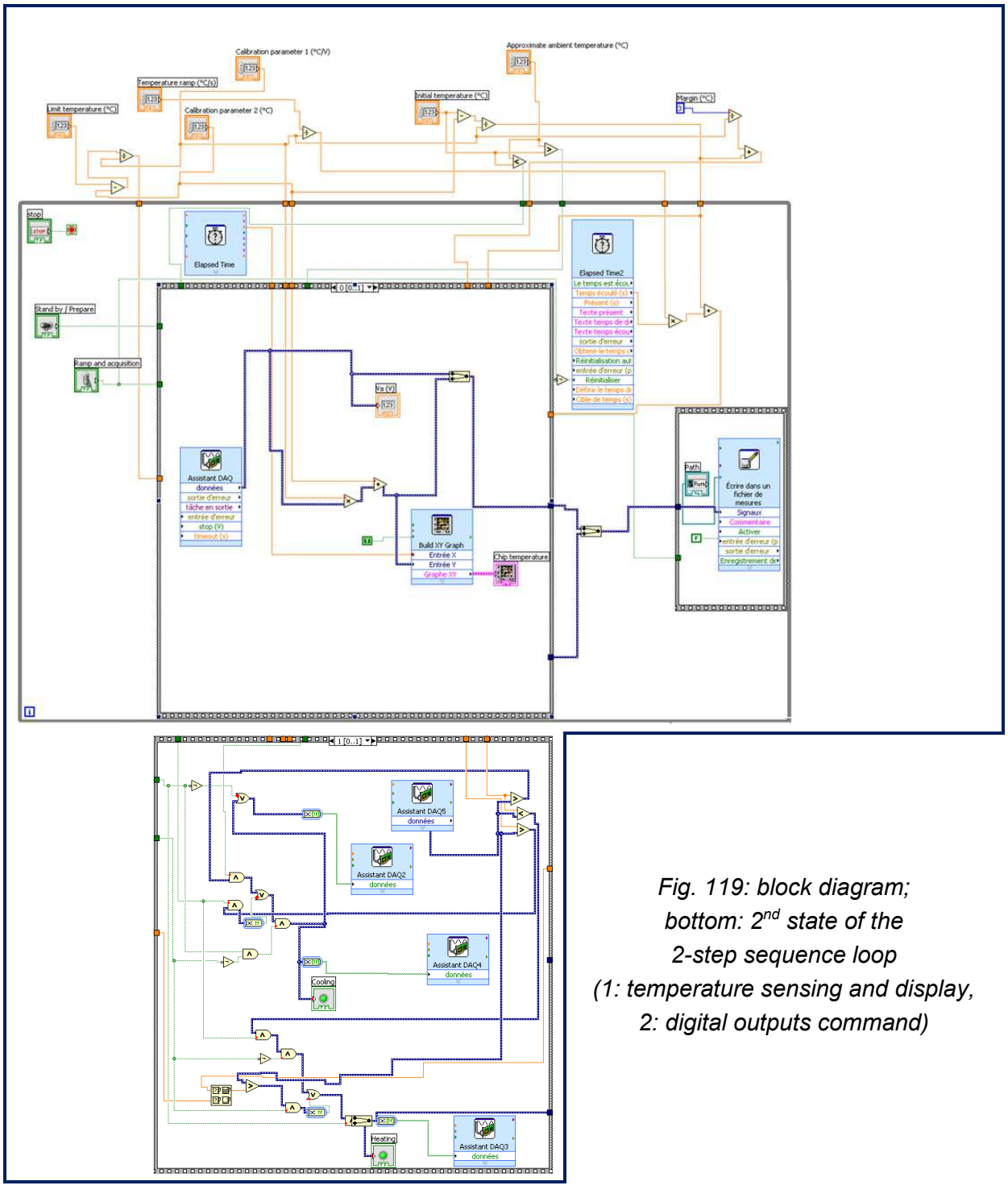


*Fig. 119: block diagram; bottom: 2nd state of the 2-step sequence loop (1: temperature sensing and display, 2: digital outputs command)*

# Abbreviations & symbols

- α: selectivity
- A: Van Deemter equation coefficient
- AFM: Atomic Force Microscopy
- As: peak asymmetry
- B: Van Deemter equation coefficient
- BCT: Buried Columns Technology
- BHF: Buffered Hydro Fluoric acid (oxide wet etchant)
- Bnz: benzene
- β: phase ratio
- C: Van Deemter equation coefficient
- C1: methane
- C2: ethane
- C3: propane
- C4: butane
- iC4: methyl-propane
- C5: pentane
- iC5: methyl-butane
- C6: hexane
- 2iC6: 2-methyl-pentane
- 3iC6: 3-methyl-pentane
- C7: heptane
- C8: octane
- C9: nonane
- C10 : decane
- cC5: cyclopentane
- cC6: cyclohexane
- CNTs: Carbon Nano Tubes
- DRIE: Deep Reactive Ion Etching
- $\Delta_r G°$: Gibbs free energy
- $\Delta_r H°$: standard enthalpy
- $\Delta_r S°$: standard entropy
- $e_f$ : stationary phase film thickness (at the middle of the channel side wall)
- ESIEE: Ecole Supérieure d'Ingénieurs en Electrotechnique et Electronique
- ESPCI: Ecole Supérieure de Physique et de Chimie Industrielles de la Ville de Paris
- FID: Flame Ionization Detector
- GC: Gas Chromatography or Gas Chromatograph
- GSC: Gas-Solid Chromatography
- H or HETP: Height Equivalent to a Theoretical Plate
- k: retention factor
- $k^\infty$: limit retention factor (at infinite T)
- K: distribution coefficient
- $K_0$: dimensionless pre-factor of the distribution coefficient
- L: column length
- MEMS: Micro Electro-Mechanical System
- MEMS TC: Schlumberger MEMS Technology Center
- N: number of plates
- $n_c$: number of carbons
- PDMS: poly dimethyl siloxane
- PLOT: Porous Layer Open Tubular
- πC2: ethene
- R: ideal gas constant (8.314 $J.mol^{-1}.K^{-1}$)
- $R_{AB}$: resolution between the peaks of compounds A and B
- $R^2$: linear regression correlation coefficient
- SEM: Scanning Electron Microscopy
- STM : Scanning Tunneling Microscopy
- $t_0$: dead time, zero retention time, flight time
- Tol: toluene
- $t_R$: retention time
- $t_{tot}$: overall analysis time
- TCD: thermal conductivity detector
- WCOT: Wall Coated Open Tubular

# Semi-indexed glossary

This very short and non-exhaustive glossary aims at both helping the reader quickly find where crucial notions definitions (such as “efficiency” or “sputtering”) can be found in this report and explaining notions too marginal to be defined in the body of the report for readability reasons (such as “dead volume” or “sample capacity”).

| Notion | Quick definition or pages references |
|---|---|
| **Capillary (column)** | Can be understood as a synonym of “open” column. |
| **Column** | p. 16, p. 29 |
| **Dead volume** | Cumulated volume in the analytical line not implied in the distribution of the analyte between the mobile phase and the stationary phase: injector and detector volumes, capillaries intern volumes, connecting elements volumes, uncoated column zones (for open column) or unpacked column zones (for packed columns). |
| **Efficiency** | p. 20 |
| **Adsorption heat** | p. 103 |
| **Gas chromatography** | p. 15 |
| **Gas solid chromatography** | Gas chromatography with a solid adsorbent as stationary phase (mineral, carbon-based material, ionic crystal, porous polymer…) |
| **Gas liquid chromatography** | Gas chromatography with a liquid as stationary phase (long hydrocarbon or organic chains, polymer in the form of gel…) |
| **MEMS technology** | p. 25 |
| **Micro machining** | |
| **Open (column)** | p. 17 |
| **Phase ratio** | p. 18 |
| **Plate (number and height)** | p. 20 |
| **Precision** | p. 102 |
| **Repeatability** | |
| **Retention factor** | p. 18 |
| **Sample capacity** | Threshold injected sample volume above which column is overloaded, peak shapes are deformed and strong deviation from conventional gas chromatography appear; it is ruled by column dimensions (including stationary phase) and separation efficiency. |
| **Semi-packed (column)** | p. 49 |
| **Separation number** | Defined as $(t_{R,A}-t_{R,B})/(w_{1/2,A}+w_{1/2,B})-1$ for two consecutive compounds in a chromatogram differing by one carbon atom, it corresponds to the number of homologous peaks that can be inserted between the two compounds. |
| **Sputtering** | p. 32 |
| **Standard enthalpy, entropy** | p. 18 |
| **Stationary phase** | p. 16 |
| **Versatility** | Ability to adapt to various requirements and situations, to show many different skills and qualities. |
| **Volatile organic compounds** | VOCs are organic chemicals that have a high vapor pressure at ordinary conditions; they include both human-made and naturally occurring chemical compounds; some VOCs are dangerous to human health or cause harm to the environment. Anthropogenic VOCs are regulated by law, especially indoors, where concentrations are the highest. |

# List of publications and communications

## A. Publications

### A.1. As first author

R. Haudebourg, J. Vial, D. Thiebaut, P. Sassiat, I. Azzouz, K. Danaie and B. Bourlon, in *Technical Proceedings of the 2012 NSTI Nanotechnology Conference and Expo,* **2012**, 106-109.

R. Haudebourg, J. Vial, D. Thiebaut, K. Danaie, J. Breviere, P. Sassiat, I. Azzouz and B. Bourlon, *Analytical Chemistry*, **2013**, 85 (1), 114-120.

R. Haudebourg, Z. Matouk, E. Zoghlami, I. Azzouz, K. Danaie, P. Sassiat, D. Thiebaut and J. Vial, *Anal Bioanal Chem*, **2013**, 1-3.

R. Haudebourg, Z. Matouk, E. Zoghlami, K. Danaie, J. Breviere, D. Thiebaut, P. Sassiat and J. Vial, submitted in **March 2014**.

### A.2. As co-author

J. Vial, D. Thiebaut, F. Marty, P. Guibal, R. Haudebourg, K. Nachef, K. Danaie and B. Bourlon, *Journal of Chromatography A*, **2011**, 1218 (21), 3262-3266.

I. Azzouz, J. Vial, D. Thiebaut, P. Sassiat, F. Marty, K. Danaie, M. Bockrath, J. Wong, R. Haudebourg and B. Bourlon, *Spectra Analyse*, **2011**, 282, 46-51.

I. Azzouz, J. Vial, D. Thiebaut, R. Haudebourg, K. Danaie, P. Sassiat and J. Breviere, *Anal Bioanal Chem*, **2013**, 1-14.

## B. Communications

### B.1. Oral communication

Podium presentation of the research work communicated by poster at the 17$^{th}$ ISSS (cf. below).

TechConnect World 2012, Conference & Expo, NanoTech, MicroTech, BioTech & CleanTech, Santa Clara, California, June 2012 (cf. technical proceeding above).

### B.2. Poster communications

17$^{th}$ International Symposium on Separation Sciences (ISSS), Cluj-Napoca, Romania, September 2011 (featuring 5 minutes « poster podium presentation »).

36$^{th}$ International Symposium on Capillary Chromatography (ISCC), Riva del Garda, Italy, May 2012 (not personally presented).

10$^{th}$ Francophone Symposium on Separation Sciences and Couplings (SEP2013), of the Francophone Association on Separation Sciences (AfSep), Paris, France, June 2013; poster rewarded (1$^{st}$ prize).

4$^{th}$ Research Symposium of the Gay-Lussac Federation (FGL) on “Chemistry in cities of tomorrow”, December 2013.

# Résumé et mots-clés

Un résumé en français du travail de thèse est proposé dans ce chapitre spécial. Il rappelle dans les grandes lignes le contexte du travail de recherche, présente les principaux résultats obtenus, et conclut sur les perspectives ouvertes par l'innovation publiée dans ce rapport.

## A. Contexte du travail de recherche

La chromatographie en phase gazeuse est une technique de choix pour l'analyse de mélanges volatils. Il s'agit d'une technologie bien connue, maîtrisée, et en constante amélioration depuis une soixantaine d'années. L'appareillage requis est cependant très volumineux, consomme beaucoup d'énergie, et est traditionnellement localisé dans les laboratoires dédiés.

Depuis une quarantaine d'années, les progrès des technologies d'usinage du silicium en salle blanche ont permis de nombreux développements, notamment dans le domaine de la micro fluidique. Les premières études portant sur des micro colonnes fabriquées dans des wafers de silicium et appliquées à la chromatographie en phase gazeuse ont été menées dès la fin des années 1970, en premier lieu pour des applications aérospatiales. Ces micro colonnes ont permis d'obtenir, en particulier, et par rapport aux systèmes conventionnels, un gain de place, en les logeant dans des puces de l'ordre du $cm^3$, un gain financier, en étant produites collectivement, et un gain en temps, en rendant possible une programmation en température très rapide. Avec les miniaturisations associées des systèmes d'injection et de détection, il est récemment devenu possible de développer des systèmes portables, pour l'analyse rapide, continue, sur site et en temps réel à l'aide de capteurs embarqués, pour des applications diverses.

Cependant, l'étape d'introduction de phases stationnaires solides conventionnelles (remplissage par des poudres) dans les colonnes s'est généralement révélée critique et peu compatible avec la miniaturisation extrême, et ce sont des phases stationnaires liquides à base de polysiloxanes qui ont été utilisées dans la quasi-totalité des applications de ces colonnes. Les inconvénients de ce type de phases stationnaires sont de 2 ordres : d'une, les composés ultra volatils comme les premiers alcanes, ne sont que peu retenus sur ce genre de support, et ne peuvent être séparés que par des colonnes de longueur conséquente, ce qui compromet la miniaturisation; de deux, l'étape d'insertion de la phase stationnaire n'est par nature ni collective (ou seulement indirectement collective), ni compatible avec la mise au point d'un procédé de fabrication intégralement réalisé en salle blanche et industrialisable.

Une première alternative intéressante, ponctuellement reportée depuis une dizaine d'années, a consisté à utiliser des nanotubes de carbone comme phase stationnaire solide; le critère d'insertion collective a été respecté (croissance des nanotubes par un procédé de salle blanche, entre la gravure des canaux et la formation de la colonne par la soudure d'un couvercle), mais des réserves ont été émises, en terme de robustesse du procédé, de

niveau de sécurité requis pour la fabrication, et de pertinence pour certaines applications chromatographiques (les supports carbonés induisent généralement de très fortes rétentions et déformation de pics pour les hydrocarbures).

L'innovation majeure présentée dans ce rapport a consisté en l'utilisation de la technique de dépôt de couches minces par pulvérisation cathodique (figure 120) pour réaliser l'étape d'insertion de la phase stationnaire. Cette technique, initialement et majoritairement utilisée en microélectronique, remplit les critères cités en terme de fabrication : elle permet le revêtement des parois des canaux par des matériaux traditionnellement utilisés en chromatographie gaz-solide (silice, alumine, graphite, etc), de manière collective, avec un procédé par nature intégrable dans la ligne de fabrication complète de la colonne en salle blanche de niveau commun.

La dernière incertitude, et la plus centrale, résidait donc dans l'évaluation des propriétés chromatographiques de telles micro colonnes ; dans le cadre d'un projet de recherche, incarné par une thèse de doctorat, supporté par Schlumberger (première entreprise de services pétroliers mondiale), et dirigé par le Laboratoire Sciences Analytiques, Bioanalytiques et Miniaturisation de l'ESPCI ParisTech, la capacité des colonnes ainsi fabriquées à retenir et séparer les composés d'intérêt premier (d'abord alcanes C1-C5, ensuite hydrocarbures volatils en général) a été testée.

Une partie du travail a consisté à estimer la précision chromatographique du procédé de fabrication puis l'influence de paramètres variés sur les propriétés thermodynamiques et cinétiques des colonnes (figure 121) : ces paramètres ont notamment inclus la structure et les dimensions de la colonne, la nature et l'épaisseur du matériau déposé, et la pression à laquelle le dépôt a été réalisé.

Une seconde partie a consisté en la mise au point et la réalisation de divers tests d'anticipation des conditions réelles d'utilisation (programmation ultra-rapide en température, séparations de mélange complexes, rétention des composés les plus légers à haute température, utilisation de l'air comme gaz vecteur, influence de l'humidité sur la rétention, intégration avec un micro injecteur et un micro détecteur).

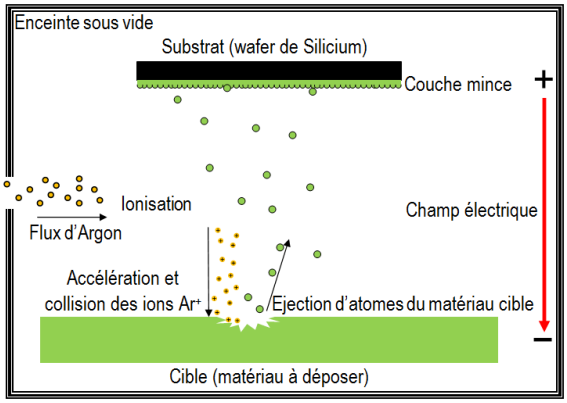


*Fig. 120 : principe du procédé de pulvérisation cathodique: un flux d'argon est ionisé et accéléré vers une cible constituée du matériau à déposer; les ions argon pulvérisent la cible et en éjectent des atomes qui se déposent ensuite en fine couche d'épaisseur proportionnelle au temps de dépôt sur le substrat.*

# B. Principaux résultats

## B.1. Observations préliminaires

Les alcanes linéaires C1-C5 purent être entièrement séparés en 6 minutes sur une micro colonne avec une phase stationnaire en silice déposée par pulvérisation cathodique (figure 122a). La silice, l'alumine, le graphite, la magnésie et le dioxyde de titane ont été testés comme matériaux pour servir de phase stationnaires dans les micro colonnes. Le tableau 19 résume qualitativement les fabrications qui ont pu aboutir et les séparations qui ont pu être obtenues, selon le matériau de la phase stationnaire et la structure de la colonne.

## B.2. Caractérisation fondamentale

La précision chromatographique de la méthode de fabrication des micro colonnes a été mesurée quantitativement, mais sur un faible nombre d'échantillons (3 colonnes d'un même wafer, et 4 colonnes de 4 wafers différents). Les résultats ont été hétérogènes (d'excellents à moyens, i.e. légèrement en-dessous des attentes) selon les différentes études menées; cependant, la majorité des causes identifiées ayant conduit à des variations de colonne à colonne peuvent raisonnablement être imputées à l'aspect recherche du travail, et évitées dans un contexte de développement industriel.

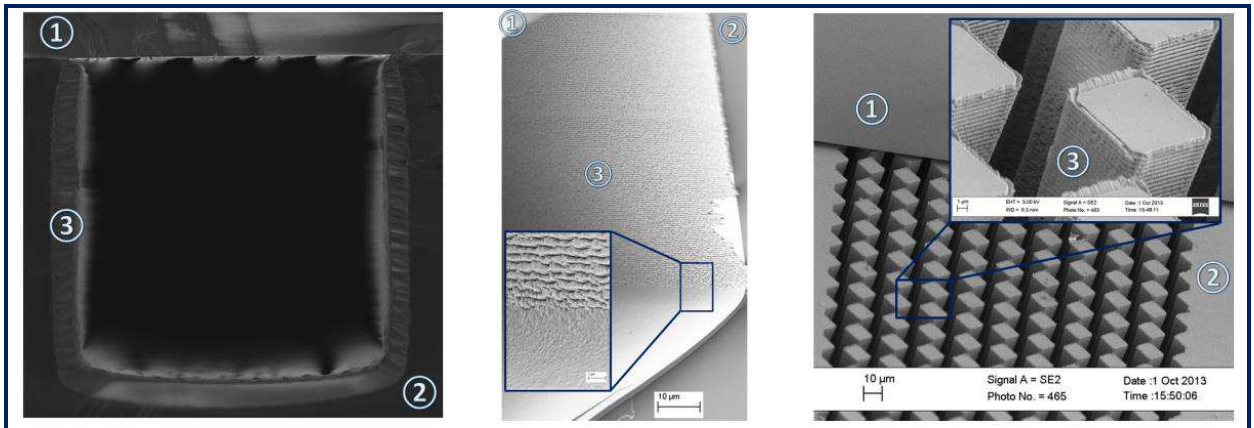


*Colonne capillaire (section vue de face) 1m x (75 x 75)µm² avec silice 6 µm*

*Colonne capillaire (section vue de ¾) 2,2m x (100x100)µm² avec graphite 2,7 µm*

*Colonne « semi-remplie » (canal vu de dessus) 1,1m x (200x100)µm² avec alumine 1 µm*

*Fig. 121 : exemples d'images MEB de micro colonnes avec phases stationnaires déposées par pulvérisation cathodique ; 1 : Pyrex ; 2 : silicium ; 3 : adsorbant.*

Dans un second temps, les grandeurs thermodynamiques (facteurs de rétention, chaleurs d'adsorption, et sélectivité), les grandeurs cinétiques (nombres de plateaux et hauteurs équivalentes à un plateau), et une grandeur mixte (résolution) ont été mesurées pour les différentes colonnes fabriquées et évaluées durant cette étude, et sont récapitulées dans le tableau 20. Les plus grandes rétentions et sélectivités ont été apportées par les colonnes de graphite, tandis que des efficacités supérieures à 5000 plateaux ont été enregistrées avec des colonnes capillaires et de la silice (correspondant à près de 955 plateaux par seconde), et que des hauteurs de plateau de 250 µm ont été obtenues avec des colonnes semi-remplies et de l'alumine ; des résolutions entre les pics du méthane et de l'éthane jusqu'à 6,6 ont été mesurées.

Une modélisation satisfaisante du comportement de ces micro colonnes à l'aide de la théorie classique de la chromatographie n'a pas pu être proposée dans la totalité des cas. La toute relative imprécision de la méthode, une moindre robustesse de la théorie de la chromatographie gaz-solide (comparée à gaz-liquide), et l'absence de mesures précises du volume de phase stationnaire (ou de la porosité de la couche), ont limité les possibilités de prédiction quantitatives.

## B.3. Caractérisation appliquée

Un système de programmation en température a été construit pour rendre possible des séparations très rapides sur ces colonnes. Ce système incluait notamment le dépôt de filaments de platine sur les puces pour la mesure de la température et l'apport de chaleur par effet Joule, un bloc de refroidissement par effet Peltier, deux cartes électroniques pour faire le lien entre le bloc de gestion en température et l'ordinateur, et un logiciel. Des mesures de puissance ont confirmé la faible consommation énergétique d'un tel système (par exemple 30 W pendant 10 secondes pour une rampe de 10°C/s de 20°C à 220°C).

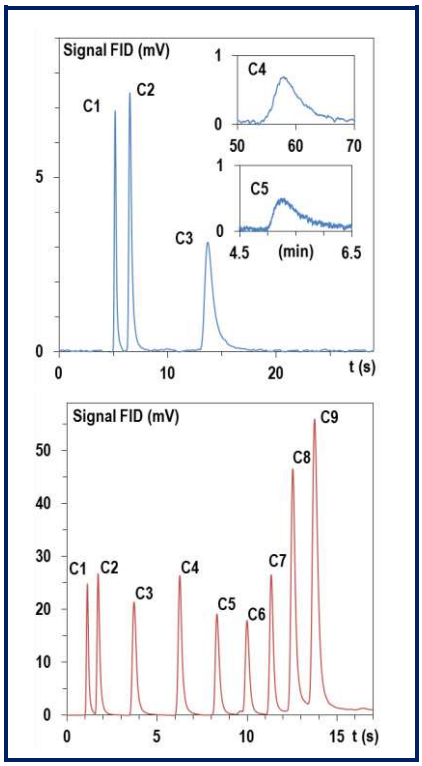


*Fig. 122 : séparations des alcanes légers sur une micro colonne capillaire (2,2 m x (100x100) µm²) avec silice (2,6 µm) ;*

*Fig. 122a (en haut) : séparation isotherme (30°C) (méthane au pentane)*

*Fig. 122b (en bas) : séparation avec programmation en température, 15°C/s (méthane au nonane)*

*Détails : voir figures 71b et 105a.*

| Phase stationnaire | Type de colonne | Fabrication réussie | Premier alcane retenu |
|---|---|---|---|
| Silice | Capillaire | Oui | Ethane |
| | Semi-remplie | Oui | Ethane |
| Alumine | Capillaire | Oui | Butane |
| | Semi-remplie | Oui | Ethane |
| Graphite | Capillaire | Oui | Ethane |
| | Semi-remplie | Oui | Ethane |
| Magnésie | Capillaire | Oui | Propane |
| | Semi-remplie | Non | - |
| Dioxyde de titane | Capillaire | Non | - |
| | Semi-remplie | Non | - |

*Tableau 19 : récapitulation simplifiée des colonnes fabriquées et des séparations possibles*

| Type | Lon-gueur | Section (µm²) | Phase station. | $t_{dépôt}$ (min) | $k_{C3}$ | $\|\Delta_r H°_{C3}\|$ (kJ/mol) | $\alpha_{C2-C3}$ | $N_{maxC2}$ | $N_{maxC2}$ (/m) | $HETP_{minC2}$ (mm) | $R_{C1-C2}$ |
|---|---|---|---|---|---|---|---|---|---|---|---|
| C | 2.2 m | 100x100 | Silice | 300 (50 mT) | 1,7 | 28,8 | 6,2 | **5731** | **2605** | **0,38** | 3,9 |
| | | | | 120 | 2,1 | 31,8 | 6,2 | 2597 | 1180 | 0,85 | 3,5 |
| | | 75x100 | | | 2,2 | - | 6,3 | 2331 | 1060 | 0,95 | 3,3 |
| | | 50x100 | | | 1,2 | - | 5,5 | 3860 | 1755 | 0,57 | 2,8 |
| | | 100x50 | | | **0,8** | - | 5,3 | 2256 | 1025 | 0,98 | 1,8 |
| | | 30x100 | | | 1,8 | - | 6,2 | 1387 | 630 | 1,6 | 2,0 |
| | | 50x50 | | 240 | 6,2 | 34,0 | 5,6 | 1318 | 599 | 1,7 | **6,6** |
| | | 50x50 | | 30 | 0,62 | 24,9 | 6,9 | 2229 | 1013 | 1,0 | 0,88 |
| | | 75x100 | | | **0,7** | - | 6,6 | **5517** | 2508 | 0,40 | 1,7 |
| | | | | 60 | 0,9 | - | 5,7 | 4425 | 2011 | 0,50 | 2,0 |
| | | | | 180 | 2,2 | - | 5,9 | 2616 | 1189 | 0,84 | 4,0 |
| | | | | 240 | 4,4 | - | 6,4 | 1988 | 904 | 1,1 | **5,5** |
| | 1 m | 75x75 | | | 3,7 | 20,1 | 8,7 | 1137 | 1137 | 0,59 | 2,2 |
| | 0.5 m | | | | 3,8 | 25,6 | 10,1 | 799 | 1598 | 0,63 | 1,3 |
| $SR_1$ | 1.1 m | 200x100 | | 120 | 3,9 | - | 6,4 | 2663 | 2421 | 0,41 | 4,1 |
| $SR_2$ | | | | | 3,2 | 26,8 | 6,7 | 2344 | 2131 | 0,47 | 4,4 |
| | | | | 30 | **0,8** | 27,8 | 5,1 | 3945 | **3586** | **0,28** | 3,3 |
| | | | Alumine | 120 | 0,7 | 30,2 | 8,6 | **4479** | **4072** | **0,25** | 0,96 |
| | | | Graphite | 60 | 12,0 | 34,9 | 16,7 | 959 | 872 | 1,1 | **6,3** |
| C | 2.2 m | 30x100 | | | - | - | - | 172 | 78 | 13 | 4,7 |
| | | 50x100 | | | - | - | - | 224 | 102 | 9,8 | 2,5 |
| | | 75x100 | | | - | - | - | 134 | 61 | 16 | 2,9 |
| | | 100x100 | | | 11,4 | 39,1 | 14,9 | 256 | 116 | 8,6 | 1,8 |
| | | | | 200 | 117 | 44,3 | 14,7 | 83 | 38 | 27 | 3,9 |
| | | | Magnésie | 562,5 | 1,0 | 20,1 | - | - | - | - | - |

*Tableau 20: résumé des résultats obtenus lors des caractérisations thermodynamique et cinétique des micro colonnes à phase stationnaire déposée par pulvérisation cathodique; les 3 meilleures valeurs en terme d'efficacité et de résolution apparaissent en rouge ; les 3 plus faibles rétentions telles que la résolution est supérieure à 1.25 apparaissent en vert ; C=capillaire, SR=semi-remplie ; voir aussi tableau 16.*

Avec ce système, des rampes de température jusqu'à 20°C/s ont pu être obtenues, permettant ainsi des séparations très rapides d'hydrocarbures variés. Le chromatogramme figure 122b montre par exemple une séparation des alcanes linéaires C1-C9 en moins de 15 secondes. D'autres séparations rapides d'hydrocarbures (isomères, insaturés, aromatiques, cycliques, en mélanges tests ou réels) ont pu être réalisées de la même manière.

Dans l'hypothèse de séparations devant être opérées à une haute température ambiante (désert, puits), où une température initiale d'analyse de l'ordre de 15-30°C serait difficilement envisageable, la résolution des composés les plus légers (méthane et éthane) pourrait être dégradée. Des solutions concrètes ont été proposées et démontrées pour anticiper cette éventuelle limitation (figure 123), en utilisant du graphite comme phase stationnaire, ou des colonnes à faible rapport de phase (petite section sur grande épaisseur de film).

Le déploiement d'appareils miniaturisés sur site requiert généralement l'utilisation de l'air à la place de l'hélium comme gaz vecteur ; une étude comparée entre l'hélium et l'azote comme gaz vecteurs a pu démontrer l'équivalence de l'utilisation de ces deux gaz avec les micro colonnes, sans perte de performance. De même, dans l'hypothèse de présence inévitable d'eau sur site (liquide ou humidité), l'effet de la percolation d'une goutte d'eau liquide sur les performances d'une micro colonnes a été étudié ; après une chute brutale immédiate de la rétention et de la résolution (de 3,7 à 1,3 pour la résolution méthane-éthane), ces quantités retrouvent leurs valeurs initiales en moins de deux heures sous le seul effet du balayage du gaz vecteur à température ambiante.

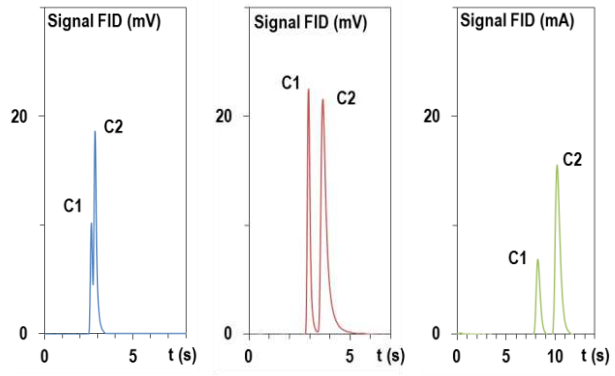


| | Gauche (ref) | Milieu | Droite |
|---|---|---|---|
| Largeur x Profondeur (µm x µm) | 100x100 | 100x100 | 50x50 |
| Phase stationnaire | Silice | Graphite | Silice |
| Epaisseur du film (µm) | 2,6 | 2,7 | 4,8 |
| T (°C) | 100 | 100 | 97 |
| $R_{C1-C2}$ | 0,8 | 2,0 | 2,3 |

*Fig. 123: séparations méthane-éthane à haute température (~100°C) (colonnes capillaires, longueur 2,2 m)*

## B.4. Paragraphe restreint à Schlumberger

## C. Conclusions et perspectives

Une nouvelle méthode d'introduction de phases stationnaires solides dans des micro colonnes de silicium a été proposée. L'utilisation de la pulvérisation cathodique comme méthode de dépôt de phase stationnaires comme la silice, l'alumine, le graphite ou la magnésie, répond à la fois aux critères de procédé d'insertion collectif et de technique industrialisable et intégrable dans une ligne de micro usinage du silicium en salle blanche conventionnelle.

Les propriétés chromatographiques de ces colonnes en termes de séparations rapides et efficaces d'hydrocarbures volatils, et d'adaptabilité à diverses exigences du terrain, en font une technologie prometteuse dans le cadre de la miniaturisation de la chromatographie en phase gazeuse pour des analyses rapides sur site, en temps réel, et éventuellement autonomes.

Bien que des études complémentaires concernant la précision de la méthode employée (fabrication, robustesse en mode cycles thermiques) doivent être menées, l'intérêt des communautés scientifiques et industrielles pour cette découverte a été démontré à plusieurs reprises par des publications et communications d'une part, et des brevets et leur application au XXXXXXXXXXX dans le but d'un déploiement industriel à court terme d'autre part.

A plus long terme, des études plus détaillées sur le sujet pourraient par exemple porter sur d'autres matériaux pulvérisables, ou sur la comparaison avec de la pulvérisation réactive; des développements pour d'autres applications, comme la surveillance de composés organiques volatils, devraient être envisagés.

**Mots clés :** micro chromatographie en phase gazeuse, pulvérisation cathodique, MEMS, hydrocarbures, alcanes, silice, alumine, graphite, magnésie, séparations rapides.

# Acknowledgements

First and foremost, I wish to thank any **reader** of this report. Thank you for your time and consideration, I hope you had a pleasant and enriching reading.

My second thanks are dearly expressed to my PhD thesis director **Jérôme Vial**, who always behaved towards me not only with honesty, transparency and scientific rigor, but also with a positive, trustful, and enthusiastic state of mind. It was a most pleasant experience to work under his supervision. In a similar manner, grateful thanks are expressed to my co-director **Didier Thiébaut**, for similar reasons. Assistance provided by **Zineb Matouk** during her 6 months master internship was greatly appreciated, as well as her tireless and joyful motivation, including through harsh technical difficulties. Still within the ESPCI, sincere and special thanks are due to **Imadeddine Azzouz** and **Fabien Brothier**, for being two of my PhD fellows, to **Patrick Sassiat**, for technical advising and support, to **Wassim Hadj Ali**, for teaching me supervising practical works, to **Joachim Fleury** for representing the unfolding of the LSABM – GeoServices collaboration, and to the **whole department staff**, from the interns and service agents to the director, through PhD students and permanent members.

Many things changed at Schlumberger MEMS TC between my arrival in March 2010 and my defense in February 2014, but obviously nothing was forgotten. My first thanks are sincerely expressed to my former supervisor **Bertrand Bourlon**: in spite of occasional disagreements, I learned a lot from him and I am most thankful to him for providing tangible industrial credit to the discovery by finding a direct and practical application of the discovery, and establishing a collaboration with GeoServices. From those early days, acknowledgements are as well due to **Eric Donzier**, **Bernard Montaron**, **Joyce Wong** and **Pierre Guibal**, without whom the project would not have been possible as well. From the latter days, I wish to acknowledge the assistance of **Emna Zoghlami** (6 month master intern) for providing significant results and perfecting my supervising skills, the technical help of **Sébastien Prangère** and **Alain Hohn**, and the availability, generosity, and wise advices of MEMS TC manager **Patrice Ligneul**. And last, but not least, I wish to mention the pleasure to share all these moments with my fellows, **Kamran Danaie**, **Maxime Projetti**, **Thomas Raillot** and **Florian Risser**, and with **all the other people at MEMS TC**.

My special thanks are naturally extended to the people involved in the project at GeoServices, firstly **Jérôme Brévière** (also invited examiner of this work) and **Pawel Kasprzykowski**, but also **Reda Karoum**, **Patrick Banik**, **Vincent Châtelet**, **François Chevillard** and **Jean-Pierre Poyet**, for their interest and commitment in the development of the application.

Other professional acknowledgements are deeply expressed to **Frédéric Marty** from the ESIEE for technical support in the early days, and to **Bruno Gallas** and **Vincent Rouessac** for very kindly accepting to operate measurements on sputter-deposited layers, and for helping understand a few key points regarding layer structure.

All the members of the thesis defense jury are mostly and gratefully thanked for their time, attention, and interest: **Carlo Bicchi** and **Jérôme Randon** (reporters), **Jacques Fattacioli**, **Franck Launay, Michel Sablier** and **Jérôme Brévière** (examiners), **Jérôme Vial** and **Didier Thiébaut** (directors).

My thanks are finally expressed to my **friends and family**, and to my dear **Pauline Valois**, who is coincidentally as well PhD student at Schlumberger and the ESPCI at the moment of this writing.

My last thought shall honor the memory of our respective grandparents.

# Abstract and keywords

A totally new solid stationary phase deposition technique for micro machined gas chromatography columns fabrication dedicated to oilfield applications was proposed: to overcome the limitations of liquid stationary phases (such as polymethylsiloxane) or occasionally reported solid stationary phases (carbon nanotubes, functionalized gold, conventional packing materials) in terms of very volatile compounds retention and/or clean room batch production, a new approach consisting of the collective direct deposition of the adsorbent in micro columns channels by sputtering was performed. The process was fully compatible with clean room fabrication flow and industry-ready, with very good (yet only partially demonstrated) precision results.

Silica, alumina, graphite and magnesia were proven able to separate volatile hydrocarbons. Various stationary phases (deposited materials and thicknesses, process pressure) and types of columns (structure, geometrical dimensions) were fabricated in the form of 2 cm x 2 cm x 1 mm silicon-Pyrex chips, and chromatographically evaluated, and their thermodynamic and kinetic properties were quantitatively reported. Retentions were qualitatively observed to increase from magnesia to graphite through alumina and silica and with phase ratio decrease, as expected; very satisfying efficiencies were obtained: more than 5700 plates for open sputter-deposited silica columns, and a plate height of 250 µm for semi-packed sputter-deposited alumina columns.

The possibility to use such columns for fast in-situ and autonomous monitoring of light hydrocarbons in oilfield environments was demonstrated by the implementation of a chip temperature-programming system and various versatility tests: a complete C1-C9 alkanes separation was performed in less than 15 s, and complex mixtures fast separations (isomers, unsaturated) were obtained as well; solutions to enable high temperature (100°C) methane-ethane separations were exhibited; use of nitrogen as carrier gas and high humidity levels were shown not to damage sputter-deposited silica columns performances.

A confidential application with GeoServices showed preliminary encouraging results and a development was planned for the year 2014.

Therefore, sputter-deposited stationary phase micro columns opened numerous perspectives for the developments of miniaturized gas chromatographic apparatuses.

**Key words: micro gas chromatography, sputtering, MEMS, hydrocarbons, alkanes, silica, alumina, graphite, magnesia, fast separations.**

**Résumé et mots-clés en français pages 172 à 178**